



Development of a Novel Electrochemical Lab-on-a-Disc, Bio-Sensors and Bio-Assays for Pathogen Capture and Detection

A thesis submitted to Dublin City University for the degree of PhD

By

Éadaoin Carthy B.Sc. (Hons)

School of Chemical Sciences,
Dublin City University,
July 2019

Supervisor:

Professor Robert J. Forster

Declaration

I hereby certify that this material, which I now submit for assessment on the programme of study leading to the award of PhD is entirely my own work, and that I have exercised reasonable care to ensure that the work is original, and does not to the best of my knowledge breach any law of copyright, and has not been taken from the work of others save and to the extent that such work has been cited and acknowledged within the text of my work.

Signed: _____

ID No.: _____

Date: _____

Table of Contents

Table of Figures.....	vii
List of Abbreviations.....	xi
Nomenclature	xv
Acknowledgements.....	xvi
Abstract	xx

Chapter 1 : Literature Review and Thesis Objective

1.1 Introduction	2
1.2 Sepsis and its Epidemiological Impact	6
1.3. Methods of Pathogen Detection	10
1.3.1 Blood Culture Techniques	10
1.3.2 Polymerase Chain Reaction Amplification Detection.....	13
1.3.3 Recombinase Polymerase Amplification	16
1.3.4 ELISA Bacterial Detection	18
1.3.4 Lateral Flow Assays	19
1.4 Impedimetric Biosensors	22
1.4.1 Electrochemical impedance Spectroscopy for Pathogen Detection	23
1.4.2 Electrochemical Biosensors.....	25
1.5 Centrifugal Microfluidics.....	29
1.6 Analyte Detection using Electrochemical Methods on a Lab-on-a-Disc.....	32
1.7 Conclusion and Thesis Outline	38
1.8 References	41

Chapter 2 : Materials and Methods

2.1 Introduction	51
2.2 Materials Justification.....	51
2.2.1 Polydimethylsiloxane (PDMS).....	51
2.2.2 Polymethylmethacrylate (PMMA)	52
2.2.3 Pressure Sensitive Adhesive (PSA).....	53
2.3 Instrumentation	53

2.3.1 Computer Aided Design (CAD).....	53
2.3.2 Laser Machining.....	54
2.3.3 Xerography.....	55
2.3.4 Dissolvable Film Tabs.....	56
2.3.5 UV Lithography.....	57
2.3.6 Casting of PDMS on Master.....	60
2.3.7 3D Printing.....	60
2.4 Experimental Procedures.....	61
2.4.1 Electrochemical Cells and Electrode Fabrication.....	61
2.4.2 Self Assembled Monolayers.....	62
2.4.3 Gold Electrode Preparation.....	62
2.4.4 Hydrophilic Treatment of Gold Electrodes.....	63
2.4.5 Electrochemical Deposition of Au on Au coated Si Electrode.....	63
2.4.6 PDMS Micro-Contact Printing Stamp Preparation.....	64
2.5 Assembly of Platforms and Clean Room Procedures.....	65
2.6 Fluid Flow in LoAD Systems.....	67
2.6.1 Types of Fluid Flow.....	68
2.6.2 Valving and Fluid Control.....	70
2.6.3 Testing of Centrifugal Devices.....	75
2.7 Bacteria Culture.....	77
2.8 Electrochemical Impedance Spectroscopy.....	78
2.8.1 Faradaic and Non-Faradaic Impedance.....	81
2.9 Imaging Systems.....	82
2.9.1 Confocal Microscopy.....	82
2.9.2 Scanning Electron Microscopy.....	83
2.10 ELONA Preparation and Detection.....	84
2.11 PCR and RPA Methodologies.....	85
2.12 Conclusion.....	89
2.13 References.....	90

Chapter 3 : Development of eLoAD for Multiple Liquid Type Handling Biosensing Platform

3.1 Introduction.....	96
-----------------------	----

3.2 Assay Requirements and Device Specifications	97
3.2.1 Converting protocol steps into microfluidic features	99
3.2.2 Chemical and biological reagents used	101
3.2.3 Materials used in manufacturing the microfluidic disc	102
3.3 Experimentation	102
3.3.1 System Design and Experimentation	102
3.3.2. Device Concept	105
3.4 Developing and optimising the ELoaD centrifugal microfluidic platform	107
3.4.1 Version 1.0	107
3.4.2 Version 2.1	110
3.4.3 Version 2.2	112
3.4.4 Version 3.1	115
3.4.5 Version 3.2	117
3.4.6 Version 3.3	118
3.4.7 Final Version (V 3.4)	120
3.5 DF Valve Triggering Frequency Optimisation	122
3.6 Waste Channel Optimisation	127
3.7 Electrode Cover Optimisation	133
3.8 Platelet and RBC inhibition Study	135
3.9 Spin Rate Study	141
3.10 Materials Characterisation	145
3.11 Second Generation Device	147
3.12 Conclusion	150
3.13 References	152

Chapter 4 : Biosensor Development and Pathogen Detection on an Electronic Lab-on-a-Disc using Label-Free Electrochemical Detection

Methods

4.1 Introduction	156
4.2 Materials and Methods	160
4.2.1 Chemical and Biological Reagents Used	160

4.2.2 Materials	161
4.3 Results and Discussion	161
4.3.1 Fabrication of label-free electrochemical biosensor for use with a three electrode electrochemical cell.....	161
4.3.2 Justification of μ CP for the single-use biosensor	175
4.3.3 Implementation of single use biosensor into eLoaD platform	182
4.3.4 Real Sample Detection for Device Validation	185
4.4 Conclusion	206
4.5 References	209
 Chapter 5 : E. coli Capture and Detection using ELONA, Apta-PCR and Apta-RPA Assays	
5.1 Introduction	216
5.2 Chemical and Biological reagents used	219
5.3 Experimentation	220
5.3.1 Enzyme linked oligonucleotide assay (ELONA)	220
5.3.2 Polymerase Chain Reaction Assays	231
5.3.3 Recombinase Polymerase Amplification	241
5.4 Conclusion	248
5.5 References	250
 Chapter 6 : Future Work and Final Conclusions	
6.1 Future Outlook	254
6.1.1 Prospective study for eLoaD for use with real samples	254
6.1.2 Integrated System for eLoaD Testing	255
6.1.3 Alternative Electrode Fabrication for eLoaD Device	255
6.1.4 Lateral Flow Assays (LFAs) detection with aptamer conjugated AuNPs.....	267
6.2 Final Conclusions	274
6.3 References	278

Table of Figures

Chapter 1

Figure 1.1 Increasing trend of number of sepsis sufferers in Irish based hospitals.....	7
Figure 1.2. Life-cycle of sepsis/septicaemia portraying the presence of multiple pathogens causing organ malfunction	7
Figure 1.3. Top 20 microbes identified from positive blood culture bottles during a 1 year period within a 1000 bed university hospital during 2013.....	12
Figure 1.4 Lateral flow assay architecture	20
Figure 1.5 Typical EC components for a non-faradaic process for pathogen detection on the working electrode in an electrochemical cell.....	24
Figure 1.6 (a) Bacteria in suspension in ions rich solution (b) Antibody-Bacteria capture.....	26
Figure 1.7 (A) portrays the setup for the eLoaD where a motor generates the centrifugal force required for on-disc filtration where the LoaD	34
Figure 1.8 (A) Conceptual design of one or eight testing sites displaying each consecutive layer of the PDMS eLoaD.....	37

Chapter 2

Figure 2.1 Contact angle measurement of hydrophobic and hydrophilic surfaces.	53
Figure 2.2 Epilog Zing CO ₂ laser used for manufacture of PMMA layers.	56
Figure 2.3 Design of a DF tab, where the top layer is the dissolvable film and the secondary Section is the PSA ring for liquid passage and adhesion of DF tab to underlying PMMA layer.	58
Figure 2.4 Micro-contact printing process.....	66
Figure 2.5 (a) PSA layer placed on alignment rig with protective plastic removed with pre-cleaned PMMA layer. (b) Alignment pins inserted through PSA layer with PMMA now attached.....	67
Figure 2.6 Portrays the basic composition of a microfluidic platform.....	68
Figure 2.7 The forces experienced on a centrifugal platform affecting flow.....	69
Figure 2.8 The forces acting upon centrifugally propelled particle in a fluid.....	71
Figure 2.9: Centrifugo-Pneumatic DF valving. A) Demonstrates the structural design and size of a DF valve.	74
Figure 2.10 Definition of the position of the fluid plug on a centrifugal system.....	76
Figure 2.11 Operating features of spin-stand instrument for testing a centrifugal testing platform.	79
Figure 2.12 Figure representing the real and imaginary vectors of the impedance modulus where φ portrays the phase angle which is formed by the mis-alignment.....	82
Figure 2.13 (a) portrays each individual element in which the Randles circuit is composed of and (b) how these individual components exist within the Nyquist plot.	83
Figure 2.14 Description of the basic PCR process.....	87
Figure 2.15 RPA process of amplification using the forward and reverse primers, recombinase proteins, recombinase primer and ATP recombinase.	89

Chapter 3

Figure 3.1. Assay requirements for automated device capable of capturing and detecting pathogens with implemented biosensor	96
---	----

Figure 3.2. (a) represents the 3D model constructed using SolidWorks, 2017 software and (b) is the real-life rapid-prototyped eLoaD device.....	102
Figure 3.3. Main reservoirs within eLoaD device where.....	103
Figure 3.4. Representation of the ELoaD assay	104
Figure 3.5 Portrays V. 1.0 of the ELoaD device design where (a) portrays the CAD drawing of the centrifugal platform with corresponding legend to further detail each component and (b) represents the electrode configuration of the sensing platform.	106
Figure 3.6. Schematic of deposited Au electrode with antibody activated cites through L-cysteine structures.	108
Figure 3.7. New electrode configuration for V2.1 device with ITO reference electrode and pre-cut Au coated Si wafer slides are utilised for the working and counter electrodes.	109
Figure 3.8. Details the additional layer inserted into V. 2.2.	111
Figure 3.9. The 9-layer device modelled off V2.1 with the additional layer-8 dubbed the “electrode cover” which has dual functionality	112
Figure 3.10. Version 3.1 of the full optimisation of the device, indicating the areas of re-design interest with a corresponding image acquired.....	115
Figure 3.11. CAD drawing of V. 3.2 of the device with the removed DF tab overflow system removed to reduce error for valving actuation.	116
Figure 3.12. (A) Contamination of counter and reference electrode (B) Additional PSA in the V. 3.3 sloped detection chamber for blood component capture to reduce non-specific binding on the sensor surfaces	117
Figure 3.13. A direct comparison of version 1 of the ELoaD device	120
Figure 3.14. A display of the reservoirs, chambers and exit channels labelled using the above legend as a reference guide to describe the two separate DF tab components implemented into the eLoaD device.....	122
Figure 3.15. Graph representing the relationship between the spin frequency and the mean radial position of the pneumatic chamber and DF tab.....	124
Figure 3.16. Dual graph portraying the linear relationship between the burst frequency (Hz) of the tab with comparison to the pneumatic chamber (mm ³) for the two tab positions on the platform.....	125
Figure 3.17. Images showing device’s microchannel and waste channels of varying widths are testing with healthy whole blood samples.....	128
Figure 3.18. Demonstrates the whole blood flow patterns between each chamber. (A) Initial loading of blood to sample chamber.....	129
Figure 3.19. Interferometer measurement of straight cut channel in PSA to determine the smoothness of the cut using the microblade in the GraphTec.....	130
Figure 3.20. Confocal images of Au electrodes post testing with sample D017-01, a gram-positive type sample	133
Figure 3.21. Confocal images of a healthy whole blood sample passed through the platform with a 7 minute incubation time where the device was a) not functionalised with fibrinogen and b) functionalised with fibrinogen.	135
Figure 3.22. Confocal images acquired from all three working electrodes per testing site to determine optimum spin-frequency parameters.....	142
Figure 3.23. The surface wettability of four separate substrates where the water contact angle was measured with ImageJ.	144
Figure 3.24. Stepwise development of the 2 nd generation device	147

Chapter 4

Figure 4.1. Typical 3-electrode cell configuration with a counter, reference and working electrode where (b) portrays the working electrode where the Au modifiable surface is shown.....	159
Figure 4.2. Stepwise process in which a planar gold surface is modified to be an antibody capture surface	161
Figure 4.3. CV of planar gold surface of a typical working electrode in 0.1 M sulphuric acid showing both the reduction and oxidation peak.....	162
Figure 4.4. Cyclic voltammograms of the three separate stages of biosensor fabrication using a gram-negative endotoxin IgG antibody	163
Figure 4.5 Schematic representation of the capacitance of the biosensor.....	165
Figure 4.6 EIS plots for the Au WE electrode immersed in 1mM DPBS solution run at OCP from 0.1 - 100,000Hz against an Ag/AgCl RE.....	169
Figure 4.7. (a) Nyquist plot of gram-negative immobilised antibody for 7 separate electrodes.....	170
Figure 4.8. Image of initial photolithographic mask used to create an array of square structures in which a labelled antibody is printed onto glass	172
Figure 4.9. Average cyclic voltammograms of the disposable gold electrodes where the separate stages of biosensor fabrication were recorded.....	174
Figure 4.10. BSA patterned surface portraying the PDMS μ -contact print stamp pattern and	175
Figure 4.11. EIS plots for the disposable electrode immersed in 1mM DPBS solution run at OCP from 0.1 - 100,000Hz against an Ag/AgCl RE	176
Figure 4.12. EIS response for the three separate functionalised electrodes where the Nyquist, Bode and Phase plots are shown	180
Figure 4.13. Nyquist and Bode plots of the eLoaD response of the difference between the GP, GN and Fungal antibody/fungal protein capture surfaces.....	182
Figure 4.14. Nyquist and Bode plots for all three working electrodes associated with a negative blood culture sample with supporting confocal images.	188
Figure 4.15. EIS results obtained for a gram-positive sepsis confirmed patient sample tested using the eLoaD.....	190
Figure 4.16. Graphical representation of all positive GP samples where the change in the Nyquist impedance value was plotted against the % surface coverage on electrodes. .	191
Figure 4.17. EIS results obtained for a gram-negative sepsis confirmed patient sample tested using the eLoaD device displaying the corresponding Nyquist	193
Figure 4.18. Graphical representation of all positive GN samples where the change in the Nyquist impedance value was plotted against the % surface coverage on electrodes. .	194
Figure 4.19. EIS results obtained for a GP and GN s confirmed patient sample tested using the eLoaD device displaying the corresponding Nyquist, Bode and Confocal images. ...	196
Figure 4.20. Image of GP electrode for patient sample 426115.18 to prove that the positive result obtained for the GP electrode	199
Figure 4.21. Graphical representation of all samples used in the St. James' Hospital validation study, where the change in the Nyquist impedance	200

Chapter 5

Figure 5.1 Recombinase polymerase amplification stepwise process.....	213
---	-----

Figure 5.2. Binding ability of streptavidin and biotin creating a SA-biotin complex, required for detection of analytes in ELONAs	217
Figure 5.3. Components of the ELONA test carried out for the detection of E. coli cells where TMB is used to determine the presence, and concentration, of the analyte present.	218
Figure 5.4. Bar chart indicating the optimum capture aptamer concentration based on the optical density of the ELONA assay against 10^4 E. coli cells.	219
Figure 5.5. Displays the decreasing optical density (OD) vs. Log of E. coli where the OD of each well was then obtained using a plate reader set to 450nm wavelength.	221
Figure 5.6. Graphical representation for the 1:100 dilution of e. coli incubated with 1000nM and 100nM reporter aptamer.....	225
Figure 5.7. PCR of eluted reporter probe for a reducing reporter aptamer concentration incubated against 10^4 cells for 30(red) and 25(yellow) cycles.....	229
Figure 5.8. PCR pilot study to determine optimum cycle conditions for eluted reporter aptamer for 5, 10, 15 and 20 cycles.	230
Figure 5.9. Gel image represents the amplicons and primers produced from 17 PCR cycles where there is a clear reduction in band intensity from lane 1 to 8.	231
Figure 5.10. Difference in amplification for ECO3R unmodified reporter.....	232
Figure 5.11. (A) Five PCR gel electrophoresis images for each concentration of reporter probes incubated against a dynamic range of E. coli cells ($10^8 - 1$ CFU/ 50 μ l).	236
Figure 5.12. Effect of incubation times for the amplification of RPA amplicons, where under-amplification is observed for 10 minutes	238
Figure 5.13. (A) Five RPA gel electrophoresis images for each concentration of reporter probes incubated against a dynamic range of E. coli cells ($10^8 - 1$ CFU/ 50 μ l)	240
Figure 5.14. Two gel images where two separate salt solutions were used to elute the reporter probe from a reducing concentration of E. coli cells.	242

Chapter 6

Figure 6.1. (a) CAD drawing of base for the SPEs where the design is cut into a PSA layer where each rectangular shape represents each of the electrodes	252
Figure 6.2. EIS nyquist and bode plots of the functionalised screen-printed carbon electrodes for GP, GN and Fungal surface.....	254
Figure 6.3. (a) Portrays the PCB electrode base acquired from PCBway	258
Figure 6.4. Comparison of four separate PCB electrodes manufactured by Mint Tek (Ireland) stamped with GP antibody solution.....	260
Figure 6.5. Two LFAs utilised for the capture and detection of E. coli cells/E. coli RPA products where 1. portrays the test line and 2. denotes the control line.	262
Figure 6.6. UV spectra of the functionalised AuNPs compared against naked AuNPs where MilliQ water was used as a control base line.	263
Figure 6.7. Functionalised AuNPs run in agarose gel to determine bound DNA where (a) portrays the UV transilluminator image.....	264
Figure 6.8. LFA where each test strip number corresponds to the sample described in Table 6.3.	267

List of Abbreviations

AB	Antibody
ABS	Acrylonitrile butadiene styrene
Ag/AgCl	Silver/ Silver Chloride
Au	Gold
AuNP	Gold Nanoparticle
BHI	Brain-Heart Infusion
BSA	Bovine Serum Albumin
BSI	Blood stream infection
CAD	Computer Aided Design
CAM	Contact angle measurements
CCD	Charged coupled device
C_{dl}	Double layer capacitance
CE	Counter Electrode
CFU	Colony forming unit
CLSM	Confocal Laser Scanning Microscopy
CRP	C-reactive protein
CV	Cyclic Voltammetry
DF	Dissolvable film
DI	Deionised
DNA	Deoxyribonucleic acid
DPBS	Dulbecco's Phosphate Buffered Solution
EC	Equivalent circuit
EDC	1-ethyl-3-[3-dimethylaminopropyl] carbodiimide hydrochloride

ED	Emergency department
EIS	Electrochemical Impedance Spectroscopy
ELISA	Enzyme linked immunosorbent assay
ELONA	Enzyme linked oligonucleotide assay
EtOH	Ethanol
FET	Field-effect transistors
GC	Genome copies
GN	Gram Negative
GP	Gram Positive
HRP	Horseradish Peroxide
H ₂ O	Water
ICU	Intensive care unit
ITO	Indium Tin Oxide
IVD	In-Vitro Diagnostics
LAMP	Loop Mediated Isothermal Amplification
LB	Lysogeny Broth
LF	Lateral flow
LFA	Lateral flow assays
LoaD	Lab-on-a-disc
LOC	Lab-on-a-chip
LOD	Limit of detection
mAb	Monoclonal Antibody
MHDA	Mercaptohexadecanoic acid
MRP	Mean radial position
MRSA	Methicillin-resistant staphylococcus aureus
NA	Nucleic Acid

NHS	N-hydroxy succinimide
OCP	Open circuit potential
OD	Optical density
OH	Oxidation and hydroxylation
OMP	Outer membrane proteins
pAb	Polyclonal Antibody
PBS	Phosphate buffer saline
PCB	Printed circuit boards
PCR	Polymerase Chain Reaction
pI	Isoelectric point
PI	Propidium iodide
PMMA	Poly methyl methacrylate
POC	Point-of-care
PSA	Pressure Sensitive Adhesive
RBC	Red blood cell
RPA	Recombinase polymerase amplification
R_{sol}	Resistivity of solution
SA	Streptavidin
SAM	Self-assembled monolayer
sccm	Standard cubic centimetres per minute
SIRS	Systemic Inflammatory Response Syndrome
SLM	Supported liquid membrane
SOP	Standard operating procedures
SPE	Screen printed electrode
SPR	Surface Plasmon Resonance
SS	Sepsis Six

ssDNA	Single stranded DNA
SWV	Square wave voltammetry
TBE	Tris/Borate/EDTA
VCV	Vacuum/Compression Valving
VNCC	Viable but non-cultural cells
WB	Whole blood
WBC	White blood cells
WE	Working electrode
WHO	World Health Organisation
Z	Impedance
μCP	Micro contact printing

Nomenclature

Symbol	Description	Units
$\Phi(t)$	Phase shift	$^{\circ}$
f	Frequency	s^{-1}
N	Newton	$kg \cdot m \cdot s^{-2}$
J	Joule	$kg \cdot m^2 \cdot s^{-2}$
V	Voltage	J/C
I	Current	Cs^{-1}
Z(t)	Impedance as a function of time	Ω : $kg \cdot m^2 \cdot s^{-3} \cdot A^{-2}$
Z'	Real impedance	Ω
Z''	Imaginary impedance	Ω
t	Time	s
R	Resistance	Ω
R _{sol}	Solution resistance	Ω
R _{ct}	Charge transfer resistance	Ω
R _{surf}	Surface resistance	Ω
C	Capacitance	F: $A^2 s^4 kg^{-1} m^{-2}$
C _{dl}	Double layer capacitance	F
C _{SAM}	Self-assembled monolayer capacitance	F
Re	Reynolds number	Ratio
ρ	Fluid density	kg/m^3
D _h	Hydrodynamic diameter	m, mm or μm
η	Viscosity	Pa.s
P _{atm}	Pressure	$kg/(m \cdot s^2)$
V	Volume	μl
ω	Angular frequency	s^{-1}
r	Radius	m or cm
θ	Theta (Angle)	$^{\circ}$
m	Mass	Kg
D	Diffusion	cm^2
x	Distance	m or mm

Acknowledgements

Firstly, I would like to thank my supervisor Professor Robert Forster. Your infectious optimism has been the driving force behind this work. Your incredible knowledge and passion for science have always been inspirational and I thank you for all the support and amazing opportunities over the years. I have learned so much from our discussions and will never look at a scene the same again!

Secondly, I would like to thank my colleagues past and present. Loanda and Fionn, I cannot tell you how much fun I've had with you both. The new dream team of the RFRG, do me proud! Monty, I have missed our tricking about the labs. You never failed to make me laugh. Sam, Bincy, Dave, Elaine, Kellie and Hazel thank you all for your help throughout the years. To all the technical staff in the NRF and School of Chemistry. You have always been so helpful and such a laugh. Dave Kinahan, your support has always meant the world to me. You've seen me throughout so many milestones here in DCU and you are to thank for all that. To all my amazing hons; Chris (aul sahn), pint man Steve, Jack, Bríona, Danielle, Phil and Ivan my days in DCU would have been so dull without you all! Niamh K, you have always been my biggest supporter! Who would have thought that we both would end up a PhD! I'm so proud of you. Best of luck with everything, you deserve the best of anything life has to offer. I am so grateful to have met such amazing people throughout my time in DCU. A special shout out goes to Sinéad. You have been such a massive support this year, I am so grateful for our carry on. You are such a bundle of joy and have always brightened up my days. I would also like to thank Princess Daz. You have been such an amazing friend. I will always value your extreme honesty and support. I can't believe we made it out alive! Ais, you mean the absolute world to me. If ever there was someone who would pick me up, motivate me, let me rant, give me advice, you were the one I could always rely on. I could not have done this without you. Thank you for everything. You are an absolute superstar!

To all my amazing Carlow hons! You have always been, and always will be, the best bunch of girls and I am so lucky to have you in my life. Anno, Ellis, Sinéad, Niamh, Ró, Shauna and Ciara. You all mean the world to me. Kate and Helen, we were the dream-team of Carberry

Road. Thanks for all the laughs after a long day in the lab! My slayage hons Cat and Arlene, I adore you both. Thank you for the endless support. Your optimism, support and overall savageness has really picked me up when I needed it the most. You are so special to me and I hope you know that! Reilly, thanks for always being such an amazing friend all these years, despite making a show of me all the time.

Cathy. I can't honestly express to you how grateful I am of our friendship. I am so proud of you and how far you've come. I love you so much. You have been a pillar of support throughout this entire process. You have always been there through the good and bad times and I could not have done this without you. We've come a long way since our summer of galivanting!

Chris. My oldest and boldest friend in the whole world. Thank you for the laughs, the outrageous stories, endless entertainment, constant encouragement and the occasional slap on the wrist. I hope I have done you proud as you have me. You are the most amazing person and I really am so lucky to call you my best friend.

I would like to also express my gratitude to you, Jack. Thank you for being so understanding. You have always been so patient with me throughout this journey. You've been a fantastic partner in crime, and long may our adventures continue. Thank you for everything!

Finally, I would like to extend a momentous thank you to my family. You have shown me how to be strong, resilient, and courageous. We have all come such a long way and I couldn't have done this without you. Your help throughout the years has meant so much to me. I love you all. Conor, Dan, Mum and Dad; this is for you. Us Carthys are capable of achieving anything we put our minds to, and hopefully this thesis will be a reminder of that.

*“This thesis is dedicated to my family, with love. Thank you for your
endless support and encouragement.”*

*“To learn, one must be humble. But
life is the great teacher”*

- James Joyce

Abstract

The development of rapid pathogenic detection continues to be at the forefront of the greatest challenges of our clinical settings to date. Sepsis is a serious systematic inflammatory response which is triggered by bacterial, viral, or fungal infections. It persists to be a primary cause of patient death despite the medical advances made in therapeutics and antibiotics development. The non-specific symptoms of sepsis are the utmost limitation of diagnosis of the condition. Delays in detection therefore leads to an increase in patient mortality. Current gold standards within microbiology laboratories are too slow, therefore a huge demand exists for a reliable method for early stage detection of sepsis. In this work, the development of biosensors and point-of-care systems for use with electrochemical, centrifugal lab-on-a-disc, Enzyme Linked Oligonucleotide Assay (ELONA), Polymerase Chain Reaction (PCR) and Recombinase Polymerase Amplification (RPA) techniques are demonstrated.

A novel integrated point-of-care LoD system has allowed a real-life application of the sensors to be studied for hospital samples. This innovative system allows pre-loading of reagents and samples which are systematically triggered using spin-frequencies where EIS techniques are adopted to give a sample to answer in under 15 minutes. These devices are single use, therefore are ideal for quick, infectious sample testing. A full optimisation of the device was required as fluid manipulation of various samples is a key-feature where samples ranging from buffer to whole blood can be tested within the same device without the need for sample pre-treatment.

A label-free electrochemical biosensor, capable of capture and detection of pathogens, was produced by using a self-assembled monolayer and antibody capture layer was fabricated and characterised to compare with the single use biosensor developed for this work. Real-cultured samples from a microbiological clinic were studied to determine the capabilities of the device for real point-of-care settings. The device, which is capable of detecting the presence of pathogens, and furthermore the category in which they lie in, has proved to be an exciting and critical step-forward in early stage sepsis detection. Further analysis allowed a specific threshold to be determined, where a change in 300

Ohms to the system signifies the presence of a pathogen on the capture surface due to changes in the interfacial capacitance of the biosensor. Using confocal microscopy, the surface coverage of the captured pathogens was determined, where a directly proportional relationship exists between the number of pathogens captured and the change in the impedance response. This highly novel system is unlike any other commercially available technology for pathogen detection.

Other methods have been explored, such as ELONA and DNA amplification. With very low detection limits of 23 CFU/ml for the ELONA, 5 CFU/ml for the PCR assay and finally 9 CFU/ml for the RPA assay. With varying assay times of 195-103 minutes, the assays were highly capable of detecting extremely low counts of E. coli in clean buffer samples. Although laborious they have also been proved to be able to detect specific E. coli pathogens which may lead the way for the development of a secondary analysis tool to specifically identify the causative pathogen for a highly precise diagnosis for patients.

Chapter 1

*Literature Review and Thesis
Objective*

1.1 Introduction

The need for the detection of pathogens is increasing with the demands of our evolving society. Advancements made with surgical procedures, mass production of food and beverages, water treatment plants, air quality, and bioprocessing fall victim to the contamination of harmful bacteria [1]. The current annual cost of pathogenic bacterial presence within the United States' food industry is an estimated \$6.5 - \$34.9 billion, with seven foodborne pathogens (*Escherichia coli*, *Campylobacter*, *Listeria monocytogenes*, *Clostridium perfringens*, *Salmonella*, *Staphylococcus aureus*, and *Toxoplasma gondii*) causing the majority of the costs of spoilage. These pathogens are also causing an estimated 3.2 – 12.3 million foodborne related illnesses and up to 3900 deaths within the US alone [2].

According to the World Health Organisation (WHO) sepsis is defined as the condition in which the body's response to an infection causes injuries to its own tissues and organs which may potentially lead to significant morbidity or death, where the majority of sepsis cases are caused by microbes [3]. It is estimated that more than 19 million people suffer from sepsis, with a reported 5 million sepsis-related deaths occur annually [4]. Sepsis was previously referred to as septicaemia, however these conditions are not the same. Septicaemia, or blood poisoning, is a condition which occurs when a bacterial infection within the body enters the blood stream where it can be displaced around the system. Sepsis is a serious complication that arises from a blood stream infection (BSI), as inflammation is a primary indication of the progressed condition. Sepsis, although primarily caused by bacteria, is also caused by fungal and viral infections [5] [6]. The exaggerated immune response can cause high blood pressure, severe high/low body temperature and dilated blood vessels, which promotes the spreading of pathogens throughout different organ systems. More severe septic shock can impair blood flow to vital organs, causing them to fail, and can create blood clots within organs and limbs leading to tissue death, known as gangrene [7]. The rate in which sepsis can cause severe complications demands a biosensor with a short analysis time. This is especially important for the shortened diagnosis and treatment time of the affected patient. This is especially important for improving patient outcome and containment of the pathogen(s).

The current standard detection methods, although accurate, can take days for a result to be obtained [8]. This involves the lengthy process of culture and agar plating bacteria to determine the growth and identification of the strains [9]. Furthermore, these conventional methods require high cost equipment. The combination of these problems portrays the strong needs for low-cost biosensors, capable of detecting deadly, disease-causing pathogens in a rapid and cost-effective manner [10]. Biosensors are integrated devices capable of analytical biological sensing of various cells, antibodies, DNA, RNA and enzymes in real time. They are capable of offering a variety of features such as high selectivity at low concentrations of the specific biomarkers and biomolecules delivering fast and accurate results, which are essential for diagnostics in clinical settings [11]. The increasing need for pathogen biosensors is evident, in that sepsis mortality rates globally reflect the huge demand for rapid, highly sensitive biosensors [12]. It's prevalent in recent years the true surge in antibiotic resistant bacteria through the over-prescriptions of drugs in an effort to reduce outbreaks of disease amongst livestock and to slow down the progression of microbial infections, before the pathogen is identified [13]. Monitoring of bio-samples for early pathogen detection can significantly reduce the over-use of antibiotics in livestock and patients, which in turn will have a knock on effect to reduce the rate in which anti-microbial resistant strains of pathogens develop [14].

The rapid growth of bacteria means that even low numbers of these disease-causing cells (<10 cells/ml) is deemed to be at a dangerous level and can lead to fatal deterioration of one's health [15]. Due to this, a pathogen biosensor must adhere to and offer a specific set of attributes capable of detecting and identifying these cells. Firstly, the biosensor must be capable of highly sensitive detection of low pathogen concentrations [16]. The rapid detection of these cells is also indispensable.

A biosensor must not be restricted to the identification of single strains of pathogens. Simultaneous detection of several types of pathogens is critical when dealing with patients suffering with sepsis. Sensors should display high specificity when targeting particular cells to allow for rapid, accurate treatment to avoid the use of broad range antibiotics within a clinical setting, as empirical broad-spectrum antibiotic administration is the current practice [17]. Finally, the sensors which portray these attributes must be able to translate the presence of the pathogen into a detectable signal. There are many

sensing methods which may be applied such as Electrochemical Impedance Spectroscopy (EIS) and Fluorescence and Surface Plasmon Resonance (SPR) [18]. According to Lazcka et al., biosensors are classified as the fourth leading method of pathogen detection, where Polymerase Chain Reaction (PCR) ranks first. Also, within the biosensor category, optical ranks first as the biosensor where electrochemical methods rank second. Nucleic Acid (NA) dependant sensing techniques often require a PCR step due to the low copy of numbers of NA's within Bacterial cells. This can often be an inhibiting factor of a biosensor, where traditional methods are relied upon for a signal-to-answer response.

The electrochemical detection based methods have become an increasingly popular choice in the development of portable biosensors utilising label-free detection methods [19]. This is an exceedingly promising technique which requires minimum user input, cost effective and has fast signal to answer response [20]. Consequently, EIS and Cyclic Voltammetry (CV) methods have been adopted to monitor analytes in real time, label free detection approaches [21].

The main objective of this body of work is the detection of disease causing microbes which may be a cause of sepsis. The fabrication of biosensors and a user friendly platform allow for a significantly reduced detection time which is pivotal for a high-impact biosensor along with bioassays with a very low detection limits with synthetic capture probes. The analytical challenge of detecting pathogens from whole blood and blood culture requires a rapid sample to answer time to allow an informed clinical decision to be made within the "golden hour". Considering that time is a critical element to the assay, label free electrochemical impedance spectroscopy was chosen as the method of detection, where changes in the interfacial capacitance caused by the binding of pathogens changes the response of the system. The user friendly, full automated LoaD also reduces assay time as all reagents and samples are loaded into the device which runs for 15 minutes, where all reagent release is due to an increase in spin frequency which triggers the dissolvable film tab system. Using Nyquist and Bode plot information, a response that exceeds a threshold will result in a positive result for pathogen detection. The non-labelling approach allows the assay time to remain short and therefore becomes highly advantageous for rapid analysis. As whole blood is an extremely complex matrix, the sensing surfaces must be highly selective towards the pathogen. By using monoclonal

antibodies, the antibody will only bind to one type of specific binding site. The intermittent sections of the antibody patterned surface also contains blocking polymers and proteins to reduce non-specific binding, where the antibodies allow the surface to be highly selective towards the analyte(s). With three biorecognition capture antibody and proteins being used, the device will also be able to discriminate between gram-positive, gram-negative and fungal pathogens, which can further inform the clinician what class of antibiotic treatment the patient may require.

Most importantly, the device and the sensing platform must be able to detect relatively low counts of pathogens in the samples ($<10^3$ CFU/ml). As low counts as pathogens are capable of triggering the sepsis response, the device must also be able to process enough sample in which pathogen would be present, but not enough that that it becomes difficult to process a large sample and keep the fluidics of the device functioning properly.

With the challenges and objectives of the platform clearly defined, the device and the testing parameters can be used as a reference point whilst designing and testing the device. Moving away from antibody usage for pathogen capture, the use of synthetic ssDNA probes is also a secondary objective of this work. These aptamers are can be highly specific towards an analyte, where E. coli cells would be captured and detected with these probes using established ELONA and DNA amplification techniques. This aspect of the project may possibly lead to a secondary testing platform where, upon a positive results from the LoAD, a sample may be tested for the specific ID of the causative pathogen against a highly specific aptamer probe.

As sepsis is a time dependent condition this system could be used to determine if:

1. The patient requires an antibiotic or another treatment plan,
2. The patient needs to undergo a sepsis treatment plan, where the antibiotic is for the treatment of Gram-Positive, Gram-Negative or Fungal microbes.
3. Measure the bacterial load to optimise the required dose of antibiotics
4. Monitor the efficiency of the provided drugs

The POC system must be as efficient, if not more so, than the current laboratory or clinic standard; whether this is a reduction in time or sample requirement. The device itself must be easy to use, where minimal training is required for its operation. A fully automated system is standard, where little or no interaction is necessary. Finally, the system must be cost effective. This is an extremely desirable attribute if the system is intended to be distributed in developing regions. These specifications for POC techniques require complex, condensed liquid handling processes which replace manual preparation of samples to simple automation which can be offered by a microfluidic system.

1.2 Sepsis and its Epidemiological Impact

According to the health service executive (HSE), 17,106 people in Ireland were diagnosed with sepsis in 2017, an increase of 13.44% from 2016, and 48.05% from 2016 [22][23] Figure 1.1. In spite of the huge advancements in antibiotic treatments and intensive care, sepsis is still a major cause of mortality in the developed world [24]. According to Nguyen et. al, 50% of all hospital based deaths are caused by an infection or sepsis [25]. The figures surrounding sepsis and its mortality rate across the globe are highly significant and continue to grow annually.

These collective conditions are one of the leading causes of emergency department (ED) and intensive care unit (ICU) admissions and represent significant morbidity and mortality rates [26], as well as a huge financial burden to that of the state and health care system. Recent epidemiological reports suggest the annual cost of patient care within a clinical setting with sepsis is \$14 billion within the USA, where the hospital cost ranges from \$22,000 and \$38,000 per patient case [27]. Databases have reported that half of these cases are admitted to the ICU, where the average length of stay is between 9 to 15 days [28]. European studies have suggested that daily hospital costs for sepsis patients range between €700 and €1033.14, depending on the severity of the case. Recent reviews suggest that 20-30% of these costs are due to drug and health care, whereas the remaining 70-80% of costs evolve from personnel costs, mainly from expensive, laborious ICU patient care [29]. Autopsies confirm that mortality rates of sepsis sufferers continue from a lack of rapid diagnostics tools capable of identifying and treating sepsis [30].

Studies have also indicated that sepsis patients who have received inappropriate antibiotic care for their blood stream infections (BSI) had a surge in hospital based mortalities to that of sepsis patients who received appropriate antimicrobial care for their pathogen based condition [31].

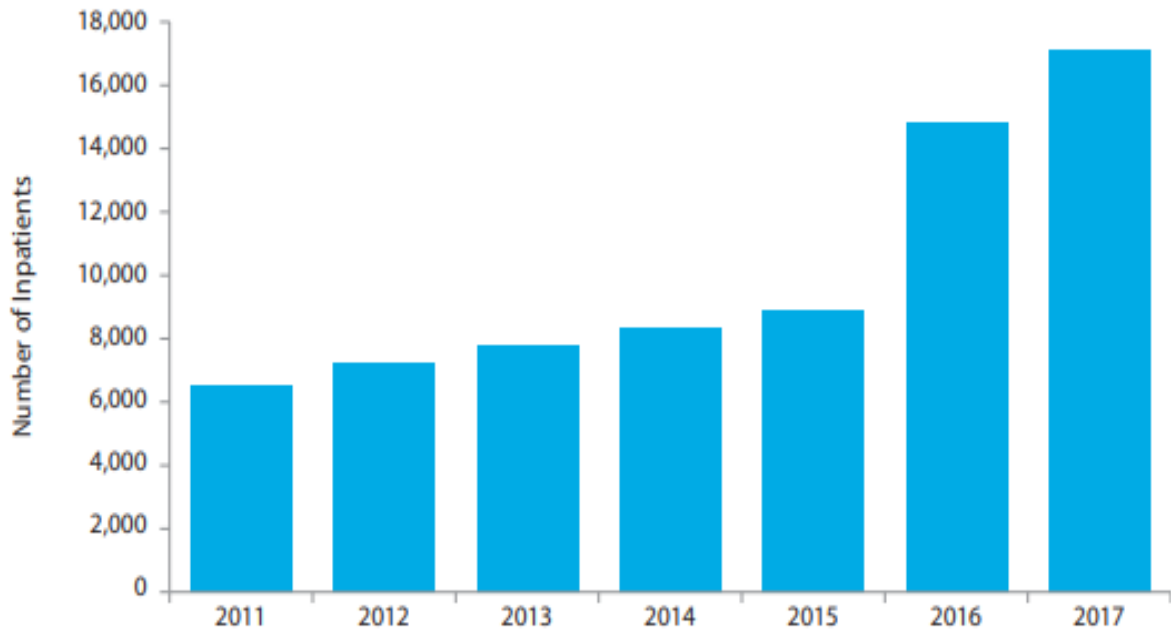


Figure 1.1 Increasing trend of number of sepsis sufferers in Irish based hospitals

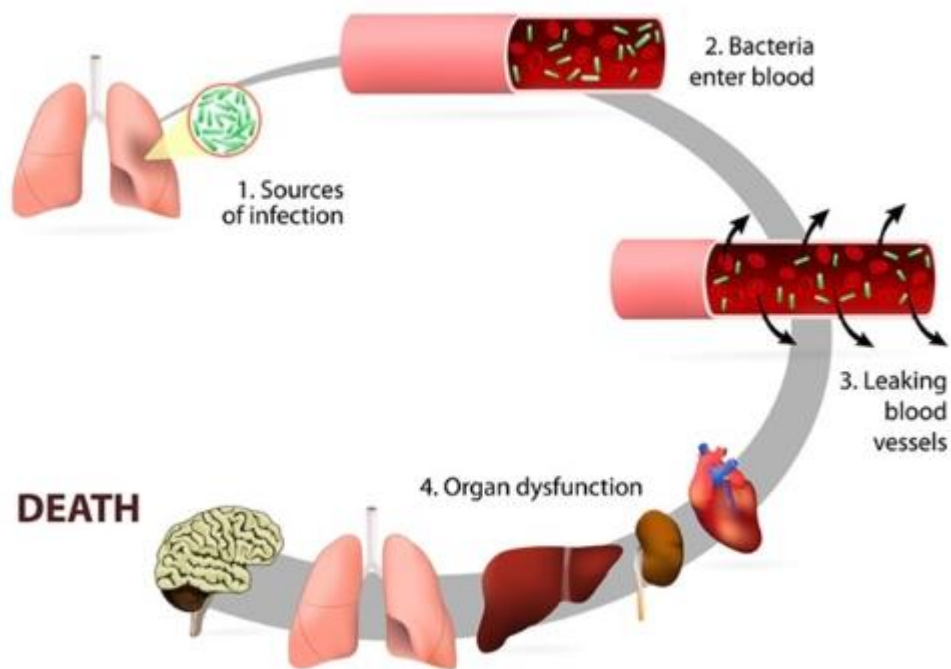


Figure 1.2. Life-cycle of sepsis/septicaemia portraying the presence of multiple pathogens causing organ malfunction [32].

The symptoms associated with the condition vary significantly between patients and appear as non-threatening. The patient suffering from sepsis may not be able to recognise the early stages of the condition, as these are very similar to that of the common flu or cold [33]. The body's ability to create compensatory mechanisms during early sepsis can conceal the severity of the symptoms, which can evolve within hours causing irreversible damage to organs [34]. The ability to recognise a patient's symptoms during the early onset of the condition allows for better patient outcomes.

These symptoms are categorised into sub-sections according to the severity of the illness. In Ireland, the current practice in place in Emergency Departments (ED) is if the patient meets two or more of the SIRS criteria (Table 1.1), the patient must undergo the "Sepsis Six" (SS) treatment plan (Table 1.2), which must be completed within the hour due to the rapid progressive nature of the disorder [17].

Table 1-1. SIRS criteria for implementation of the Sepsis Six treatment programme [22].

Infection Suspected + Any 2 or more Systemic Inflammatory Response Syndrome (SIRS) criteria	
Respiratory rate > 20 (bpm)/Hypoxia	White blood cell count <4 <u>or</u> >12 (x 10 ⁹ /L)
Heart rate > 90 (bpm)	Acutely altered mental state
Temperature <36 <u>or</u> >38.3 (°C)	Bedside glucose >7.7mmol/L

The SS criteria is displayed in Table 1.2, where it is estimated that an extra 1 in 5 septic shock patients will survive if the SS plan is implemented within the hour [35].

Table 1-2. Sepsis Six criteria for implementation within the first hour of diagnosis [36].

Sepsis Six	
Take 3	Give 3
1. Blood Culture – Take blood culture prior to administering antimicrobials unless this leads to delay > 45 mins	4. Oxygen – Range 21% to 100%. Titrate to saturations of 94%-98%, 88%-92% in chronic lung disease cases
2. Blood tests – POC lactate (venous/arterial).	1. Fluids – Range 0 – 2000mls

<p>3. Urine output – POC urinalysis and assess urine output as part of volume/perfusion status assessment. For patient with existing sepsis/septic shock, monitor hourly</p>	<p>2. Antimicrobials – Administer antimicrobials as per local antimicrobial guidelines bases on site of infection, community or healthcare associated infection and the patient’s allergy status</p>
--	--

With the current practice in place within the Irish clinical setting, sepsis-suspect patients are prescribed antimicrobials whilst a blood sample is sent to the microbiology department. These samples come back negative in over 90% of all cases, acuminating a huge waste on hospital resources and time [37]. Within the time-frame for blood cultures to be returned, antibiotics have been wrongly administered, increasing the risk of an antibiotic resistant bacterial outbreak within the hospital [38].

Rapid containment and control of infection is one of the main goals in direct sepsis therapy, as mortality rate increases by 7.8% every hour [39]. It must be noted that implemented treatment plans regarding antibiotic use differ from that of other medical regimens such as diabetes, as they can be from an abstract point of view. As medical treatment for diabetes is limited to a specific care package per patient and will have no impact on others, antibiotic therapies may induce specific pressure on bacterium which may develop antibiotic resistant strains, which may put the entire hospital population at risk [40]. As the catalogue of resistant strains of bacteria increases, the ICU is challenged to treat the microbial infection with an accurate antibiotic treatment plan in order to reduce the detrimental effects of sepsis and septic shock, reduce mortality rates within the clinical setting, save time with a treatment plan, reduce the use of broad-spectrum antibiotics, and not endanger future care-plans for other patients [41].

Due to a severe delay of up to several days regarding pathogen information and antibiotic susceptibility to the clinician, present practice mandates a “blind” course of antibiotic treatments, based on the knowledge and experience of the acting physician, the site of infection if known, and known resistance pattern emerging from that specific hospital [42]. The current challenge is to rapidly inform the physician of the pathogen ID, so the correct adjustments of the therapy plan may be implemented.

1.3. Methods of Pathogen Detection

A variety of techniques can be applied for the detection of harmful pathogens, such as blood culture methods, PCR, ELISA assays and electrochemical detection techniques [43]. In the majority of cases of infection, rapid test analysis is a priority. In sepsis management, the critical time for appropriate antibiotic treatment is determined to be less than 6 hours according to the “surviving sepsis campaign” [17]. The patient’s survival is reported to be linearly correlated to time of appropriate antibiotic care [44]. This time-frame is commonly referred to as “the golden hours” of sepsis care [45].

1.3.1 Blood Culture Techniques

Micro-organism identification within the microbiology lab has profoundly altered with the routine ID of pathogens using Matrix-Assisted Laser Desorption Ionization Time-of-Flight Mass Spectrometry (MALDI-TOF MS) [46] [47]. Yeast and bacterial ID is possible with this technique and is adopted within microbiology labs which eradicates time-consuming subculture routines and unseeing phenotypic ID methods [48]. This process involves mixing the sample with a matrix and applied to a metal plate where a pulsing laser triggers ablation and desorption of both the sample and matrix. The analyte molecules are then ionised and accelerated into a mass spectrometer for analysis. [48].

Existing sepsis management guidelines state that for optimum ID of causative microorganisms, two sets of blood cultures must be obtained, in aerobic and anaerobic culture bottles, before therapy with “*at least one drawn percutaneously and one drawn through each vascular access device, unless the device was recently (<48h) inserted*” [41]. Despite only 30% of sepsis blood cultures becoming positive [49]. The turn-around time for a positive result depends on a variety of factors, such as the volume of patient’s blood taken, type of pathogen, chemistry of blood culture bottle, the time taken for the blood culture bottle to reach the incubator, the previous treatment of the patient before the sample was taken and the growth capacity of the present pathogen. The average time for a positive result is about 15 hours, however some samples may return an answer in 4 hours whereas some may take several days [50].

The quantity of pathogens in a blood stream infection ranges from 1 to 10 colony forming unit (CFU)/ml to 1×10^3 and 1×10^4 CFU/ml. [51]. The volume of sample acquired from a patient ranges from 40-80mL to be capable of detecting the microbial agent in 80-96% of cases [52]. These culture bottles include BD BACTEC (BD Diagnostics, Franklin Lakes, NJ, USA) and BacT/ALERT 3D (bioMérieux, Durham, NC, USA). These standard collection bottles have been designed for the growth of aerobic/anaerobic bacterial types. Each is designed to accommodate 10mL of samples however paediatric samples have been modified to hold <3mL of patient sample, due to the difficulty in obtaining a large volume of blood. Antibiotics which are administered prior to blood sampling are neutralised within the bottle due to the presence of resins and charcoal. The recovery and growth of microbes that have undergone endocytosis by phagocytes is promoted due to the presence of lytic agents within the growth media. Typical turn-around incubation periods last for 5 days for the recovery of bulk of microbes, including known HACEK (Haemophilus, Aggregatibacter, Cardiobacterium, Eikenella and Kingella Bacterium) fastidious bacteria group.

Slow growing microbes such as the Mycobacteria species and fungi will require longer incubation times. Automated incubators monitor the presence of positive microbial samples by detecting CO₂ production from growing organisms. The presence of CO₂ will alter pH levels which are detected by colour change, red-ox variations and fluorescence signal. Up to one-third of positive culture bottles are a result of contamination which occurs from micro-organisms which are not present in the blood. These microbes are introduced into the broth bottle during sample collection. Skin flora organisms, such as Coagulase negative Staphylococci, may cause a false positive result, even when samples are drawn under aseptic condition [53]. Contamination rates are interestingly linked with the patient's blood access point is drawn from, whether peripheral venepuncture (36%), central venous access (10%) or arterial accesses (7%) [54].

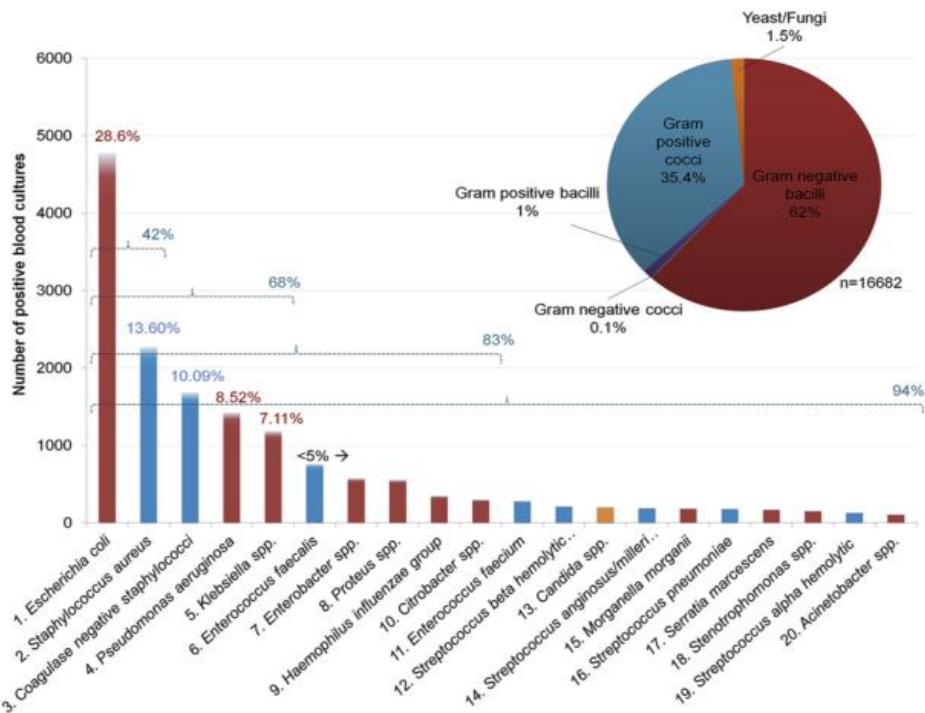


Figure 1.1. Top 20 microbes identified from positive blood culture bottles during a 1 year period within a 1000 bed university hospital during 2013 [58].

Once a positive blood-culture is acquired, a gram-staining procedure is carried out using a blood-culture aliquot. This is an essential step in order to confirm the presence of bacteria/fungi within the sample. From here, the morphology of the microbe may indicate the aetiology of the infection source. Specific ID is acquired directly from the positive blood culture broth bottles, using various methodologies such as (a) ID from a subculture, (b) nucleic acid based microarrays directly from a positive blood culture, and (c) post bacterial enrichment and purification for a bacterial pellet, which may be used in conjunction with matrix-assisted laser desorption ionisation time-of-flight mass spectrometry (MALDI-TOF_MS). A variety of influencing factors may portray the significance of a positive blood culture, such as the number of positive bottles, site of sampling, time difference between positive sampling between drawing times and sites [55]. Opota *et. al* have identified the top 20 microorganisms which are identified from positive blood culture during 2013, adapted from a total of 16,682 samples were tested and have quantified the common microbes per morphotype as shown in Figure 1.3 [56]. Blood culture techniques have been the gold standard for microbe testing, but results can take up to 5 days, depending on the initial concentration of pathogen within the sample,

and are rarely performed outside a laboratory setting [57]. However, this mainstream laboratory approach lacks and is highly impaired by the delay in the time to result for certain pathogens [48]. With the current gold standard lacking a quick sample to answer time, alternative methods of pathogen detection will be explored and compared with the proposed electrochemical centrifugal platform described in the main objective in Section 1.1.

1.3.2 Polymerase Chain Reaction Amplification Detection

Polymerase Chain Reaction (PCR) is a simple enzymatic assay which allows for the specific target and amplification of a DNA strand [59]. This technique can be performed using DNA from a variety of sources, such as blood, saliva, urine and microbes. The concentrations of DNA from the source needed for basic PCR methods is: Bacterial DNA – 1pg, Fungal DNA 10ng, Plasmid DNA – 1pg and mammalian DNA – 1ug [60]. These masses are adequate to produce enough copies for analysis, deeming PCR to be a sensitive assay. It is reported that the lower limit to achieve this DNA concentration is 20 cells for bacteria [61]. PCR provides multiple advantages for bacterial detection.

This molecular method is faster than the typical blood culture routine adopted by clinicians as they are culture independent reducing the detection times to hours rather than days. PCR methods are capable of providing a specific ID during the time to positivity, reducing a need for further analysis. Despite PCR being a valuable, sensitive technique, its sensitivity can be a hindrance. Any form of contamination from trace amount of DNA can provide misleading results, therefore, incorrect diagnosis of the patient [63]. The design for PCR primers relies on previous knowledge of the sequence is required, where two types of primers can be used (forward and reverse). Therefore, this technique can only distinguish the presence or absence of a known gene or pathogen.

For this form of NA testing, the amount of genome copies (GC) present within the sample is of more importance than the CFU. The GC also includes that of the DNA recovered from **dead** bacterial cells and pathogens engorged by phagocytes. With results obtained from PCR and electrospray ionisation mass spectroscopy (ESI-MS) it's estimated that during a typical bloodstream infection (BSI), there are approximately 10^3 and 10^4 GC/mL present,

which exceeds the bacteria DNS load above the limit of detection (LOD) of most PCR methods, compared to the typical 1-10 CFU/mL from whole bacterial cell used for blood culture [65]. A limiting factor of whole blood processing is the quantifiable amounts of human DNA which inhibit probes and primers during a PCR reaction. The removal of white blood cells (WBCs) before DNA extraction will reduce the concentration of human DNA. Using methods which are specifically designed to degrade or remove this interfering DNA after the extraction of NAs has also been proven to reduce the risk of false results [66]. In some cases, a simple dilution of whole blood can resolve the interfering components, however some well-known PCR inhibitors, such as immunoglobins, iron and heparin should be completely removed before PCR is ran. Iron, sourced from haemoglobin, the pigment associated with erythrocytes, and lactoferrin from leucocytes are well-known PCR inhibitors as they specifically obstruct DNA synthesis [67].

Despite these limiting factors associated with whole blood processing using PCR techniques, working with this sample type has proven to be advantageous when reducing the time to results. This type of microbe detection is independent of blood culture enrichment. The time taken for positivity of a blood culture test can vary hugely; 8hours (for rapid-growth type bacteria), to several days (slow growing microbes such as fungi). PCR methods allow for microbe ID which is culture independent, unlike the majority of phenotypic techniques. SeptiFast carried out a study on 78 nosocomial sepsis cases where the rates of microorganism detection by blood culture and PCR were 34.2% and 47.9% [68]. The rapid analysis time allows for a superior insight of what is happening in the bloodstream during an infection, allowing for close monitoring of the patient's condition [58]. The reduced LOD of specific PCR makes the method more sensitive than blood culture, however this attribute is largely counterbalanced by the low sample input required.

PCR methods are highly unaffected to previous antibiotic treatment a patient may have received during a symptomatic BSI. Quantitative real-time PCR (qPCR) may aid the clinician in interpreting positive results, as contamination is characterised by low amounts of microbes. As bacteraemia is often regarded as a paucibacterial infection (low CFU), the data collected for quantitative analysis is useful when high bacterial presence is documented. This method is also applicable in the event of poly-microbial infections, as

it will allow for the relative quantities of each pathogen to be determined. The levels of bacteria established from a PCR test may also indicate the severity of infection which may be a useful indication of the level of treatment required. The measure of GC/mL is a useful diagnostic method to monitor the levels of infection post antibiotic treatment [69].

The method of qPCR, also known as real-time PCR, attains the ability for continuous monitoring of product formation throughout the reaction. This method supplies the user with simultaneous, rapid amplification and specific sequence-based detection. A major benefit of qPCR is that the product requires no further amplification and also disregard imaging detection such as gel electrophoresis, which significantly reduces the analytic time-period [70]. The LightCycler SeptiFast (Roche Molecular System, Switzerland) is an automated system capable of identifying 19 pathogens; 6 Gram-Positive bacteria, 8 Gram-Negative bacteria, and 5 fungi. A sample size of 1.5 mL of whole blood is required and a time to positivity is obtained within 8 hours. The target pathogenic DNA is amplified using broad-range PCRs. The ID at species level is delivered by analysis of the melting curves of the specific probe strands. The relatively short result time is the main advantage of the SeptiFast PCR system compared to the blood culture methods.

SeptiFast offers good clinical sensitivity, as low as 3-30 CFU/mL for bacteria and 100 CFU/mL for fungal microbes [71], [72]. The true positive rate however has a broad range between 43-95% with a varying selectivity of 60-100% [73]. This may be a result of the selected patient pool acquired for the study. Blood culture methods and Septifast are complementary as they correlate rates of 43 – 83%. Other molecular-based diagnostic methods from whole blood only exhibit a limited correlation with the gold-standard blood culture for microbe ID. Therefore, these PCR methods are not intended to replace culture methods but are complementary to this type of diagnosis. SeptiFast performs a semi-quantitative analysis rather than complete qPCR. Cut-offs used for the interpretation of the potential contaminants may lead to false negative results [73]. As the test is only capable of detecting a limited number of pathogens (n=19) but this represents more than 90% of the commonly detected pathogens found in BSIs. This instrument is highly capable of specific ID of the causative pathogen, however the time to answer is still considerably slow. This method provides many positives in the push for rapid, accurate measurements however in emergency situations, this method would fail to deliver the necessary

information a clinician may require. Methods that require an amplification process will always considerably extend the assay time and therefore, referring back to the objective of an EIS eLoaD, a platform capable of capturing whole cells and detecting the changes to the electrode interface would significantly reduce assay times.

1.3.3 Recombinase Polymerase Amplification

Recombinase polymerase amplification (RPA) is an **isothermal technique** that has been widely used for the molecular diagnosis of infectious diseases. This technique may be more advantageous as the single temperature requirement allows for simple heating apparatus and can amplify low levels of DNA to detectable quantities in just ten minutes real-time [74]. It is an alternative approach of pathogen detection to PCR, qPCR and Loop Mediated Isothermal Amplification (LAMP). This method has many attractive qualities, which contributes to the rising interest in this technique such as high sensitivity (LODs of 1GC have been reported), affordable price per test ~€4-5 per test and short reaction time. As the method is subject to a single temperature, no costly thermocyclers are required, therefore driving down the cost of equipment [75], [76].

Shanin *et. al* have reported the development of an RPA assay for the rapid detection of the pathogenic bacteria *Francisella noatunensis* in aquaculture environments. They established a novel real-time *Francisella*-RPA methodology for the rapid and accurate detection of the pathogen which proved high sensitivity and specificity which rivalled that on already established qPCR techniques. The RPA method also showed highly promising results with clinical samples with better tolerances to amplification inhibitors used in PCR. The whole process of RPA amplification was a mere 20 minutes, in comparison to the multiple cycle lengths of PCR, promising good results for RPA to establish itself and a worthy analytical tool [77]. RPA assays have also been used in conjunction with other detection tools such as lateral flow assays (LFAs), ELISA assays and hybridisation in microarray formats [78]. Xing *et al.* provide highly promising outcomes of real-time RPA to detect 0.9fg of disease causing *S. japonicum* DNA in just 15 minutes with the capability of distinguishing between different strains. 60 patient samples were testing indicating 100% sensitivity and specificity compared to ELISA plate results which only provided accurate information in 82.5% of the tests. It was proven that the RPA was superior to the

other detection methods used for this pathogenic species with respect to time and sensitivity [79].

Rosser *et. al* utilised the robust RPA assay in conjunction with an oligochromatographic lateral flow (LF) technology to detect a lower limit of 100fg of the amplified *S. haematobium* DNA. The assay was successful at amplifying the target DNA using RPA methodology at 30-45°C for 10 minutes. The amplicons were also detected in urine samples of up to 5% crude volume. Cross amplification studies were also carried out where amplification occurred for different species of the pathogen, however no other urine microorganism DNA was amplified. The LF system was capable of detection for extremely low concentrations of the DNA where the positive results obtained provide a great indication that RPA is a promising technology for molecular diagnostics for uropathogenic species detection which can be used with LF strips [80].

Finally, Santiago-Felipe developed an RPA and ELISA assay as a DNA based amplification detection strategy for food analysis. Traditionally this type of assay is performed using PCR products for detection with standard ELISA procedures, however the use of RPA amplicons reduces detections time as the constant temperature of 40 °C is only required for 40 minutes, compared with the studied PCR time of 205 minutes reported required for the same amplification outcomes. With this assay, the hybridisation of the labelled products to the specific biotinylated probe/streptavidin coated microtiter plates at room temperature for use with the colorimetric immunoassay is carried out. The RPA-ELISA procedures were applied to food safety screening, where common threats in foodstuffs, such as allergens and pathogenic bacteria [78]. With all the reported literature using RPA DNA products, this method has not been used for any commercial product or test capable of detecting pathogens. The RPA assay, although easy to run, requires very specific primer design and a specific “know-how”, where PCR has dominated the DNA amplification field. With a lower detection time, it is interesting that this method has not been used to date for pathogen detection in a commercial sense. PCR remains to be the most commonly used amplification techniques due to the existing automated instruments.

1.3.4 ELISA Bacterial Detection

Enzyme linked immunosorbent assay (ELISA) is one of the most commonly used immunological assays used for detection of foodborne pathogens, which may lead to a BSI. This method is extremely accurate and sensitive for hapten and antigen detection [81]. Conventional ELISA usually involves chromogenic substrates and reporters that are capable of the production of an observational colour change which indicates the presence of the analyte or antigen. The “sandwich” assay is the most robust form of ELISA, because antigens from the enrichment culture which are to be measured are bound between two types of antibodies; the capture antibody and detection antibody. The acrylic walls of microtiter plater wells are the most commonly used support, however ELISAs have been developed using dipsticks, membranes and various other solid matrices [81]. Bolton et al. discussed the bioline Salmonella ELISA investigation for Salmonella spp; which is a simplistic, rapid, convenient assay for foodborne Salmonella detection. The LOD for this particular ELISA kit was as low as 1 CFU per 25g of sample. The majority of foodborne toxins recognition relies heavily on the presence of an immunological reaction used for specifically for toxin detection.

ELISAs are universally used for this type of detection, and have been evolved for staphylococcal enterotoxins a, b, c and e. The detection levels for these types have been quantified as less than 0.5ug per 100g in minced beef. ELISAs have also been utilised for the detection of enterotoxins and botulinum toxins produced by the Gram-negative bacteria, E. Coli [81]. ELISA-based methods have been proven to be more rapid than culture based methods, as testing time ranges between 1-2 hours compared to 5-7 days for specific ID. This method can also be automated to reduce the assay turn-around time and to reduce manual labour, where a large throughput of samples can be obtained with larger ELISA automated instruments [82]. Improvements to the ELISA technique have been realised through a combination with advanced nanomaterials. Silica nanoparticles (NPs) conjugated with polyacrylic acid which acts as a catalase container which increase the enzyme loading of the assay. Chen *et al.* reported a plasmonic sandwich ELISA technique for the detection of *Listeria monocytogenes* for lower concentrations to previously reported work [83]. The LOD of 80 CFU/ml ranged from two to five orders of magnitude lower than other conventional catalase plasmonic ELISA and basic horseradish peroxidase (HRP) ELISA research.

Wei *et al.* reported a simply prepared enzyme labelled antibody which combined the biorecognition unit, carrier unit and signal amplification (HRP) in a one-pot reaction [84]. This was applied to a portable ELISA detection for the pathogenic E. coli strain 0157:H7 reporting sensitivity of 10 CFU/ml for the concanavalin A-glucose oxidase reporter and 60 CFU/ml for the HRP detector reporter [84], [85]. Immunosensors, created around specific antibody-antigen interaction, are capable of detecting antigens attaching to antibodies by an immobilised reaction to the surface of the transducer. This converts the change in surface parameters into a measurable electrical signal [81].

Immunological reactions are problematic to measure in real-time, due to the diffusion limitation of antigens and immobilised antibodies, specifically for low concentrations of the target antigen. Nonetheless, the majority of immunosensors are capable of producing results within the hour, which is far more rapid than conventional PCR and traditional ELISAs. With this, the results are converted into digital signals, making it user-friendly compared to the more laborious techniques such as blood culture [81]. ELISA techniques have proven to have many benefits around pathogen detection however there it is difficult to determine the viability of the cell and whether it is stressed or damaged. There is also a need for pre-sample enrichment depending on the complexity of the sample matrix. Finally, it has also been reported that there can be high cross-reactivity with similar antigens for bacterial detection, reducing the specificity of the assay [86]. Depending on the capture antibody, the assays are capable of distinguishing between species which would allow for specific treatment plans for patients to relate back to the clinical need.

1.3.4 Lateral Flow Assays

Lateral flow assays (LFAs) are a type of immunoassays which is comprised of a chromatographic technique with an immunochemical reaction. The basic working principal of the LFA is based on an antibody-antigen interaction. The sample is introduced to the system via the absorbent sample pad where it comes into contact with the gold nanoparticles (AuNPs), where the sample migrates along the test strip through capillary action. During this time, the sample and gold nanoparticle (AuNP) conjugate interact with

the test and controls lines, where a signal response is obtained in 5-10 minutes [87], [88] as shown in Figure 1.4. Once the test strip is fabricated, LFAs have a huge potential for pathogen detection due to its simplicity, low cost, rapidity and portability.

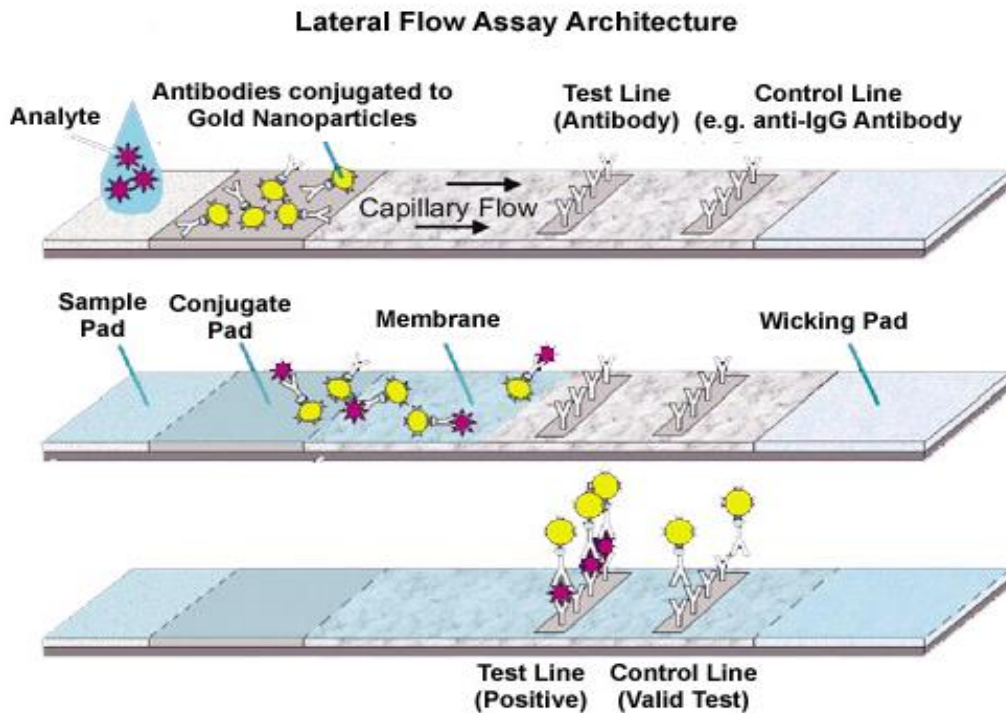


Figure 1.4 Lateral flow assay architecture displaying the sample pad, conjugate pad, membrane and wicking pad. For a positive test to occur, the AuNP antibody conjugate must bind with the antibody functionalised test line and control line [10].

The visual aspect of the LFA is typically realised using AuNPs however fluorescent materials and magnetic beads have also been adopted to enhance the visual detection of analytes [89]. For the majority of LFAs, colloid gold is the most commonly used label due to its intense colour for visual detection and has been used for a huge range of foodborne pathogen detection research. Park *et al.* presented detection of both *E. coli* O157:H7 and *Salmonella* with the paper-based LDA dipstick where AuNPs were used as the label. The LOD for found to be 10^5 CFU/ml and 10^6 CFU/ml respectively [89]. LFAs can be used for specific detection of analytes due to the functionalised control line, which is specific to the analyte, which allows the device to have high specificity. This is also a limiting factor of the technology as each antibody may only be specific to certain strains of the pathogen, where multiple LFAs may need to be utilised to detect to desired analyte.

FebriDx is a new, unique product on released to the market in May 2019, where the test reports to provide a clinician within 10 minutes an assessment of the immune response to a respiratory infection. The device, which incorporates lateral flow technology, reportedly can distinguish between a bacterial and/or viral infection. The use of biomarkers to determine this only for a very low sample volume requirement (5 µl) from a fingerpick test. The use of the C-reactive protein (CRP) for bacterial infection detection, and Myxovirus (Myx) resistance protein A for viral detection, allows the assessment to be made through a colour change on the lateral flow strip in such a short time [129]. The use of biomarkers allows for the rapid response time; however, biomarker detection may lead to false positive detection due to the nature of the biomarker itself. C-reactive protein exhibits elevated expression during inflammation caused by rheumatoid arthritis, some cardiovascular diseases, and infection. CRP levels also tend to alter dramatically between patients of different gender, age, smoking status, lipid levels and blood pressure [130],[131]. The highest concentrations of CRP are found in serum, with some bacterial infections increasing levels up to 1,000-fold, however these levels are only achieved in extreme cases of infection [132]. Myx biomarker has been strongly associated with viral infections, where no other illness or immune response has an effect on the body producing this biomarker. However, Myx does increase the levels of CRP and procalcitonin levels in the bloodstream and therefore may possibly cause a false positive for a bacterial infection [133].

With a clinical trial carried out in the US in 2018, the sensitivity of the device ranges from 59-93% with specificity of 89-97%. FebriDx may help to identify clinically significant immune responses associated with bacterial and viral upper respiratory infections (URI) however as the test itself cannot quantify the amount of the biomarker in the sample, it is impossible to determine if the elevated levels of CRP may come from a genuine infection or from an inflammation response from another disorder. The test itself is compact and rapid and therefore does have potential to be incorporated into the decision making process for the clinician, however the test is more suited towards determining whether or not the illness is viral. CRP levels have been known to fluctuate and therefore it is a possibility to why the device is aimed at determining a URI rather than a sepsis response.

1.4 Impedimetric Biosensors

Electrochemical detection procedures carried out using transduction-type systems which can be designed to quantify and identify pathogens [91]. These biosensors can be categorised into impedimetric, potentiometric, amperometric and conductometric responses, based on certain parameters such as potential, current, conductance and impedance [81]. Electrochemical detection methods have many advantages over optical methods, where real-time analysis of target/analyte binding events can be obtained. Electrochemical bio-sensing methods coupled with microfluidic lab-on-a-chip (LOC) platforms have gained traction in the integrated sensor field of research in recent years. As microfluidics is a rapidly emerging field of study, integrated sensors and microfluidic platforms are only being developed and studied with various well-established methods. Electrochemical detection methods can be utilised in conjunction with LOCs. Electrochemical sensors have gained particular attention due to the ease of fabrication of microelectrodes through screen-printing and photolithographic methods [92]. These microelectrodes can easily be installed within microchannels or micro-reservoirs structures for bacterial capture or detection. The high surface to volume ratio increases the detection efficiency by huge factors [93].

Electrochemical biosensors designed for simultaneous multiplex analysis of pathogens predominantly employ Electrochemical Impedance Spectroscopy (EIS) as the transduction method, consequently providing high throughput, label-free microbe detection [81]. This powerful technique allows for the study of interfaces and conductive surfaces. With this technique, a sinusoidal wave function with a small amplitude and varying frequency is applied to the transducer, where the output current is employed to calculate impedance at specific frequencies. Impedance biosensors used for the detection of microbes are therefore based upon changes of electrical properties associated with cells attaching to the electrode surface. EIS is a commonly applied technique for biosensors, once combined with disposable, screen-printed electrodes (22,23). The low-cost nature of these disposable chips makes electrochemical biosensors very appealing in the field of microbiology due to the ease of fabrication and high sensitivity.

1.4.1 Electrochemical impedance Spectroscopy for Pathogen Detection

Previous literature has stipulated changes to the capacitance recorded by the EIS are variants formed in the electrical double layer capacitance. The C_{dl} is the outer capacitance that exists at the solid/liquid interface which relies upon the concentration of the ionic solution where-as the interfacial capacitance is reliant upon an adsorbed species formation on the working electrode surface [95]. The majority of pathogen cells are electrically charged so the immobilisation of said cells will produce variations in the biosensor. Attachment of pathogenic cells containing negatively charged proteins may decrease the double layer formed by attracting the oppositely charged ions from the electrolyte solution which may condense the C_{dl} .

The change in surface conductivity therefore can be due to the electrical charge produced by the cells or the additional of surface layer capacitance. Label free impedance has gained particular interest over the last decade due to a reduced detection time compared with growth based impedance approaches as the method is not reliant upon cell replication within a culture media solution for the production of metabolites from the cells. Most bacterial impedimetric biosensor studies have focused on functionalised surfaces where immobilised biorecognition elements are used for cell capture [96].

Antibodies, proteins and aptamers are just some examples of biorecognition elements which have a specific affinity towards the analyte. This complex formation will typically alter the electrical properties of the sensor where the biorecognition molecule will form the first response and the target complex will form the second response. A multitude of strategies can be incorporated to increase the immobilisation of the capture biorecognition elements on the biosensing surface, which in thiol self-assembled monolayers (SAMs), thin polymers, bio-affinity layers and chemical grafting. The choice the capture molecule is ordinarily determined by the nature of the biomolecule, its cost and reproducibility, stability and ease of immobilisation [97], [98].

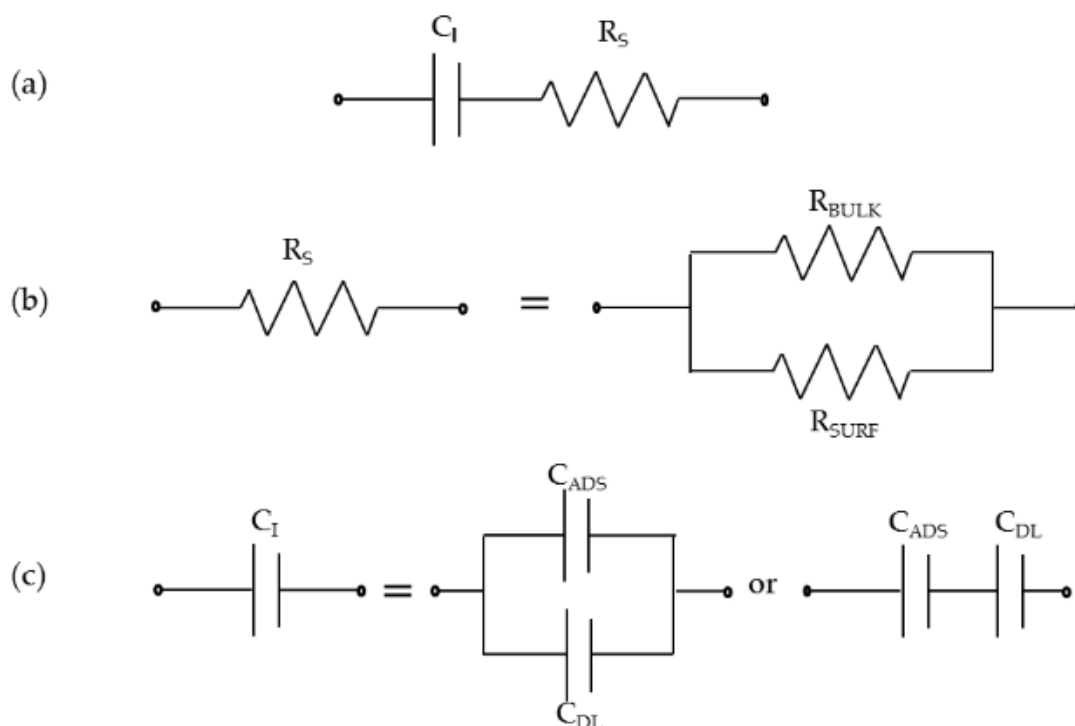


Figure 1.5 Typical EC components for a non-faradaic process for pathogen detection on the working electrode in an electrochemical cell (a) The standard circuit components consist on the C_{dl} and the R_s (b) The total resistance R_s may depend on the bulk solution resistance and the resistance of the electrode surface (c) Whole cell adsorption on the surface can result in a secondary source of capacitance which may be in series or parallel with the double layer capacitance of the electrolyte depending on the amount of pathogenic cells present.

Figure 1.5 portrays the fundamental elements of the equivalent circuit modelling for a non-faradaic process. Without a redox probe present in the electrolyte solution, no faradaic process will occur, and electron transfer is not produced. In this case, the changes in interfacial capacitance will be observed [94]. The main advantage associated with immunosensors is the sensitivity and specificity of the interaction between the antibody layer and the antigen where advances made with the production of antibodies through genetic engineering have been improving the stability and binding ability on the sensing surfaces [99]. Nonetheless, a major drawback still exists with the use of antibodies, as they can become unstable as many types cannot maintain their binding activity. This issue has hindered the widespread use of immunosensors of this type [99].

1.4.2 Electrochemical Biosensors

Recent advancements with micro-fabricated devices has allowed for functionalisation of electrode surfaces with molecules capable of capturing microbe cells [100][101]. In the work carried out by Yang *et. al* the R_{et} and C_{dl} are reliant on the electrical properties of the electrolyte and electrode interface, which is monitored to determine if molecules and cells have adhered themselves on the surface [102], [103]. Due to these bio-recognition reactions, this technique is capable of detecting specific types of pathogens, with high selectivity amongst complex matrices. The Salmonella typhimurium bacteria grows within the media where the impedance was measured at hourly interval at four frequencies of 10, 100, 1000, 10,000 Hz. A detection limit of 6.5×10^5 CFU/ ml was recorded at 6 hours, where the limit significantly dropped to 7.6×10^1 at 13.3 hours. The C_{dl} changes due to the medium growth recorded at 10 kHz showed the greatest change, where this frequency is directly associated with the capacitance of the double layer at the bacteria interface. With a good detection limit, this is only specific to one bacteria. A larger range of pathogens studied would make a more robust study, as the growth rate of the bacteria is specific to each species and therefore may alter dramatically between various types of microbes.

Unlike a variety of detection methods, electrochemical sensing may not require a labelling step which is a highly desirable attribute of a sensing platform. Boehm et al. fabricated a silicon chip with thin platinum microelectrodes capable of measuring the change in impedance in a fixed volume chamber [104]. This microfluidic pathogen sensor contains a 15 μm deep chamber pre-functionalised with specific target antibodies. Bacteria suspended in various DPBS solution were passed through a microchannel into the chamber where the bacteria selectively attached to the corresponding capture antibody. As the bacterial membrane acts as an insulator and displaced a specific amount of conductive solution within the chamber, a change in impedance was recorded to prove the capture of the bacteria and therefore, its presence in solution. It was stated that the change in conductance and capacitance decreases the recorded impedance. The cell membrane acts as an insulator at low signal frequencies, the presence of cells in solution displacing the ions would change the signal response. Boehm et al. could differentiate between two types of bacteria using this sensing technique; Escherichia coli (E. coli) and Moraxella catarrhalis (M. catarrhalis) by using different capture antibodies. This method was capable of detecting 9×10^5 colony forming unit (CFU) mL^{-1} of the E. coli strain. The

detection limit was possibly so high as the displacement of ions by one pathogen may be extremely low. Despite the high LOD, the monitoring of the cell presence was carried out in real time.

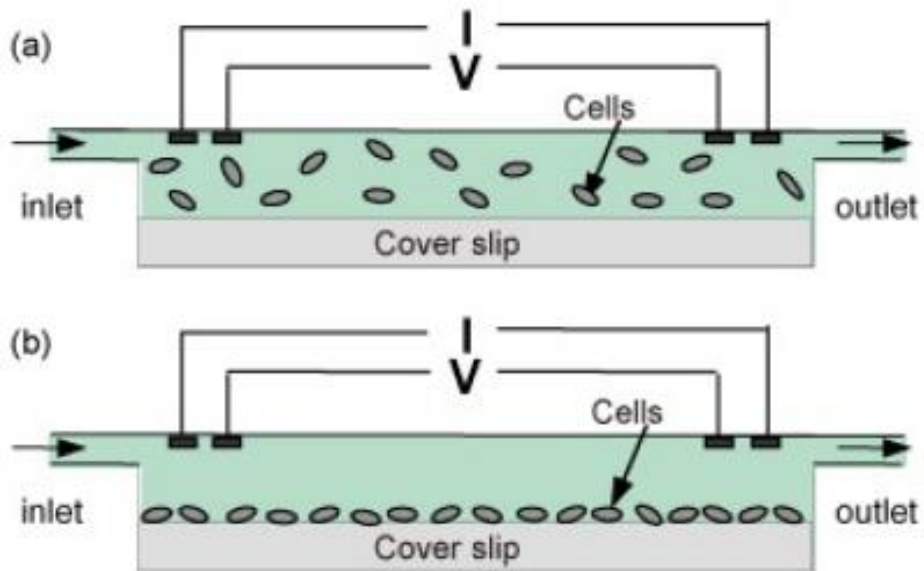


Figure 1.6 (a) *Bacteria in suspension in ions rich solution* (b) *Antibody-Bacteria capture*. [11]

Acquiring an impedance signal has been proven to be a fast detection method, an attractive attribute for a POC device. Here, this device has justified the cross-over of micro-fabricated device with impedance detection for a high-throughput device. A reduction in the fluid cross-section area in the sensing region increases the ratio of cell volume to the total volume of the sensing region, thereby increasing the sensitivity. Once a cell is captured, various solutions can be readily perfused through the channel and the resulting changes in cell volume can be followed *via* impedance

It is expected that by reducing the size of the measurement capture features, the microfluidic device may be modified for a lower detection limit, suitable to pathogen detection [60].

Whilst Boehm *et al.* observed changes in the real and imaginary impedance due to the insulating quality of the bacterial cell membrane and displacements of conducting ions, Cheng *et al.* developed a cheap, simple micro-device comprising of two glass slides separated by 50 μm PDMS gasket capable of detecting ions and therefore the reduction

of impedance across a known surface [106]. The intracellular solution within the bacterial cell released from cell lysis causes a change in the conductivity of the surrounding medium due to the released ion from the cells, which is monitored in real-time. As the total ionic concentration of a cell is insignificant, the total change caused by the cell lysis can be quantified for a total lysed cell number count. Cheng et al. documented that the entire concentration of the present solution's conductance increased linearly with the isolated cells which provided the ions during the lysis.

The basic setup of the device comprised of a protein modified glass substrate for specific cell capture, which are then lysed, and the conductance is measured across the microchannel area and the micro-patterned electrodes. This device proved to have a high sensitivity, capable of detecting 20 cells μl^{-1} or 2×10^4 CFU/ml. This cell count, although high, was again carried out in real time where no culturing was used. The electrochemical sensing of this device eliminates the requirement of Nucleic Acid (NA) amplification, a favourable attribute for quick fabrication and analysis of a target probe [107]. This device reported by Cheng *et al.* was developed to capture, detect and quantify CD4 cells, commonly associated with HIV patients, however by changing the capture protein, it can be easily modified for bacterial cells.

According to Cheng *et al.*, this device provided enough evidence to prove that this setup, for immobilised cells, is one of the most sensitive, non-optical approaches for cell detection. Due to its size, ease of fabrication, and highly sensitive, this device could potentially serve as a single use platform used fast, affordable bacterial cell detection and counting for a hand-held point-of-care device. It can be argued that multiple types of chips would need to be fabricated in order to specifically identify an unknown bacterial cell, which wouldn't be a feasible option in a clinical setting. With such a high detection limit, the device itself couldn't be used as a POC platform as pathogens counts that high wouldn't exist in real sample without the need for culturing which significantly increases the time to answer. The device setup is too specific to only one capture probe, unlike the traditional method of PCR where a read-out of the primer sequence is displayed for highly specific identification of the present pathogen [108]. Another method of label-less sensing and detection is electrochemical impedance spectroscopy (EIS) of probing biomarker interactions upon a conductive surface. A wide range of conductive metal can be used as

the electrode surface, making the fabrication a robust and possible cheap alternative to an optical sensing approach [109]. As the surface of the site is being examined during the EIS, the electrode surface must be modified to maximise antibody adhesion [110]. The altered surface chemistry will allow for a highly sensitive antibody functionalised surface.

Liao et al. developed a micro-fabricated electrochemical sensing device equipped to detect pathogens in human urine samples [111]. The device contained 16 sensing sites, each fabricated as a single layer gold, three electrode system, i.e. counter, reference and working electrode. Each working electrode within the system was functionalised with a different capture probe, specific to a common urinary pathogen. Some of the probe library consisted of *E. coli*, *Enterococcus* spp., *Pseudomonas aeruginosa* and *Enterobacter* strains. The pathogens were cultured and lysed where the capture probes were specific to a 16S rRNA released by the pathogen where 10 µl of the sample was incubated on the electrode. The detection of the probe-target hybrid was accomplished with the addition of Horseradish Peroxide (HRP) conjugated antibody to the detector probe located on the working electrode. Using a fixed potential of -200mV, species detection was obtained for the uropathogenic bacteria.

The sensitivity of the probes was recorded as low as 2600 CFU/ml pathogenic cells in culture, with a complete assay to answer in 45 minutes, without the need for pre-sample purification. This in theory was a good yield, as common UTI contain >10,000 CFU/ml. Further feasibility studies proved the sensor had a 98% sensitivity for Gram Negative (GN) bacteria within the integrated system. This work demonstrates the working capacity of the device, validating the use of electrochemical sensors within a micro-fabricated platform as a POC mechanism. The rapid, single uropathogenic identification was accomplished and ratified using this platform and could be applied in a clinical setting for urinary tract infection diagnostics. This amperometric electrochemical detection has been reported throughout available literature, with similar detection of low concentration of target probes within an assay runtime of 45 minutes [112]. The multiplexed testing area provides the user with a highly robust device capable of distinguishing between pathogens that may be present in a sample. This detecting capability specifically pinpoints the bacterial strain present which will allow for specific antibiotic administration for the patient. The bodies of work discussed have provided automated LOCs with integrated

biosensors capable of detection of pathogens. Both highly specific platforms and array based sensors have been explored, revealing the high prospects that can be offered using the combination of these techniques. This method was capable of differentiating between species, however not reports have been made regarding sub-species detection. A common attribute of the majority of these sensor platforms is that the capture probe is only specific to one pathogen. This may be used to monitor the growth, decay of pathogen levels within an already established sample, but would be difficult to apply to an unknown clinical case. To date, there has been no commercial success with an impedimetric sensor that is capable of capturing whole cells for determining whether a sample contains pathogens. EIS methods allow for rapid sensing as no label is required, however the methods previously described all have high detection limits. Many EIS systems require sample pre-treatment, whether it is to lyse the cell or culture the pathogen to a detectable CFU count. As the sepsis condition is time-dependent there is a clear gap in this market where an EIS platform capable of whole cell detection without the need for culturing or labelling.

Overall, these immunosensors have proved to be highly accurate, where a 98% selectivity towards GN bacteria was reported with a fast screening processes but will face the challenge to become more robust when compared to the slow but highly accurate PCR methods which have been established for decades. Where the issue of speed has been addressed with the electrochemical immunosensors, the sensitivity of the sensors appears to still be an issue. These immuno-response analysis results can possibly be further confirmed using PCR methods and can be more commercially available if coupled with a hand-held or bench top operating device. These portable analysers have been released the market in recent years due to the high output of various LOCs that have been commercially developed by large companies such as Lonza, Gen-Probe and Novartis.

1.5 Centrifugal Microfluidics

Microfluidics is the study of fluid flow on the micron, and submicron, scale [113]. Centrifugal microfluidics is a branch of this field, where rotating lab-on-a-disc (LoaD) platforms propels fluid from the centre of the disc in an outward direction through

centrifugal forces, through a system of microfabricated structures. As LoDs can manipulate fluids on the microscale, scaling effects must be considered [114]. Different forces take precedence when the liquid volume is reduced, therefore there must be a re-distribution of effects. On macroscopic levels, forces such as gravity and atmospheric pressure dominate whilst in micro-systems capillary forces and surface tension govern. A full comprehension of hydrodynamics is important whilst designing and developing these microfluidic systems. Theoretical flow will be discussed in this section with particular attention paid to flow types and microscale forces that effect small volume liquids. These platforms are also capable of performing fluid manipulation operations such as mixing, metering and separating and metering, and mixing can be carried out using a clever network of microchannels and reservoirs [115].

Centrifugal based microfluidics has emerged as a quick analysis tool for biomedical diagnostics and poses to be an exciting development for point-of-care (POC) devices, as many of the required steps for any fluidics analysis can be miniaturised and amalgamated onto a LoD. Due to the multiple possible analysis steps which may be incorporated into a platform, this has allowed to development of sample-to-answer devices known as micro total analysis systems (μ TAS). Centrifugal microfluidics allows for ease of use, as no external pumps or devices are needed for the propulsion of liquids through the system. A simple motor, with variable spin-rates, is sufficient in provided all the forces necessary for fluid control. The evolution of manufacturing techniques allows for production of LoDs with rapid testing methodologies are now achievable [116]. Complex device operation requirements incorporated onto the platform can be realised on a single polymer disc which contains all microfluidic architecture. Thermoplastics or acrylics are used and therefore the cost per test can be significantly reduced compared to other in-vitro diagnostic (IVD) techniques. The optical transparency can also be advantageous for direct visualisation of the test and allows for optical detection methods to be implemented.

Many immunoassays have been implemented onto existed commercially available centrifugal platforms. Immunoassays often require many assay steps such as blood separation, sample incubation, washing and elution steps and detection. These stages have been proven to be implemented on robust microfluidic flow controlled platforms. Gyros AB™ has proven commercial success with a first generation centrifugal testing

platform for immunoassay application. The device utilises hydrophobic regions to control a sequential flow within an injection moulded disc which allows for on-board metering of reagents. One device provided by the company has up to 112 channels which allows for high throughput of the sample where the users own specific biomarker may be detected. The Gyrolab Bioaffy CD allows for nanolitre immunoassays to be tested which minimises sample and reagent usage where fluorescence detection from the assay is reportedly obtained within the hour. The selling point of the device is that specific immunoassay can be designed for implementation on the device based on the required dynamic range and analyte concentration where the company itself will provide support whilst designing the LoAD assay. With many advantages regarding assay volume sizes being realised with this platform, there are many clear drawbacks with the concept. The company does not provide with “ready to use” devices, where all assays and binding pairs for the sandwich protein assay require specific user knowledge. Again, as the assay detects protein biomarkers which will require some form of sample separation which cannot be performed on-disc therefore the device cannot be a POC platform and can only be used in a centralised lab [134],[135].

In 2013, Samsung released the LabGEO IB10 to the market. The integrated system combines a microfluidic platform and analyser for cardiac biomarker detection from whole blood which is the only user required input into the device. Proteins such as troponin, CK-MB and Myoglobin are extracted and tested in 20 minutes where an optical density reading over 10 specific wavelengths are obtained in the custom built centrifuge analyser platform [136]. The centrifugal disc contains freeze-dried reagents for blood chemistry analysis. All fluid flow is controlled by laser actuated ferrowax microvalves where all processing of the sample is carried out automatically, where a total of 350 μ l of whole blood is required. Other centrifugal devices have incorporated a testing and optical density analysis conjoined system [137] however, Samsung appear to be the only competitors on the current market which have been able to provide the user with analysis from whole blood on a POC system , where the analyser system is portable and handheld with an integrated interface and Bluetooth technology where the clinician may receive results directly to their smart phone.

1.6 Analyte Detection using Electrochemical Methods on a Lab-on-a-Disc

Recent developments in microfluidic research has allowed for the integration of well-established detection methods, such as optical or electrochemical, to create robust platforms capable of a sample-to-answer within a significantly reduced time [54]. The use of centrifugal microfluidic platforms allows for complex sample handling on-board, reducing the efforts of the user significantly. LoAD research manipulates microfluidics through the use of centrifugal forces which possesses many advantages. For fluid pumping throughout the system, only a compact motor is required to generate these forces. This transportation is highly efficient and significantly reduces reagent usage. Sample separation is also possible due to density based fluid, such as whole blood where the dense blood components settle to the bottom of the chamber where the plasma remains on the top as it's less dense. These attributes have contributed to the surge in research surrounding centrifugal microfluidics, where the exciting integrated fields of electronic LoADs (eLoAD) allows for rapid detection and analysis of biomolecules, significantly reducing data acquisition time [55]. For the majority of eLoADs, the electrodes are integrated onto the platform, however to platform must be static for the electrochemical readout [56]. Carbon brushes in contact with a metal slip ring have been applied the eLoAD and motor during centrifugation, however high background electrical noise may greatly interfere with the electrical readout signal, which results in an instable measurement [57].

Nwankire *et. al*, developed an eLoAD capable of capturing and quantifying ovarian cancer cells (SKOV3), extracted from whole blood. With antibody functionalised gold electrodes, sensitive detection of the cells is obtained using label-free detection methods. The flow control system on-board is facilitated by the intricate use of siphons, capillary action and centrifuge-pneumatic DF valves. Due to the small-amounts of sample and reagents loaded into the platform, up to five different testing sites exists, allowing for multiple assays being carried out in parallel. An 87% capture efficiency was reported over a dynamic range of three orders of magnitude with a lower LOD of 214 cells/mm², where the lower LOD is comparable to just 2% of the electrode surface. The detection method of label-free

impedance allowed for rapid analysis of the cancer cell detection. Electrochemical biosensors of this type have attracted major interest for label free analysis with reduced complexity during assay running time and signal acquisition. They attain sensitivity and simplicity which makes them a practical and quantifiable diagnostic method for detection of whole cells [120]. Using a label free method also reduces the cost of the system therefore, the eLoaD is a highly efficient and sensitive diagnostic tool. The use of cost-effective sputter-coated electrodes allows for the platform to be disposed of after a single-use, making this type of POC device economical [121]. These results give a true insight into the huge potential that exists for eLoaDs as they are an efficient prognostic devices where minimal sample preparation is required and can be further developed for clinical applications.

Andreasen *et al.* produced a centrifugal system to entrap a sample within a microfluidic chamber during analysis where CV measurements are acquired at a variety of spin-speeds, where the electrochemical response is not altered. It was possible to extract data from the system under centrifuge conditions, simplifying the interpretation and collection of data. The group established real-time and continuous observation of a sample under electrochemical conditions. Additionally, all transitional sample handling steps were monitored using amperometric detection of analyte mixing (ferricyanide and PBS) on-disc [122]. Where this is an exciting prospect of real-time monitoring of an electrochemical process on an eLoaD under centrifugal conditions, a high error does exist whilst the platform's spin speed exceeds 10Hz due to high noise with the carbon brushes. For many fully integrated LoADs where valving is used to automate the device, spin-speeds much greater than this are often required [123].

Another centrifugal platform capable of capturing and detecting pathogens is documented by Sangar *et al.* The robust platform contains an integrated sample pre-treatment system where square wave voltammetry (SWV) techniques are applied for the cell free detection of a secondary metabolite, p-Coumaric acid (pCHA) which is generated by genetically modified strains of E-Coli. Like most common LoADs, the device contains multiple testing sites each containing individual electrochemical detection regions. A total of eight regions are available for individual testing, where a 0.2 μm membrane unit exists in each section for the sample filtration. Filtration occurs under centrifugal conditions for

5 minutes at 700 RPM or 11.67 Hz, where the supernatant is metered and passed into the detection chamber. Unlike the previous eLoaD, the sensors are patterned onto the PMMA base layer of the device using e-beam evaporation utilising 20nm chromium as a supportive adhesive layer for the 200nm of deposited gold. Contact points exist through the depth of the LoaD to establish an electrical connection through a slip-ring using a magnetic clamping system which enables ease of assembly with adjoining electrical components portrayed in Figure 1.7. All measurements were acquired under static conditions and showed very promising results for the detection and quantification of the two E. coli p-Coumaric acid metabolites compared to results obtained from HPLC, where the detected quantities existed in the μM range [124].

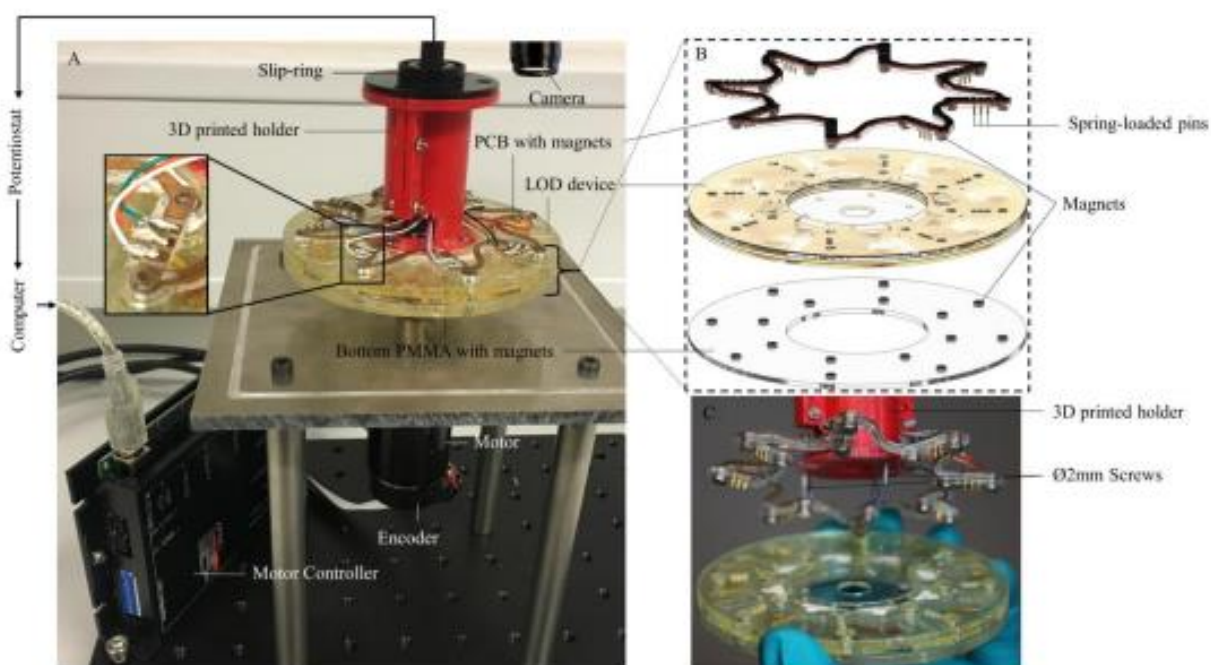


Figure 1.7 (A) portrays the setup for the eLoaD where a motor generates the centrifugal force required for on-disc filtration where the LoaD in B) shows the clamping system in which electrical contact is made with the device [12].

Similarly, the group also demonstrated a new, on-disc pre-treatment based on supported liquid membrane (SLM) technology where this extraction technique is used to purify and enrich analytes directly from complex matrices such as saliva and urine [126], [127]. Using the SLM to implement on-disc separation, the main interfering compound Tyrosine is removed and the pHCA is enriched. The device enables multiple readings to be acquired at certain stages of the production process when the target analyte is quite low (typically $100 \mu\text{M}$). As the device is deemed as low-cost it was aimed to be a single use device,

however it has been shown that the device can be re-used using typical electrode cycling to clean the surfaces. This work poses a significant insight into the exciting advantages and potential of on-disc sample pre-treatment and electrical detection for analytes in a compact, portable testing [125].

Amperometry is often used as a detection technique when coupled with eLoaD platforms. A constant potential is maintained at the working electrode via the reference electrode where the current is recorded due to oxidation and reduction of the electrolyte. In cases where the supporting solution of the analyte is not electrochemically active, the target analyte cannot be measured directly. Screen-printed carbon electrodes which were modified using graphene-polyaniline nanocomposites were incorporated onto a LoaD to enhance electrochemical detection of glucose. The glucose and enzyme solutions are loaded into separate chambers where they mix in a serpentine channel under centrifugal conditions. This produces an electrochemically active hydrogen peroxide solution through an enzyme reaction in under 8 minutes. The quantity of produced hydrogen peroxide is then measured to systematically deduce the amount of glucose present. The LOD for the system was reported to be 0.29mM. Glucose present in serum samples were also tested where the recorded amounts detected with a certified reference serum sample [128]. Common interfering compounds such as uric acid and ascorbic acid were tested where the sensor was only specific towards glucose. This was an important effort to determine to working capability of the sensor for real-life applications.

Another electronic LoaD platform for whole blood (WB) analysis was developed by Li *et al.* where the systems main functionality was to perform basic metabolic testing. Different concentrations of uric acids, lactate and glucose in WB spiked samples with the target were analysed within minutes [118]. WB is a complicated and different matrix to work with, as the blood components non-specifically bind to sensor surfaces. Figure 1.8 portrays the system setup in which a nano-porous Au plated Si electrode with carbon nanotubes increases the electrode surface area to increase the immobilisation of Prussian blue (catalyst) and the analytes. A small sample size of 16 μ l was required to perform each test, where each PDMS LoaD platform contained eight individual testing sites. LODs of 0.3mM of glucose, 0.1-0.2mM of uric acid and 0.7-1.5mM of lactate were obtained using this simplified, rapid diagnostic test. The loading of a WB sample, in which centrifugation

separates the blood components and plasma allows for the detection of analytes present within the less dense fluid for testing. To further determine the potential of this device, a comparison study was carried out using a commercial colorimetric method, where the results indicated deviations for glucose, lactate and uric acid of 4.2%, 5.2% and 6.0%, respectively between both methods.

Another example of eLoaD has been reported by Kim *et al.*, where amperometric detection methods for the cardiac marker, C-reactive protein (CRP), were capable of a prognosis in 20 minutes. The implementation of an ELISA assay on-disc followed by the electrochemical detection through gold electrodes, fabricated using E-beam lithography. 300 Å of chromium was deposited acting as an adhesion layer, followed by deposition of 3000 Å of gold to create the desired electrode pattern [119]. The use of ferrowax valves allows for on-board reagent storage and actuation through a mobile laser. Individual triggering of the valve can only occur under static conditions [121]. The recorded LOD for this system for CRP was deemed to be 4.9pg/ml. This was reportedly a 17-fold improvement in quantification by optical density (OD) which is the common approach for ELISA detection for microbiologists. This microfluidic platform adds to the very small research bracket of microfluidic-electrochemical cross over for successful detection for very low levels of desired biomarkers. Whilst the recorded data showed good results, the sample type was spiked buffer with CRP.

As the sample type was in reality the simplest fluid suspension for the analyte, it would be very interesting to determine the true capability of the platform using a more complex matrix, such as serum of whole blood. All bodies of work exploit centrifugal propelled fluid flow for the actuating of liquid throughout the LoaD. Fluid flow has been proven to increase the capture efficiency of the analyte to the capture site [122], which for all cases is induced by the motor. Using a spin-stand setup, the centrifugal platform does not require expensive pumping equipment to induce flow. A simple DC motor can generate up to 60Hz, which is a substantial spin-frequency.

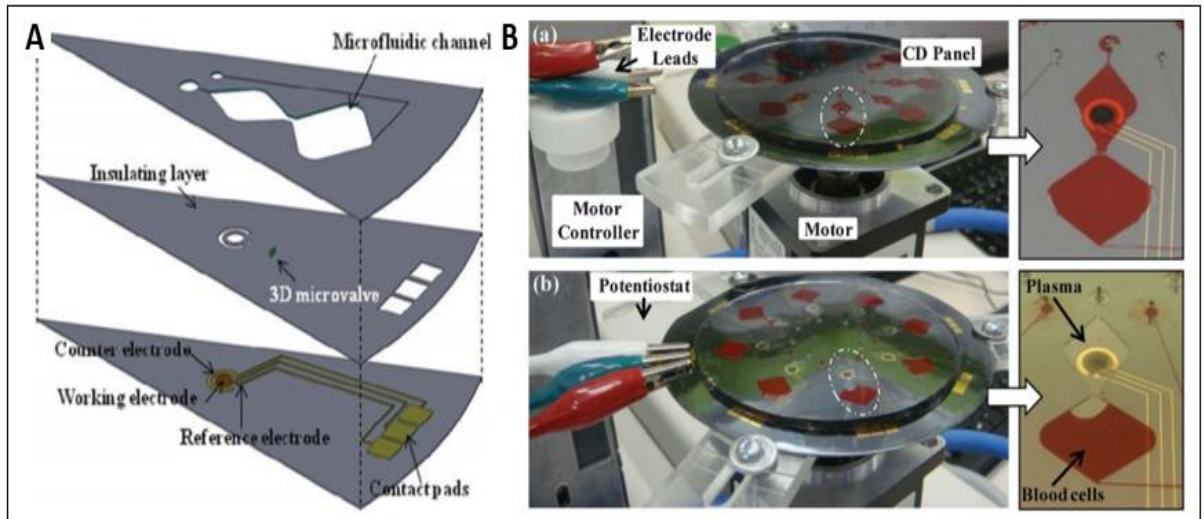


Figure 1.8 (A) Conceptual design of one or eight testing sites displaying each consecutive layer of the PDMS eLoaD (B) Real image of the eLoaD where whole blood is loaded and centrifuged to separate plasma for detection [13].

The research discussed here shows the huge advantage for this emerging field of research. The combination of centrifugal microfluidics and electrochemistry has proved that a real-point of care system is attainable where quantifiable results can be obtained in minutes.

It only appears that the cost of instrumentation is relatively cheaper in comparison to optical methods required for standardised testing of biomarkers. Although most results for eLoaD can only be achieved through static conditions, the developments of carbon brushes and slip rings for the motor and potentiostat via the platform itself proves very promising results for real-time detection with reduced noise. Very little work has been published in this field, where Nwankire *et al.* appears to be the only research published for whole cell detection on this type of platform using electrochemical techniques for detection [118].

1.7 Conclusion and Thesis Outline

As detailed in this review, the need for rapid low cost pathogen detection is an essential aspect for sepsis diagnosis. As the current gold standard for pathogen identification can range from hours to days due to the reliance on cell growth, blood culturing techniques although the most established technique, is an outdated method. Biosensors for pathogens must be highly sensitive and selective as detection of pathogens in complex matrices such as blood is a key factor. As the “Golden-hour” for sepsis treatment is vital, emerging technologies designed for pathogen detection must have a rapid response time. This body of work has explored the epidemiological effects of pathogens in society and various methods of detection used by clinician’s to-date. A huge gap is presented in the time frame for sepsis diagnostics, where hospital staff are pressurised to analyse a patient’s symptoms and decide whether a sepsis-influenced treatment plan must be adhered to. Current technologies implemented with a clinical setting are too slow with varying factors of inaccuracies due to the complexities of the processes. Methods such as PCR, RPA and ELISAs have proven to be highly selective between pathogen species and sensitive (<10 CFU/ml) however they still require a prolonged amount of time and a highly skilled technician to perform the bioassay.

EIS for immune-sensing has been of particular interest in the last as there is no need for sample amplification due to the label-free detection capabilities of the functionalised electrodes. The changes of the interfacial impedance allow for quick detection times of the sample of interest in a significantly reduced amount of time (< 1 hour) in comparison to other methodologies. In this critical analysis of existing literature, electrochemical biosensors have been used for very specific detection of pathogens in more complex matrices such as whole blood have not been truly explored.

Centrifugal microfluidics is an exciting, evolving field and its importance as a real point-of-care device is still to be fully recognised. With the constant emergence of scientific fields, new applications of LoDs are being realised and utilised for various sensing systems., mass-production of Lab-on-Chip (LOC) and Lab-on-a-Disc (LoaD) are now possible and inexpensive. In this body of work, biosensors and pathogen detection are at

the forefront of the research aim. Other competitors in the market have also been explored who adopt these various methods of pathogen or biomarker detection which may be indicative of a sepsis response. The proposed electrochemical eLoaD described in the main thesis objective have also been compared to justify why this novel platform is pushing the boundaries of sepsis detection.

Chapter 2 of this monograph presents the various materials and methodologies explored for each individual project, where material rationale is given. For the techniques used, the theory is explained to also justify the use of that specific method.

Chapter 3 portrays the development and optimisation of an eLoaD capable of handling complex matrices such as blood culture and whole blood samples. The development stage discusses in detail the design changes and their implications and how the spin parameters and functionalisation of certain chambers within the device allows for better capture of pathogens present in samples with no pre-treatment.

Chapter 4 discusses the sensor fabrication techniques used, where the SAM method of antibody attachment to sensors was initially explored. EIS methods were used to determine the effect of the various fabrication steps on the sensor response. This method was then compared to the single use biosensor which would be incorporated into the eLoaD. With this altered method in which the antibody is absorbed on to the surface the EIS response was examined once more to determine the changes induced by the new fabrication method. Finally, the biosensors were incorporated into the eLoaD which again were examined and how the EIS response compared to previous methods. Samples received from St. James' Hospital were tested on the platform to determine how the device would operate with real complex samples. A full study was carried out with these blood culture samples where the true capabilities of the device or determined.

Chapter 5 explores the use of aptamers as a capture biorecognition molecule for the capture and detection of E. coli cells for use with PCR and RPA methods as an alternative approach of microbe detection, where aptamers may be applied to increase stability of reduce the cost of the sensors.

Chapter 6 comments on the possible future work is also described to portray the next steps in furthering the research to develop their potential. Preliminary data shown determines how the previously discussed work may be developed. This chapter also concludes the body of work. Each working chapter is summarised to determine the effectiveness of the experimental work

1.8 References

- [1] H. F. S. Freitas and C. M. G. Andrade, "A brief review on biosensors for bioprocesses," no. 999, 1962.
- [2] S. HOFFMANN, M. B. BATZ, and J. G. MORRIS, "Annual Cost of Illness and Quality-Adjusted Life Year Losses in the United States Due to 14 Foodborne Pathogens," *J. Food Prot.*, 2012.
- [3] J. Hajj, N. Blaine, J. Salavaci, and D. Jacoby, "The 'Centrality of Sepsis': A Review on Incidence, Mortality, and Cost of Care," *Healthc. (Basel, Switzerland)*, vol. 6, no. 3, p. 90, Jul. 2018.
- [4] K. E. Rudd et al., "The global burden of sepsis: barriers and potential solutions," *Crit. Care*, vol. 22, no. 1, p. 232, Sep. 2018.
- [5] I. M. Sheldon, "Detection of Pathogens in Blood for Diagnosis of Sepsis and Beyond," *EBioMedicine*, vol. 9, pp. 13–14, 2016.
- [6] F. R. Coelho and J. O. Martins, "Diagnostic methods in sepsis: the need of speed," *Rev. Assoc. Med. Bras.*, vol. 58, no. 4, pp. 498–504, 2012.
- [7] S. Wang et al., "Portable microfluidic chip for detection of *Escherichia coli* in produce and blood," *Int. J. Nanomedicine*, vol. 7, pp. 2591–2600, 2012.
- [8] R. Singh, M. Das Mukherjee, G. Sumana, R. K. Gupta, S. Sood, and B. D. Malhotra, "Biosensors for pathogen detection: A smart approach towards clinical diagnosis," *Sensors Actuators B Chem.*, vol. 197, pp. 385–404, Jul. 2014.
- [9] J. Heo and S. Z. Hua, "An overview of recent strategies in pathogen sensing," *Sensors (Switzerland)*, vol. 9, no. 6, pp. 4483–4502, 2009.
- [10] N. D. Toan et al., "Clinical features, antimicrobial susceptibility patterns and genomics of bacteria causing neonatal sepsis in a children's hospital in Vietnam: protocol for a prospective observational study.," *BMJ Open*, vol. 8, no. 1, p. e019611, 2018.
- [11] P. Speck, "Antibiotics: Avert an impending crisis," *Nature*, vol. 496, no. 7444, p. 169, 2013.
- [12] J. Almagor, E. Temkin, I. Benenson, N. Fallach, Y. Carmeli, and on behalf of the D.-A. consortium, "The impact of antibiotic use on transmission of resistant bacteria in hospitals: Insights from an agent-based model," *PLoS One*, vol. 13, no. 5, p. e0197111, May 2018.
- [13] et al. Alberts B, Johnson A, Lewis J, *Molecular Biology of the Cell*. New York, 2002.
- [14] M. Wallden, D. Fange, E. G. Lundius, Ö. Baltekin, and J. Elf, "The Synchronization of Replication and Division Cycles in Individual *E. coli* Cells," *Cell*, vol. 166, no. 3, pp. 729–739, 2016.
- [15] V. Schneider-Lindner, L. HA, and M. Thiel, "Definitions for sepsis and septic shock," *JAMA*, vol. 316, no. 4, p. 457, Jul. 2016.
- [16] A. Kleiman and J. P. Tuckermann, "Glucocorticoid receptor action in beneficial and side effects of steroid therapy: Lessons from conditional knockout mice," *Mol. Cell. Endocrinol.*, vol. 275, no. 1–2, pp. 98–108, 2007.

- [17] R. Daniels, "Surviving the first hours in sepsis: Getting the basics right (an intensivist's perspective)," *J. Antimicrob. Chemother.*, vol. 66, no. SUPPL. 2, pp. 11–23, 2011.
- [18] O. Lazcka, F. J. Del Campo, and F. X. Muñoz, "Pathogen detection: A perspective of traditional methods and biosensors," *Biosens. Bioelectron.*, vol. 22, no. 7, pp. 1205–1217, 2007.
- [19] H. J. Hwang et al., "High sensitive and selective electrochemical biosensor: Label-free detection of human norovirus using affinity peptide as molecular binder," *Biosens. Bioelectron.*, vol. 87, pp. 164–170, Jan. 2017.
- [20] H. Y. L. Ee, J. S. C. Hoi, P. G. Uruprasath, and B. L. Ee, "An Electrochemical Biosensor Based on a Myoglobin-specific Binding Peptide for Early Diagnosis of Acute Myocardial Infarction," vol. 31, no. July, pp. 699–704, 2015.
- [21] N. Wang et al., "Electrospun fibro-porous polyurethane coatings for implantable glucose biosensors," *Biomaterials*, vol. 34, no. 4, pp. 888–901, Jan. 2013.
- [22] "HSE stats," 2017.
- [23] H. S. Executive, "National Sepsis Outcome Report 2017," 2017.
- [24] C. D. Garcarena, T. M. McHale, I. Martin-Loeches, and S. W. Kerrigan, "Pre-emptive and therapeutic value of blocking bacterial attachment to the endothelial alphaVbeta3 integrin with cilengitide in sepsis," *Crit. Care*, vol. 21, no. 1, 2017.
- [25] H. B. Nguyen et al., "Early goal-directed therapy in severe sepsis and septic shock: Insights and comparisons to ProCESS, ProMISE, and ARISE," *Crit. Care*, vol. 20, no. 1, 2016.
- [26] K. E. Rudd, L. K. Tutaryebwa, and T. E. West, "Presentation, management, and outcomes of sepsis in adults and children admitted to a rural Ugandan hospital: A prospective observational cohort study," *PLoS One*, vol. 12, no. 2, pp. 1–13, 2017.
- [27] F. B. Mayr, S. Yende, and D. C. Angus, "Epidemiology of severe sepsis," *Virulence*, vol. 5, no. 1, pp. 1–11, 2014.
- [28] C. Fleischmann et al., "Fallzahlen und sterblichkeitsraten von sepsis-patienten im krankenhaus," *Dtsch. Arztebl. Int.*, vol. 113, no. 10, pp. 159–166, 2016.
- [29] H. Burchardi and H. Schneider, "Economic aspects of severe sepsis: a review of intensive care unit costs, cost of illness and cost effectiveness of therapy," *Pharmacoeconomics*, vol. 22, no. 12, pp. 793–813, 2004.
- [30] E. M. Dannemiller, "Impact of Time to Antibiotics on Survival in Patients with Severe Sepsis or Septic Shock in whom Early Goal-directed Therapy was Initiated in the Emergency Department," *J. Emerg. Med.*, vol. 39, no. 3, p. 393, 2010.
- [31] J. Chvojka and M. Matějovič, "[International guidelines for management of severe sepsis and septic shock 2012 - comment].," *Vnitřní lékařství*, vol. 60, no. 1, pp. 59–67, 2014.
- [32] B. L. Thomas, "Recovery from Post - Sepsis Syndrome :," pp. 1–5.
- [33] National Clinical Effectiveness Committee (NCEC), "Sepsis Management, National Clinical Guideline No. 6," no. 6, p. 110, 2014.
- [34] D. M. Yealy et al., "Recognizing and managing sepsis: What needs to be done?," *BMC Med.*, vol. 13, no. 1, pp. 1–10, 2015.

- [35] "Dr Vida Hamilton MB FCARCSI JFICMI National Clinical Lead Sepsis."
- [36] HSE, "Sepsis Form - In-Patient Adult," vol. 4, pp. 1–2.
- [37] S. Gupta, A. Sakhuja, G. Kumar, E. McGrath, R. S. Nanchal, and K. B. Kashani, "Culture-Negative Severe Sepsis: Nationwide Trends and Outcomes," *Chest*, vol. 150, no. 6, pp. 1251–1259, Dec. 2016.
- [38] M. Jin and A. I. Khan, "Procalcitonin: Uses in the Clinical Laboratory for the Diagnosis of Sepsis," *Lab. Med.*, vol. 41, no. 3, pp. 173–177, 2010.
- [39] A. Kumar et al., "Duration of hypotension before initiation of effective antimicrobial therapy is the critical determinant of survival in human septic shock," *Crit. Care Med.*, vol. 34, no. 6, pp. 1589–1596, 2006.
- [40] J. P. Lynch, N. M. Clark, and G. G. Zhanel, "Evolution of antimicrobial resistance among Enterobacteriaceae (focus on extended spectrum β -lactamases and carbapenemases)," *Expert Opin. Pharmacother.*, vol. 14, no. 2, pp. 199–210, 2013.
- [41] R. Dellinger, M. Levy, and A. Rhodes, "Surviving Sepsis Campaign: international guidelines for management of severe sepsis and septic shock, 2012," *Intensive care ...*, vol. 41, no. 2, pp. 580–637, 2013.
- [42] F. M. Brunkhorst et al., "Effect of empirical treatment with moxifloxacin and meropenem vs meropenem on sepsis-related organ dysfunction in patients with severe sepsis: A randomized trial," *JAMA - J. Am. Med. Assoc.*, vol. 307, no. 22, pp. 2390–2399, 2012.
- [43] M. Sinha, J. Jupe, H. Mack, T. P. Coleman, S. M. Lawrence, and S. I. Fraley, "Emerging Technologies for Molecular Diagnosis of Sepsis," *Clin. Microbiol. Rev.*, vol. 31, no. 2, Apr. 2018.
- [44] L. Bissonnette and M. G. Bergeron, "Diagnosing infections--current and anticipated technologies for point-of-care diagnostics and home-based testing," *Clin. Microbiol. Infect.*, vol. 16, no. 8, pp. 1044–1053, 2010.
- [45] S. L. in. Chong, G. Y. K. Ong, A. Venkataraman, and Y. H. we. Chan, "The golden hours in paediatric septic shock--current updates and recommendations," *Ann. Acad. Med. Singapore*, vol. 43, no. 5, pp. 267–274, 2014.
- [46] A. Mellmann et al., "Evaluation of matrix-assisted laser desorption ionization-time-of-flight mass spectrometry in comparison to 16S rRNA gene sequencing for species identification of nonfermenting bacteria," *J. Clin. Microbiol.*, vol. 46, no. 6, pp. 1946–1954, 2008.
- [47] P. Seng et al., "Ongoing Revolution in Bacteriology: Routine Identification of Bacteria by Matrix-Assisted Laser Desorption Ionization Time-of-Flight Mass Spectrometry," *Clin. Infect. Dis.*, vol. 49, no. 4, pp. 543–551, 2009.
- [48] L. Ferreira et al., "Identification of fungal clinical isolates by matrix-assisted laser desorption ionization-time-of-flight mass spectrometry," *Rev. Esp. Quimioter.*, vol. 26, no. 3, pp. 193–197, 2013.
- [49] G. Peralta, M. J. Rodríguez-Lera, J. C. Garrido, L. Ansorena, and M. P. Roiz, "Time to positivity in blood cultures of adults with *Streptococcus pneumoniae* bacteremia," *BMC Infect. Dis.*, vol. 6, pp. 1–8, 2006.
- [50] A. Afshari, J. Schrenzel, M. Ieven, and S. Harbarth, "Bench-to-bedside review: Rapid molecular diagnostics for bloodstream infection - a new frontier?," *Crit. Care*, vol. 16, no. 3, 2012.

- [51] J. Wain et al., "Quantitation of Bacteria in Blood of Typhoid Fever Patients and Relationship between Counts and Clinical Features, Transmissibility, and Antibiotic Resistance Quantitation of Bacteria in Blood of Typhoid Fever Patients and Relationship between Counts an," vol. 36, no. 6, pp. 1683–1687, 1998.
- [52] F. R. Cockerill et al., "Optimal testing parameters for blood cultures.," Clin. Infect. Dis., vol. 38, no. 12, pp. 1724–30, 2004.
- [53] W. I. Gonsalves, N. Cornish, M. Moore, A. Chen, and M. Varman, "Effects of volume and site of blood draw on blood culture results," J. Clin. Microbiol., vol. 47, no. 11, pp. 3482–3485, 2009.
- [54] R. G. Patton and T. Schmitt, "Innovation for reducing blood culture contamination: Initial specimen diversion technique," J. Clin. Microbiol., vol. 48, no. 12, pp. 4501–4503, 2010.
- [55] C. Kassis, G. Rangaraj, Y. Jiang, R. Y. Hachem, and I. Raad, "Differentiating culture samples representing coagulase-negative staphylococcal bacteremia from those representing contamination by use of time-to-positivity and quantitative blood culture methods," J. Clin. Microbiol., vol. 47, no. 10, pp. 3255–3260, 2009.
- [56] O. Opota, A. Croxatto, G. Prod'hom, and G. Greub, "Blood culture-based diagnosis of bacteraemia: state of the art," Clin. Microbiol. Infect., vol. 21, no. 4, pp. 313–322, Apr. 2015.
- [57] T. J. Kirn and M. P. Weinstein, "Update on blood cultures: How to obtain, process, report, and interpret," Clin. Microbiol. Infect., vol. 19, no. 6, pp. 513–520, 2013.
- [58] O. Opota, K. Jaton, and G. Greub, "Microbial diagnosis of bloodstream infection: Towards molecular diagnosis directly from blood," Clin. Microbiol. Infect., vol. 21, no. 4, pp. 323–331, 2015.
- [59] L. Garibyan and N. Avashia, "Research Techniques Made Simple: Polymerase Chain Reaction (PCR)," J. Invest. Dermatol., vol. 133, no. 3, pp. e6–e6, Mar. 2013.
- [60] T. C. Lorenz, "Polymerase Chain Reaction: Basic Protocol Plus Troubleshooting and Optimization Strategies," J. Vis. Exp., no. 63, p. 3998, May 2012.
- [61] F. M. Munari et al., "A combined enrichment/polymerase chain reaction based method for the routine screening of Streptococcus agalactiae in pregnant women," Brazilian J. Microbiol., vol. 43, no. 1, pp. 253–260, 2012.
- [62] C. J. Smith and A. M. Osborn, "Advantages and limitations of quantitative PCR (Q-PCR)-based approaches in microbial ecology," FEMS Microbiol. Ecol., vol. 67, no. 1, pp. 6–20, 2009.
- [63] "Microfluidics and Microfabrication  Coverage of the fundamentals of microfluidics at a level accessible to multi-disciplinary researchers, and with a balance of mathematical details and physics principles  Shows how the life sciences and chemistry can," vol. 49, no. 0, p. 6221, 2010.
- [64] a Akane, K. Matsubara, H. Nakamura, S. Takahashi, and K. Kimura, "Identification of the heme compound copurified with deoxyribonucleic acid (DNA) from bloodstains, a major inhibitor of polymerase chain reaction (PCR) amplification.," J. Forensic Sci., vol. 39, no. 2, pp. 362–372, 1994.
- [66] J. Hoorfar, P. Wolffs, and P. Rådström, "Diagnostic PCR: Validation and sample preparation are two sides of the same coin," Apmis, vol. 112, no. 11–12, pp. 808–814, 2004.

- [67] C. Feldman et al., "Severity of illness scoring systems in patients with bacteraemic pneumococcal pneumonia: Implications for the intensive care unit care," *Clin. Microbiol. Infect.*, vol. 15, no. 9, pp. 850–857, 2009.
- [68] J. A. Carriço, A. J. Sabat, A. W. Friedrich, and M. Ramirez, "Bioinformatics in bacterial molecular epidemiology and public health: databases, tools and the next-generation sequencing revolution , on behalf of the ESCMID Study Group for Epidemiological Markers (ESGEM)," *Eurosurveillance*, vol. 18, no. 4, pp. 1–9, 2013.
- [69] X. Zhao, C. Lin, J. Wang, and D. Oh, "Advances in rapid detection methods for foodborne pathogens," *J. Microbiol. Biotechnol*, vol. 24, no. 3, pp. 297–312, 2014.
- [70] J. P. Casalta, F. Gouriet, V. Roux, F. Thuny, G. Habib, and D. Raoult, "Evaluation of the LightCycler® SeptiFast test in the rapid etiologic diagnostic of infectious endocarditis," *Eur. J. Clin. Microbiol. Infect. Dis.*, vol. 28, no. 6, pp. 569–573, 2009.
- [71] H. Westh et al., "Multiplex real-time PCR and blood culture for identification of bloodstream pathogens in patients with suspected sepsis," *Clin. Microbiol. Infect.*, vol. 15, no. 6, pp. 544–551, 2009.
- [72] D. Bravo et al., "Diagnostic accuracy and potential clinical value of the LightCycler SeptiFast assay in the management of bloodstream infections occurring in neutropenic and critically ill patients," *Int. J. Infect. Dis.*, vol. 15, no. 5, pp. 326–331, 2011.
- [73] M. D. Moore and L.-A. Jaykus, "Development of a Recombinase Polymerase Amplification Assay for Detection of Epidemic Human Noroviruses," *Sci. Rep.*, vol. 7, p. 40244, Jan. 2017.
- [74] A. T. Hall, A. M. Zovanyi, D. R. Christensen, J. W. Koehler, and T. D. Minogue, "Evaluation of Inhibitor-Resistant Real-Time PCR Methods for Diagnostics in Clinical and Environmental Samples," vol. 8, no. 9, pp. 1–8, 2013.
- [75] J. Macdonald, F. Von Stetten, and J. Macdonald, "Review: a comprehensive summary of a decade development of the recombinase polymerase amplification," vol. 144, no. 1, 2019.
- [76] K. Shahin, J. G. Ramirez-paredes, G. Harold, B. Lopez-, A. Adams, and M. Weidmann, "Development of a recombinase polymerase amplification assay for rapid detection of *Francisella noatunensis* subsp . *orientalis*," no. 1582014, pp. 1–21, 2018.
- [77] W. Xing et al., "Field evaluation of a recombinase polymerase amplification assay for the diagnosis of *Schistosoma japonicum* infection in Hunan province of China," pp. 1–7, 2017.
- [78] A. Rosser, D. Rollinson, M. Forrest, and B. L. Webster, "Isothermal Recombinase Polymerase amplification (RPA) of *Schistosoma haematobium* DNA and oligochromatographic lateral flow detection," *Parasit. Vectors*, pp. 1–5, 2015.
- [79] C. Vernozy-Rozand, C. Mazuy-Cruchaudet, C. Bavai, and Y. Richard, "Comparison of three immunological methods for detecting staphylococcal enterotoxins from food," *Lett. Appl. Microbiol.*, vol. 39, no. 6, pp. 490–494, 2004.
- [80] R. Ye et al., "Bioinspired Synthesis of All-in-One Organic – Inorganic Hybrid Nanoflowers Combined with a Handheld pH Meter for On-Site Detection of Food Pathogen," pp. 3094–3100, 2016.
- [81] R. Chen, X. Huang, H. Xu, Y. Xiong, and Y. Li, "Plasmonic Enzyme-Linked

- Immunosorbent Assay Using Nanospherical Brushes as a Catalase Container for Colorimetric Detection of Ultralow Concentrations of *Listeria monocytogenes*,” *ACS Appl. Mater. Interfaces*, vol. 7, no. 51, pp. 28632–28639, Dec. 2015.
- [82] T. D. Tran and M. Il Kim, “Organic-Inorganic Hybrid Nanoflowers as Potent Materials for Biosensing and Biocatalytic Applications,” *BioChip J.*, vol. 12, no. 4, pp. 268–279, 2018.
- [83] T. Wei, D. Du, M.-J. Zhu, Y. Lin, and Z. Dai, “An Improved Ultrasensitive Enzyme-Linked Immunosorbent Assay Using Hydrangea-Like Antibody–Enzyme–Inorganic Three-in-One Nanocomposites,” *ACS Appl. Mater. Interfaces*, vol. 8, no. 10, pp. 6329–6335, Mar. 2016.
- [84] T. K. Mandal and N. Parvin, “Rapid Detection of Bacteria by Carbon Quantum Dots,” vol. 7, no. 6, pp. 846–848, 2011.
- [85] M. Sajid and M. Daud, “Designs , formats and applications of lateral flow assay : A literature review,” *J. Saudi Chem. Soc.*, vol. 19, no. 6, pp. 689–705, 2015.
- [86] W. Lai and Y. Xiong, “Author ’ s Accepted Manuscript,” *Biosens. Bioelectron.*, 2015.
- [87] J. Park, J. H. Shin, and J. K. Park, “Pressed Paper-Based Dipstick for Detection of Foodborne Pathogens with Multistep Reactions,” *Anal. Chem.*, vol. 88, no. 7, pp. 3781–3788, 2016.
- [88] S. Shan, W. Lai, Y. Xiong, H. Wei, and H. Xu, “Novel Strategies To Enhance Lateral Flow Immunoassay Sensitivity for Detecting Foodborne Pathogens,” *J. Agric. Food Chem.*, vol. 63, no. 3, pp. 745–753, Jan. 2015.
- [89] W. Chen et al., “LATERAL FLOW TEST STRIP APPROACHES FOR RAPID DETECTION OF FOOD CONTAMINANTS AND PATHOGENS : REVIEW been recommended using two different methods . This strategy comprises :,” vol. 1, no. 12, 2015.
- [90] J. Park, J. H. Shin, and J.-K. Park, “Pressed Paper-Based Dipstick for Detection of Foodborne Pathogens with Multistep Reactions,” *Anal. Chem.*, vol. 88, no. 7, pp. 3781–3788, Apr. 2016.
- [91] Cytodiagnosics, “Lateral Flow Immunoassays - Cytodiagnosics.” [Online]. Available: <http://www.cytodiagnosics.com/store/pc/Lateral-Flow-Immunoassays-d6.htm>. [Accessed: 19-Feb-2019].
- [92] F. Abbasian, E. Ghafar-Zadeh, and S. Magierowski, “Microbiological Sensing Technologies: A Review,” *Bioengineering*, vol. 5, no. 1, p. 20, 2018.
- [93] S. Liébana et al., “Design and development of novel screen-printed microelectrode and microbiosensor arrays fabricated using ultrafast pulsed laser ablation,” *Sensors Actuators B Chem.*, vol. 231, pp. 384–392, Aug. 2016.
- [94] Z. Chang, M. Michel, M. Callanan, N. Johnson, C. Bravo Almeida, and C. Iversen, “Evaluation of indirect impedance for measuring microbial growth in complex food matrices,” *Food Microbiol.*, vol. 42, pp. 8–13, 2014.
- [95] B. Byrne, E. Stack, N. Gilmartin, and R. O’Kennedy, “Antibody-based sensors: Principles, problems and potential for detection of pathogens and associated toxins,” *Sensors (Switzerland)*, vol. 9, no. 6, pp. 4407–4445, 2009.
- [96] L. Yang, Y. Li, C. L. Griffis, and M. G. Johnson, “Interdigitated microelectrode (IME) impedance sensor for the detection of viable *Salmonella typhimurium*,” *Biosens. Bioelectron.*, vol. 19, no. 10, pp. 1139–1147, May 2004.

- [97] L. Yang, C. Ruan, and Y. Li, "Detection of viable *Salmonella typhimurium* by impedance measurement of electrode capacitance and medium resistance," *Biosens. Bioelectron.*, vol. 19, no. 5, pp. 495–502, Dec. 2003.
- [98] M. S. Chiriaco et al., "Towards pancreatic cancer diagnosis using EIS biochips," *Lab Chip*, vol. 13, no. 4, pp. 730–734, 2013.
- [99] E. Primiceri et al., "Automatic transwell assay by an EIS cell chip to monitor cell migration," *Lab Chip*, vol. 11, no. 23, pp. 4081–4086, 2011.
- [100] D. A. Boehm, P. A. Gottlieb, and S. Z. Hua, "On-chip microfluidic biosensor for bacterial detection and identification," *Sensors Actuators B Chem.*, vol. 126, no. 2, pp. 508–514, Oct. 2007.
- [101] A. Manuscript and E. Dysfunction, "NIH Public Access," vol. 25, no. 8, pp. 713–724, 2015.
- [102] D. A. Boehm, P. A. Gottlieb, and S. Z. Hua, "On-chip microfluidic biosensor for bacterial detection and identification," *Sensors Actuators B Chem.*, vol. 126, no. 2, pp. 508–514, Oct. 2007.
- [103] Carbonaro A, "Cell characterization using a protein-functionalized pore.," *Lab Chip*, pp. 1478–85, 2008.
- [104] M. E. Brecher and S. N. Hay, "Bacterial Contamination of Blood Components," vol. 18, no. 1, pp. 195–204, 2005.
- [105] P. J. L. Carson, P. F. Sieber, D. R. Cook, L. Beaupre, P. W. Macaulay, and P. G. G. Rhoads, "Cell detection and counting through cell lysate impedance spectroscopy in microfluidic devices," *Lab Chip*, vol. 385, no. 9974, pp. 1183–1189, 2015.
- [106] V. Gau, S. C. Ma, H. Wang, J. Tsukuda, J. Kibler, and D. A. Haake, "Electrochemical molecular analysis without nucleic acid amplification," *Methods*, vol. 37, no. 1, pp. 73–83, 2005.
- [107] S. A. Barghouthi, "A Universal Method for the Identification of Bacteria Based on General PCR Primers," *Indian J. Microbiol.*, vol. 51, no. 4, pp. 430–444, 2011.
- [108] A. Albulbul, "Evaluating Major Electrode Types for Idle Biological Signal Measurements for Modern Medical Technology," *Bioengineering*, vol. 3, no. 3, p. 20, 2016.
- [109] P. Velásquez et al., "SEM, EDX and EIS study of an electrochemically modified electrode surface of natural enargite (Cu_3AsS_4)," *J. Electroanal. Chem.*, vol. 494, no. 2, pp. 87–95, Dec. 2000.
- [110] J. C. Liao et al., "Use of Electrochemical DNA Biosensors for Rapid Molecular Identification of Uropathogens in Clinical Urine Specimens," vol. 44, no. 2, pp. 561–570, 2006.
- [111] S. Singh, A. Kaushal, S. Khare, and A. Kumar, "DNA chip based sensor for amperometric detection of infectious pathogens," *Int. J. Biol. Macromol.*, vol. 103, pp. 355–359, 2017.
- [112] N. B. Arnfinnsdottir, V. Ottesen, R. Lale, and M. Sletmoen, "The Design of Simple Bacterial Microarrays: Development towards Immobilizing Single Living Bacteria on Predefined Micro-Sized Spots on Patterned Surfaces," *PLoS One*, vol. 10, no. 6, p. e0128162, Jun. 2015.
- [113] D. R. Tobergte and S. Curtis, "Microfluidics- a review," *J. Chem. Inf. Model.*, vol. 53,

no. 9, pp. 1689–1699, 2013.

- [114] R. Gorkin et al., “Centrifugal microfluidics for biomedical applications,” *Lab Chip*, vol. 10, no. 14, p. 1758, 2010.
- [115] J. Ducreé, S. Haeberle, S. Lutz, S. Pausch, F. von Stetten, and R. Zengerle, “The centrifugal microfluidic Bio-Disk platform,” *J. Micromechanics Microengineering*, vol. 17, no. 7, pp. S103–S115, Jul. 2007.
- [116] R. Burger, L. Amato, and A. Boisen, “Detection methods for centrifugal microfluidic platforms,” *Biosens. Bioelectron.*, vol. 76, pp. 54–67, 2016.
- [117] C.-H. C. and M. O. Shaikh, “Label free Impedance Biosensors for Point of Care Diagnostics,” pp. 119–142.
- [118] C. E. Nwankire, A. Venkatanarayanan, T. Glennon, T. E. Keyes, R. J. Forster, and J. Ducreé, “Label-free impedance detection of cancer cells from whole blood on an integrated centrifugal microfluidic platform,” *Biosens. Bioelectron.*, vol. 68, pp. 382–389, Jun. 2015.
- [119] J. Banothu, M. Khanapur, S. Basavoju, R. Bavantula, M. Narra, and S. Abbagani, “Integrating Electrochemical Detection with Centrifugal Microfluidics for Real-Time and Fully Automated Sample Testing,” vol. 2, pp. 22866–22874, 2014.
- [120] T. H. G. Thio et al., “Theoretical development and critical analysis of burst frequency equations for passive valves on centrifugal microfluidic platforms,” *Med. Biol. Eng. Comput.*, vol. 51, no. 5, pp. 525–535, May 2013.
- [121] The Lancet, “Food industry must act to safeguard the future of antibiotics,” *Lancet*, vol. 390, no. 10109, p. 2216, 2017.
- [122] S. Z. Andreasen et al., “Extraction, Enrichment, and in situ Electrochemical Detection on Lab-on-a-Disc: Monitoring the Production of a Bacterial Secondary Metabolite,” *ACS Sensors*, 2018.
- [123] M. Tudorache, I. A. Zdrojewska, and J. Emnéus, “Evaluation of progesterone content in saliva using magnetic particle-based immuno supported liquid membrane assay (m-ISLMA),” *Biosens. Bioelectron.*, vol. 22, no. 2, p. 241–246, Aug. 2006.
- [124] J. H. Shin, Y.-C. Na, J. H. Chung, S. Gorinstein, and Y. G. Ahn, “Quantitative analysis of heterocyclic amines in urine by liquid chromatography coupled with tandem mass spectrometry,” *Anal. Biochem.*, vol. 447, pp. 169–176, Feb. 2014.
- [125] O. Chailapakul et al., “An Electrochemical Compact Disk-type Microfluidics Platform for Use as an Enzymatic Biosensor,” *Electroanalysis*, vol. 27, no. 3, pp. 703–712, 2015.
- [126] M. Madou et al., “Flow-enhanced electrochemical immunosensors on centrifugal microfluidic platforms,” *Lab Chip*, vol. 13, no. 18, p. 3747, 2013.
- [127] J. M. Park, Y. K. Cho, B. S. Lee, J. G. Lee, and C. Ko, “Multifunctional microvalves control by optical illumination on nanoheaters and its application in centrifugal microfluidic devices,” *Lab Chip*, vol. 7, no. 5, pp. 557–564, 2007.
- [128] K. Sanger et al., “Lab-on-a-disc platform for screening of genetically modified *E. coli* cells via cell-free electrochemical detection of p-Coumaric acid,” *Sensors Actuators, B Chem.*, vol. 253, pp. 999–1005, 2017.
- [129] W. H. Self *et al.*, “Diagnostic Accuracy of FebrIDx: A Rapid Test to Detect Immune

Responses to Viral and Bacterial Upper Respiratory Infections," *J. Clin. Med.*, vol. 6, no. 10, p. 94, Oct. 2017.

- [130] M. P. Corcoran, M. Meydani, A. H. Lichtenstein, E. J. Schaefer, A. Dillard, and S. Lamou-Fava, "Sex hormone modulation of proinflammatory cytokine and C-reactive protein expression in macrophages from older men and postmenopausal women," *J. Endocrinol.*, vol. 206, no. 2, pp. 217–224, Aug. 2010.
- [131] N. R. Sproston and J. J. Ashworth, "Role of C-Reactive Protein at Sites of Inflammation and Infection," *Front. Immunol.*, vol. 9, p. 754, Apr. 2018.
- [132] S. U. Eisenhardt, J. R. Thiele, H. Bannasch, G. B. Stark, and K. Peter, "C-reactive protein: How conformational changes influence inflammatory properties," *Cell Cycle*, vol. 8, no. 23, pp. 3885–3892, Dec. 2009.
- [133] V. P. Zav'Yalov, H. Hämäläinen-Laanaya, T. K. Korpela, and T. Wahlroos, "Interferon-inducible myxovirus resistance proteins: Potential biomarkers for differentiating viral from bacterial infections," *Clin. Chem.*, vol. 65, no. 6, pp. 739–750, 2019.
- [134] A. P. Joyce *et al.*, "One mouse, one pharmacokinetic profile: Quantitative whole blood serial sampling for biotherapeutics," *Pharm. Res.*, vol. 31, no. 7, pp. 1823–1833, 2014.
- [135] O. Strohmeier *et al.*, "Centrifugal microfluidic platforms: advanced unit operations and applications," *Chem. Soc. Rev.*, vol. 44, no. 17, pp. 6187–6229, 2015.
- [136] B. S. Lee *et al.*, "Fully integrated lab-on-a-disc for simultaneous analysis of biochemistry and immunoassay from whole blood," *Lab Chip*, vol. 11, no. 1, pp. 70–78, 2011.
- [137] M. Czugala *et al.*, "CMAS: Fully integrated portable centrifugal microfluidic analysis system for on-site colorimetric analysis," *RSC Adv.*, vol. 3, no. 36, pp. 15928–15938, 2013.
- [138] Cytodiagnosics, "Lateral Flow Immunoassays - Cytodiagnosics." .

Chapter 2

Materials and Methods

2.1 Introduction

This Chapter is a compilation of all the fabrication methods and the associated materials used throughout this work and an outline of the basic working principles of the instrumentation. This Chapter only deals with basic methodologies, any specific information regarding particular specific experiments will be discussed in the associated results Chapters.

2.2 Materials Justification

A wide range of materials are used in modern microfluidics and nanoengineering. As reproducibility and accuracy is a top priority for microfluidic chip production, material properties play a huge role in the LOAD/chip functionality. Glass substrates were originally utilized for its appealing optical properties. However, the complicated manufacturing process associated with the material drove the development of the other materials [1]. Polymers such as Poly (dimethyl siloxane) (PDMS) and Poly(methyl-methacrylate) (PMMA) are the main materials associated with microfluidics due to their excellent optical properties, cost and ease of fabrication [2]. PDMS cast from UV lithography master Si wafers have also been commonly used for micro-contact printing of antibody surfaces, which is demonstrated in Chapter 4. The microfluidic devices described in Chapter 3 and 4 were fabricated using layers of PMMA with different thicknesses to create various reservoir depths to comply with the function of the device.

2.2.1 Polydimethylsiloxane (PDMS)

This material has been associated with the manufacture of microfluidic chips for decades due to its optical, mechanical and ease of fabrication attributes [2]. The production of silicon masters using traditional UV based photolithography can give rise to extremely intricate designs and channel passageways in PDMS moulds which is highly advantageous at microlitre volume manipulation of fluids [1]. PDMS is a silicon based organic polymer

which is also non-toxic and inert. PDMS is referred to as a two-part system where the siloxane must be mixed with a curing agent at specific ratios. Through-out this body of work a ratio of 10:1 is required to produce specific mechanical properties of moulded PDMS. Increasing the ratio of the cross linking agent increases the rigidity of the PDMS and a decrease of ratio increases the flexibility [3]. This ratio is ideal for the production of PDMS antibody stamps required to produce the biosensor outlined in Chapter 4, as it is rigid enough to manually handle and flexible enough to easily remove from the mould. PDMS itself is naturally hydrophobic in nature, with a contact angle $> 90^\circ$ therefore it may need to be treated to increase the wettability for biological applications [4]. The classification of hydrophobicity and hydrophilicity for a droplet on a surface is shown in Figure 2.1

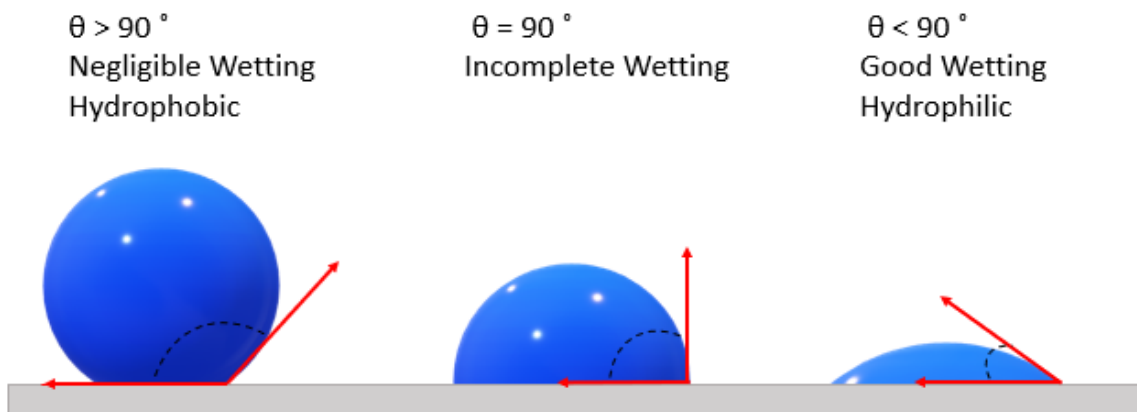


Figure 2.1 Contact angle measurement of hydrophobic and hydrophilic surfaces.

2.2.2 Polymethylmethacrylate (PMMA)

PMMA is an excellent polymer to use in conjunction with other materials to form a microfluidic device [5]. It's non-toxic and a cheap alternative to glass and other optically transparent substances [6]. The fabrication processes associated with PMMA are simple and non-time consuming, compared with glass chip prototyping. Due to its cost effective nature and ease of manufacturability, PMMA is for ideal for LoD manufacturing as it attains desirable qualities for a POC devices [6]. The polymer itself is suitable for bio-processes as it non-toxic and matter inert. The relatively low melting point of PMMA (160°C) is also appropriate for laser ablation for fabrication processes [7]. The hydrophobic nature of PMMA may be seen as undesirable however many surface

treatment techniques have been reported where PMMA's surface chemistry can be altered, through use of plasma or UV/ozone treatments [8].

2.2.3 Pressure Sensitive Adhesive (PSA)

PSA (Pressure Sensitive Adhesive, Adhesives Research, Limerick, Ireland) is a thin roll of Polyethylene Terephthalate (PET) coated with adhesive glue on each side. This material is a strong adhesive substrate which has dual functionality within microfluidic platforms. For the purpose of this work PSA acts as a layer which adjoins corresponding PMMA layers and also contains pre-cut microchannels which have a consistent height of 86 μm . The thickness of the PSA therefore defines the channel height, where the width and length of the channels is then defined by the design and manufactured into the substrate. The PSA experiences adhesive energies of $\sim 100 \text{ J/m}^2$ [9]. The hydrophilic nature of the adhesive layer provides desirable flow characteristics within the assembled devices which also allows the PSA to adhere to low-energy surfaces for correct bonding and sealing. Sheer pressure is applied to the PSA to activate the mechanical properties of the material. This is carried out using a hand roller or a pneumatic laminator [8]. Due to the strong adhering qualities of the adhesive material, the material cannot be reused

2.3 Instrumentation

2.3.1 Computer Aided Design (CAD)

All parts to be manufactured using the instrumentation detailed in Sections 2.3.2, 2.3.3, 2.3.4, and 2.3.7 were originally designed using Computer Aided Design (CAD) software such as Solidworks (2016-2018) and AutoCAD (2017). Dimension size plays a key role in determining the route of manufacture for templates and device layers. The resolution of the physical features needed are an influential factor on the feature sizes in the microfluidic platform to manipulate fluids, which must be determined before the design is created [1]. Soft lithography photomasks can obtain a resolution as low as 0.4 μm where-as the rapid-prototyping can achieve feature widths as low as 400 μm and CO₂ machining can obtain feature sizes of 500 μm . Therefore, the precision and reproducibility were the first determining factor of fabrication methods and must be considered when

designing and manufacturing devices for their intended purpose. For small micron features, photolithographic methods must be implemented as rapid-prototyping of devices with PSA and PMMA constructed layers can only achieve minimum sized features of 400-500 μm . Once the design has been produced using the SOLIDWORKS CAD software, DXF files are extracted and used to produce various components required for experimental work. PMMA layers are produced using CO₂ laser machining (Table 2.1) which can be adhered to pre-cut PSA layers which are produced using a knife cutter-plotter to develop rapid-prototype devices. These layers are then sealed together using alignment rigs and a pressure driven laminator in a clean room setting. Individual specifications for the fabrication processes are discussed below.

2.3.2 Laser Machining

The CO₂ laser machine is primarily used to cut PMMA (Radionics™) of various thicknesses. DXF files are loaded into CorelDraw software which is used to operate the machine. The basic working principle of the Epilog Zing 16 (Epilog Laser, USA) is melting and vaporising the polymers once the focused CO₂ beam encounters the top surface of the PMMA. The laser bed has a working area of 400mm x 300mm, allowing for multiple layers to cut at once. The machine has a high resolution of 1000 DPI with a max wattage output of 30W, capable of cutting pieces up to a thickness of 17mm. The laser used for the duration of this work has a focal length of 50.8mm and a spot size of 0.1016mm according to the Epilog Zing user guide. Laser parameters are altered to suit the specifications of the cut needed. *Table 2-1* provides these optimised settings for the cutting of different thicknesses of PMMA.

Table 2-1 *CorelDraw parameters necessary for complete laser ablation of varying thicknesses of PMMA*

PMMA thickness	Vector Speed (%)	Vector Power (%)
2 mm	18	35
1.5 mm	20	24
1 mm	25	20
0.5 mm	20	18

A secondary raster setting option can be included to create etched wells or features onto the surface of the PMMA which is displayed in *Table 2-2*.

Table 2-2 CorelDraw parameters necessary for etched features of certain depths on PMMA surfaces

Raster Depth	Raster Speed (%)	Raster Power (%)
0.6mm	35	95
0.3mm	50	75

For LoAD manufacturing, four layers are produced using the CO₂ laser; i.e., Vents, Reservoirs, Midlayer and Raster Base. These are discussed in detailed in Chapter 3.

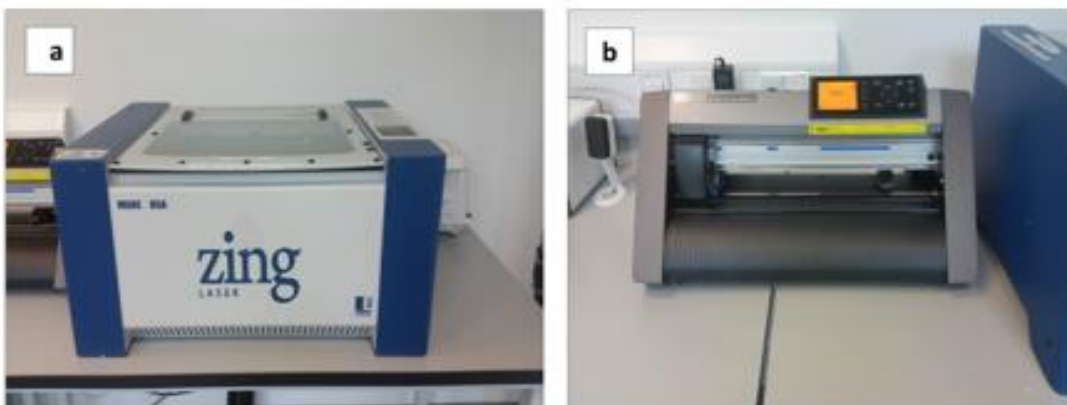


Figure 2.2 Epilog Zing CO₂ laser used for manufacture of PMMA layers (b) GraphTec cutter-plotter used in the production of PSA layers.

2.3.3 Xerography

Xerography is the process of graphics production into PSA segments used for the rapid prototyping of microstructures in the adhesive layer. This method is widely used in microfluidic rapid prototyping [10]. Commonly referred to as a motorised knife plotter-cutter, the Graphtec Cutter Plotter CE6000-40 (MDP Supplies, Ireland) was here. Designs extracted from the 3D SolidWorks model are loaded into the GraphTec studio software. PSA layers are adhered to a transfer sheet and loaded into the machine, where the origin point and cutting forces are set. Both speed and cut forces are adjusted for specific PSA layers. These parameters will be discussed when associated with specific layers in later working Chapters. The reproducibility of microchannel deteriorates with widths of 400

μm and lower where microscope images to determine channel widths of set dimensions of $400 \mu\text{m}$ produced channels of varying distances of $386.23 \pm 190.6 \mu\text{m}$.

2.3.4 Dissolvable Film Tabs

Dissolvable films (DFs) are used in microfluidic LoDs for reagent storage and timed released mechanisms for integrated and automated assay deliverance which allows for a continuous test and eliminates the need for pipetting and reagents loading throughout the test [11]. They act as a liquid barrier in the platform by sealing off the liquid path due to a pressure build up. Once this pressure is overcome by an external force and the DF is wetted, the liquid can be transported to the secondary channel or reservoir. In accordance to the following work, these DFs are designed in a valve format and physically inserted into the LoD [8]. DFs play an extremely important role in the automation of the devices optimised in this work. They allow for a full assay to be performed with pre-loaded reagents which is highly beneficial for minimising cross-contamination [12].

Throughout this work, one main type of DF was used. The low-cost Embroidery film (Barnyarns, Ripon, UK; Avalon) is composed of mostly PVA. Extensive characterisation has been carried out to test the dissolution times of this DF [13]. Further characterisation studies have been carried out and discussed in Chapter 3.

The GraphTec is utilised for the production of the DF tabs. An array of inner and outer circles or slots are created on the GraphTec studio software. The GraphTec is programmed to cut the inner array of structures first, which must be removed first. This inner hole is the liquid passageway through the tab. The top clear protective plastic is removed, and the DF is carefully placed upon the exposed PSA and firmly secured by applying pressure using a hand roller. The secondary cut is applied, and the outer circle or slot is cut to give the shape of the tab. These tabs are stored in a zip-lock bag until assembly to avoid air moisture weakening the DF. Figure 2.3 displays the basic example of a DF tab, where in inner diameter is 1.5mm and outer diameter is 3mm.

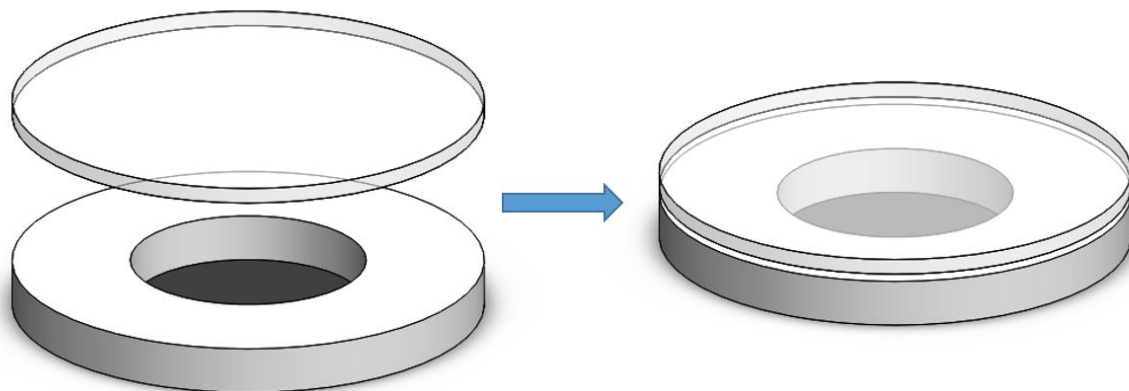


Figure 2.3 Design of a DF tab, where the top layer is the dissolvable film and the secondary Section is the PSA ring for liquid passage and adhesion of DF tab to underlying PMMA layer.

2.3.5 UV Lithography

Photolithography is a multi-stage process in which a photomask is designed and produced and is used in conjunction with a mask aligner and UV source lamp to produce cross-linked structures on a SU-8 covered Si wafer. Soft lithography was used to create a silicon master in which PDMS was poured to create the antibody transferring stamps used in Chapter 4 for micro contact patterning of the capture probes on electrode surfaces. This process can yield high resolution structures of approximately $0.4\ \mu\text{m}$. The desired designed in created using SolidWorks and AutoCAD for the photomask production. The negative master platform is manufactured within clean-room settings where is undergoes surface treatment for PDMS moulding.

A photomask is required for the manufacture of the Si master. The desired file is used in conjunction with the Heidelberg DWL 66fs, where the instrument uses highly accurate lasers to polymerise the image file upon a pre-coated photoresist chrome mask. The photomask used was an opaque glass plate with patterned transparencies that allowed the UV light to shine through in a defined sections which polymerises the photoresist underneath. Chrome is a common material, called the absorber, used to create the surrounding pattern due to its opacity and adhesion properties. Chrome is highly efficient as an anti-reflective coating in the UV spectrum which would minimise reflection onto the polymer causing double exposure to the resist. It and can also have a

very thin stack of 100nm which allows the photomask and resist coated Si wafer to come into close proximity to one another [14].

The resist used for chrome photomask production was a positive resist, meaning the areas exposed to the laser are un-polymerised where-as the area unexposed to the laser were polymerised. The chrome mask must be developed to remove the unpolymerized resist once laser etching is complete. The developer used was AZ 351B Developer (Microchemicals™). A development time of 60 seconds is sufficient in order to produce the chrome photomask. A ratio of 1:4 with DI water was used for this step. The photomask was washed with DI water and gently dried with N₂. The photoresist slide is then coated with chrome, by placing the mask into a glass bath of chrome etch 18 (MRT, UK) solution for 90 seconds. The chrome mask was rinsed with DI water and dried again with N₂. The production of the chrome photomask allows the production of the Si masters for PDMS production.

2.3.5.1 Fabrication of the negative silicon master with 25 μm structure height, using SU-8 2000 photoresist

The basic procedure of UV photolithography is composed of seven separate process steps. Firstly, the substrate was pre-treated. This ensures no impurities exist the surface which may affect the photoresist structures forming correctly. In this case, Si wafers are used. The wafer can be immersed in Piranha etch or ethanol, rinsed with DI water and dried with N₂. The wafer was then carefully placed onto the spin coater and attached using a vacuum jig, where the mixture was slowly added to the centre of the wafer. 4ml of the negative photoresist was dispensed onto the middle of the surface.

The selected program has a spin speed of 500 rpm (accelerated with a rate of 100 rpm/s) for 5-10 seconds once the speed of 500 rpm was reached and increased to 3000 rpm (accelerated with a rate of 300 rpm/s) for 30 seconds. This creates a thin layer of the thinned SU-8 mixture on the surface. This will give an approximate film thickness of ~25μm. This film thickness is due to the viscosity of the SU8 and the spin-speed applied. Next, the wafer undergoes a soft-bake, where for features of 25-40 μm a temperature

range of 65 °C for 3 minutes was used followed by an increase to 95 °C for 6 minutes. This process was to ensure that the solvent evaporates to make the SU8 more rigid.

The SU8 wafer is placed underneath the chrome mask in the mask aligner before the UV lamp is switched on. Using the X and Y stage dials, the mask must be adjusted to sit directly over the wafer. A Z dial is also present to bring the wafer into contact with the mask. An interference pattern is visible once the Z positioning is achieved. The “hard contact” switch is activated to ensure direct contact between mask and wafer to minimise diffraction patterns once the UV lamp was active and to minimise light scattering which affects feature size.

The UV bulb radiation has an intensity of 250 W/cm². Safety goggles must be worn to avoid retinal damage during this time. The wafer now undergoes a post exposure bake where the wafer is placed on a hot plate for 1 minute at 65°C and increased to 95°C for 6 minutes. The UV exposure provides the SU8 with the energy required to activate the photoactive component of the resist, however the post exposure bakes provides the additional energy for the completion of the reaction. The wafer was then removed and allowed to cool to room temperature. The wafer is then placed in a developer bath for 4-5 minutes at 70 oscillations per minute. The wafer is rinsed with IPA and dried with N₂ and hard baked for 30 minutes at 150 °C. This step evaporates any residual solvent and improves cross-linking. This procedure was adapted from the MicroChem protocol for a variety of SU8 types [15]. Once the silicon master was cooled the surface must be treated to become hydrophobic. The surface treatment will allow to the master to be re-usable as the PDMS will easily release from the surface once cured.

A simple method to create a hydrophobic surface was to place 1µl of Octadecyl trichlorosilane (OTS) (Sigma Aldrich, Ireland) in a 2mL centrifuge tube and place within a vacuum chamber with the master. This was left under vacuum for one hour, where the OTS evaporates. The wafer was then placed on a hot plate at 100° for 30 minutes. Plasma cleaning may also be used to create a hydrophilic surface.

2.3.6 Casting of PDMS on Master

The negative silicon master produced by photolithography was adhered onto the base of a large cell culture dish using PSA. This master containing the desired pattern onto which a PDMS mixture is poured. A 10:1 ratio of the siloxane and curing agent was mixed thoroughly. The visible bubbles within the mixture provide evidence of good mixing through the PDMS. This is poured onto the master and placed under vacuum for one hour to remove the trapped air bubbles that may cause defects within the mould. The PDMS was then placed in an oven for one hour at 70°C for curing.

2.3.7 3D Printing

The purpose of the 3D printed segments was to provide an alternative approach to manufacturing various components of the microfluidic platforms for mass production of the components. 3D printing can be quite slow for part production and can take hours for a complete model to be manufactured. For mass production to be feasible using this type of machine, multiple printers would have to be used in tandem. Injection moulding is the ideal solution for true mass production, as the part-per cycle time ranges from two seconds to two minutes, depending on the complexity of the part [16]. The cost of initial setup for injection moulding can be very expensive, as the tooling of the mould is an intricate process. It is advised to optimise the part using 3D printing and then use injection moulding as the final, mass production stage [17].

Three-dimensional (3D) printing has the ability to produce complex structures with good resolution and is widely used in microfluidic LOC production [18]. The basic working principle of the 3D printed model is a free-form model created by laying down successive layers of solid and support material. This process continues to build up until all the CAD data sets have been realised. It has been reported that microchannels can be printed with a high resolution of 100µm [19], making the production of a LOC a simple, elegant process where no further assembly or modification is necessary [20]. The 3D printer utilised for this work was a µPrint Plus (Stratasys, Germany). The µPrint Plus is capable of creating a layer thickness of 0.254 mm and a resolution of 0.254 mm, where the max build size is

203.2 × 203.2 × 152.4 mm. The material used is Acrylonitrile butadiene styrene (ABS) polymer.

2.4 Experimental Procedures

2.4.1 Electrochemical Cells and Electrode Fabrication

A typical electrochemical cell contains a 3-electrode setup. The electrochemical measurements were carried out on the CH instruments 760 E model potentiostat. Initially, all gold electrodes must be polished to ensure a smooth, uniform surface free of any contaminants. The 2mm gold disc is polished with 0.3 μm alumina paste on a polishing pad, followed by polishing with a 0.05 μm alumina paste for up to 10 minutes with a wash step in between. The electrode is then washed thoroughly with Milli-Q water and ethanol followed by a 5 minute sonication in MilliQ water. The cell was used at room temperature (20 ± 2°C) for measurement acquisition. In all cases where this setup is used, the reference electrode was a silver/silver chloride (Ag/AgCl in 3M KCl), the counter is a large area coiled platinum wire, and the working electrode is a 2mm gold disc electrode. To determine the surface roughness of an electrode, and therefore, how clean it is, cyclic voltammetry (CV) was carried out in 0.1 M degassed H₂SO₄. This CV measurement determines the microscopic area and the roughness factor, which is a result of microscopic to geometric area. The scanning parameters consist of scanning between 0 V and 1.5 V at a scan rate of 0.1 V/s. The area under the gold oxide reduction peak (typically around 0.8 V) is used to analyse the roughness factor and electrochemical area. Three equations are applied to determine the geometrical area of the electrode A_g (0.0314 cm²), the electrochemical area EA where A_p is the area under the reduction peak and RF, the roughness factor of the electrode. Equation 2-1, Equation 2-2 and Equation 2-3 detail each set required to calculate the surface roughness.

Equation 2-1

$$A_g = \pi r^2$$

Equation 2-2

$$A_p = \frac{A_p}{390 \mu C cm^{-2}}$$

$$RF = \frac{A_p}{A_g}$$

2.4.2 Self Assembled Monolayers

For the purpose of the pathogen sensor fabrication outlined in Chapter 3 the gold disc electrodes are placed in 16- MHDA acid (1mM in EtOH) for 24 hrs to allow time for the adsorption of the layer onto the gold surface. They are rinsed with 0.1 M DPSB and dried using N₂. The carboxylic acid of the 16-MHDA self-assembling monolayer (SAM) layer is converted to an active NHS ester by incubating the electrode with EDC/NHS (15mM/5mM) for 15 minutes at room temperature. SAMs were formed by adsorbing the alkanethiol onto the gold surface through the formation of an alkanethiol functional group. An EDC/NHS coupling layer was incubated on the surface of the freshly cleaned gold disc electrodes to form a carboxyl group which will form a complex with a primary amine. The NHS solution stabilised the amine reactive intermediate by converting it to an amine-reactive Sulfo-NHS ester and therefore increasing the efficiency and stability of the EDC mediated coupling reaction. The SAM modifies the surface to allow for biomolecular layers to form and remain stable.

2.4.3 Gold Electrode Preparation

For the microfluidic platform developed in Chapter 3 and tested in Chapter 4, disposable bacterial sensors were developed to be utilised for the capture and detection of harmful pathogens. Gold coated surfaces were chosen as the sensor base due to its excellent electrochemical response and high biocompatibility [21]. The gold electrode surfaces used in Chapter 4 are modified to increase hydrophilicity to promote antibody adhesion which is discussed in this Section 2.4.4. To modify the surface for antibody cell capture, the 4" Au coated Si wafers (Platypus) must be diced into 30mm x 5mm sized electrodes. This was carried out using a wafer scribe. Similar to the GraphTec, the wafer scribe uses a blade to trace out the inputted parameters to separate the Au wafer to the individual electrode sizes. The preparation of the Au diced electrodes was carried out by Dr. Elaine Spain in the CRANN institute in Trinity College, Dublin.

2.4.4 Hydrophilic Treatment of Gold Electrodes

The single use diced Au electrodes displayed hydrophobic properties, an unfavourable characteristic whilst dealing with biosensors [20]. This was possibly caused by contaminants on the surface. In order to clean the surface to reveal the hydrophilic characteristics of the Au surface the electrodes were prepared using a two-step system. Firstly, the electrodes were sonicated in EtOH for 10 minutes. This cleans organic matter off the Au surface and therefore will make the surface hydrophilic [22]. When an organic contaminant is present on the surface, the contact angle of a water droplet with the surface will be high, therefore after the contaminant is removed, the contact angle will be reduced, increasing the wettability of the surface [23].

Secondly, the electrodes were rinsed with DI water and dried with N₂ and placed into the UV Ozone Cleaner – ProCleaner™ Plus (Bioforce, Nanosciences) for forty minutes. The UV/Ozone treatment is intended to remove any remaining organic contamination on the surface. It operates using a high intensity mercury vapor lamp which was capable of generating 254 nm light which detaches molecules from a surface. A secondary emission of 185 nm light converts the present atmospheric pressure into reactive ozone. This penetrates smaller molecules and cleaves them from the Au veneer [24].

2.4.5 Electrochemical Deposition of Au on Au coated Si Electrode

In order to make the Au coated Si electrodes more suitable for antibody adsorption a thin layer of electrochemically deposited gold was grown on the surface. This increases the surface roughness of the electrode which allows for between antibody layer formations [25]. A traditional three electrode system was setup; where a platinum wire Counter Electrode (CE), Ag/AgCl Reference Electrode (RE), and the desired gold working electrode (WE) on which gold is to be deposited, are immersed into a 25mL beaker containing the gold plating solution (Technic Inc., USA). Applying the amperometric IT curve program on the Metrohm Autolab potentiostat (Metrohm, UK) with the parameters of -0.7 V for the starting potential, with a current of 10mA for 4 seconds. The gold electrode is then removed and washed with dH₂O, dried with a N₂ and placed under vacuum until use.

2.4.6 PDMS Micro-Contact Printing Stamp Preparation

Micro-contact printing was used to create an antibody patterned surface on the single use gold electrodes. This process was used to control the antibody functionalised section on the electrode. The PDMS photomask was prepared using the stated procedure in Section 2.3.5. An array of $10\mu\text{m} \times 10\mu\text{m}$ squares form the pattern with a $10\mu\text{m}$ pitch present on the Si master was used for micro-contact printing stamp production. A 10:1 mixture of PDMS elastomer and curing agent is thoroughly mixed and carefully poured over the silicon master. This was placed under vacuum for one hour to degas the PDMS and avoid air bubbles causing defects on the PDMS mould. The PDMS was cured for one hour in a convection oven where the polymer is now rigid and can be easily removed from the pre-treated silicon master. PDMS is inherently hydrophobic and required further treatment to alter the surface chemistry. The PDMS mould is placed into a O_2 RF Plasma generator under vacuum conditions, with 100 mTorr of O_2 for 5 minutes. This process is shown in Figure 2.4

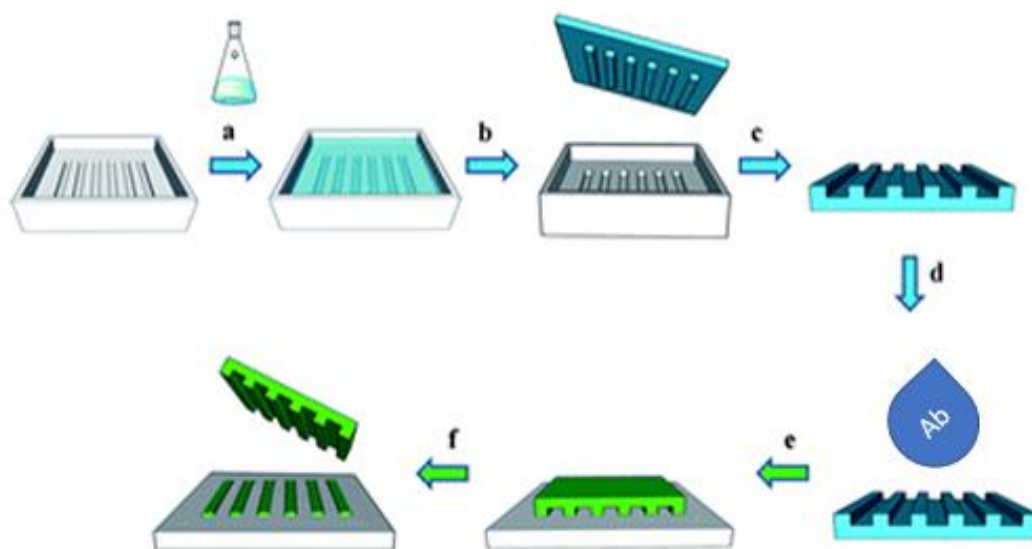


Figure 2.4 Micro-contact printing process (a) PDMS is poured onto the silicon master (b) The cured PDMS is removed revealing (c) the micropillars. The PDMS is diced squares (d) the antibody is incubated onto the stamp and dried with N_2 , (e) the antibody incubated stamp placed on gold electrode, (f) antibody patterning on the surface is observed.

2.5 Assembly of Platforms and Clean Room Procedures

Once all PMMA and PSA layers are fabricated, the Lab-on-a-disc (LoaD) platform was assembled in a class 1000 clean room. The equipment shown in Figure 2.5 was needed to ensure correction alignment of layers between the lamination process. All PMMA layers are cleaned with 70% isopropanol and dried with N₂. PMMA layers are adhered to PSA cut-outs. The LoaDs were built up, layer by layer, with consecutive lamination between each build. A standard centrifugal microfluidic disc consists of four PSA layers and four PMMA layers, as shown in Figure 2.6.

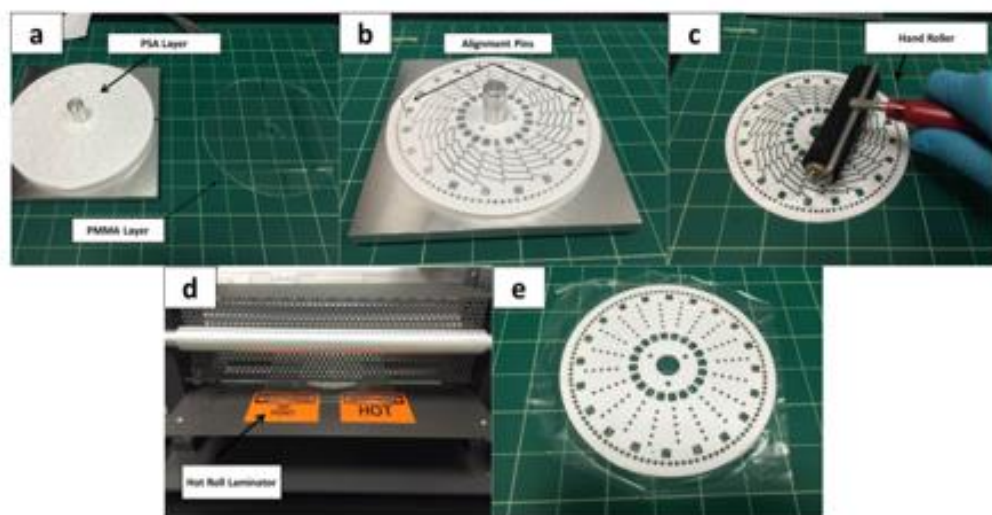


Figure 2.5 (a) PSA layer placed on alignment rig with protective plastic removed with pre-cleaned PMMA layer. (b) Alignment pins inserted through PSA layer with PMMA now attached. (c) PMMA and PSA layers and rolled together using hand-roller. (d) Disc is inserted into hot roll laminator for correct adhesion (e) Fully assembled disc vacuum sealed for testing. Credit: Danielle Chung

Layer 1 of the device is comprised of 2mm PMMA containing an array of holes acting as entry points for loading samples and reagents into the lower layers of the device. These holes are also used as venting mechanisms to ensure fluid flow throughout the system.

Layer 2 of the device contains an assortment of microchannels necessary for the routing of liquid between specific reservoirs. These microchannels also act as a means of flow

control, where channels are connected to air and pressure chambers. The height of the microchannels is 86 μ m which is defined by the PSA.

Layer 3 of the device is comprised of 2mm PMMA which has an assortment of reservoirs which are required for the storage of the sample, reagents and the waste. This layer also gives depth to the device which is needed for the volume of liquids used.

Layer 4 is the secondary PSA layer which contains access points to the DF tabs once routing of the liquid to their position is activated. This layer also contains air passages needed for air circulation and air compression to aid the control of burst frequency desired for the DF tabs.

Layer 5 is mirrored against layer 4, where the only difference lies with a Section for the DF tab placement. DF tabs are fixed upon this layer, where they will act as a liquid barrier between microchannels and lower-channels,

Layer 6 of the device is the third 2mm PMMA layer which contains reservoirs for storage of the sample, reagent and waste. Once activated, this layer provides passage for liquid travelling from the microchannels, through the DF tab towards lower channels.

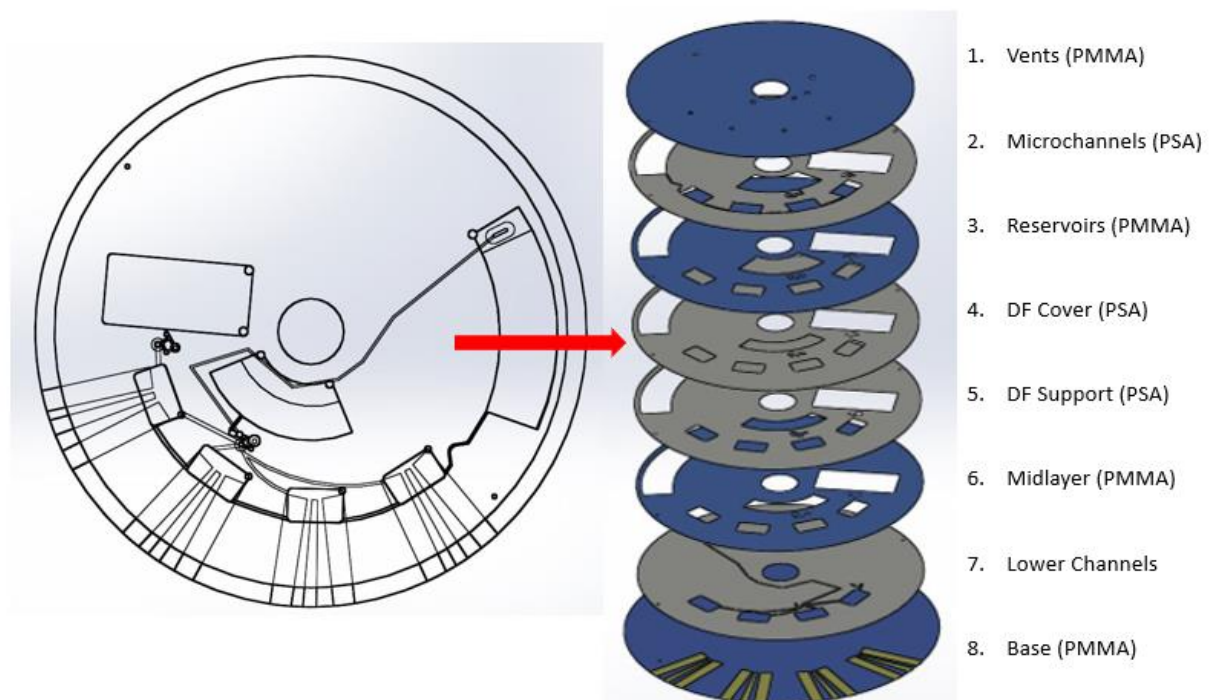


Figure 2.6 Portrays the basic composition of a microfluidic platform. Layers 1, 3, 6 and 8 are PMMA used for liquid storage and rigidity where the remaining layers act a liquid microchannels and through holes for liquid displacement.

Layer 7 contains microchannels for the displacement of liquid from the reagent storage chambers to the detection chamber, and finally the waste chamber.

Layer 8 of the device is a PMMA base disc. The acts as a rigid base and a platform for the insertion of Au electrodes for biological capture and electrochemical detection.

The DF tabs are part of the intricate DF valving system present in the platform between layers four and five. These tabs restrict fluidic movement between the layers of the disc by creating pressure blockade as the fluid approaches the valve. The pressure is overcome by an increase in the angular velocity of the platform and will be discussed in further detail in Chapter 4.

2.6 Fluid Flow in LoD Systems

Certain centrifugally induced forces influence the way in which fluid acts within a disc-based platform [38] and are demonstrated on Figure 2.7. The Coriolis force operates in a perpendicular direction to the centrifugal force. This force can be harnessed in sections of rotating platform where alternating flow-directions are required for particle separation or drift [38]. The Coriolis effect can be considered for these applications however it is typically much smaller in magnitude to that of the centrifugal force, there is often disregarded [39].

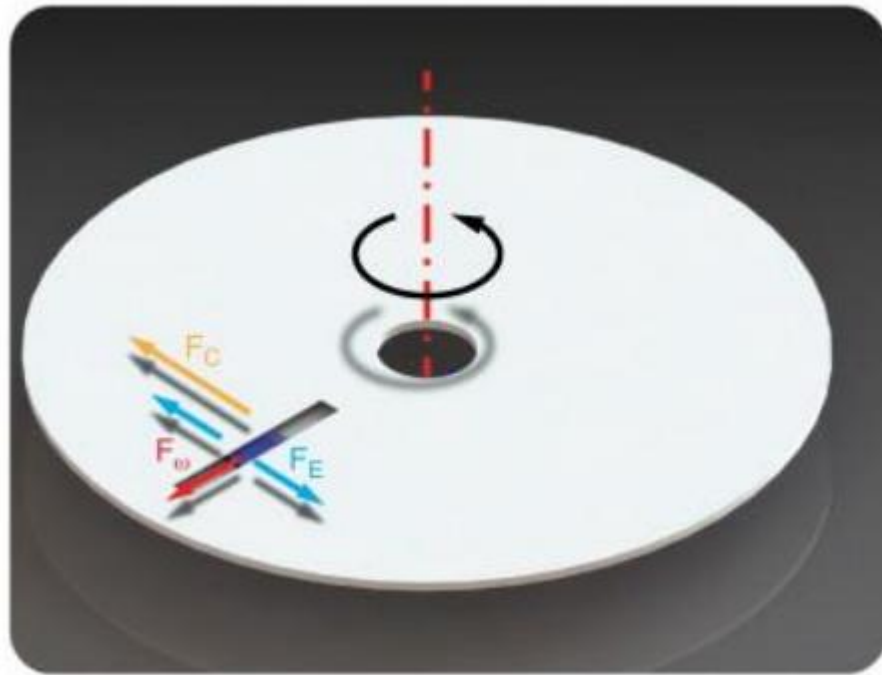


Figure 2.7 The forces experienced on a centrifugal platform affecting flow. F_ω is the centrifugal force, F_E is the Euler force and F_c is the Coriolis force. Adapted from Burger et al. [14].

2.6.1 Types of Fluid Flow

Laminar flow is defined as non-turbulent fluid flow and transpires naturally within a microfluidic structure. The movement of fluid must be considered as overlapping sheet like structure of fluid which travel in the same direction. With this type of flow, no mixing occurs between adjacent layers. Fluid viscosity relates to the flow, where the liquid's viscosity is the opposing resistance to flow. This can often be described as non-turbulent or streamline. As the lamina does not allow for liquid mixing, molecules can pass through these sheet-like fluid layers through diffusion [40].

When discussing fluid flow within a system, the Reynolds number (Re) must be determined to dictate whether the fluid is laminar or turbulent. This is the measure of the ratio between inertial and viscous forces. Laminar flow that occurs naturally within these microfluidic systems exist at $Re < 2300$, where turbulent flow occurs at $Re > 2300$ [41]. The Reynolds number can be characterised by the length, D , and the velocity, V with respect to the mass density of the fluid within the channel. This may also be referred to using the hydraulic diameter, D_h . With respect to biomedical diagnostics, mixing is a necessary procedure required for certain assay steps. The Reynolds number within

microchannels is commonly a low figure, which refers to laminar flow (< 2000). This number may be as significantly low as 10, therefore viscous forces play a major role in the characterisation of fluid flow [42].

This can be deemed unsuitable for certain experiments where mixing is required. This will imply that on the micro scale, diffusion methods are the only means of mixing which can take up to several minutes [41]. Suitable methods to overcome this is the rapid oscillation of the disc or including structures which will cause turbulence in the fluid flow. A particle that is present within a liquid will experience the laminar or turbulent flow, along with the common forces associated with centrifugal microfluidics under a rotational velocity. These forces also include that of Stokes drag forces and buoyancy forces, which are the opposing effects of the centrifugal force [42] (Figure 2.8). These are the forces that pathogens or other cells will experience within a Load and therefore it is important to understand these dynamics when designing a system.

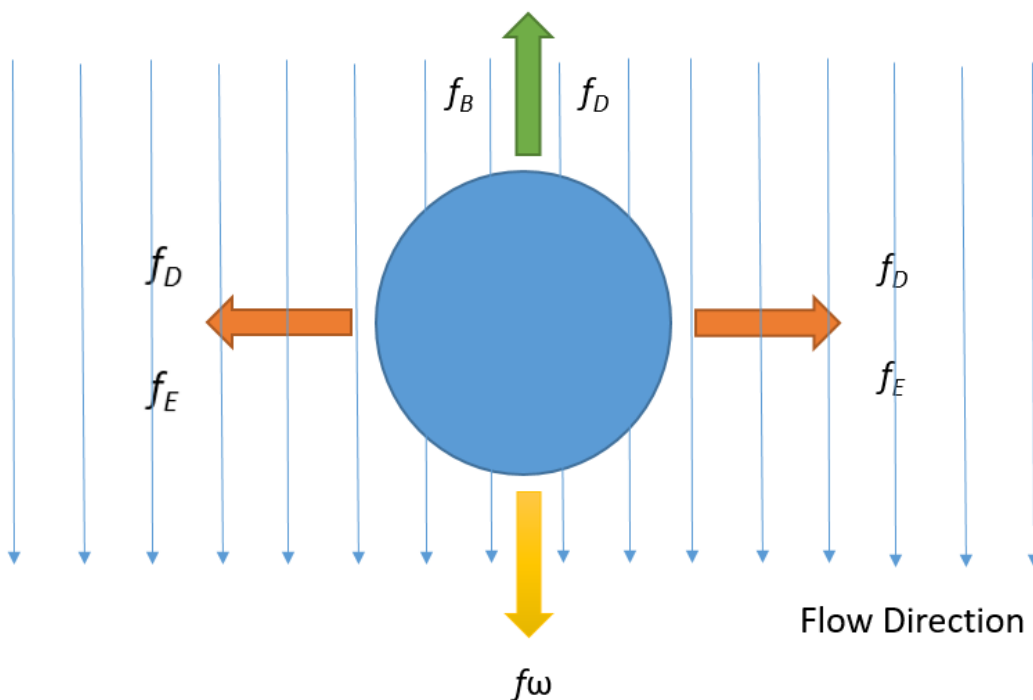


Figure 2.8 The forces acting upon centrifugally propelled particle in a fluid. The particle undergoes a centrifugal force (f_ω) which is opposed by the drag (f_D) and buoyancy (f_B) forces which are unique to the fluid. The lateral forces in the form of Euler (f_E) and Coriolis forces (f_C) still exist within the rotating system.

This is most apparent when the fluid is in a stationary phase within the system with particles moving throughout. The buoyancy and Stoke drag forces are an upward force that a fluid exerts on a body which opposes the mass with regards to gravity of the immersed body [43]. The Stokes drag force also defines the force related to the opposing direction fluid flow, where viscosity of the sample is a determining factor of the magnitude of the drag force exerted on a particle. It is important to understand the relevant formulae to predict particles interaction within a liquid medium within a rotating system.

2.6.2 Valving and Fluid Control

With the mechanics of the surface tension and fluid flow discussed, the way in which fluid moves within a system and how to implement an assay must be understood. With flow control systems, valving methods are implemented to control fluid movement. With passive valving, no other forces are experienced bar the forces previously described related to the spinning of the rotating platform. Passive valving is actuated by increasing or decreasing the spin frequency of the platform, which influences the centrifugal forces acting upon the fluid within the system compared to the relative forces that don't change, such as capillary force. Capillary valves are predominantly controlled by the LoADs rotation [44]. Passive valves are open channels within the system and therefore do not seal. This attribute controls vapour movement within the device there this passive valving method cannot be utilised for long-term reagent storage with the device for long periods of time [45].

Capillary action is a liquid feature by where it can flow through micro-channels and other miniscule passages without the assistance of, or even countering, peripheral forces such as gravity. The effect transpires through intermolecular adhesion forces between the liquid interface and the surrounding surfaces. The magnitude of this action is proportional to the cross-sectional area of the channel, and combined with surface tension, the liquid height can be lifted due to capillary action.

Once a balance is obtained between centrifugally stimulated pressure and capillary action within the system, fluid flow is hindered. If the platform rotational speed is increased, the centrifugal pressure will increase and overpower the capillary force and the liquid will flow through the valve. However, capillary action will ensue if a fluid is being forced from a small microchannels to a larger reservoir. Surface tension forces will be generated and will slow down or hinder the movement of liquid. For this to be overcome, the centrifugal pressure must exceed that of the capillary pressure. The platform spin frequency ω_c , which is known as the burst frequency, must be achieved in order to override the capillary pressure. Surface tension is finally overcome, and the fluid can continuously flow through the device.

As capillary valving is the most commonly used fluid control mechanism used with centrifugal devices, it exhibits limitations. In certain cases, the supporting material used for the microfluidic device may be hydrophobic, while some channels or chambers are required to be hydrophilic. In these instances, additional surface treatments steps are mandatory during the fabrication process. This valving type performance relies heavily upon contact angle and this may vary over time with certain LoAD platforms if incorrectly stored. The burst frequency is also dependent on the geometries of the channels and the reliability of the manufacture, including that of edge definition and surface roughness. These manufacturing limitations therefore require a compromise between the performance of capillary valving and cost of manufacture [46]. Dissolvable film (DF) technology was first introduced by Gorkin et al. and are categorised as passive valving (Figure 2.9). This work established a novel valving system that was integrated on a LoAD to perform fluid manipulation and full automation of assay steps [47].

In this system (B), the DF tab is fixed in a pneumatic chamber between the initial sample loading chamber and the collection chamber. This creates a compartment of trapped, pressurised air in the LoAD. At low rotational frequencies, the liquid present in the sample loading chamber is unable to flow over the DF due to the pressurised air. On increasing the speed spin of the platform, the fluid located in the loading chamber exceeds the pressure created by the trapped air and is forced to flow into the pneumatic chamber due to the increased centrifugal force. This consequents in the wetting of the DF tab. Once saturated, the DF valve weakens, and dissolves and the fluid can find passage to the

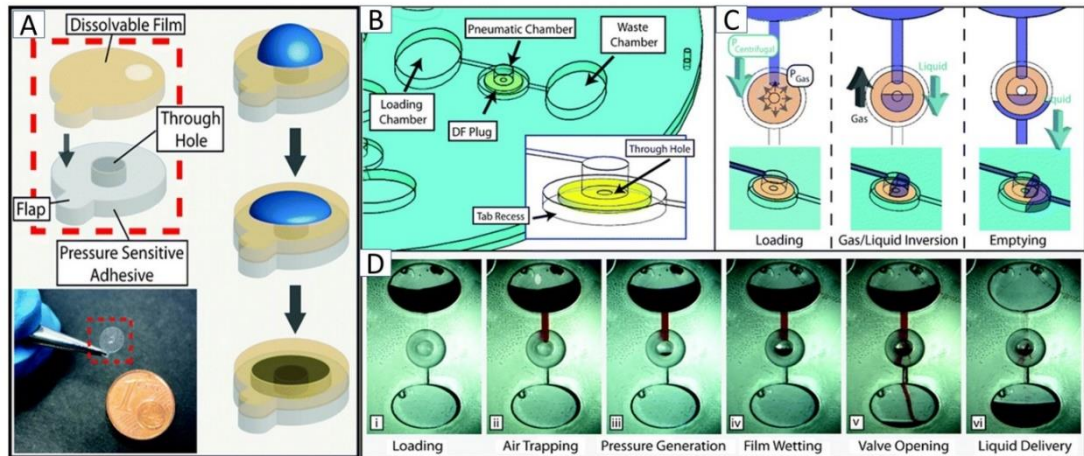


Figure 2.9: Centrifugo-Pneumatic DF valving. A) Demonstrates the structural design and size of a DF valve. The film deteriorates upon contact with liquid until complete dissolution. Liquid moves through the remaining structure B) Expresses the centrifugo-pneumatic valving concept. The integration of a DF valve with a Load. C) Portrays the DF valve in contact with liquid in a microfluidic system under centrifugal conditions. The operation at the point of loading, during liquid/gas inversion and after film destruction and emptying of the sample fluid D) Coloured dyes are exercised to demonstrate the DF valve operation. At low spin frequencies the air is entrapped, air is compressed at increased rotational spin frequencies resulting in air inversion in the chamber. The liquid introduced into the valve results in the fragmentation of the DF and valve opens. Adapted from Gorkin et al. 2012 [15].

adjoining chamber. The time in which the DF dissolves depends on the film used. Under spinning conditions, DF tabs have reported to burst in 45 seconds. This time can be increased by introducing a thicker DF.

The manipulation of fluid movement can be achieved by implementing DF valves as a fluid barrier. One key attribute of utilising DF valves is the selection of dissolution times of certain films used when fabricating the tabs. Different thicknesses and composition allow for a range of liquefying times in water. This fashions a more automated platform with a highly controllable valving process [47]. Furthermore, additional characteristics of the valve allow for more influential factors for the bursting of the tabs. The pneumatic chamber size which is situated above the tab can play a critical role in controlling the burst frequency of the valve. Large chambers require lower burst frequency to allow the liquid to come into contact with the tab. Testing has been carried out to ensure the properties of tuning specific valves. The DF valving mechanism is highly dependent on the balance, and disruption of balance, between the critical yield pressure P_{crit} and the pressure head ΔP . These pressures arise from the system being centrifugally provoked, and are consequential of the equation of hydrostatic pressure;

Equation 2-4

$$\Delta P = \rho g h$$

where g is the angular acceleration, or ω^2 , and h is equal to Δr .

As the centrifugal force acting on the liquid interface increases with radial positioning, the equation can be denoted as:

Equation 2-5

$$\Delta P dr = \rho \omega^2 r dr$$

By integrating this equation and applying the bounds of the liquid element, and therefore applying the limits, the absolute pressure is measured by:

Equation 2-6

$$P_{abs} = P_{\omega} = \rho \Delta r \bar{r} \omega^2 + P_{atm}$$

where the density is represented by ρ , Δr is the radial length from the centre of the Load, \bar{r} is the mean position of the liquid plug and ω is the angular frequency.

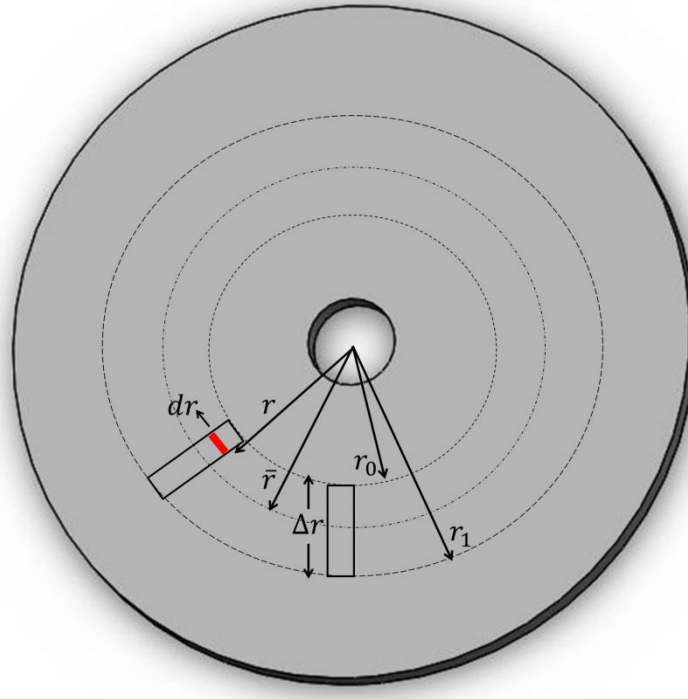


Figure 2.10 Definition of the position of the fluid plug on a centrifugal system. r_0 is the radially inwards point of the fluidic plug and r_1 is the radially outward location of the fluid plug. To calculate the centrifugally induced hydraulic pressure at location r_1 , the key dimensions are Δr , which is the radial length of the fluid element $[(r_1-r_0)]$, and \bar{r} , which is the average radial position of the fluid plug $[(r_0+r_1)/2]$. dr is an infinitesimal element and r is its distance from the centre.

By applying the values, depicted Figure 2.10, the burst frequency is calculated using the following formula:

Equation 2-7

$$\omega = \sqrt{\frac{P_{atm} \left(\frac{1}{1 - \frac{\Delta V}{V}} - 1 \right)}{\rho \Delta r \bar{r}}}$$

Where ω is the angular velocity in rad/s and the burst frequency Hz is equal to $\omega/2\pi$.

In the original findings presented by Gorkin et al, surface tension stabilises the liquid-gas interface, where the liquid head can protrude through a pneumatic chamber as P_ω is increased. The surface tension, in effect, cannot sustain the hanging liquid volume ΔV , where eventually the liquid plug is disrupted and inverts the liquid-gas arrangement at

the specific burst frequency. On contact with the emerging liquid face, the DF tab dissolves and allows fluid passage to the adjoining chamber [48]. With common geometries designed for this purpose, the pneumatic volume is low, but it contains a degree of unreliability due to the unpredictable nature of surface tension forces [49]. The DF tabs tend to rupture rather than dissolve. This may be beneficial as the films, although reported as inert bio-friendly polymers, may have an effect on electrodes or modified surfaces which may be in the adjacent chamber. Systems containing the tabs have a difficult task for mass manufacture of the devices, where the fragile nature of the film will make a “pick and place” mechanism a difficult, if not impossible, method to create the automated devices.

These microfluidic platforms are generally manufacturing using inexpensive acrylic materials, this making the LoDs cost effective. As the discs are typically disposable and single use, they become prime candidates for point-of-care for human diagnostics. Centrifugal microfluidics has gained traction in the last decade as a hugely influential tool for diagnostics, as multiple analysis steps can be performed on a these highly robust devices [50]. Mass-production of LoDs is carried out utilising injection moulding techniques which is the process of transported thermoplastic materials in the form of melted pellets extruded under high pressures into a mould cavity [51]. This material solidifies under high pressure, and decreasing glass-transition temperatures, until the polymer has set. Once this temperature is reached, the piece is ejected and the cycle repeats. Depending on the complexity of the device, cycle times can range from seconds to minutes. This process has a huge set of advantages for commercially available microfluidic devices as there a wide range of thermoplastics available for full automation and short cycle times, highly-cost effective for disposable platforms and low maintenance of equipment compared to lithographic methods [52], [53].

2.6.3 Testing of Centrifugal Devices

As the LoDs operate using centrifugal force, a spin-stand was developed for the operation of the devices. For optimisation purposes, the instrument was coupled with a motion powered stroboscope camera and imaging software for real-time fluidic analysis. The performance and reproducibility of the platforms were studied using this in-motion

observation software to determine if the device's operating features were functioning. Valve actuation times and frequencies are studied, along with liquid incubation times, which are vital for the optimised performance of the LoDs. The operation of the live-imaging feed depends on the acquisition of a series of images, captured once per motor revolution. The motor and camera strobe are synchronized and once a revolution has been achieved by the motor/LoD the signal is fed back into camera software. As the centre of rotation is fixed throughout the test, the disc appears to be stationary throughout the live feed, despite the maximum rotational frequency of 80Hz which can be achieved.

Figure 2.11 displays the spin-stand instruments fabricated for centrifugal microfluidic testing. The disc is attached to the spindle motor (CMMS-AS Servo Motor, Festo, Germany), where it was secured. The disc is spun at a low spin frequency to optimise the strobe parameters, such as brightness and focus. These are directly adjusted on the charged coupled device (CCD) camera (PCO Pixelfly). The spin-frequency and acceleration of the motor were controlled using LabView software. Once the optical parameters have been selected, the pre-loaded disc was secured to the motor spindle. Once the spin frequency of the disc was selected, a series of single-frame images appeared in sequence to give the appearance of a live-feed despite the disc appearing stationary whilst the liquid flow was observed.

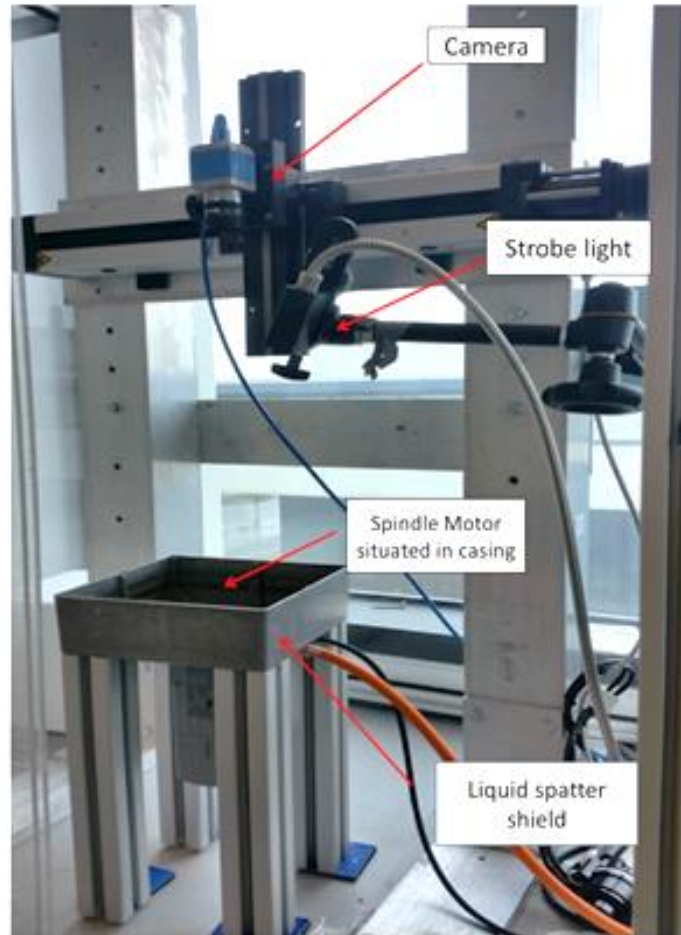


Figure 2.11 Operating features of spin-stand instrument for testing a centrifugal testing platform.

2.7 Bacteria Culture

Preparation of cultured bacteria is necessary for the validation of the pathogen sensing platform. A serial dilution of the bacteria is prepared and adhered to the electrode, functionalised with the appropriate antibody. Different agar plates must be prepared for the specific culture of the pathogen groupings, as shown in *Table 2-3*.

Table 2-3 Agar plate composition for gram positive and gram negative bacteria culture.

Bacteria Culture Type	Gram Positive	Gram Negative
Bacteria Media Type	Brain-Heart Infusion (BHI)	Lysogeny Broth (LB)
Agar Plate preparation	37g of BHI	10g tryptone

	15g Agar	5 g of yeast extract 10 g of NaCl (mw 58.44g) 15 of agar
--	----------	--

12.50g BHI or LB is mixed with 500mL deionised (DI) water for produce the desired media. For the preparation of the agar plates, the appropriate agar plate ingredients are added to an autoclaved 2L flask, pre-rinsed with DI water. A litre of DI water was added, and the sealed flask is sonicated to promote the dissolving of particles. For the LB agar, 0.5 mL of 4M NaOH was added. The solution was autoclaved at 121°C for 15 minutes for sterilisation of the solution. Once the agar flask to cool enough to handle the flask was placed within a sterilised fume hood. All plates were dated and poured within the fume hood. The lid of the sterile plate was slightly lifted and approximately 30mL of the agar was poured quickly, then covered. The plates were left undisturbed for 30 minutes to allow it to solidify. Plates were incubated at 37°C overnight, upside down to avoid condensation forming on the agar. If plates were contaminated, cloud type structures were visible. Plates can be stored for up to 3 months at 4°C.

For the preparation of the Staphylococcus Aureus, the 1000 CFU bacterial pellet (ATCC, Ireland) was placed in a sterile sample tube with 5mL of nutrient broth and left in a shaker for 24-48 hours at 37°C at 200 RPM to ensure correct growth of bacteria. A cloudy consistency was an indication of good bacterial growth. For the serial dilution, a 1:10 dilution of bacterial solution into Dulbecco's Phosphate Buffered Solution (DPBS) was prepared where 100uL of each diluted step is plated and spread using inoculation loops. The plates are inverted and incubated overnight at 37°C. Colonies formed were counted to determine the CFU/ml of the initial bacteria stock.

2.8 Electrochemical Impedance Spectroscopy

For the purpose of the experiments carried out in Chapters 3 and 4 EIS techniques were adopted for pathogen detection. For the duration of the studies a CH 760 E potentiostat (CH Instruments, Inc., USA) was used. The three electrode electrochemical cell was used

at room temperature ($20\pm 2^\circ\text{C}$). EIS measurements were carried out at the open circuit potential (OCP), in 1 mM Dulbecco's phosphate-buffered saline (DPBS) within the frequency range of 0.01–100,000 Hz, with a 25mV AC amplitude using the three electrode system placed inside a faraday cage [26]. The OCP must be recorded per experiment as this value is unique to each experiments. The OCP is the measure of the potential between the reference and working electrodes. The initial voltage of the EIS measurement is set to the OCP as a potential exists at the interface of the electrode when no current is flowing through the cell. Electrochemical reactions are slight, but the setup is changed to the electrode's OCP to avoid interference from these interfacial reactions [27]. The typical value of the OCP was found to lie within the range of 0 and -0.1 V.

EIS has the inherent potential of a non-destructive analysis of a sample, where the response of the electrochemical cell is measured using a low amplitude sinusoidal perturbation of the system is a function of frequency [54]. This frequency response in turn provides much information regarding the electrode surface of interest. A number of research articles have reported the use of impedance in microbiology, where impedance changes due to pathogen growth in culture media causes a change in the conductance due to charged ions produced during microbial growth or cell adhesion on the working electrode surface which in turn would alter the interfacial capacitance [55]–[58].

EIS determines the impedance Z is governed by the applied voltage which causes a perturbation of a sinusoidal wave of a given amplitude where the current response is measured. The impedance of a system is given by:

Equation 2-8

$$Z(t) = \frac{V(t)}{I(t)} = \frac{V_0 \sin(2\pi ft)}{I_0(2\pi ft + \varphi)}$$

where V_0 and I_0 are the maximum voltage and current signals applied to the system, f is the frequency of the sinusoidal wave, t is the time, and ϕ is the phase shift between the current–time functions and the voltage–time [54], [59]. Equation 2.8 is a modified ohmic law relationship where Z is considered a complex value because the current can alter in

terms of phase shift and amplitude compared to the time-voltage function. Figure 2.12 portrays the relationship between V , I , the phase shift φ , the impedance modulus $|Z|$ which is a vector function of the real impedance Z_{re} and the imaginary impedance Z_{im} .

For impedimetric measurements, the two most commonly methods of evaluating the extracted data from the system is the Bode plot and the Nyquist plot. The Nyquist plot consists of the real data (Z') against the imaginary data (Z''). A typical Nyquist plot comprises of a semi-circle which approaches the X axis followed by a straight line which exists at an angle. At high frequencies, the semi-circle segment relates to the electron transfer limited process when used in conjunction with a redox probe, while at lower frequencies the straight angled line represents the diffusion limited process [60]. In other cases, the semi-circle shape may also be attributed to the change in capacitance at the corresponding frequency. As EIS is a study of the response of an electrochemical system of the voltage at different frequencies, it is evident that the lack of frequency information from the Nyquist plot is its main disadvantage. To rectify this issue, the Bode plot can be observed, where the amplitude and phase over the applied frequency range is analysed. The Bode is the logarithm of the modulus of both the phase and impedance plotted against the logarithm of the frequency [61].

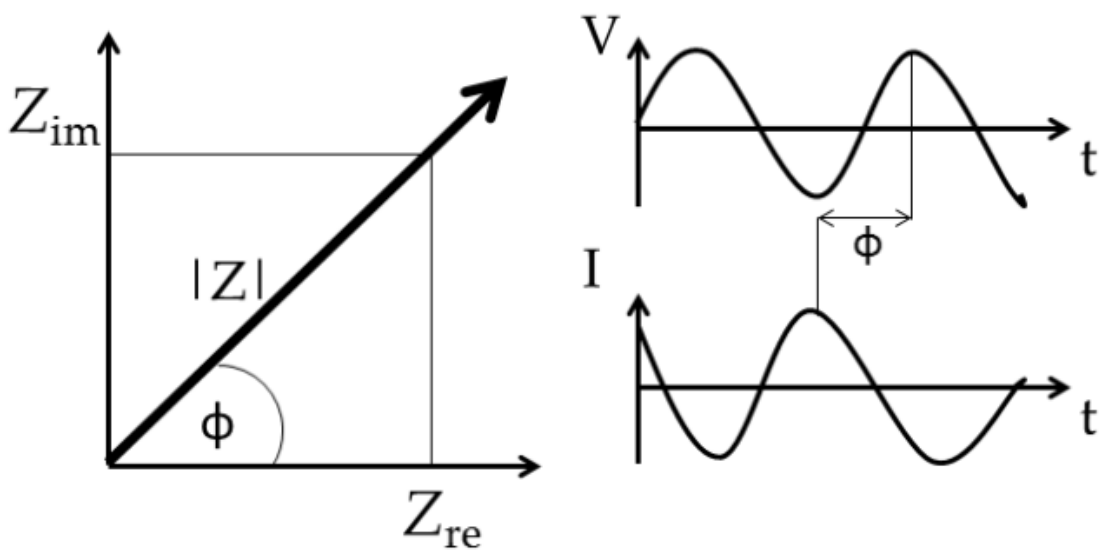


Figure 2.12 Figure representing the real and imaginary vectors of the impedance modulus where φ portrays the phase angle which is formed by the mis-alignment, or phase shift, of the V and I sinusoidal waves [16].

2.8.1 Faradaic and Non-Faradaic Impedance

EIS is the analysis and understanding of the response spectra using equivalent circuit (EC) which is a combination of resistances and capacitances in series or parallel. For EIS measurements which is performed with a metal, working electrode in an electrolyte solution that contains an electroactive compound, the EC elements are known. The double layer capacitance (C_{dl}), charge transfer resistance (R_{ct}), the ohmic resistance of the electrolyte (R_s) and the Warburg impedance (Z_w) are all typical components of an electrochemical biosensor cell in a faradaic process which can be further described using Randles circuit in Figure 2.13 [62]. The C_{dl} is defined as by the electrical double layer that exists at the electrode interface and its surrounding electrolyte. This double layer is formed as ions from the electrolyte form an ion barrier on the electrode surface. The charges that exists on the electrode are separated from the charges of these ions from the solution, where the separation distance is in the order of angstroms. Charges which are separated by an insulating layer are deemed a capacitor were the value of the C_{dl} depends on many variables such as electrode potential, temperature, ionic concentrations, types of ions, electrode roughness, impurities and adsorption,

In the case where a redox probe is not present in the electrolyte solution, the process is described as non-faradaic. The procedure relies upon the impedimetric electrode interfacial properties and the conductivity of the electrolyte used.

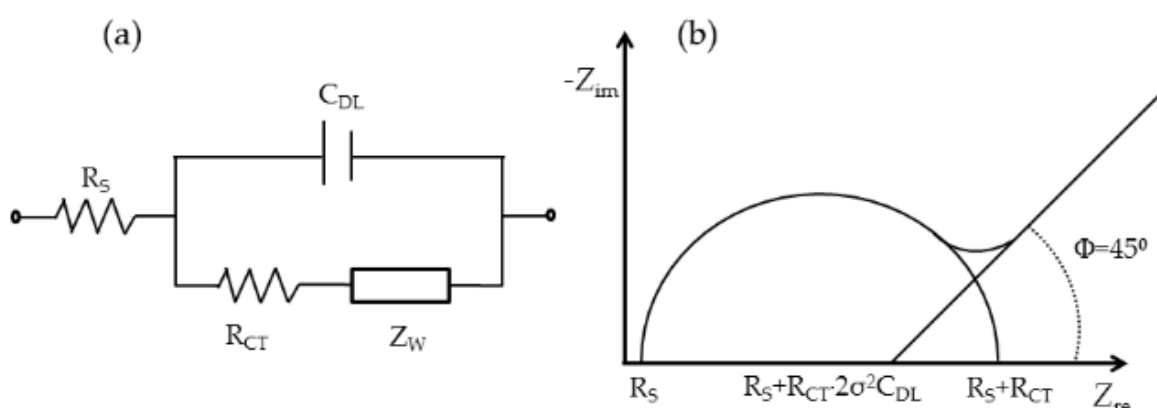


Figure 2.13 (a) portrays each individual element in which the Randles circuit is composed of and (b) how these individual components exist within the Nyquist plot.

The capacitance value will change when thickness of the C_{dl} or when the dielectric constant of the transducer surface changes due to an alteration of the surface's composition. The development of bio-chemical reactions may cause the addition of a capacitor in series (Equation 2-9) or parallel (Equation 2-10) with the C_{dl} depending on the process being observed. As the biosensor surface, antibody, blocking proteins etc. have an individual capacitance, when all are used together to form the finished biosensor, some of these capacitances may be in series or parallel. The sum of capacitors in series reduces the overall capacitance and increases when in parallel format.

Equation 2-9

$$\frac{1}{C_{total}} = \frac{1}{C_1} + \frac{1}{C_2} + \dots + \frac{1}{C_N}$$

Equation 2-10

$$C = C_1 + C_2 + \dots + C_n$$

2.9 Imaging Systems

2.9.1 Confocal Microscopy

Confocal Laser Scanning Microscopy (CLSM) operates on the basis of utilising lasers to excite fluorescent labelled samples, where only a specific focused area of the sample is detected by the light source [28]. Compared to more traditional methods of light microscopy, this greatly improves the resolution and quality of the obtained image. CLSM employs pinholes which act as scattered light rejecters which lie outside of the focal plane for enhanced image quality [29]. By guiding both excited and detected light beams through pinholes, any out of focus back scattering is eliminated. Two pin-holes exist; one placed before the sample at the excitation line, and a pinhole directly after the sample at the detector. Fluorescence given off from the sample is collected using a photomultiplier tube (PMT). For image acquisition, the sample is scanned in the XY plane by the laser and the image is developed on a per-pixel basis [30].

For the purpose of the experiments detailed in Chapter 4, the following procedure was adopted for imaging the bacterial cells. Firstly, the electrode area must be prepped for confocal using a 10% glutaraldehyde (Sigma-Aldrich, Ireland) solution to fix the any bound cells onto the surface. The solution was incubated on the surface for 15 minutes and rinsed with DI H₂O. This step was necessary for the preservation of the cell as it prevents autolysis of the structure. The bound cells' membranes are permeabilised using a 1% Triton-X 100 solution (Sigma-Aldrich, Ireland). It is a non-ionic surfactant which disrupts the hydrogen bonding in the lipid bilayer structures, creating pores in the membrane structure [31]. This solution was incubated for 15 minutes on the surface, which was removed and replaced with a 2% solution of BacLight (*BacLight* Bacterial Viability, Thermo-Fischer Scientific, Ireland). This red-fluorescent propidium iodide (PI) nucleic acid stain penetrates bacteria with damaged or permeabilised membranes. This solution was incubated on the surface for 15 minutes. The prepared electrodes were then fixed onto a glass slide using fluoroshield (Sigma-Aldrich, Ireland), a mounting medium which preserves the fluorescence of cells. The images were recorded on a Zeiss LSM510 Meta confocal microscope using a 64× oil immersion objective lens. For the excitation of the uptaken dye, a 540 nm HeNe laser was used.

[2.9.2 Scanning Electron Microscopy](#)

Prior to SEM imaging, all non-conductive samples must be coated in a conductive material. For all SEM imaging carried out, the samples were sputter coated with 10nm of gold at 2.5kV and 36mA for 38 seconds in a N₂ chamber. All samples were secured to SEM stubs with carbon tape as imaging takes place under vacuum conditions. All SEM images were acquired using the Hitachi S300N scanning electron microscope. Images were obtained between a range of accelerating voltages of 5-20 kV. An increase in the accelerating voltage results in a smaller probe diameter and thus higher resolution of images however it will also increase the charge on the sample surface and potentially damage specimens that are non-conductive and beam sensitive [32]. The probe current of 25-35 mA was applied to the system.

2.10 ELONA Preparation and Detection

Maleimide coated 96-well plates required to perform the ELONA assays were acquired from Thermo- Scientific (Spain). Each plate must be thoroughly washed three times with PBS Tween20 (0.05%) (PBST) using a multichannel pipette. 100µl of the specific capture aptamer of a given concentration is incubated within each well overnight at 4 °C. The capture aptamer was removed, and the plate was washed three times again with PBS Tween (0.05%). 100µl of a blocking agent was incubated within each at room temperature (20±2°C) and left under rocking conditions for 1 hour. Blocking agents are used to block the surface of the well where no capture aptamer has attached. For a highly successful ELONA plate, low background signal must be acquired, which was achieved through the blocking of the test wells using an inert protein [33].

The plate was washed again four times to ensure the full removal of unbound blocking proteins. Next, the analyte and reporter probe (50µl of each) was mixed and placed in each well and incubated at room temperature (20±2°C) and left under rocking conditions for 1 hour. Here, the solution was removed and washed three times. From this point, the assay can be finalised using two approaches; typical ELONA colorimetric detection or eluting the reporter for PCR and RPA amplification (Section 2.11).

For ELONA colorimetric detection, each well was incubated with 50µl of streptavidin Poly-HRP for 30 minutes at room temperature. This conjugate is biotin binding protein which is conjugated with polymers of horseradish peroxidase (HRP) which allows for signal amplification of biotin bound probes. SA Poly HRP was prepared by diluting 0.5 µl (50ng/ml) in 10mls of PBBS. This solution was removed, and each plate was washed five times to ensure to completed removal of unbound SA-Poly HRP. 50µ l of Tetramethylbenzidine (TMB) was added for 5-10 minutes where a colour change can be visibly observed due the presence of the analyte. The reaction was stopped using 1M sulphuric acid. The plate was transferred to the Spectramax 340 PC (bioNova, Scientifica (Spain)) spectrophotometer.

All results obtained are based upon the Beer Lambert law where the concentration of compound has a linear correlation to its absorbance at a defined wavelength at a constant pathlength. The absorbance values obtained are converted to an excel file in which analysis can be carried out to determine the LOD of the assay.

2.11 PCR and RPA Methodologies

PCR and RPA are two methods used for the amplification of an unmodified reporter probe. Firstly, it's a simple method providing rapid results [63], and highly sensitive as its capable of producing vast amounts of copies of specific targets for sequencing and analysis [64] [65]. This technique requires a varying range of temperatures per cycle.

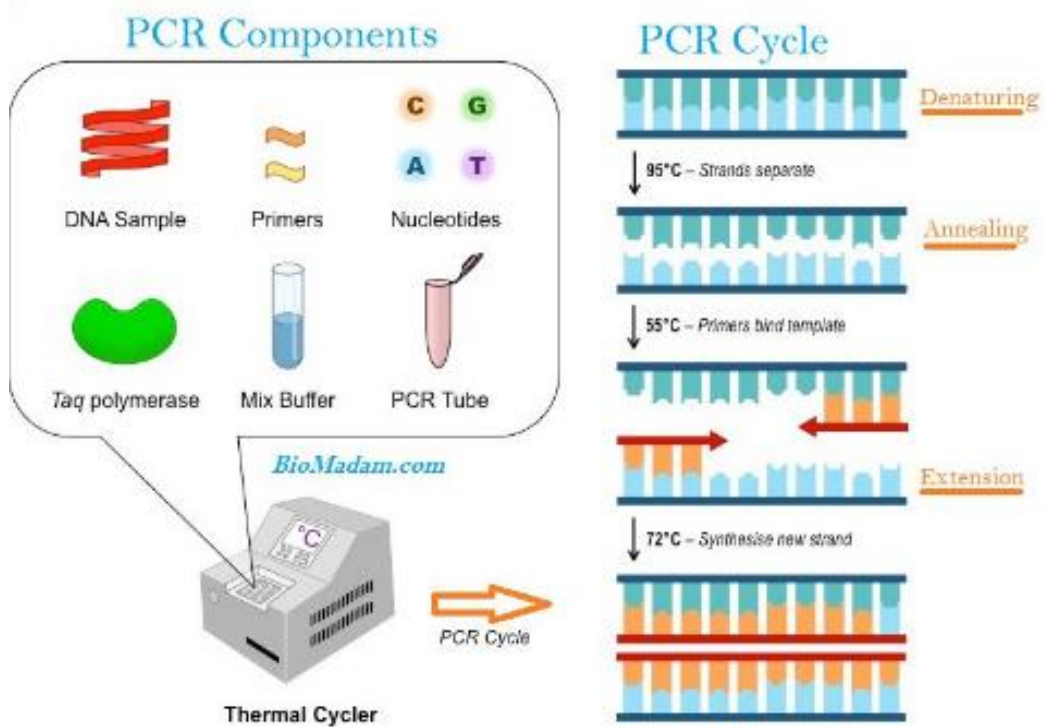


Figure 2.14 Description of the basic PCR process. Denaturation of the target DNA melting at 95 °C. The secondary stop of annealing allowing got the primers to attach to the single stranded DNA. New strands of DNA are synthesized which directly correlated to the DNA template by the DNA polymerase at 72 °C during the final step in the cycle [17].

The first step of basic PCR is denaturation at 94 °C for one minute. Primers are annealed to the now, single stranded DNAs, as the temperature is decreased to between 40-60 °C. This second step is followed by an increase to 72 °C to allow for sufficient time for primer extension. The temperatures applied for denaturation and annealing are the most critical elements. A failure to attain the target temperature for these stages results in the failure of DNA melting, therefore no amplification will occur. Low temperatures lead to mis-priming of non-target sequencing, whereas over-heating the sample leads to non-amplification as base pairs won't anneal at high temperatures [66].

PCR enables the amplification of short regions of DNA in an *in-vitro*, enzyme driven process. The amplification is performed by DNA polymerase in the presence of two oligonucleotide primers which allows the process to be carried out. The primers bind to opposite ends of the specified target DNA and trigger the target DNA sequence to replicate as the polymerase advances along the sequence region between the opposing primers, therefore the region of interest expands exponentially. The cycle repetition allows for high amplification rates, where millions of strands of target DNA can be generated and detected [67]. This process is portrayed in Figure 2.14.

The other DNA amplification method used in Chapter 5 termed RPA operates as follows. The basic reaction mechanisms of the RPA method are subject to a synthetic adaption of the natural cellular process called homologous recombination. The standard RPA kit comprises of three reaction reagent proteins (recombinase, recombinase loading factor, and ss-binding protein). These proteins thus coordinate with the DNA polymerase, energy components and salt molecules to carry out the RPA reaction. For the RPA reaction, the recombinase binds to the primers which is aided by the loading factor. This forms the nucleoprotein that locates the homologous sequence in the ds-DNA. The complex then invades the DNA and forms a D-loop structure which begins a strand exchange reaction where the unravelled strand is stabilised by the ss-binding proteins. The recombinase then detaches from the nucleoprotein filament once the strand exchange is complete and is available for the next set of forward and reverse primers. The next step comprises of the DNA polymerase to extend from the 3' end of the primers. As this polymerisation process continues, the parent strands then begin to detach and form two duplexes. The process

then repeats until stopped using a high temperature to denature the enzymes/proteins or the addition of a reaction ending protein as shown in Figure 2.15 [67].

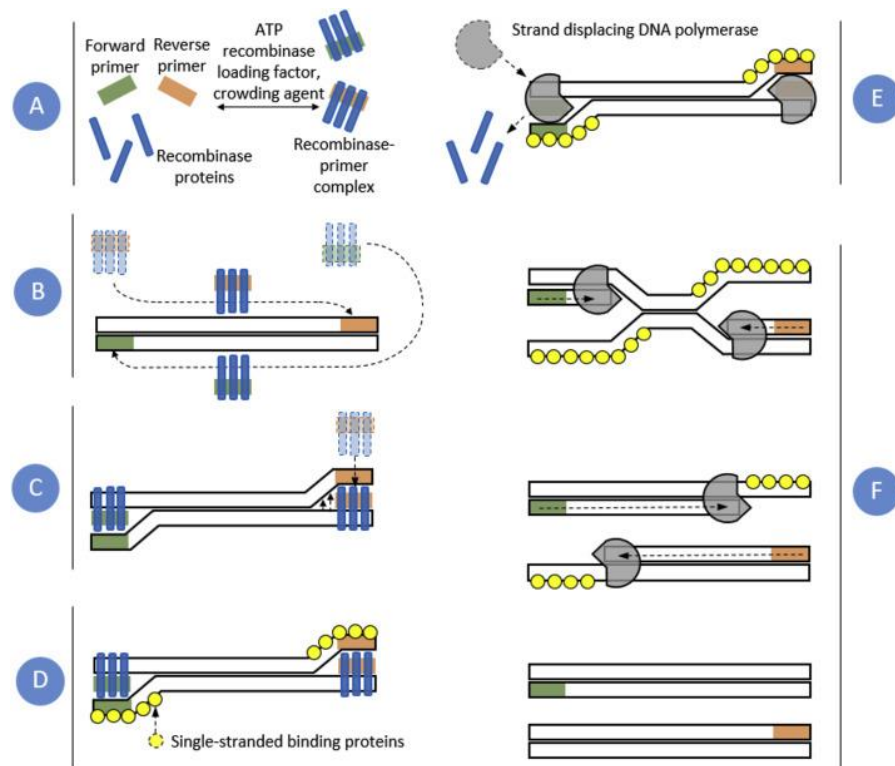


Figure 2.15 RPA process of amplification using the forward and reverse primers, recombinase proteins, recombinase primer and ATP recombinease.

For the purpose of experimentation in Chapter 5, eluted unmodified reporter aptamer was amplified using both procedures. The eluted aptamer was obtained using the same protocol outlined in Section 2.10, where instead of the addition of the SA Poly HRP, 20 μ l of MilliQ water heated to 95 °C and added to each well for 3 minutes. Salt solutions, such as NaCl and NaOH, may also be used for elution purposes. The MilliQ water was aspirated and placed into autoclaved PCR tubes and can be stored in -20 °C. 1 μ l of eluted sample was mixed with 9 μ l of PCR or RPA master mix, which contains the relevant components for each type of amplification. 5 μ l of this total sample was mixed with 4 μ l of loading buffer (Thermo Scientific, Ireland), where this 9 μ l sample was loaded into a pre-made gel. A DNA ladder (1 kb) is added to the first well to determine the concentration of the DNA whilst imaging using the UV transilluminator. PCR thermocyclers are instruments utilised for the amplification of DNA segments using the PCR thermal cycles. The programmable

instrument typically contains a thermal block which can facilitate up to 96-PCR tubes which contain individual samples for amplification.

The device then raises and lowers the temperature of both the thermal block and lid to induce the thermal conditions required for a PCR reaction. The temperature and duration of each step can be inputted on the user interface of the instruments to allow for any conditions to be applied to the samples. For the PCR and RPA work carried out in this monograph, the BioRad T100 thermocycler (BioRad, Spain) was used. Once the amplification process was complete the samples are removed for fragment separation. Agarose gels are prepared for use with a standard gel electrophoresis setup. Different percentages of agarose can be used in the production of the gels depending on the DNA fragment size. The gel pores can be altered by changing the agarose concentration, which controls how fast the amplicons will travel in the gel during electrophoresis. The concentration of the gels effects the resolution of the amplified DNA separation. A 0.8% agarose gel gives good separation large 5–10kb DNA fragments, while 2% agarose gel gives good resolution for small 0.2–1kb fragments.

To cast a gel, the agarose was weighed out and dissolved in the buffer in which the gel will be run. For all gels fabricated throughout this work, a 1.3g of agarose was dissolved, by heating, in 50ml of Tris/Borate/EDTA (TBE) buffer. 5uL of Gel Red (Biotium, UK) dye was then added to the gel mixture and cast in the gel docking pre fixture with the 15-tooth comb for 30 minutes.

Once all solutions have been added to the individual wells, the gel was placed into the gel electrophoresis dock, which was prefilled with TBE buffer. The gel dock is then attached to a power supply and run at 120V for 20 minutes. The use of running buffer and applied voltage is also a determining factor in which controls the migration of the amplicons [34]. The use of an electromotive force (EMF) for DNA migration is due to the applied voltage between the anode and cathode port in the apparatus. As DNA has a negatively charged backbone, the DNA amplicons will travel towards the cathode port, forcing fragments of different weights to travel different distances within the gel. [35], [36] The gel was then placed in a UV transilluminator for image acquisition. A UV transilluminator was set to

mirror the absorbance, emission profile of the chosen dye loaded into the agarose gel where images are acquired [37].

2.12 Conclusion

The materials, instrumentation and processes used for this thesis was described in detail as a comprehensive breakdown. The experimental processes for each results chapter was portrayed as a series of standard operating procedures (SOP) guidelines. The production of Au sensors for use in an electrochemical cell and within a microfluidic POC device have been portrayed as well as the fabrication of microfluidic centrifugal platforms. DNA amplification and detection techniques have also been discussed as a step-wise approach.

2.13 References

- [1] D. J. Lipomi, R. V. Martinez, L. Cademartiri, and G. M. Whitesides, *Soft Lithographic Approaches to Nanofabrication*, vol. 7. Elsevier B.V., 2012.
- [2] C. W. Tsao, “Polymer microfluidics: Simple, low-cost fabrication process bridging academic lab research to commercialized production,” *Micromachines*, vol. 7, no. 12, 2016.
- [3] J. Friend and L. Yeo, “Fabrication of microfluidic devices using polydimethylsiloxane,” *Biomicrofluidics*, vol. 4, no. 2, pp. 1–5, 2010.
- [4] T. Trantidou, Y. Elani, E. Parsons, and O. Ces, “Hydrophilic surface modification of PDMS for droplet microfluidics using a simple, quick, and robust method via PVA deposition,” *Microsystems Nanoeng.*, vol. 3, no. November 2016, p. 16091, 2017.
- [5] D. J. Guckenberger, T. E. de Groot, A. M. D. Wan, D. J. Beebe, and E. W. K. Young, “Micromilling: A method for ultra-rapid prototyping of plastic microfluidic devices,” *Lab Chip*, vol. 15, no. 11, pp. 2364–2378, Jun. 2015.
- [6] Y. Chen, L. Zhang, and G. Chen, “Fabrication, modification, and application of poly(methyl methacrylate) microfluidic chips,” *Electrophoresis*, vol. 29, no. 9, pp. 1801–1814, 2008.
- [7] U. Ali, K. J. B. A. Karim, and N. A. Buang, “A Review of the Properties and Applications of Poly (Methyl Methacrylate) (PMMA),” *Polym. Rev.*, vol. 55, no. 4, pp. 678–705, Oct. 2015.
- [8] R. Ortiz, J. L. Chen, D. C. Stuckey, and T. W. J. Steele, “Poly(methyl methacrylate) Surface Modification for Surfactant-Free Real-Time Toxicity Assay on Droplet Microfluidic Platform,” *ACS Appl. Mater. Interfaces*, vol. 9, no. 15, pp. 13801–13811, Apr. 2017.
- [9] A. Jagota, “Mechanics of Adhesion Through a Fibrillar Microstructure,” *Integr. Comp. Biol.*, vol. 42, no. 6, pp. 1140–1145, 2002.
- [10] D. A. Bartholomeusz, R. W. Boutté, and J. D. Andrade, “Xurography: Rapid prototyping of microstructures using a cutting plotter,” *J. Microelectromechanical Syst.*, vol. 14, no. 6, pp. 1364–1374, 2005.

- [11] "Microfluidics for Biologists_ Fundamentals and Applications - Google Books." .
- [12] G. R. *et al.*, "Centrifugo-pneumatic valving utilizing dissolvable films," *Lab Chip*, vol. 12, no. 16, pp. 2894–2902, 2012.
- [13] J. D. Kinahan *et al.*, "Baking Powder Actuated Centrifugo-Pneumatic Valving for Automation of Multi-Step Bioassays," *Micromachines* , vol. 7, no. 10. 2016.
- [14] R. Robbins and R. Robbins, "Photomask Making," *Univ. Texas Dallas Sch. Eng.*, pp. 1–24, 2007.
- [15] P. Epoxy and N. Photoresist, "Permanent Epoxy Negative Photoresist," 2000.
- [16] C. Kaynak and S. D. Varsavas, "Performance comparison of the 3D-printed and injection-molded PLA and its elastomer blend and fiber composites," *J. Thermoplast. Compos. Mater.*, p. 892705718772867, Apr. 2018.
- [17] K. Takagishi and S. Umezu, "Development of the Improving Process for the 3D Printed Structure," *Nat. Publ. Gr.*, no. June 2016, pp. 1–10, 2017.
- [18] R. Gorkin III *et al.*, "Centrifugo-pneumatic valving utilizing dissolvable films," *Lab Chip*, vol. 12, no. 16, pp. 2894–2902, 2012.
- [19] Y. Zhou, "The recent development and applications of fluidic channels by 3D printing," *J. Biomed. Sci.*, vol. 24, no. 1, p. 80, 2017.
- [20] R. K. Lade, E. J. Hippchen, C. W. Macosko, and L. F. Francis, "Dynamics of Capillary-Driven Flow in 3D Printed Open Microchannels," *Langmuir*, vol. 33, no. 12, pp. 2949–2964, Mar. 2017.
- [21] A. Ferrario, M. Scaramuzza, E. Pasqualotto, A. De Toni, and A. Paccagnella, "Development of a Disposable Gold Electrodes-Based Sensor for Electrochemical Measurements of cDNA Hybridization," *Procedia Chem.*, vol. 6, pp. 36–45, Jan. 2012.
- [22] Moran---Mirabal, Research, and Group, "Piranha Cleaning – Glass Surfaces," pp. 3–5, 2014.
- [23] G. Bracco and B. Holst, *Surface science techniques*, vol. 51, no. 1. 2013.
- [24] D. A. Hook, J. A. Olhausen, J. Krim, and M. T. Dugger, "Evaluation of oxygen plasma and UV ozone methods for cleaning of occluded areas in MEMS devices," *J.*

Microelectromechanical Syst., vol. 19, no. 6, pp. 1292–1298, 2010.

- [25] S. Bhakta, M. S. I. Seraji, S. L. Suib, and J. F. Rusling, “Antibody-like Biorecognition Sites for Proteins from Surface Imprinting on Nanoparticles,” *ACS Appl. Mater. Interfaces*, vol. 7, no. 51, pp. 28197–28206, Dec. 2015.
- [26] E. Spain *et al.*, “Detection of prostate specific antigen based on electrocatalytic platinum nanoparticles conjugated to a recombinant scFv antibody,” *Biosens. Bioelectron.*, vol. 77, 2016.
- [27] M. Pedrero, S. Campuzano, and J. M. Pingarrón, “Electroanalytical sensors and devices for multiplexed detection of foodborne pathogen microorganisms,” *Sensors*, vol. 9, no. 7, pp. 5503–5520, 2009.
- [28] J. P. B. T.-M. in C. B. Robinson, “Chapter 4 Principles of confocal microscopy,” in *Cytometry*, vol. 63, Academic Press, 2001, pp. 89–106.
- [29] E. Wang, C. M. Babbey, and K. W. Dunn, “Performance comparison between the high-speed Yokogawa spinning disc confocal system and single-point scanning confocal systems,” *J. Microsc.*, vol. 218, no. 2, pp. 148–159, 2005.
- [30] T. Sakurai, A. Lanahan, M. J. Woolls, N. Li, D. Tirziu, and M. Murakami, “Live Cell Imaging of Primary Rat Neonatal Cardiomyocytes Following Adenoviral and Lentiviral Transduction Using Confocal Spinning Disk Microscopy,” *J. Vis. Exp.*, no. 88, p. 51666, Jun. 2014.
- [31] D. Koley and A. J. Bard, “Triton X-100 concentration effects on membrane permeability of a single HeLa cell by scanning electrochemical microscopy (SECM),” *Proc. Natl. Acad. Sci. U. S. A.*, vol. 107, no. 39, pp. 16783–16787, Sep. 2010.
- [32] B. Hafner, “Scanning Electron Microscopy Primer by University of Minnesota’s Characterization Facility,” pp. 1–29, 2007.
- [33] R. P. Pratt, “Comparison of Blocking Agents,” *ThermoScientific*, p. All, 2014.
- [34] P. Y. Lee, J. Costumbrado, C.-Y. Hsu, and Y. H. Kim, “Agarose gel electrophoresis for the separation of DNA fragments,” *J. Vis. Exp.*, no. 62, p. 3923, Apr. 2012.
- [35] N. C. Stellwagen, “Electrophoresis of DNA in agarose gels, polyacrylamide gels and in free solution,” *Electrophoresis*, vol. 30 Suppl 1, no. Suppl 1, pp. S188–S195, Jun. 2009.

- [36] R. Westermeier, A. Biosciences, and E. Gmbh, "Gel Electrophoresis," pp. 1–6, 2005.
- [37] H.-Q. Wang and Z.-X. Deng, "Gel electrophoresis as a nanoseparation tool serving DNA nanotechnology," *Chinese Chem. Lett.*, vol. 26, no. 12, pp. 1435–1438, 2015.
- [38] C. Yang, H. Huang, J. Castro, and A. Yi, "High-aspect-ratio microfeature injection molding."
- [39] U. M. Attia, S. Marson, and J. R. Alcock, "Micro-Injection Moulding of Polymer Microfluidic Devices," vol. 7, no. 1, pp. 1–28, 2009.
- [40] L. X. Kong, A. Perebikovskiy, J. Moebius, L. Kulinsky, and M. Madou, "Lab-on-a-CD: A Fully Integrated Molecular Diagnostic System.," *J. Lab. Autom.*, p. 2211068215588456-, 2015.
- [41] A. Bacconi et al., "Improved sensitivity for molecular detection of bacterial and Candida infections in blood.," *J. Clin. Microbiol.*, vol. 52, no. 9, pp. 3164–74, Sep. 2014.
- [42] J. Koo and C. Kleinstreuer, "Liquid ow in microchannels: experimental observations and computational analyses of micro uidics effects," *J. Micromechanics Microengineering*, vol. 13, pp. 568–579, 2003.
- [43] K. W. Oh and C. H. Ahn, "A review of microvalves," *J. Micromechanics Microengineering*, vol. 16, no. 5, pp. R13–R39, 2006.
- [44] J. Siegrist et al., "Serial siphon valving for centrifugal microfluidic platforms," *Microfluid. Nanofluidics*, vol. 9, no. 1, pp. 55–63, 2010.
- [45] R. Gorkin et al., "Centrifugo-pneumatic valving utilizing dissolvable films.," *Lab Chip*, vol. 12, no. 16, pp. 2894–902, Aug. 2012.
- [46] G. R. et al., "Centrifugo-pneumatic valving utilizing dissolvable films," *Lab Chip*, vol. 12, no. 16, pp. 2894–2902, 2012.
- [47] N. Dimov et al., "Solvent-selective routing for centrifugally automated solid-phase purification of RNA," *Microfluid. Nanofluidics*, vol. 18, no. 5–6, pp. 859–871, 2015
- [48] D. J. Kinahan, S. M. Kearney, N. Dimov, M. T. Glynn, and J. Ducreé, "Event-triggered logical flow control for comprehensive process integration of multi-step assays on centrifugal microfluidic platforms," *Lab Chip*, vol. 14, no. 13, pp. 2249–2258, 2014.
- [49] A. S. Balankin, J. C. Valdivia, J. Marquez, O. Susarrey, and M. A. Solorio-Avila, "Anomalous diffusion of fluid momentum and Darcy-like law for laminar flow in media with fractal porosity," *Phys. Lett. Sect. A Gen. At. Solid State Phys.*, vol. 380, no. 35, pp. 2767–2773, 2016.
- [50] R. Burger et al., "Centrifugal microfluidics for cell analysis," *Curr. Opin. Chem. Biol.*, vol. 16, no. 3–4, pp. 409–414, 2012.
- [51] R. Burger and J. Ducreé, "Handling and analysis of cells and bioparticles on centrifugal microfluidic platforms," *Expert Rev. Mol. Diagn.*, vol. 12, no. 4, pp. 407–421, May 2012.
- [52] M. Tang, G. Wang, S. K. Kong, and H. P. Ho, "A review of biomedical centrifugal microfluidic platforms," *Micromachines*, vol. 7, no. 2, 2016.
- [53] T. Li, Y. Fan, Y. Cheng, and J. Yang, "An electrochemical Lab-on-a-CD system for

- parallel whole blood analysis," *Lab Chip*, vol. 13, no. 13, pp. 2634–2640, 2013.
- [54] W. Lee, W. Fon, B. W. Axelrod, and M. L. Roukes, "High-sensitivity microfluidic calorimeters for biological and chemical applications," *Proc. Natl. Acad. Sci.*, vol. 106, no. 36, pp. 15225–15230, 2009.
- [55] D. J. Jeanmonod, Rebecca, K. et al. Suzuki, and M. Hrabovsky, "Impedimetric Sensors for Bacteria Detection," *Intech open*, vol. 2, p. 64, 2018.
- [56] S. Brosel-Oliu, "Impedimetric Sensors for Bacteria Detection," N. Uria, Ed. Rijeka: IntechOpen, 2015, p. Ch. 9.
- [57] F. Yu, X. Dai, T. Beebe, and T. Hsiai, "Electrochemical impedance spectroscopy to characterize inflammatory atherosclerotic plaques," *Biosens. Bioelectron.*, vol. 30, no. 1, pp. 165–173, Dec. 2011.
- [58] E. I. Spectroscopy and N. Eis, "Impedance Basics," no. 1.
- [59] L. Yang and R. Bashir, "Electrical/electrochemical impedance for rapid detection of foodborne pathogenic bacteria," *Biotechnol. Adv.*, vol. 26, no. 2, pp. 135–150, 2008.
- [60] G. Ertürk and B. Mattiasson, "Capacitive Biosensors and Molecularly Imprinted Electrodes," *Sensors (Basel)*, vol. 17, no. 2, p. 390, Feb. 2017.
- [61] A. Bratov, N. Abramova, M. P. Marco, and F. Sanchez-Baeza, "Three-Dimensional Interdigitated Electrode Array as a Tool for Surface Reactions Registration," *Electroanalysis*, vol. 24, no. 1, pp. 69–75, Jan. 2012.
- [107] C. Berggren, B. Bjarnason, and G. Johansson, "Capacitive Biosensors," *Electroanalysis*, vol. 13, no. 3, pp. 173–180, Mar. 2001.
- [62] V. Perumal and U. Hashim, "Advances in biosensors: Principle, architecture and applications," *J. Appl. Biomed.*, vol. 12, no. 1, pp. 1–15, 2014.
- [63] A. Ståhlberg, C. Thomsen, D. Ruff, and P. Åman, "Quantitative PCR Analysis of DNA, RNAs, and Proteins in the Same Single Cell," *Clin. Chem.*, vol. 58, no. 12, p. 1682 LP-1691, Dec. 2012.
- [64] E. K. Sackmann, A. L. Fulton, and D. J. Beebe, "The present and future role of microfluidics in biomedical research.," *Nature*, vol. 507, no. 7491, pp. 181–9, 2014.
- [65] A. K. Bej, "Amplification of nucleic acids by polymerase chain reaction (pcr) and other methods and their applications," *Crit. Rev. Biochem. Mol. Biol.*, vol. 26(3/4), pp. 301–334, 1991.
- [66] R. K. Saiki et al., "Primer-Directed Enzymatic Amplification of DNA with a Thermostable DNA Polymerase Published by: American Association for the Advancement of Science Stable URL: <http://www.jstor.org/stable/1700278> REFERENCES Linked references are available on JSTOR for t," vol. 239, no. 4839, pp. 487–491, 2016.
- [67] R. Puchades and A. Maquieira, "Analytica Chimica Acta Recombinase polymerase and enzyme-linked immunosorbent assay as a DNA amplification-detection strategy for food analysis," *Anal. Chim. Acta*, vol. 811, pp. 81–87, 2014.

Chapter 3

Development of eLoaD for Multiple Liquid Type Handling Biosensing Platform

3.1 Introduction

POC systems have significant benefits; where near patient testing becomes a reality and reduces the need for centralised laboratories. With the reduced sample-to-answer time, early diagnosis of disease is obtainable, which is a highly desirable attribute for the identification of blood stream infections such as bacterial meningitis [1] ,[2], [3] With a shorter sample-to-answer timeframe, faster treatment plans can be devised for patients. POC devices also reduce sample and reagent consumption which will drive the cost of care down, as well as reduce the length of stay within an emergency room and outpatient clinical visits which ensured optimum use of the clinician/consultant's time. The benefits associated with POC devices are quite evident, however in order to implement these procedures and maximise the key advantages, POC methods must meet specific criteria [4].

In this chapter, a novel electronic Lab-on-a-Disc (eLoaD) platform has been developed and optimised for the capture and detection of biohazardous analytes which may be present in buffer, culture media and whole blood. The centrifugal microfluidic device is capable of sample-to-answer in 15 minutes, where EIS techniques are used for detection purposes. The device is able to distinguish whether bacteria is present within the sample and if the present bacteria are Gram-Positive, Gram-Negative, Fungal, or a combination on the integrated biosensor which is physically inserted into a modified PMMA base.

Using LoaD technology, the sample and liquids within the device is propelled through a series of channels by centrifugal forces which are applied to the system using a motorised spin-stand apparatus. The flow rate and thus the incubation of the sample over the electrode area can be altered by adjusting the spin-frequency of the platform. Using dissolvable film (DF) technology, the device is fully automated through the triggering of wash and electrolyte steps though an increase of the spin-rate. DF tabs offer full automation of the device, where the spin frequency of the device controls the reagent triggering system. This is a simpler alternative to wax valving, or laser actuated valving, as no additional external mechanism is required to actuate DF tabs [8]. By creating an integrated, fully automated system, the device becomes user friendly and highly

applicable for a POC setting. The device is composed of three identical testing sites, where 1.7mLs (x3) of the acquired sample is injected into the preloaded device. Small volumes of blood were used to have a desired concentration of pathogens within the sample without having a large amount of interferences from blood components such as white and red blood cells. As the pathogen count can be as low as 1-10 CFU/mL in a sepsis sufferer blood sample, 5.1mLs of blood must be acquired from the patient to increase the capture efficiency of the platform. This sample response from the platform is averaged out to improve the validity to minimise false-positives and false-negatives.

Each pre-loaded water step is simply DI H₂O (Deionised water) where the electrolyte step was 1mM DPBS (Dulbecco's phosphate buffered saline) for electrochemical detection purposes. The small sample volumes also will reduce biohazardous waste and also allows the platform to be a reasonable size for user handling. Each disc was produced using rapid-prototyping techniques and is a one-use, disposable platform. Direct detection of the analyte avoids lengthy amplification times of the target i.e. by blood culture, and costly filtration and purification steps. With such a short response time, it is proposed that such a device would be close to an ideal near-patient or POC system.

With this system, we can provide rapid confirmation for patients and clinical staff if sepsis is present. This would overall reduce the overuse of antibiotics within hospitals, and also reduce the amount of blood cultures delivered to the Microbiology laboratory.

3.2 Assay Requirements and Device Specifications

To determine the optimal approach of the automated device design, a basic breakdown of the platform's requirements from the user are collected and detailed in Figure 3.1. Each step of the test is described, where for this case the user input, the performance of the test, and the time dependency stages are detailed. Each protocol step was required in order for a fully functional assay to be achieved.

The diagram illustrates each essential assay step, where the range of external, user inputs, assay stages and time dependent stages are colour coded to determine the specific tasks of the microfluidic device. Extracting information from this guide, along with sample conditions (type of sample, viscosity and volume), the design parameters for the microfluidic platform can be determined. For an automated device, reagents are required to be pre-loaded. A valving system must be implemented, where flow regulators can control the reagents storage and actuation depending on the triggering response. Three separate fluids are required for the assay completion. The sample and incubation times are the only variables with the device, which have a direct correlation due to viscosity factors. The DI H₂O wash and DPBS electrolyte steps are recurrent reagents, therefore can become fully integrated in the system to allow the device be user friendly and automated past the point of sample injection. From this guide, five main chambers must be designed for the platform. A main sample reservoir, an electrode incubation chamber, two reagents compartments and the waste collection point. Channels connecting sequential chambers must also be designed to control flow and manipulate the displacement of these fluids.

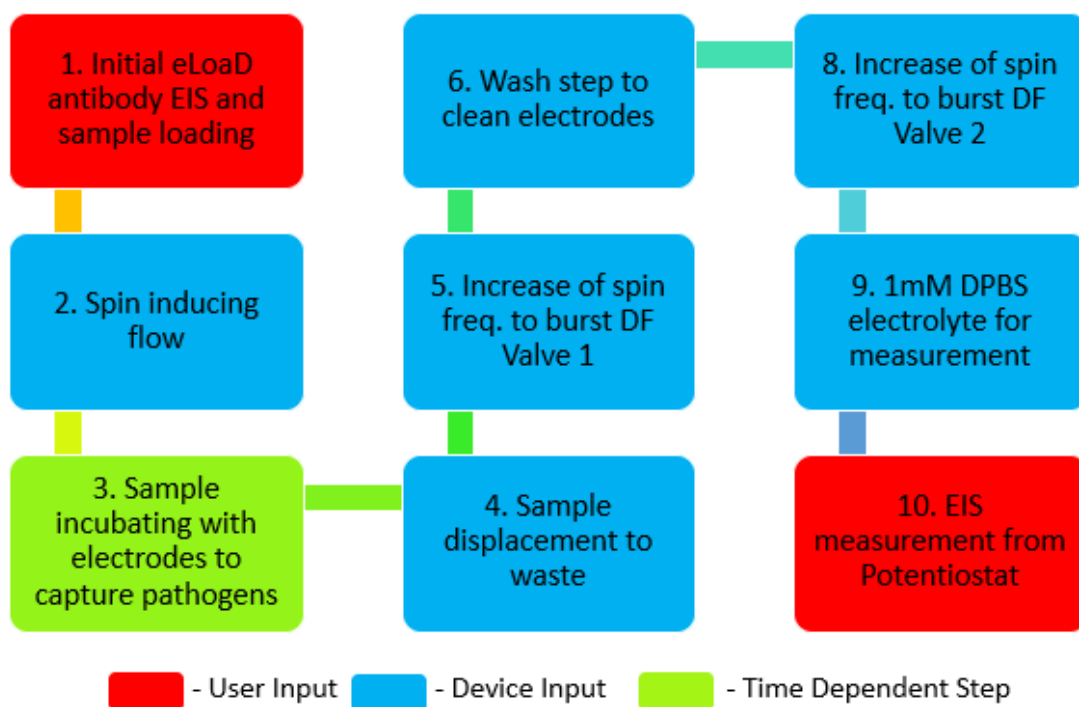


Figure 3.1. Assay requirements for automated device capable of capturing and detecting pathogens with implemented biosensor

3.2.1 Converting protocol steps into microfluidic features

The initial stage of the assay is the loading of the sample. Firstly, the type of sample must be considered. The viscosity and volume were examined, as this would determine how the fluid will flow through microchannels, how long they will remain in each chamber, its effect on incubation times within the electrode detection chamber, and its displacement time into the waste chamber. For the insertion of the fluid into the device, loading holes must be applied to the design, as well as adequately sized reservoirs. As patient samples for pathogen testing may come in many fluid types (blood, urine, saliva, tracheal intubation swab elution), the device must be capable of testing various viscosity types. Pathogens may be suspended in DPBS buffer, cultured samples in BacT or BacTec, and whole blood. The viscosities of each sample type are determined in Table 3-1.

Table 3-1 Viscosity of fluid types tested within eLoaD device

Sample Type	Viscosity (1 cP = 10^{-3} Pa·s)
Whole Blood (37°C)	3 - 4
Whole Blood (20°C)	3.8 - 5.04
Plasma	1.65
Serum	1.4
Culture Media	1.1
PBS	1
Water	0.91

Blood is a non-Newtonian fluid; therefore, its viscosity depends on shear rate. At high shear, blood cells disaggregate, deform and align in the flow direction which reduces viscosity. However, at low shear the blood cells can aggregate which induces a higher viscosity. Other factors that influence the viscosity of blood are the deformability of RBCs and temperature [9], gender and health status of the patient. The percentage of haematocrit (presence of macro-molecules) contributes to the varying viscosity from sample to sample, as a haematocrit of 40% (40% volume of RBCs/ total liquid volume) has a viscosity of 3~4cP but increasing the haematocrit to 60% doubles the viscosity to 8cP. Temperature must always be considered as for each 1°C decrease, there is a 2% increase in blood viscosity [10]. According to Cinat *et. al* A decrease in whole blood temperature

from 36.5°C to 22°C causes a 26.13% increase in the viscosity of the sample with a 34.73% decrease in erythrocyte deformability and 18.71% increase in plasma viscosity. When the temperature of blood increases from 36.5°C to 39.5°C, sample viscosity decreased by 10.8%, where the plasma viscosity decreased also by 4.99% [11]. As the platform itself is not temperature controlled, a fail-safe must be implemented to overcome the possibility of the changing viscosity of blood containing samples which may affect the flow and incubation times of the sample and the biosensor surfaces.

This will essentially determine the temperature in which the samples must be tested or stored. Considering these factors, specific design criteria must be implemented to assist the flow of blood through reservoirs and channels without aggregation to avoid channel blocks and over-incubation of the samples over the electrodes. For the sample flow to be controlled, microchannels are designed and implemented between reservoirs. The design of these channels essentially effects the flow rates and incubations times, how the reservoirs fill and empty, and where the fluid is displaced.

The sample liquid was expected to be passed from the initial sample chamber to the succeeding functionalised electrode reservoir, where sample-to-antibody mixing occurs, thus an essential microchannel is required. Often the dimensions of these channel types aren't considered critical, however due to the complex nature of the desired samples they potentially can be. Liquids encountering microchannel openings have a low cross-sectional area in rapid prototyping microfluidics. As the ratio of scales between depth and length differs greatly ($\mu\text{m}:\text{mm}$), capillary action is a predominant force within this channel. The ratio of molecular cohesion forces within the sample or reagent, and adhesion forces existing between the fluids and the surrounding material and have a huge effect on the flow rate of the sample. If the flow rate is an important factor for the assay, the cross-sectional area of the channel must be optimised. As the PSA used has a fixed thickness of 86 μm , the width and length of the channels must be optimised to control the flow of sample displacement between reservoirs [12]. As centrifugal forces are the primary fluid driving force for the platform on a 2-dimensional plane, the height of the channel placement within the device can also be manipulated to provoke sample mixing. As the aim is to capture low CFU/ml in a sample size ~ 1.7 ml in a short amount of time, a large electrode incubation chamber must be employed for several reasons;

- House the 5-electrode system for capture and detection of pathogens
- Contain a large amount of sample received from the sample chamber
- Provoke sample mixing
- Act as the mediating chamber between sample and waste reservoirs
- Controlling reservoir for sample incubation times
- Ensure all pathogens come into contact with the electrode surface

The secondary channel, located between the electrode incubation chamber and the large waste collection chamber must also be connected by a microchannel, dubbed the “waste channel”. This too must follow similar specifications previously detailed for the microchannel. Again, the length and width of this channel will determine the exit flow rate of the sample entering the waste chamber. If the flow rate is too fast, the sample will have little interaction with the electrodes, reducing the chance of pathogen capture, if the flow rate is too slow, there is a large chance of surface contamination from blood components non-specifically binding to the electrode surfaces causing false-positive results. An optimum channel dimension must be achieved to regulate the sample interaction with the functionalised electrodes.

Once the chamber and channel arrangements have been decided through fluidic testing of the platform, their position on the device must be determined. Centrifugal forces act in an outward radial position; therefore, the location of these features is important as the fluid in each chamber experiences different factors of the driving force of the platform at a given spin frequency. Different spin-rates are applied to the system from an external motorised system, in which the device is attached.

[3.2.2 Chemical and biological reagents used](#)

GTX40307 Gram Negative Endotoxin [308] Mouse Monoclonal Antibody, GTX36804 Gram Positive bacteria LTA [3801] Mouse Monoclonal Antibody and Native Candida Rugose Cholesterol Esterase Purified Protein purchased from Genetex (USA). Peg₈-thiol purchased from Quanta (USA). Bovine Serum Albumin (BSA), Glutaraldehyde, Triton, DPBS, Flourosshield mounting media, Ethanol, IPA, Tween and Saponin all purchased from

Sigma Aldrich (Ireland). The Live/Dead bacteria viability kit purchased from Life Sciences. BD BacTec Culture Media bottles were purchased from BD (UK). Gold plating solution purchased from Technik Inc. (UK).

3.2.3 Materials used in manufacturing the microfluidic disc

The ELoaD was manufactured from varying layers off 2mm PMMA and PSA (ARcare7840) from Radionics and Adhesive Research respectively. The discs were assembled using the rapid-prototyping process as outlined in Section 2.3. The Au coated Si wafers were purchased from Platypus, which are diced into 30mm x 5mm Au electrodes. M77 glue was acquired from Scotch (United Kingdom).

3.3 Experimentation

3.3.1 System Design and Experimentation

The electrode configuration is pre-functionalised, ready for testing. Once functionalised, the electrochemical impedance spectroscopy (EIS) response of the antibody surface was obtained. This impedance value was used for a before and after comparison between antibody (EIS 1), and antibody plus sample (EIS 2). This change in impedance ($\Delta\text{EIS}/\Delta Z$) would be an indication of whether an analyte has been captured or not, and depending on the change, whether it is a high or low concentration of the captured pathogen.

The eLoaD assay was kept simple in order to reduce sample-to-answer time to keep within the margins of the “golden-hour” sepsis diagnosis rule. The simplified assay consisted of sample incubation for analyte capture, a DI H₂O wash step following by an analyte to trigger into the detection electrode chamber for EIS measurement purposes.

The eLoaD device was manufactured using the protocol outlined in Section 2.3. The final device was a nine-layer microfluidic device. Each layer of the device described in *Table*

3-2, the internal architecture of the device is further described in Figure 3.2. The platform itself is portrayed in Figure 3.2 and visually translates the concept to physical device transition.

Table 3-2. Describes each layer of the ELoad device, with each material and function described in detail.

Layer No.	Description
1. Vents (2mm PMMA)	Rigid layer containing an array of holes acting as entry points for loading samples and reagents into the lower layers of the device. These holes are also used as venting mechanisms to ensure fluid flow throughout the system
2. Microchannels (86µm PSA)	Contains an assortment of microchannels necessary for the routing of liquid between specific reservoirs. These microchannels also act as a means of flow control, where channels are connected to air and pressure chambers.
3. Reservoirs (2mm PMMA)	Contains reservoirs which are required for the storage of the sample, reagents and the waste. This layer also gives depth to the device which is needed for the volume of liquids used.
4. DF Cover (86µm PSA)	Location of access points to the dissolvable film (DF) tab once routing of the liquid to their position is activated. This layer also contains air passages needed for air circulation and air compression to aid the control of burst frequency desired for the DF tabs.
5. DF Support (86µm PSA)	Mirrored against layer 4, where the only difference lies with a Section for the DF tab placement and securement.
6. Midlayer (2mm PMMA)	Another PMMA layer which contains reservoirs for storage of the sample, reagent and waste. Once activated, this layer provides passage for liquid travelling from the microchannels, through the DF tab towards lower channels.

<p>7. Lower-Channels (86µm PSA)</p>	<p>Microchannels for the displacement of liquid from the reagent storage chambers to the detection chamber, and finally the waste chamber.</p>
<p>8. Electrode Cover (86µm PSA)</p>	<p>PSA layer which only exposes the functionalised area of the electrodes whilst also exposes the top of the counter and reference electrodes which is vital for impedance detection within the device.</p>
<p>9. Raster Base With electrodes (2mm PMMA)</p>	<p>Final 2mm Section of the device which contains 3 sets of the 5 electrode configuration. 2mm PMMA has rastered Sections of 0.8mm depth to accommodate electrodes. These functionalised electrodes capture the pathogens which induces an impedance change.</p>

With each layer of the device described in *Table 3-2*, the internal architecture of the device is further described in *Figure 3.3*. The platform itself is portrayed in *Figure 3.2* and portrays the concept from CAD design transitioning to a physical prototype.

Individual layers are exported as .DXF files to use with either the Epilog Zing laser for PMMA cutting or the GraphTec for the production of PSA layers. The device is composed of three identical testing sites. The inner diameter is 15.4mm to correspond with the motor spindle, where a wing-nut locks in the platform to secure the disc during rotation.

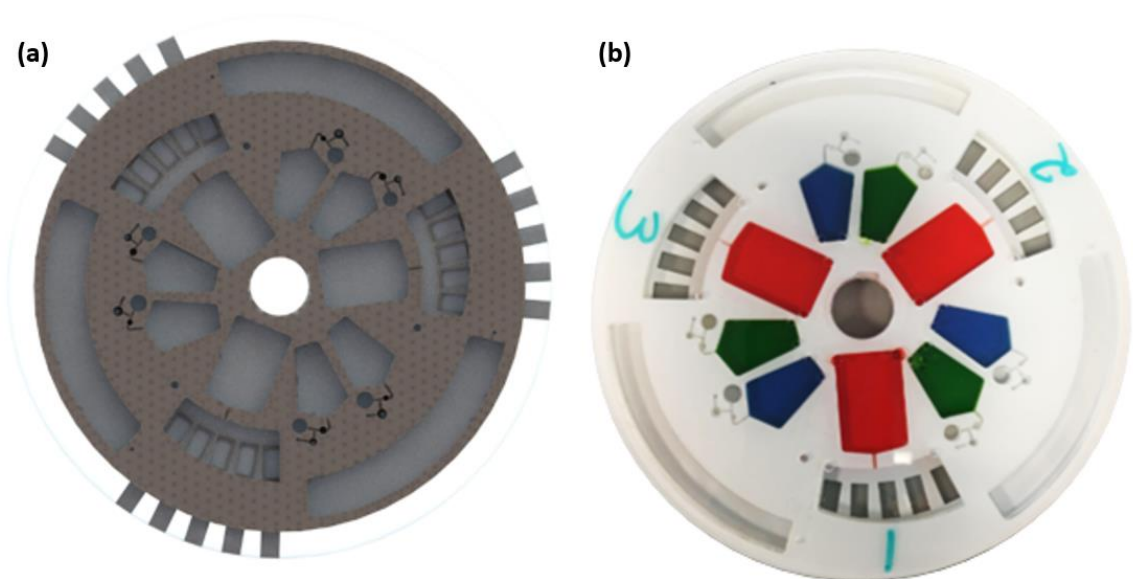


Figure 3.2. (a) represents the 3D model constructed using SolidWorks, 2017 software and (b) is the real-life rapid-prototyped ELoaD device.

3.3 2. Device Concept

The platform consists of five main reservoirs, all connected through microchannels of different sizes to control flow. These reservoirs are portrayed in Figure 3.3, below. Chamber **A** denotes the sample chamber, where two entry point located at the top of each reservoirs allow for loading and venting purposes. Chamber **B** depicts the 5 – electrode incubation chamber, where a controlled area of the antibody area is exposed through the electrode cover (layer 8 of the device, *Table 3-2*). The waste collection chamber is denoted by **C**, where both reagent chambers are marked by **D** and **E**.

All channels are sloped in a downwards radial position to aid fluid flow from a central position on the platform, to the most radially outward positioned chamber. The sample and reagents are loaded into the device were the centrifugal force (F_{ω}) generated by the motorised spin-stand forces the sample into the 5-electrode incubation chamber, and then into the waste. Each reservoir has its own distinct function, as outlined in *Figure 3.4*.

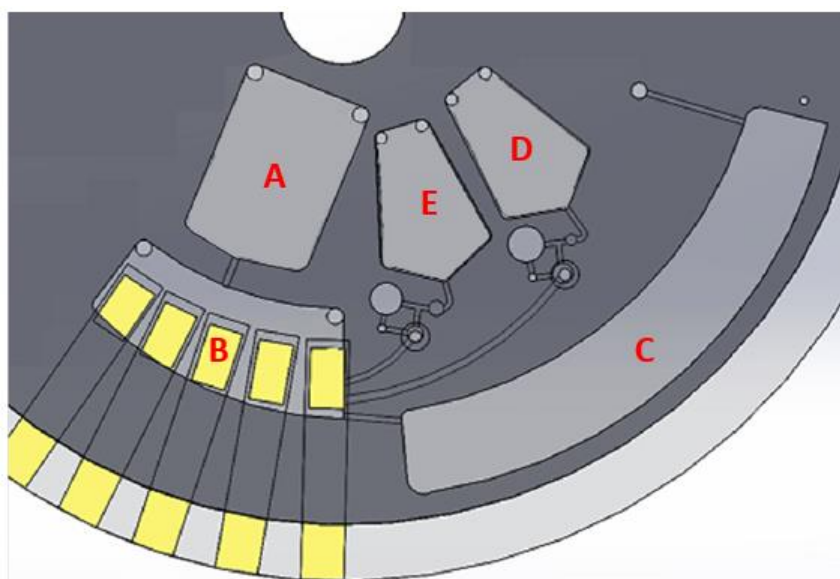


Figure 3.3. Main reservoirs within eLoadD device where; **A** denotes the main sample chamber, **B** represents the electrode incubation chamber which is connected to **C**, the collection waste reservoir. **D** and **E** represent the reagent storage chambers.

Chamber **A** contains 1.7 mL of sample which flows into chamber **B** by applying a spin frequency of 7-10Hz to the system. During this time, the sample builds up and incubates with the exposed electrodes, where any specific analytes will bind to the specific

electrode(s). This liquid was then displaced during this time into chamber **C**. The channel connecting **B** and **C** allows the flow of the sample, whilst also preventing backwards mixings due to its radially downward position on the platform. Once all the sample was displaced, the spin frequency of the platform was increased which trigger chamber **D**, contains the DI H₂O wash step. This removed any unbound components from the electrode surfaces which may have settled. Once the entire wash step was displaced to chamber **C**, the waste was now full, blocking off the channel connecting both chamber **B** and **C**. The final increment in the spin frequency triggers chamber **E**, which releases the 1mM DPBS step, remains in chamber **C** for detection purposes. The outer electrodes are connected to the potentiostat via crocodile connecting clips where the CH760E software will runs impedance measurements using specific input parameters. Each platform contains three identical, separate testing sites, which are used simultaneously. The detection of the analyte is determined from the change in impedance ($\Delta EIS/ \Delta Z$) i.e. EIS 1 – EIS 2.

The difference of these values determines whether pathogens are present in the sample and if so, what category they fall under. This entire process is portrayed in Figure 3.4. As the device is composed of nine-overlapping layers, a full optimisation of the device was essential for reproducibility purposes.

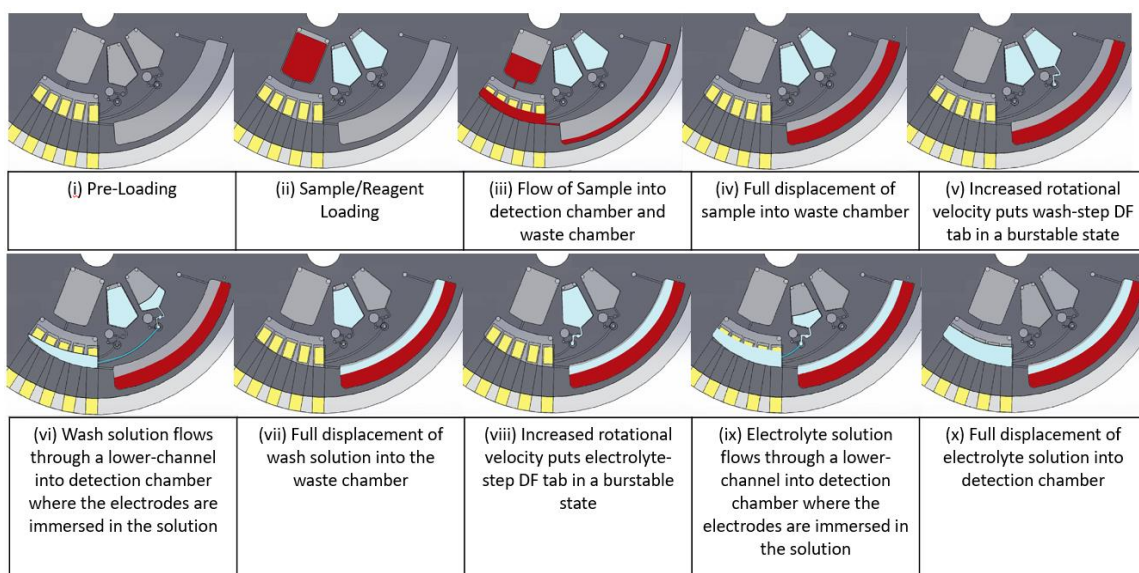


Figure 3.4. Representation of the ELoaD assay where (i) displays the testing site before pre-loading of sample and reagents compared to (ii) loading of all components. (iii) Applying a spin-frequency displacing sample into the electrode incubation chamber. (iv) Full displacement of sample to waste. (v) An increase in spin frequency puts the wash tab into a burstable state where (vi) Triggering of wash step into the electrode incubation chamber, completely filling the waste chamber and blocking the waste channel. (vii) Increment in spin-frequency placing the wash step (vii) into a burstable state where the 1mM DPBS flows into the electrode incubation chamber only (ix). EIS measurements (x).

3.4 Developing and optimising the eLoaD centrifugal microfluidic platform

Section 3.3 described the final fully automated device; however, the platform underwent many design modifications to fully optimise the performance. Both fluidics and biosensor integration techniques were employed. The development of the eLoaD has undergone a vast optimisation and characterisation procedure to ensure that the final product was a robust, easy to use device. Each design stage is outlined with specific attention paid to the dimensions of microchannels and automation of the platform. The optimisation of the platform is broken down into three categories. Version 1 of the device used sputter coated electrodes of the base for the sensors. Version 2 and its sub versions used Au coated Si electrodes and an Indium Tin Oxide (ITO) reference electrode where Version 3 and its sub versions used five Au coated Si electrodes for the embedded sensors.

3.4.1 Version 1.0

The initial platform designed contained three electrodes within each chamber. This version was to determine the use of sputtered Au electrodes on a PMMA base. An n=3 for each platform can be determined through the design of 3 identical testing sites. For the development of this device, the base was fabricated using the standard laser-cutter procedure outlined in Chapter 2. The CAD drawing of V. 1.0 is detailed in Figure 3.5 (a).

The three electrode system mimics that of the system observed in typical electrochemical cells where Figure 3.5 (b) denotes the counter, working, and reference electrodes where only a specific area of the electrode system was exposed in the electrode incubation chamber. Each feature of the device is outlined using a coloured legend to highlight each specific reservoir function, where each channel and DF tab system is titled. The working order of the assay follows that of the procedure previously explained in this chapter. Microchannel A is placed at an angle of 40° to reduce flow rate, as it's placed at a slant against the centrifugal forces applied to the system. This channel was strategically placed

over the working electrode to allow maximum contact with the sample and the functionalised working electrode.

Siphon **B** connects both the electrode incubation chamber and the waste chamber, where it has dual functionality. Firstly, during rotation, the channel will only prime to that of the liquid head in the electrode chamber, forcing the sample to remain to incubate within the for that constant spin state. Here the centrifugal forces are greater to the capillary force experienced within the siphon channel. Reducing the spin frequency of the rotating platform reduced the centrifugal forces applied to the eLoaD, therefore the capillary forces become predominant, allowing the channel to prime and to carry out its second function of sample displacement to the waste chamber. The electrode incubation chamber itself is sloped at an angle towards the siphon channel to encourage flow towards the waste chamber and to ensure all sample get displaced.

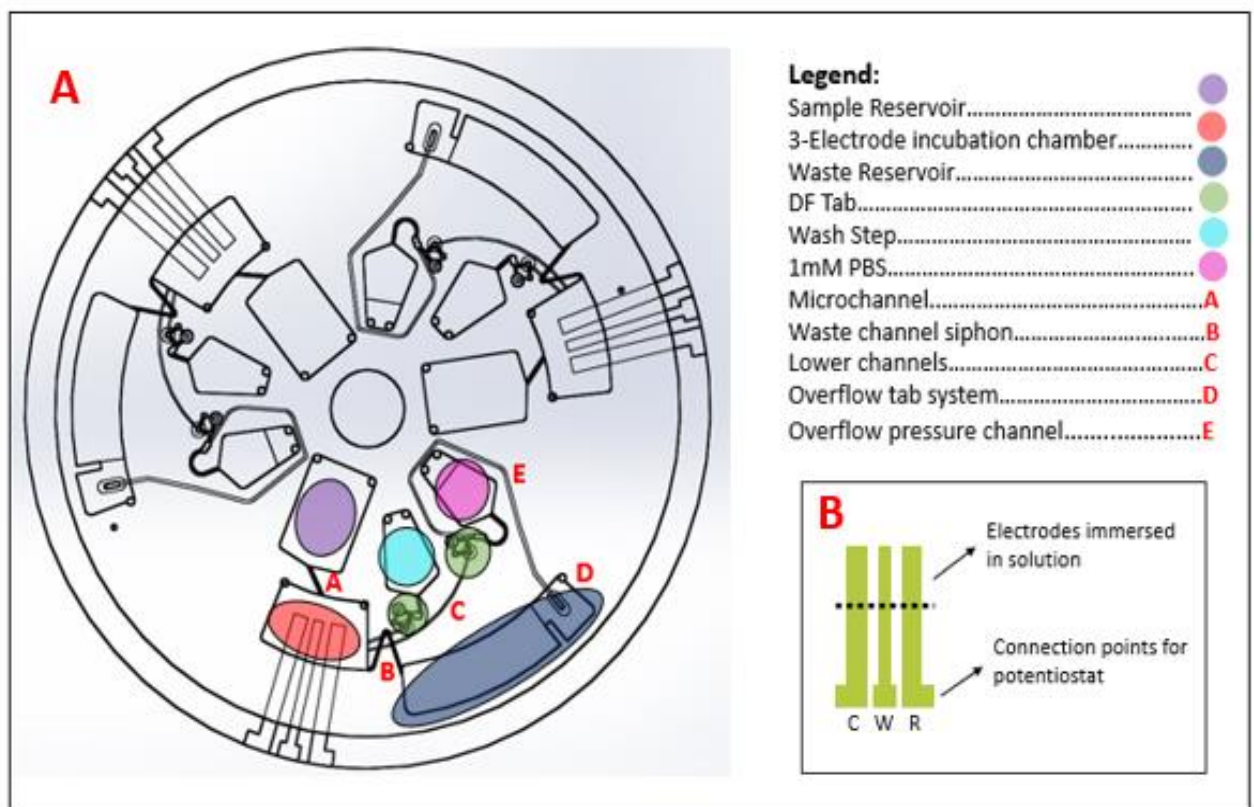


Figure 3.5 Portrays V. 1.0 of the ELoaD device design where (a) portrays the CAD drawing of the centrifugal platform with corresponding legend to further detail each component and (b) represents the electrode configuration of the sensing platform.

The waste chamber itself was divided into two separate Sections, where a small wall feature within the chamber separates the main waste collection area and the DF tab overflow system **D**. Once the sample was fully displaced into the waste, it would remain in the main waste collection site. With an increase of the spin frequency, the DF tab connected to the wash step reservoir would burst, triggering the flow of the DI H₂O into the electrode incubation chamber via a lower channel **C**. As the siphon was previously primed, the water would then displace directly into the waste. Here, the water flows into the waste, and overflows over the small partition into the second Section of the waste chamber. The DI H₂O would then come into contact with the slot DF tab **D** which will relieve pressure accumulated in the overflow pressure channel **E** and allow the second DF tab associated with the 1mM electrolyte to be put into a burstable state. With another increase in the spin frequency, the 1mM DPBS was displaced into the electrode incubation chamber, where it will cover the electrodes without displacement to the waste chamber. The eLoaD assay was complete, where it was then connected to the potentiostat for a readout. The device was an 8-layer device, where layers 1-7 follows the same layout as described in *Table 3-2* where layer 8 is a base layer which contains the biosensor surface.

The fabrication of the gold electrode configuration was initially used in conjunction with the Au sputtering, as the sensors deposited onto the surface are so thin that the device can be pressure laminated together with no gaps forming between the lower channel layer and the base. The sputtering coater (Quorum Technologies, UK) technique also allows an array of electrode dimensions to be explored, as the mask template was created using CAD software and fabricated using the GraphTec equipment. To adhere the Au to the surface on the PMMA, a high voltage is applied to the gold targets to forcefully transfer the Au atoms to the PMMA surface through the mask design for 2 minutes. Literature indicates that the thickness of Au coating in N₂ gas can be determined at 2.5kV where the thickness of gold (angstroms) = $7.5 * I * t$, where the distance from sample to target is 50mm. The current was measured in mA and time in minutes where the parameters for 80nm of gold to be deposited are $I = 36\text{mA}$ and the time is set to 3 minutes [13].

The pre-cut disc was immersed in 1M L-Cysteine solution for 1-hour and dried at room temperature ($20\pm 2^{\circ}\text{C}$). The L-cysteine coating electrodes can readily bind to antibodies, therefore can be functionalised with a variety of antibodies, proteins or amino acids [14] as portrayed in Figure 3.6 below.

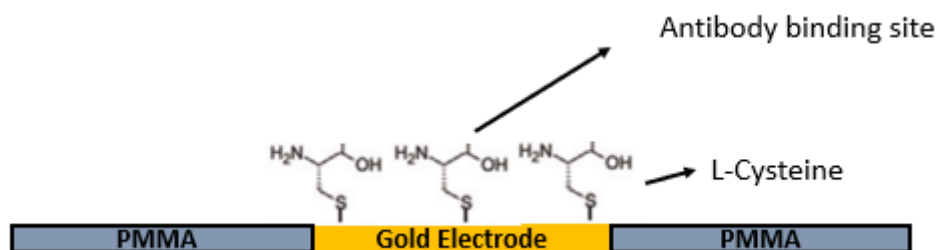


Figure 3.6. Schematic of deposited Au electrode with antibody activated sites through L-cysteine structures.

EIS measurements were carried out but the Au electrodes became unstable in aqueous solution and became slightly damaged after EIS 1 was obtained. Despite the device being designed for single use, the two separate EIS measurements that must be obtained, the electrodes became unstable after the initial measurement. With unstable sensors, the test outcomes are unreliable and therefore this was the first major issue which was dealt with.

3.4.2 Version 2.1

Issues to address from the previous version are detailed in *Table 3-3* below,

Table 3-3 Troubleshooting guide 1 for eLoad

Issue with previous version	Rectification
Unreliable sputtered sensors	Change working electrode to more stable gold surface

To address the electrode issue for the V 1.0 device, diced Au coated Si wafer electrodes (30mm x 5mm x 0.5mm) were fabricated for use with the device. Only the base layer and electrodes were developed in V 2.1, as the microfluidics of the device were functioning as required. To reduce cost, ITO acted as reference electrode. To implement both types of electrodes, a variety of rastering steps were carried out. To avoid leaking over the electrodes, they must be within a range of 0.2 - 0.3mm range from the top Section of the

platform. This range allows a gap to form to avoid the cracking of the Au electrodes whilst only requiring little amounts of glue to impede flow over the electrodes where the glue doesn't interfere with the electrical signal from the potentiostat. To optimise conditions used, a raster checkerboard was created to determine the optimum depths and laser settings, as shown in *Table 3-4*.

Table 3-4. Raster laser settings for optimum electrode depth

Raster Settings	Power (%)	Speed (%)
Au electrodes	100	32
ITO	90	85

As Au coated Si electrodes replaced the original electrode arrangement, the functionalisation of the electrodes was altered for a more stable antibody layer. The test itself evolved from one working electrode in each test site, to three separate working electrodes, each functionalised with different antibodies. Figure 3.7 portrays the new electrode configuration where Reference (R), Gram positive antibody capture surface (WE1), Gram negative antibody (WE2), Fungal protein capture (WE3), and Counter (C) electrodes. The sensor fabrication was optimised and detailed in Chapter 4.

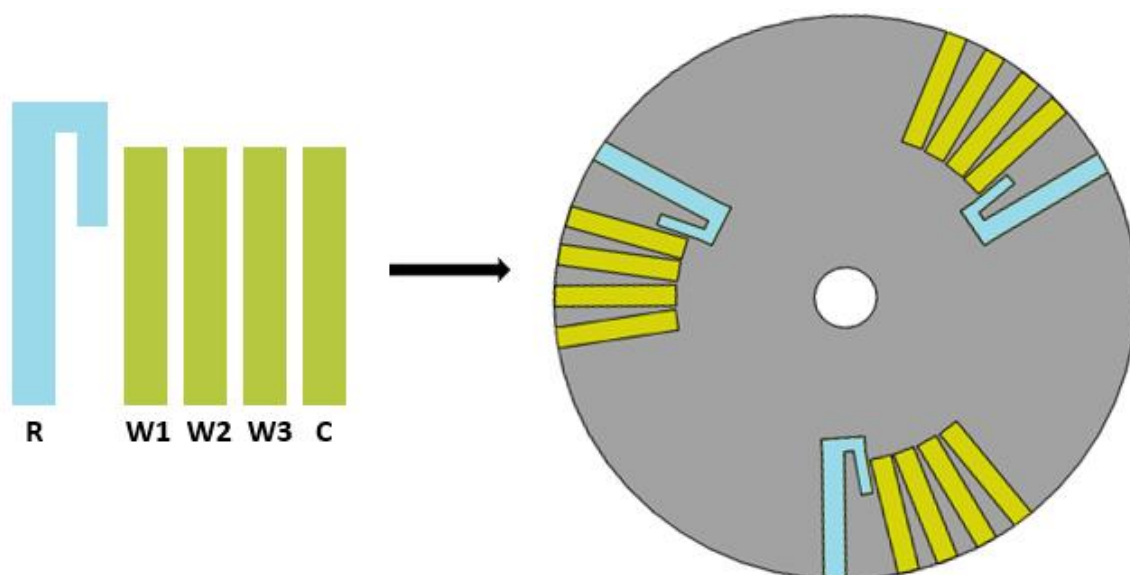


Figure 3.7. New electrode configuration for V2.1 device with ITO reference electrode and pre-cut Au coated Si wafer slides are utilised for the working and counter electrodes.

The ITO reference electrode was slightly hydrophobic therefore sealing issues were addressed by using glue. The hydrophobicity of the reference electrode wouldn't allow for the PSA of the adjacent device layer to seal the device and therefore leaking over the electrodes was observed under spinning conditions. To create the ITO reference electrodes, PSA was adhered to the back of an ITO sheet and cut into individual electrodes using the CO₂ laser. This allowed for uniform manufacture of the electrodes. To accommodate the extra electrodes, the electrode incubation chamber was altered. No other device changes were made. Initial testing of the device it was discovered that, after glue was placed around the perimeter of the base and top Section of the disc, leaking was observed over electrodes at low spin frequencies as low as 6Hz.

Minimal amounts of a soft glue were used as it contained a low-acetone concentration which can affect the surface chemistry of the gold electrode. In an effort to reduce the amount of glue used in the device fabrication an additional layer was implemented, as detailed for version 2.2.

3.4.3 Version 2.2

Version 2.2 was modelled off V 2.1, where all fluidics and reservoirs remained the same, however an additional layer was located between layer 7 and the base. The new layer 8 was dubbed the "electrode cover" and acted as an adhesive layer with individual opening sections, exposing fixed regions over each electrode. The layer allowed additional PSA to impede fluid flow over electrodes, as with careful preparation of the joining of both surfaces allowed sealing between electrodes and between the Au surface and PSA. A simple hand-roller was utilised to adjoin both parts, as care had to be taken to not interfere with the antibody functionalised Sections of the electrodes. This electrode cover became a method of determining the amount of the electrode surface exposed to the electrolyte solution and could be utilised as a way of varying the working electrode areas.

The fabrication of the device altered slightly with the addition of the electrode cover (layer 8). Layers 1-7 were assembled as previously described. The counter, reference and pre-functionalised electrodes were glued into the rastered base layer, where the electrode cover was carefully adjoined to the base using two alignment pins. The two Sections of

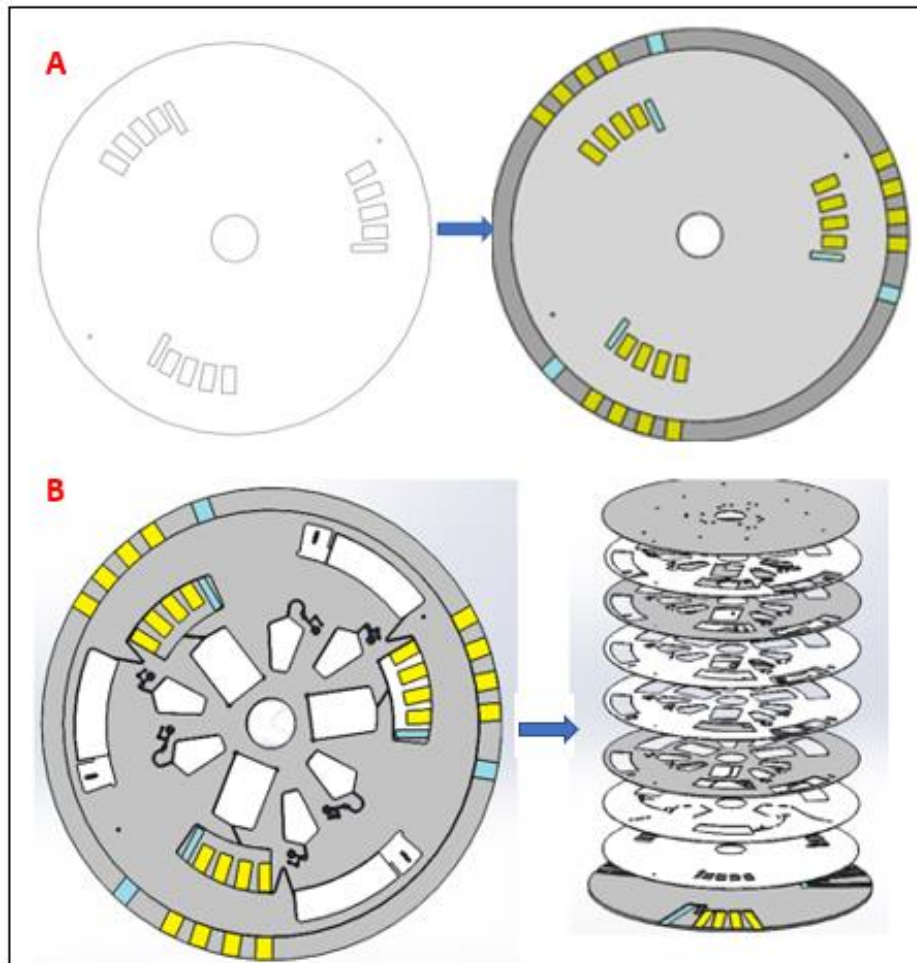


Figure 3.8. Details the additional layer inserted into V. 2.2. (a) The electrode cover (layer 8) design where once adhered to layer 9 of the device (b) shows V 2.2 of the device with the additional layer inserted.

the discs were then joined together where a hand roller was used to apply the required pressure to join the PSA layers without damaging the electrodes. The perimeter of the 130mm disc (i.e.

layer 8) required glue to fill any gaps between the electrodes and the device. Carefully placing minimal glue over the contact points for the potentiostat. The devices were physically clamped overnight @ 20 PSI to allow the glue sufficient time to set.

For a true indication of the platform's functionality with real-clinical samples, V.2.2 provided many insights into a range of necessary adjustments. 20mL bottles of BacT with real blood samples were acquired from the Coombe Hospital, Dublin. All previous versions of the platform were tested fluidically with food dye and DI H₂O, therefore the

microchannel and siphon were never tested with a viscous fluid. These blood culture samples were used to test the ability and working function of the sensor surface. A 1:10 dilution of the real samples was passed through the device using the aforementioned assay. Fifteen total blood culture samples were tested where false positive results were reported for all the samples. The EIS measurements for each of the antibody surfaces were determined to be very low, and with such a high discrepancy for each antibody surface the electrode arrangement itself was examined as the cause of the error. With the average of the antibody EIS values for the electrodes too low (ranging from 690 – 780 \pm 390 ohms) to detect a viable signal change, the electrodes again appeared to be the issue with the detection element of the device, which is described in detail in Chapter 4

The ITO electro-active surface became unstable after a single use, as air bubbles would form on the surface and making it very difficult to obtain an accurate EIS response, therefore was unsuitable to take multiple reading using the 1mM DPBS. With a different surface chemistry of the reference electrode compared to the Au coated Si electrodes, the EIS measurements obtained were unreliable due to a varied potential on the reference electrode providing false potential values for which the counter electrode utilises to drive current through the working electrode [14]. Literature indicates that ITO can become unstable in aqueous solution, where for the device in question, EIS measurements and optimisation may lead to 1mM DPBS being present in the chamber for up to one hour [15].

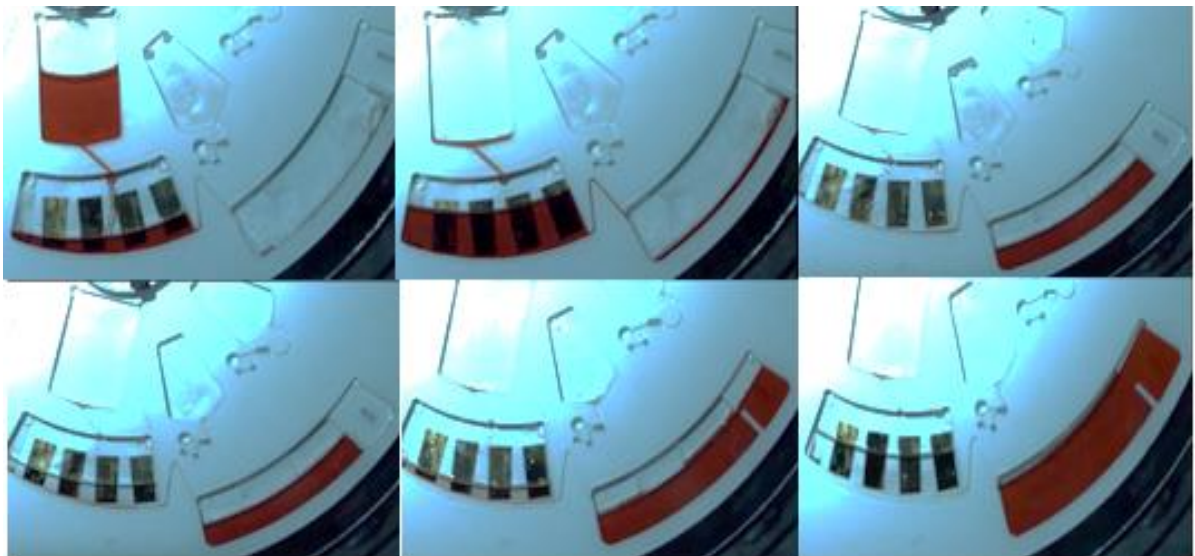


Figure 3.9. *The 9-layer device modelled off V2.1 with the additional layer-8 dubbed the “electrode cover” which has dual functionality; 1). Prevent leaking over electrode during LoaD rotation and 2). Expose specific areas of the electrodes which are exposed in the electrode incubation chamber.*

3.4.4 Version 3.1

Issues to address from the previous versions are detailed in the table below,

Table 3-5 Troubleshooting guide 2 for eLoaD

Issue with previous version	Rectification
Unreliable EIS response	Change working electrode to more stable gold surface
Design change required to implement Au reference electrode	Modify layer 8 electrode cover
Real samples blocking in microchannel A	Channel re-design for more viscous samples
DF burst frequency irregular	Remove the over-flow triggering system from the waste chamber

The blood culture samples obtained from the Coombe hospital were again used to test the functionality of this disc version V. 3.1. As previously described, blood is a non-Newtonian fluid, hence the spin-frequency applied to the system must be adequate to move the sample between chambers whilst not aggregating the sample which will cause channel blocks. Throughout testing, it was observed that microchannel **A** and the siphon channel **B** were unpredictable, where the same sample on one eLoaD was inconsistently running on the different testing sites due to clotting and blocking within different channels.

To address these problems, the microchannel **A** was re-designed to flow directly downwards, in an equal vector to the centrifugal force. This channel was repositioned to overhang over the middle of the electrode incubation chamber to equally distribute the sample over the three working electrodes. The length of channel was reduced from 5.2mm to 3.32mm to decrease the channel resistance to allow more viscous samples to flow. The channel itself was also widened from 0.65mm to 0.85mm, again, the reduced resistance whilst also maintain the capillary force which allows the sample to prime the passageway when no external forces are applied to the system.

The siphon channel **B** was replaced with a straight waste channel, which is discussed in Section 3.6. The electrode cover was modified to allow the replacement of the ITO reference electrode with an Au electrode to make all sensors in the device consistent. To allow the addition of the electrode, all raster setting for the 2mm PMMA base layer were set to 100% power and 37% speed. The wash chamber was increased in size to maximise liquid to electrode contact times whilst the waste collection chamber was also increased to accommodate the volume increase in the assay. All modifications to V. 3.1 are shown in Figure 3.10.

EIS measurement acquired with the new 5-Au electrode system provided excellent, replicable results with the new reference electrode, as fully described in Chapter 4. Gold is regarded as an ideal metal for electrodes in aqueous media and therefore would be the ideal electrode type for all electrodes within the system as two EIS measurements are required [16] With multiple tests carried out on this device, the triggering system for the DF tabs was determined inconsistent, with the PBS triggering out of sequence despite the waste chamber tab being contact. Further examination with spin frequencies, explained further in this chapter, deemed the triggering frequency of the device too high, essentially damaging the captured bacteria in the electrode incubation chamber and interfering with the EIS reading. A number of modifications were implemented to incorporate a reduced maximum spin frequency profile for the device.

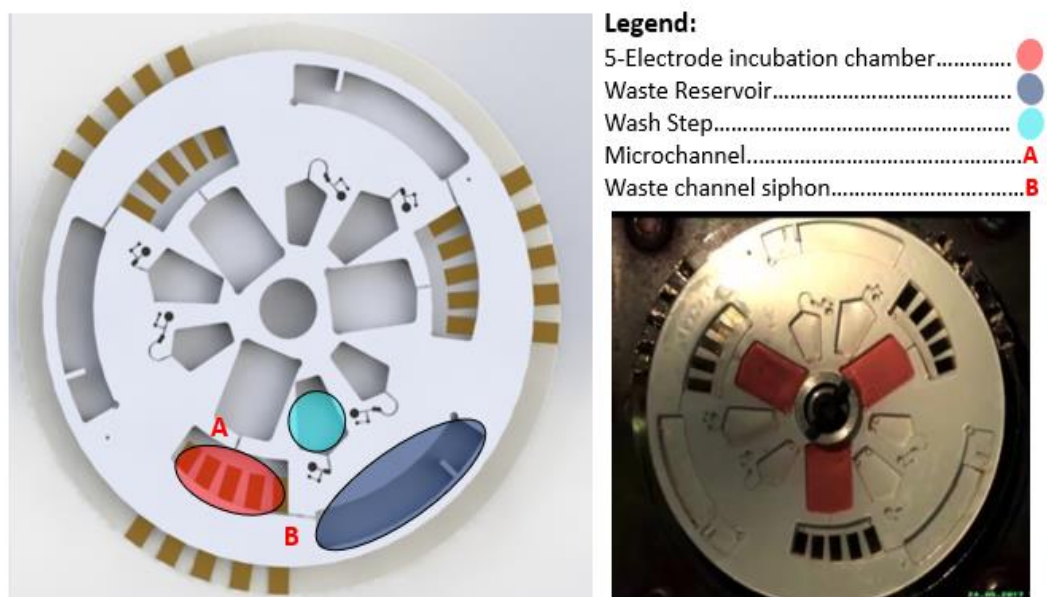


Figure 3.10. Version 3.1 of the full optimisation of the device, indicating the areas of re-design interest with a corresponding image acquired during the real time testing of the device.

Regarding the full automation of the platform's issues for V. 3.1, a number of modifications were implemented. One of the main modifications for V. 3.2 is the electrode incubation chamber. The volume was significantly decreased from 1.7mls to 1.3mls in an attempt to maximise the sample to functionalised electrode contact time to enhance the capture probability of the system. All exposed sections of the electrodes were made equal in an attempt to determine if shorter electrodes may be a possibility, reducing costs for sensor production. This only exposed 5 mm² of each electrode, making all sensing surfaces equal in the electrode incubation chamber. The overflow DF tab system was removed in an effort to reduce the spin-frequency of the platform. The full DF tab optimisation was discussed further in Section 3.5. With the removal of the overflow system, the internal structure of the device became simplified. The waste chamber volume increased to adjust to the new volumes of fluids in the platform. The overflow channel **E** was also removed as it was no longer required, where both reagent chambers are controlled by a DF tab system dependent of the pressure build up due to surrounding architectures and positioning on the platform, further outlined later in this chapter. The DPBS chamber was increased also due to available space on the platform. With the reduced volume in the

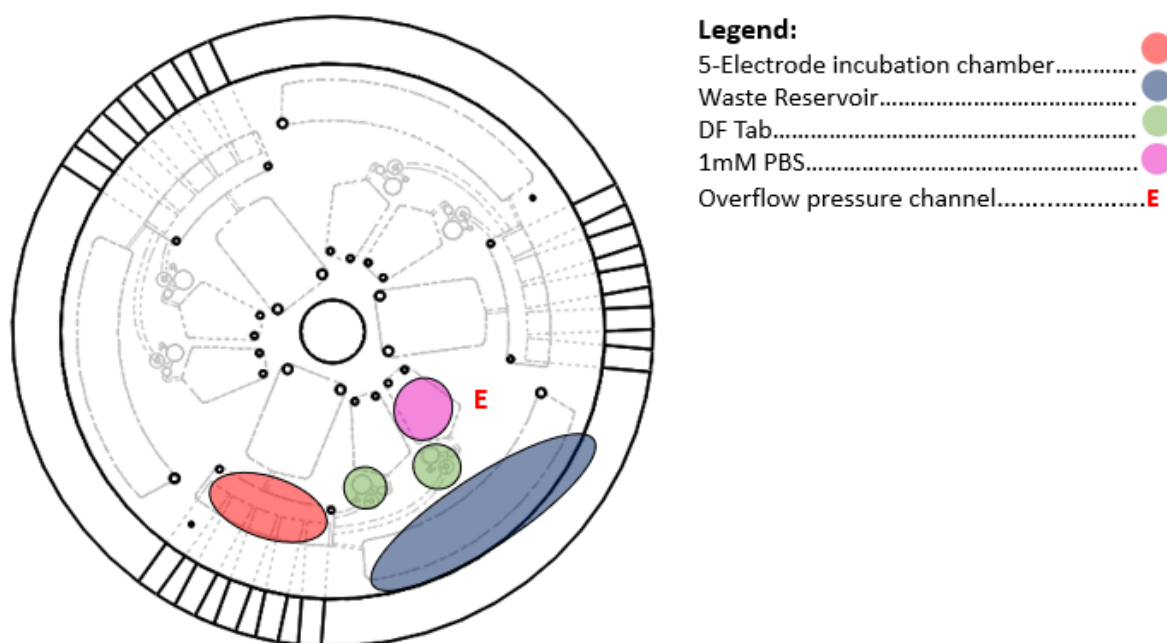


Figure 3.11. CAD drawing of V. 3.2 of the device with the removed DF tab overflow system removed to reduce error for valving actuation.

electrode incubation chamber, all reagents comfortably fill up over the electrodes ensuring the best wash step possible for the device.

The modified Sections of the device are portrayed in Figure 3.11. EIS measurements acquired utilising this design unfortunately gave insignificant results, where little changes (< 150 ohms) between the impedance data for real samples meant the new electrode configuration was not capable of providing a significant change in the EIS, where the final threshold of the device was later discovered and discussed in Chapter 4, Section 4.4.1. Further examination into the electrode shapes determined that the similar exposed electrode areas within the incubation chamber **B** was incapable of providing information regarding the captured analytes as the reference and counter electrodes were the same size. Traditionally in electrochemistry the counter electrode is usually 10x bigger than the reference electrode [17]. For this small, enclosed system the counter size for V 3.1 gave better results, as the volume size of the chamber and ion availability of the solution is slightly larger for the previous version. This led to an electrode cover investigation detailed in Section 3.7.

3.4.6 Version 3.3

With the evolution of the device through constant testing with blood culture samples, more information was extracted to finely tune the performance of the eLoaD. V 3.3 of the device focused on the electrode incubation chamber only. Confocal images acquired of the electrode post sample testing showed a significant number of platelets adhered to the surface of the counter and reference electrodes. In an effort to decrease this, an additional functionalisation step of the device is described further in this chapter, however to minimise the build-up of settled platelets and RBCs the chamber was altered to mimic that of the

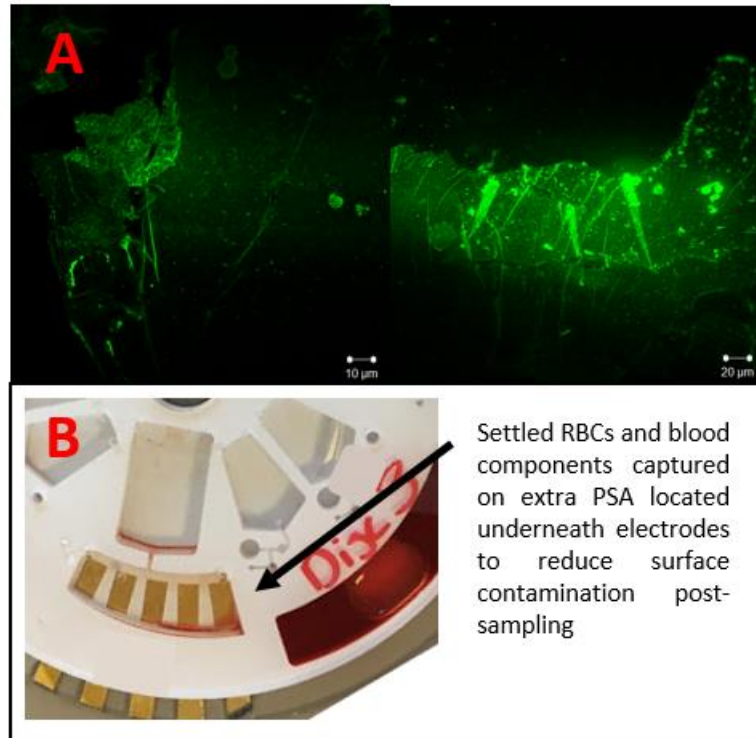


Figure 3.12. (A) Contamination of counter and reference electrode (B) Additional PSA in the V. 3.3 sloped detection chamber for blood component capture to reduce non-specific binding on the sensor surfaces

chamber implemented in V. 3.1 with a more angled slope to essentially create a blood component “trap” where these larger elements could settle before being relocated to the waste chamber as shown in Figure 3.12 (A). The slanted chamber shown in Figure 3.12 (B). This reduces the amount of non-specific binding within the chamber and proved to be an important aspect of the design. The modifications for versions 3.1 -3.3 are detailed below in *Table 3-6*

Table 3-6 Troubleshooting guide 3 for eLoad.

Issue with previous versions	Rectification
Non specific binding on counter and reference electrode	Incubation chamber B sloped to capture residual blood components post sampling
DF tab triggering system	Overflow system removed and DF tab triggering finely tuned
Blockages in channels	Siphon removed and replaced with angled channel to waste chamber C

3.4.7 Final Version (V 3.4)

Vents located on the platform have a dual functionality, to act as entry points for fluids and to relieve pressure build up to allow the proper flow of fluids in the device. A vent is necessary in the waste chamber to allow the sample to be easily displaced whilst also allowing for proper disposal of the sample once testing is complete. While the waste chamber can accommodate for the sample, wash and some of the PBS liquids, overspinning the platform can result in the waste overflowing and exiting the eLoad. As each sample loaded into the device, it is impossible to determine the exact moment when to finish the test to only have the 1mM PBS in the electrode incubation chamber and not over-spilling into the waste forcing liquid out the waste vent. To ensure the user can simply load all reagents, and leave the test unsupervised, additional vents were inserted into the waste chamber termed the “lollipop vent”.

This vent was designed to be 1mm wide, where the entry point is located at circular point ahead of the incubation chamber, therefore the balance acquired during spinning the device, liquid can never overflow out of this vent. The fabrication of the device was altered also for V. 3.4. The raster base technique was removed as the electrode wells were too rough for the electrodes, causing the electrode slides to snap under pressure, becoming a fabrication issue. 144mm plain bases were cut out where the electrode slots were milled instead of rastering significantly reducing the roughness of the electrode well base. The milled electrode slots were created using a tool piece, creating a smooth well for the electrodes to sit. The rastered sections were created by scanning the CO₂ laser over defined sections, creating a rough well surface. The glue for underneath the electrodes was degassed for 5 minutes under vacuum conditions and placed into each well to secure each electrode. These bases were dried overnight in a bio-safety cabinet to ensure no contamination of the antibody surfaces. The excess glue was removed using a tweezers to ensure a uniform, flat surface. The electrode was carefully placed on the base and adjoined to the base using a hand roller, securing the PSA layer. The top disc (layer 1-7) was then pressure rolled onto the base using the laminator apparatus at 80 PSI. A high-pressure roll was now achievable as the electrodes all lie on a uniformly flat surface. A 20ul pipette was then used to fill in any gaps above and between electrodes using super glue. The disc is again left in the bio-safety cabinet at room temperature again until dry.

A comparison between the original device V 1.0 and the fully automated V. 3.4 is depicted in Figure 3.13 and Table 3-7. All major changes are highlighted using a legend to indicate the different chambers where their volumes are tabulated for direct comparison. Figure 3.13 (a) portrays the initial design containing lower volumes for sample and reagents, where a siphon channel controlled the incubation of the sample over the electrodes. The DF overflow triggering system was evidently too unreliable, as well as the ITO reference electrode. Figure 3.13 (b) displays V. 3.4 which has addressed all the troubleshooting issues where manufacturing of the electrode base with the physically inserted electrodes has allowed for the stable electrode system. With higher volumes of sample and reagents, a more reliable assay can be performed on-disc.

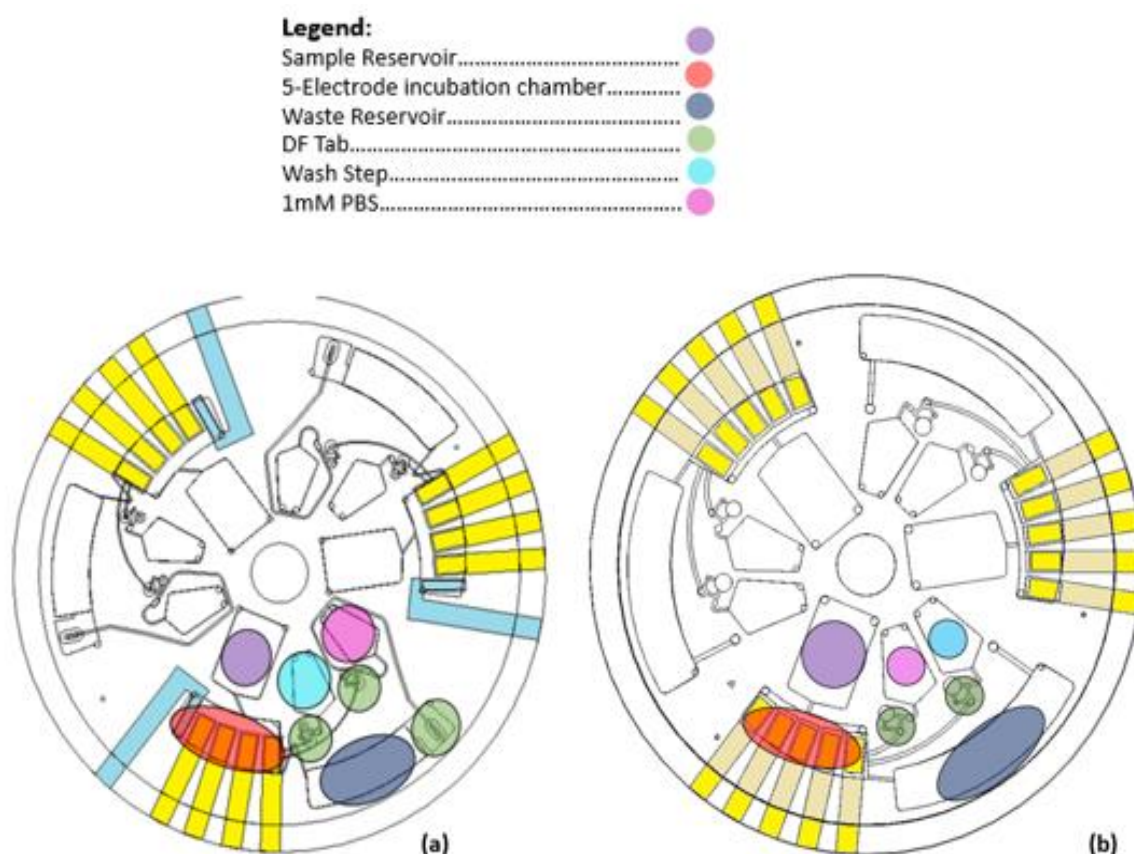


Figure 3.13. A direct comparison of version 1 of the ELoaD device (a) to the current device V 3.4 (b) optimised for bacterial detection where a legend indicates the intended application of each reservoir within the system.

Table 3-7. Comparison of original device (a) reservoir parameters to that of the current device (b)

Version of device	Device (a) – Original Design	Device (b) – Fully Optimised
Sample Chamber size	1.5mls	1.7mls
5-Electrode Incubation Chamber size	1.9mls	1.7mls
Electrode arrangement	ITO reference 4 Au plated electrodes	5 Au plated electrodes
Waste Reservoir size	2.2mls	2.65mls
DF Tab system	Event triggered and burst frequency	Burst frequency only
DI H₂O Step	0.65mls	0.85mls
1mM DPBS	0.65mls	0.85mls

V. 3.4 concluded the optimisation work to develop the automation of the device, where the major design components are specifically looked at in further detail in this chapter.

3.5 DF Valve Triggering Frequency Optimisation

For the automation of the device, a dissolvable film (DF) tab system was implemented for reagent storage which can be activated by augmenting the platform's spin frequency. Many parameters were considered while designing the various components of the DF tab surrounding architecture. The mean radial position of the tab, the size of the main pneumatic chamber connected to the tab chamber via microchannels, size of the liquid resistance chamber to prevent premature channel priming, and the exit channel length as portrayed in Figure 3.14. As two reagent chambers exist, a clear gap between DF tab activation frequencies must be implemented in order to ensure the reagents trigger in sequence to preserve the integrity of the assay. It has been reported that three main relationships exist for tab initiation. The burst frequency (Hz) is inversely proportional to

the volume of pneumatic chamber (mm^3), exit channel length (mm) and directly proportional to the mean radial position (mm) to the centre of the tab [18].

The architecture of the DF tab system is portrayed using Figure 3.14. As both the DF tabs are separated, the parameters of the existing channels and chambers sizes are the determining factors of the burst frequency. These factors are discussed further, relating to *Table 3-8* and *Table 3-9*. The optimisation of the specific spin-frequencies required for the activation of the valves underwent many iterations, however for ease of comparison, a first edition tab system is compared to the fully optimised device used to date. Below is a comparison of two separate sets of parameters for the components of the DF tab structure.

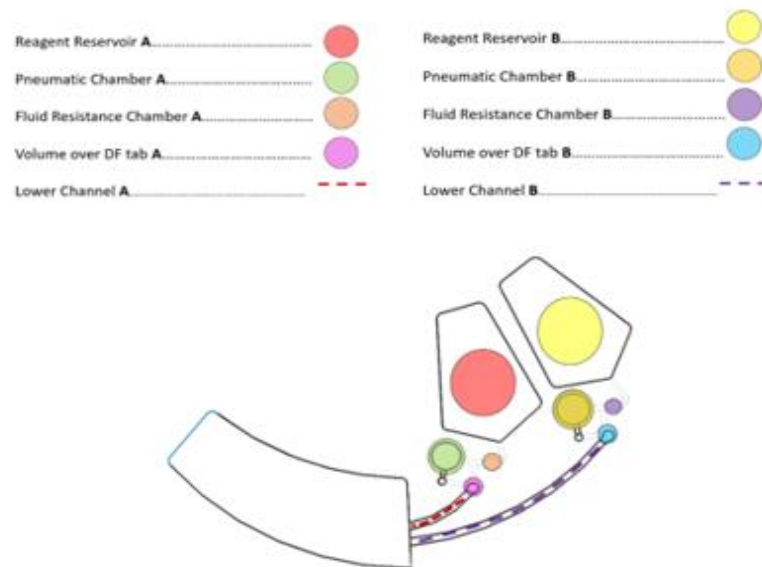


Figure 3.14. A display of the reservoirs, chambers and exit channels labelled using the above legend as a reference guide to describe the two separate DF tab components implemented into the eLoaD device.

Table 3-8 displays the parameters associated with a high spin frequency activation for both the wash and electrolyte steps. As the burst frequency for both steps has a large intermediate range, it was an unreliable system, as the higher end trigger for the wash step may cause the DF tab for the electrolyte step to burst. For this DF tab setup, the wash

step was located at “Reagent Reservoir A” and the electrolyte step was step was located at “Reagent Reservoir B”. As these parameters were deemed unsuitable for the system, an optimisation study concluded that the burst frequency must be reduced in order to minimise the burst range for each DF tab.

Table 3-8. A comparison table between the dimensions associated with the components of the DF tab architecture.

	Wash Step	1mM DPBS Step
Burst Frequency (Hz)	20-25	25-30
Mean Radial Position to centre of tab (mm)	42.25	42.25
Resistance Chamber (mm³)	8.6	8.6
Pneumatic Chamber (mm³)	68	53.7
Volume over DF tab (mm³)	1.9	1.7
Exit Channel Length (mm)	10	8.8
All Other Channel Widths (mm)	0.8	0.8

Table 3-9 displays the parameters associated with the fully optimised DF tab system in place with the current ELoaD device. The change in design parameters made the device more stable and reproducible for scaling-up measures. For the fully optimised setup, the wash and electrolyte steps were switched in order to maximise the exit channel length for the wash step.

Table 3-9. Fully optimised DF tab system design parameters implemented into the eLoaD device.

	Wash Step	1mM DPBS Step
Burst Frequency (Hz)	14-15	19-20
Mean Radial Position to centre of tab (mm)	43.5	42.5
Resistance Chamber (mm³)	6.69	13.65
Pneumatic Chamber (mm³)	69.1	54.95
Volume over DF tab (mm³)	21.33	13.65
Exit Channel Length (mm)	31.3	10.13

All Other Channel Widths (mm)	0.65	0.65
--------------------------------------	------	------

This fully optimised system was implemented onto the eLoaD for the full optimisation of the device, which can now have a set program to control the flow of all fluids, with no supervision. The various parameters which were examined and altered for the purpose of the automation of the platform and adjusted for use with fluids of a low viscosity.

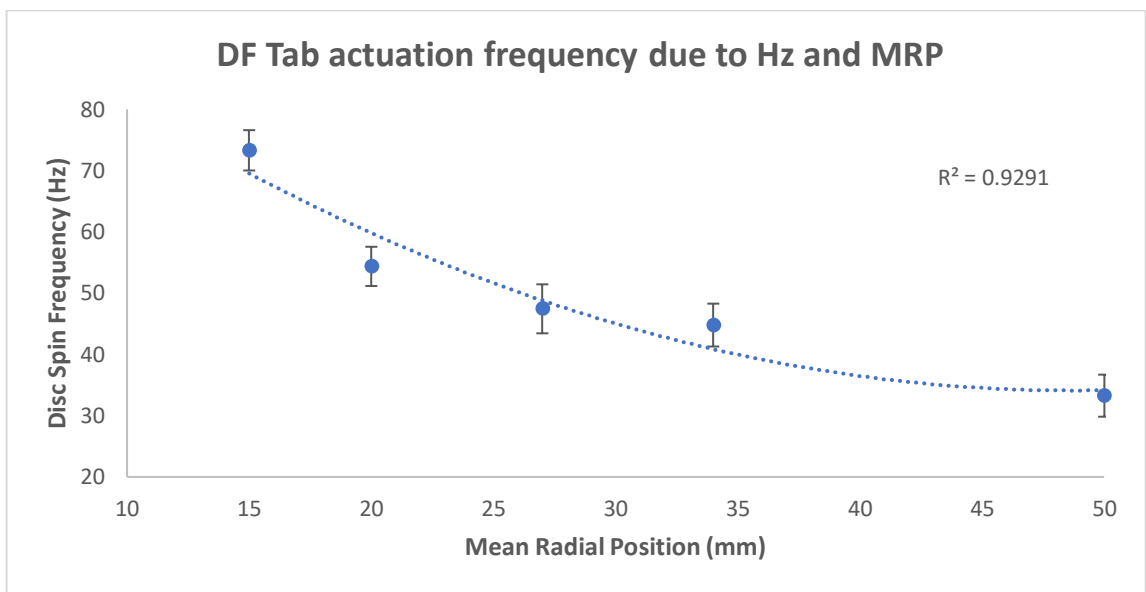


Figure 3.15. Graph representing the relationship between the spin frequency and the mean radial position of the pneumatic chamber and DF tab.

Figure 3.15 relays results obtained with a DF tab radius of 0.75mm. The mean radial position (MRP) of the DF tab plays an important role in DF tab architecture design. If a low DF tab triggering frequency is desired, then a larger radial platform must be designed [19]. This must be considered when the space available on the device is limited. Other factors such as exit channel length, and pneumatic chamber size influences the burst frequency of the tab also. The further away the DF tab is located from the centre, the higher the F_{ω} induced by the spin-frequency is at that given radius. As the spin-frequency is still relatively high at a radius of 50mm, the effect of the pneumatic chamber size is also examined. The relationship between the spin frequency of the device and the MRP was derived from the equation:

Equation 3-1

$$F_c = m\omega^2 r$$

$$\frac{F_c}{r} = m\omega^2$$

$$\therefore \frac{1}{r} \propto \omega^2 \text{ (where } \omega = 2\pi f \text{)}$$

$$\therefore \frac{1}{r} \propto f^2$$

$$\therefore \frac{1}{\sqrt{r}} \propto f$$

The initial equation outlined in Equation 3-1 is the standard centrifugal force equation where F_c denotes the centrifugal force of the platform, m is the mass, ω is the angular velocity, r is the radius and f is the frequency in which the platform is spinning. By rearranging this formula, the relationship of frequency and radius was established, where the graph shown in Figure 3.15 portrays this relationship. The graph shows the characteristics of a $y = \frac{1}{\sqrt{x}}$ graph.

Figure 3.16 displays the effect of the chamber size at the two MRPs of the tabs located on V. 3.4 of the device. The MRPs of the wash and DPBS steps were 43.5mm and 42.25mm respectively. A proportional relationship exists between spin frequency (Hz) and volume of the pneumatic chamber surrounding the DF tabs. A combination of the pneumatic chamber size and MRP of the tab allowed for a reduction in the spin frequency for valve actuation. Gorkin *et. al* "stated the burst frequency shrinks with increasing chamber size V_0 " for their DF tab system based upon the direct relationship between frequency, f , and pressure P . As detailed in the work, $f \propto \frac{1}{\sqrt{V}}$, where V is the volume of the chamber [20], [21].

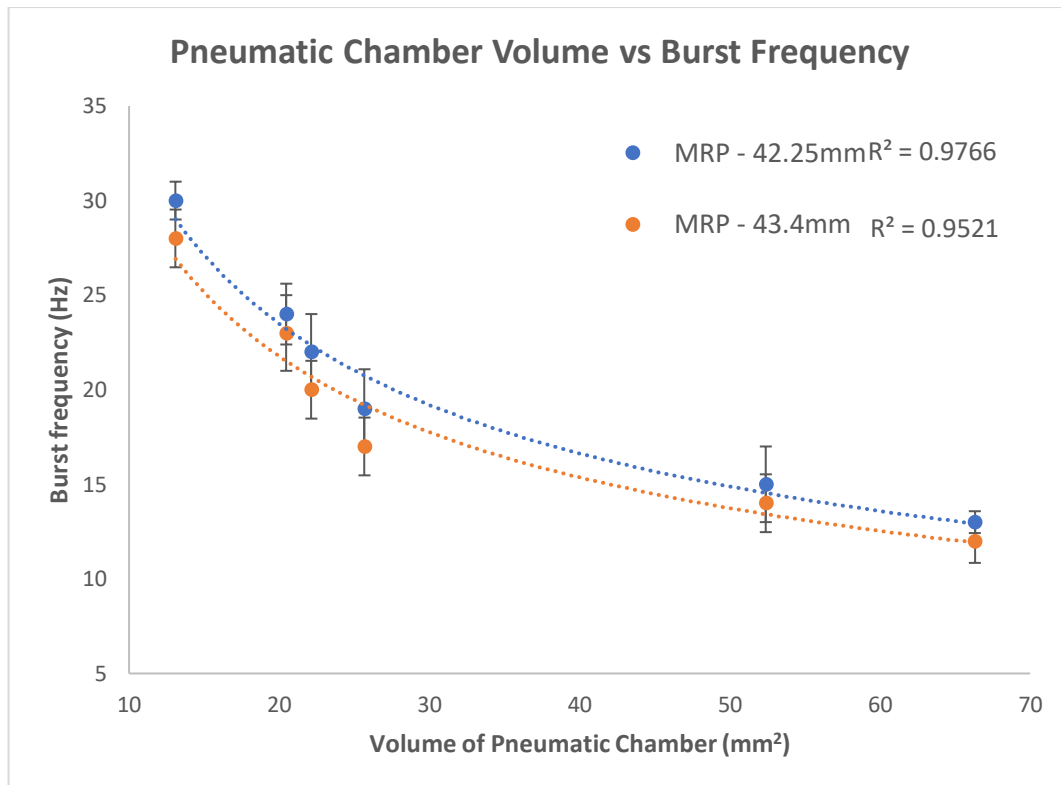


Figure 3.16. Dual graph portraying the linear relationship between the burst frequency (Hz) of the tab with comparison to the pneumatic chamber (mm³) for the two tab positions on the platform.

The graph corresponds with an inversely proportional graph, where the DF tab system used for the device correlates well with the literature. Where the larger of the two MRPs shown in Figure 3.16, the burst frequency required for the DF tab actuation was lower, which verifies the information provided by the graph shown in Figure 3.15. With a larger DF chamber volume and a larger radial position, the frequency required to burst the tab is lowered.

3.6 Waste Channel Optimisation

A variety of waste channel dimensions were studied throughout the course of development. The waste channel **B** governs the incubation time of the sample within the chamber, which must also have a continuous flow to eradicate the chance of clotting and interference. As the channel is a 3-dimensional structure, a variety of widths and lengths are examined. The depth of a single layer of PSA governs the set value of $86 \pm 5 \mu\text{m}$.

Initially, DI H₂O was used to determine optimum channel dimensions. For final version of the device, low viscous samples were tested with a channel width of 0.75mm and a length of 6.33mm. For this channel length, the sample entering the electrode incubation chamber filled above the electrode point, as the resistance in the waste channel **B** was adequate to maintain the sample within the electrode incubation chamber for a period of 7-8 minutes. With $\frac{3}{4}$ of the sample displaced within the incubation chamber, the pressure head of the fluid becomes greater than the channel B resistance and the sample begins to flow into the waste under a constant spin frequency of 7Hz.

Similar to this, with a constant spin-rate of 10Hz applied to the device, the sample follows the same flow profile as the sample exhibits under 7Hz, however the incubation reduced greatly to 3-4 minutes. To eliminate the possibility of the microchannel **A** blocking, a slow acceleration to 10Hz is set to avoid an immediate force being applied to the sample which may aggregate within the channels. Sample slowly enters the waste chamber under a constant spin of 10Hz, however the majority of flow doesn't occur until the electrode incubation chamber is $\frac{3}{4}$ full. This occurs after 45seconds and begins to empty at this time. Full displacement of the sample is achieved after 4 minutes for all low viscous samples.

For blood culture samples, an incubation time of 3-4 minutes was deemed the optimum timeframe for pathogen capture, as detailed in Section 3.9. Extensive optimisation had to be carried out for healthy whole blood, to determine the optimum channel dimensions to transport the sample to the electrode incubation chamber, a specific timeframe for incubation before displacement to the waste, to avoid clotting and blocking of channels, and to achieve uniform results on all three testing sites. The conditions used for the blood culture samples were tested with directly collected whole blood samples (20±2°C). The initial optimisation of whole blood was carried out using v. 3.2. where all microchannels **A** and waste channels **B** have a fixed length of 3.31mm and 6.98mm respectively and varying widths as shown in *Table 3-10*.

Table 3-10. Channel parameters to determine design conditions for flow rate of samples

Test Site	Microchannel A width (mm)	Lower-Channel B width (mm)	Lower-Channel Pressure (mbar)	Reynolds Number
-----------	---------------------------	----------------------------	-------------------------------	-----------------

1	0.85	0.75	0.771	4.696
2	0.85	0.85	0.629	4.289
3	1	1	0.537	3.697

All calculations of the Reynolds number were based on a flow rate of 0.5mL/min, giving rise to a fluid velocity of 0.129199m/s which slightly decreases with a decrease in channel pressure for whole blood at room temperature. The viscosity of whole blood 4.4 cP (Pa. s/10³) and fluid density is 1.06 g/cm³ (kg/m³ x 10³), where the blood viscosity is dependent on a multitude of factors, where temperature is the only one considered for these calculations shown in the above *Table 3-10*.

The test sites correspond with Figure 3.17 where the same sample was evenly distributed between all three testing sites. All spin conditions were originally set to 12Hz, however after 15 minutes of sample to electrode contact time, the spin frequency was increased to 15Hz. It was evident that the microchannel in test site 3 displaced the sample to the electrode incubation chamber the fastest, however test site 2 fully displaced the sample to the waste chamber. The sample run time was 19 minutes long, for the whole blood only.

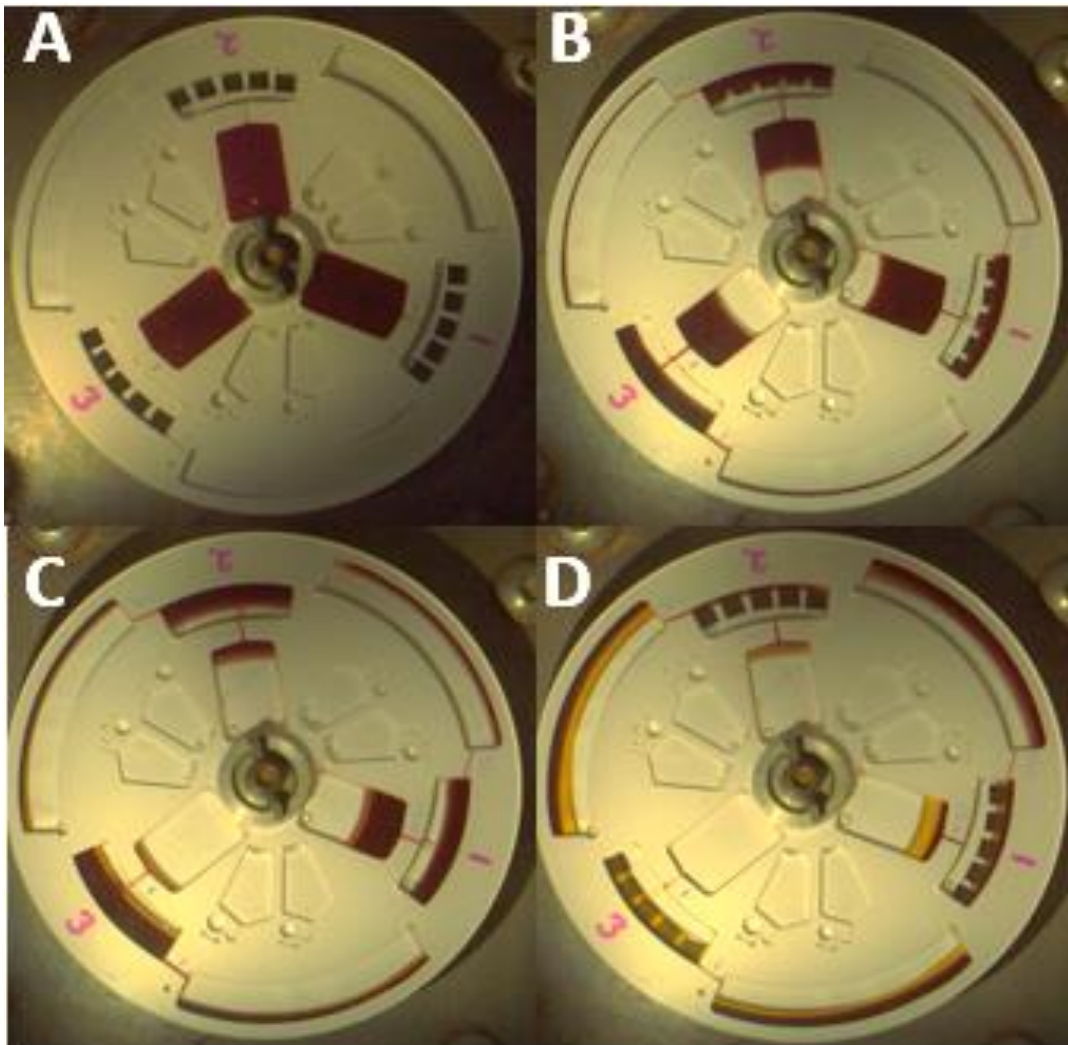


Figure 3.15. Images showing device's microchannel and waste channels of varying widths are testing with healthy whole blood samples. (A) Initial loading of the sample to the sample chamber, (B) spin frequency of 12Hz applied (C) shows sedimentation of whole blood in test site 3, D) Test site 2 shows best results after 20 minutes, where blocking of test site 1 microchannel impeded the sample flow.

The separation of the whole blood to plasma and components is evident in Figure 3.17 (C) and (D) which is a further indication that the sample is being processed for too long. The test itself would also be too long compared to the clinical sample test of 15 minutes from start to finish. With supporting images in Section 4.xx (incubation times), it is shown that with an increasing incubation time, the increase in the on-specific binding between blood components and all electrodes. With a redesign of V. 3.2 to V 3.3, the electrode incubation

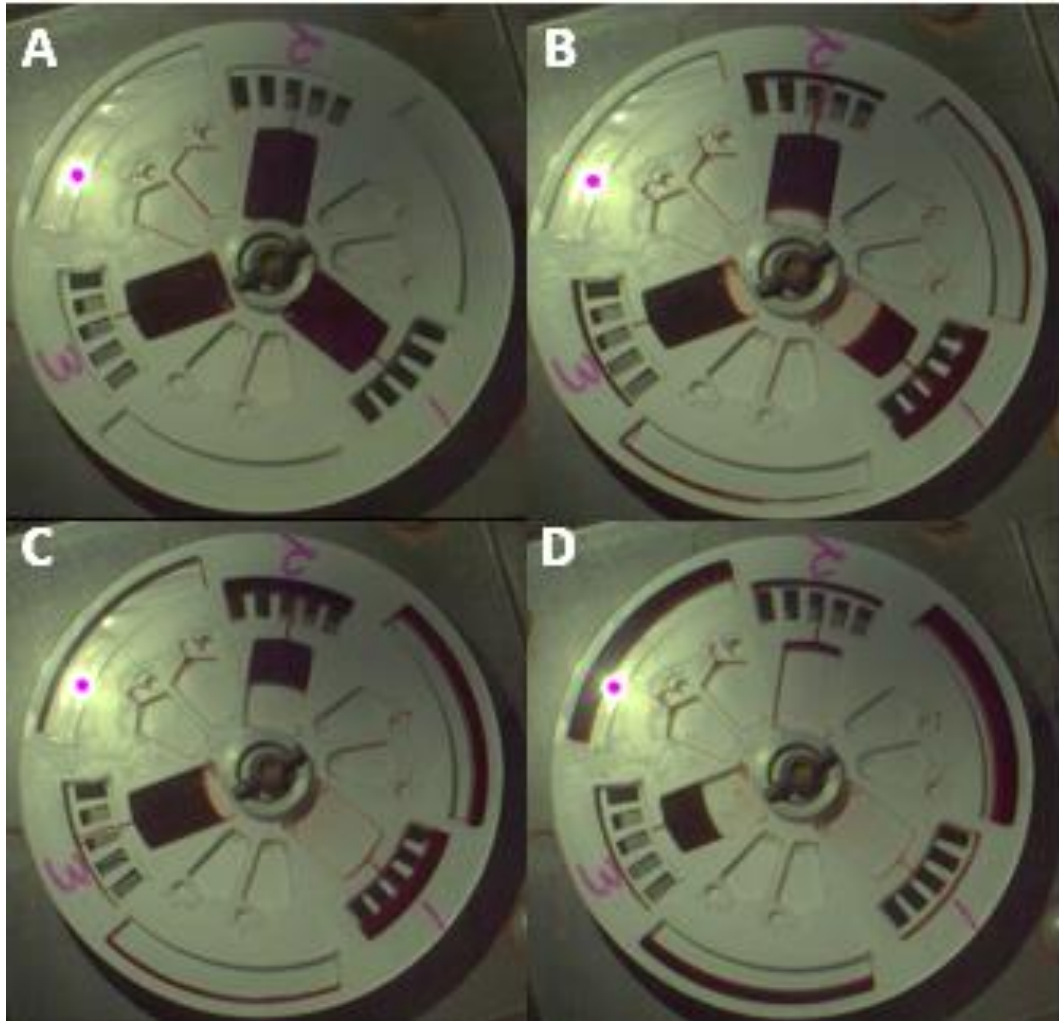


Figure 3.16. *Demonstrates the whole blood flow patterns between each chamber. (A) Initial loading of blood to sample chamber (B) A spin-rate of 10Hz applied to device (C) Uneven flow of sample between testing sites. (D) Test 1 and 2 complete, with test 3 sample failed.*

chamber volume increase was explored. For the previous waste channel, it was determined that the channel resistance itself was too high to allow a smooth fluid flow. With aqueous sample, an increase in spin-frequency can overpower this resistance to allow the fluid to be easily displaced, however as whole blood acts abnormally under these conditions, another option to explore was to increase the depth. Two PSA layers were joined and cut using the GraphTec as normal. This gave additional depth to reduce the incubation time of the test. Figure 3.18 displays a sub-version of V.3.3 where the lower channel is reduced in length, to 3.32mm to mirror the same length as the microchannel A, where the pressure experiences within the channel is 4.6×10^{-2} mbar. A total sample to waste chamber time of 9 minutes was recorded for test site 1 and 2, however the whole blood did not reach the top of the electrodes. Therefore, there was minimal contact between the functionalised electrode area and sample which would lead to low pathogen

capture efficiency. It was evident that there was insufficient channel pressure to cause the sample level to be greater than the electrode area.

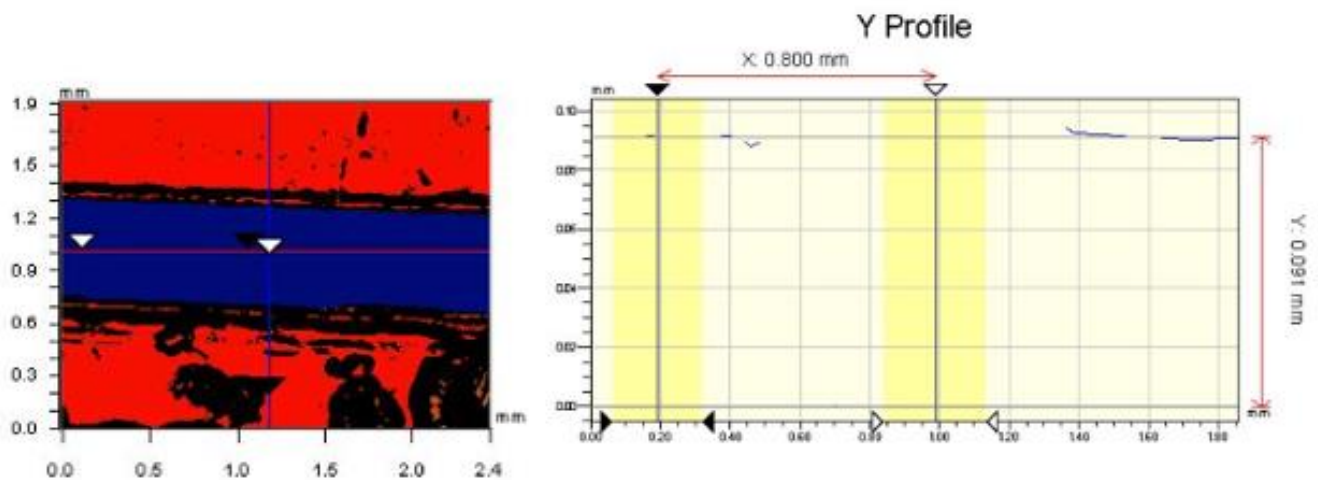


Figure 3.17. Interferometer measurement of straight cut channel in PSA to determine the smoothness of the cut using the microblade in the GraphTec.

The double layer of PSA created excessive channel volume which created little fluid resistance which led to rapid emptying. Further examination of the PSA channels was carried out to ensure the correct cutting of channels. Inconsistencies between the identical microchannels was a cause for concern, as spin-frequencies would need to be altered depending on how well the sample is flowing between test sites.

Interferometry images were acquired of a 0.8mm straight channel to determine if the channels contain any discrepancies which may create features which cause RBC aggregation. The straight channel PSA layer was pressure rolled at 70 PSI to a flat 1.5mm PMMA cut chip. The channel was coated with a thin layer of sputtered Au for use with the interferometer (Bruker, 3D Optical microscope, UK). With no evidence of abnormal channel structures, the channel fabrication method was considered satisfactory. The sample type itself appeared to cause the issues due to changing viscosities. The fabrication of the device itself was altered to include Tween20 to the microchannels to act as a lubricant to reduce the effect of aggregation of blood components within the channels. The device was laminated as previously described from layer 1 to layer 7. The device was inverted and 10 μ L of tween was pipetted into the microchannel and waste channel for each testing site. The device was then joined with layer 8 and the electrode

base. The lower channel was fabricated using one layer of PSA, with a channel width of 0.85mm and a length of 6.98mm. The tween in the microchannels allowed for a more uniform distribution of blood from the sample chamber to the electrode chamber. A spin frequency of 7-8 Hz allowed the sample to enter the electrode incubation chamber without flowing into the waste, until the spin-frequency was increased to 10Hz, which triggers the sample to enter the waste, without aggregation. A range of incubation times between 5-7 minutes was investigated for whole blood samples, which should allow adequate contact time between sample and functionalised electrodes

For testing of various samples all buffer, blood culture and whole blood samples were run on the V. 3.4 device, where Tween20 was only applied to the devices used for whole blood pathogen detection.

3.7 Electrode Cover Optimisation

The electrode cover was an additional layer incorporated into the device design at an early stage to prevent mid-Sectional leaking. Despite the addition of glue to the outer perimeter of the device, sample could still potentially leak from the top/bottom of the slotted electrodes under spinning conditions which is highly dangerous whilst testing biohazardous samples. The electrode cover has three sets of five electrode exposure sites, which only exposes the top area of the electrodes, whilst sealing around the perimeter with correct positioning of the layer. The area of the exposure areas on the electrode cover also has a significant role in the sensitivity of the detection aspect. Comparing the electrode cover used for version 3.2 of the device previously shown in Figure 3.11, all electrodes in the system had an exposed area within the electrode cover of 5mm². The dimensions of the electrode cover were altered over the course of the device optimisation. With the stamped area of the electrode being 5mm², this electrode cover design only allows for the antibody and protein modified surfaces to be exposed, however upon further investigation, the EIS measurements acquired for this system showed no significant difference before and after exposure to sampling. As previously stated, the counter electrode is traditionally 10 times larger than the working electrode as it provides the current to the working electrode for the system response to be obtained. In this case, no observable difference was observed when high pathogen count samples were used,

possibly due to the counter and working electrodes all being the same size. Due to size restraints, the counter electrode cannot possibly be ten times larger in this device, however the dimensions detailed in *Table 3-11* were applied to the electrode cover, used for the final device depicted in *Figure 3.13 (b)*.

Table 3-11. *Electrode cover dimensions for each of the 5 rectangular exposed areas over each electrode based on layer 9*

Electrode Type	Exposed Area (mm ²)	% CE > WE
Reference	121.98	NA
WE 1	129	24.2%
WE 2	135.88	17.9%
WE 3	139.32	14.98%
Counter	160.2	NA

The percentage in which the counter electrode is greater than the GP, GN and fungal electrodes is 24.2%, 17.9% and 14.98% respectively. All results shown in Chapter 4 utilise this electrode cover and associated dimensions. With the 1mM DPBS electrolyte being added to the detection chamber, this adds an electrolyte resistance. This is one of many influencing factors on the EIS measurements however in this instance, this impedance change is also influenced by the area of the electrode. With an increased area, the greater number of ions may adsorb onto the gold surface, altering the capacity response. In this case, the greater the size of the electrode, the lower the EIS response for that electrode configuration. The GP antibody EIS measurements always provided the highest Z (ohms) value for the Nyquist plot. The average of 15 antibody EIS measurements for the three electrodes are shown in *Table 3-12*, where the average values decrease as the working electrode area increases [22].

Table 3-12. *Values of antibody EIS measurements using the final electrode cover acquired from a set of 15 of each type of working electrode*

	Gram + AB	Gram - AB	Fungal AB
Average R (ohms)	2075	1868	1647
Standard Dev	114	104	128

3.8 Platelet and RBC inhibition Study

Throughout the development of the device, EIS measurements were acquired to ensure the alterations of the device didn't reduce or impede the EIS signal of the biosensor. It was discovered that whole blood and darker blood culture samples contained a high platelet and RBC count, which in turn would non-specifically bind to the reference and counter electrode, as well as the three working electrodes. This has huge effects on the EIS signal, as it can cause false positive and false negative read-outs. For this optimisation, real patient samples and healthy whole blood were collected and stored at room-temperature ($20\pm 2^\circ\text{C}$) for use that day. A constant contamination inhibited the response of the system and could generate enormous results.

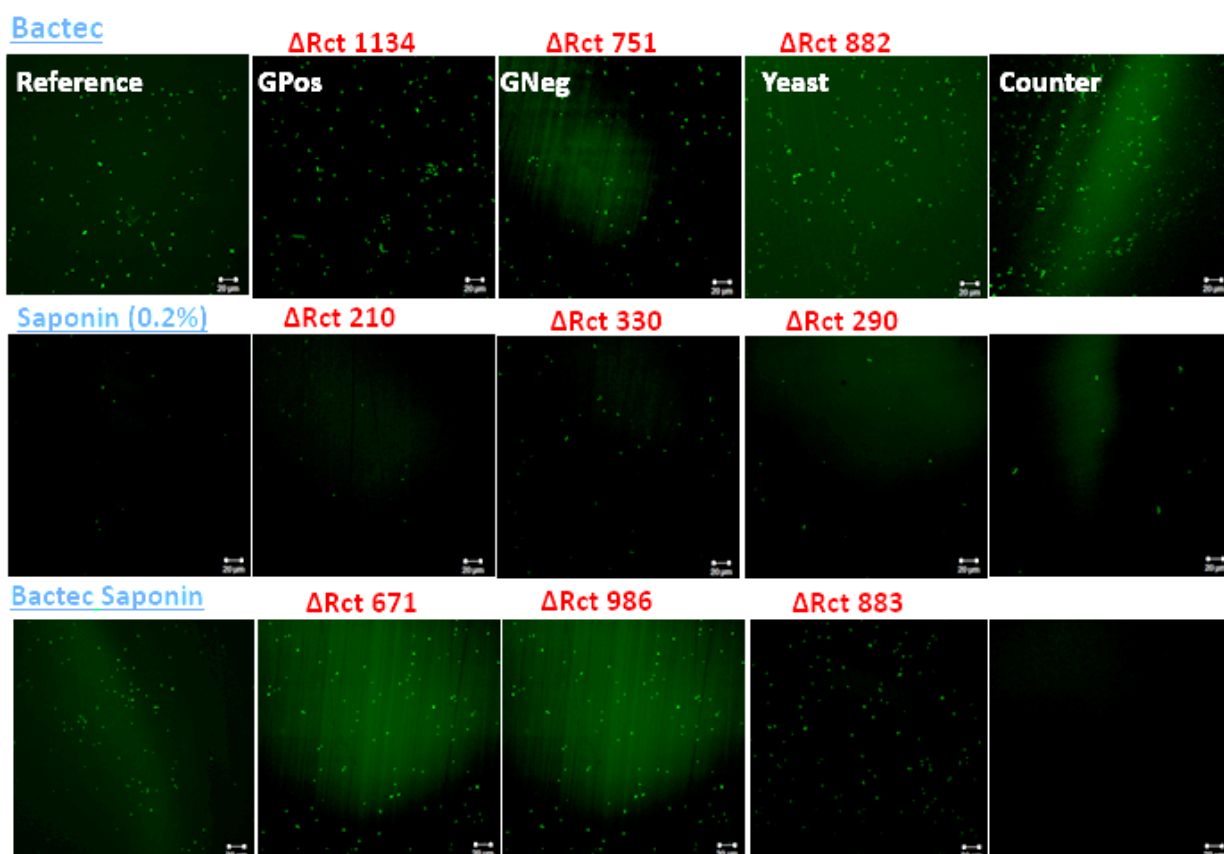


Figure 3.18. Confocal images of Au electrodes post testing with sample D017-01, a gram-positive type sample, to determine optimum pre-treatment of samples before testing with all devices. All images were acquired by Dr. Kellie Adamson

A variety of pre-treatments were applied to the sample before insertion to the device. The addition of DI H₂O, PBS, BacTec, Lactic acid and Saponin with the sample at different mixtures and ratios were used to examine the effect on platelet and RBC count reduction on the electrodes. The concept of pre-lysis of the RBCs before the addition of the sample to the device was examined. The addition of saponin had an immediate visual change to the sample, where whole blood appeared to break down after 10 minutes of adding 0.2% saponin. Sample D17-01, a gram-positive type sample, was used to determine an effective solution to the non-specific binding of pathogens and blood components to the sensor surfaces

Table 3-13. *Effect sample pre-treatment on the $\Delta EIS/R$ using a Gram-positive sample D17-01 acquired from St. James' Hospital where the initial antibody – sample ohm value is displayed*

Sample Type	ΔZ (ohms)		
	Gram Positive	Gram Negative	Fungal
Clinical Sample D017-01			
D017-01: Bactec	1134	751	882
D017-01 Saponin 0.2%	210	330	290
D017-01 Bactec Saponin	671	986	883
Healthy Whole Blood (WB)			
Healthy Whole Blood w/ Bactec	650	30	140
WB Saponin 0.2%	350	400	640
WB Bactec Saponin	570	210	373
Healthy Blood Separated RBC Layer			
Separated Blood RBC Bactec	140	340	40
Separated Blood RBC Bactec Saponin	120	0	20
Separated Blood Saponin	1457	648	732

As the D017-01 sample should yield only a positive result for the gram-positive EIS measurement. The best response for this was the 1:1 dilution of the sample with Bactec culturing media. Despite all three electrodes providing positive results, the highest change in the ohmic response was recorded with the gram-positive. From Figure 3.20 the confocal images report that there is non-specific binding to the counter and reference and all three working electrodes. The addition of saponin to sample D017-01 appeared to break down

all cell components, including the pathogen, therefore no positive result was acquired from the testing. All EIS values were below the determined threshold, therefore the use of 0.2% saponin would not be used for future testing. A mixture of the sample, saponin and BacTec also provided false positive results for the sample.

For platelet inhibition, the use of fibrinogen was examined. In a study carried out by Mikhailidis *et. al*, human fibrinogen induced platelet aggregation in up to 65% of platelet rich plasma samples tested [23], [24]. PDMS stamps, pre-treated with O₂ plasma, were coated with fibrinogen solution (500µg/ml) for 15 minutes. The solution was removed, dried with N₂ and adhered to the top Section of PMMA of the sample chambers and electrode incubation chambers of a pre-fabricated disc. The corresponding sections of the electrode cover were also stamped. This stamp was incubated with the surfaces for 15 minutes and removed. In order to allow time for the sample to come into contact with the fibrinogen coated Sections in the device, the samples were injected into the device and left for 5 minutes before a spin-frequency was applied to the device. Confocal images were acquired to determine the effectiveness of the fibrinogen modified surfaces for platelet capture so as to reduce non-specific binding of the platelets to all five electrodes within the electrode incubation chamber.

Figure 3.21 portrays the effect of RBC and platelet adhesion on the counter electrode with the use of fibrinogen stamped within the sample chamber **A** and the electrode detection **B**. A healthy whole blood sample was allowed to incubate with the fibrinogen functionalised sample chamber **A** for 5 minutes before a spin frequency of 10Hz was applied to the system to allow for a 7 minute incubation of the sample over the electrodes.

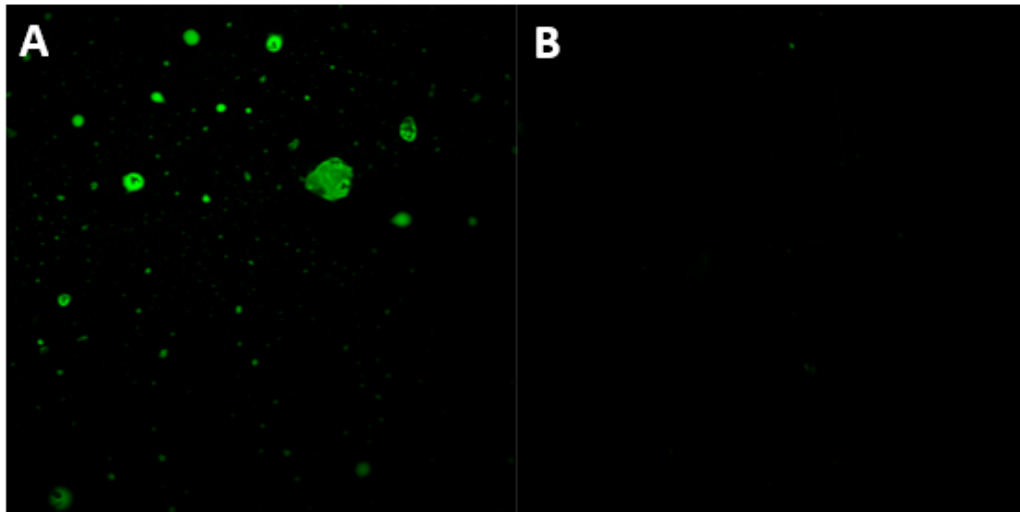


Figure 3.19. *Confocal images of a healthy whole blood sample passed through the platform with a 7 minute incubation time where the device was a) not functionalised with fibrinogen and b) functionalised with fibrinogen.*

To keep the device as user-friendly, the fibrinogen stamped sections were located in the top and bottom layers of both the sample and electrode incubation chamber where the sample comes in direct contact with both chambers through-out the testing. *Table 3-14* represents the ΔZ (Ohms) acquired for a sample set of blood culture samples acquired from the Coombe hospital. This table shows that with no fibrinogen within the device, a notable change is recorded for each of the three working electrodes, detailing a “false positive” result for each sample for all three working electrodes. With the use of fibrinogen within the device it was found that 3 out of 4 samples are positive for a type of pathogen, where a false positive exists for the fungal ΔZ (Ohms).

Yellow denoted the false positive due to platelet adhesion to the counter/reference, green signifies the correctly identified pathogen whilst red represents the contamination due by fungal spores. As BacT and BacTec contain a yeast extract, this can affect the results of the overall fungal ΔZ (Ohms) while the sample was tested undiluted.

Table 3-14. Table of various samples acquired from the Coombe Hospital, Dublin to show to effect of testing the platform with and without fibrinogen functionalisation

Treatment	Sample Name	Gram + AB	Sample		ΔZ (Ohms)	Gram - AB	Sample	ΔZ (Ohms)	Fungal Protein	Sample	ΔZ (Ohms)
No treatment of sample or functionalisation of platform	D101	1940	350		1590	1740	400	1340	1750	452	1298
	D102	1730	619		1111	1860	564	1296	1600	492	1108
	D103	1380	525		855	1310	556	754	1660	575	1085
	D104	1360	346		1014	1444	623	821	1800	717	1083
	D105	1960	407		1553	1910	414	1496	1790	364	1426
	D106	1730	1100		630	1730	883	847	1880	679	1201
	D109	1240	293		947	1500	327	1173	1620	308	1312
	D114	1960	401		1559	1760	362	1398	1580	400	1180
	D116	1880	1250		630	600	400	200	1920	918	1002
	D119	2150	733		1417	737	564	173	1780	676	1104
	D120	1820	725		1095	707	556	151	1720	748	972
D121	1800	799		1001	1750	720	1030	1800	932	868	

	D122	1870	1260		610	1930	1230	700	1790	1100	690
	D124	1850	605		1245	1970	599	1371	1720	559	1161
Addition of fibrinogen to sample and detection reservoirs	D101	1540	832		708	1500	1108	392	1490	913	577
	D108	1050	861		189	914	476	438	912	485	427
	D109	871	825		46	934	901	33	753	725	28
	D1010	892	435		457	841	788	53	860	285	575

3.9 Spin Rate Study

The effect of spin-frequency on the capture of pathogens was examined to confirm the choice of operating frequency parameters. Initially, a low spin value was chosen to reduce the chances of leaking over the electrodes. Two spin-frequencies (7Hz and 20Hz) were examined to determine its effect on pathogen capture on the biosensor surface.

For this study, sample D017.10 (Gram-negative containing sample) was used. According to previous literature, the large pressure drop that exists between channels and reservoirs has a large effect on the particles within the fluid [25]. As the bacteria flow through a microchannel of length 3.31mm, the initial ~200-300µL must travel 5-times that distance on it reaches the base of the electrodes in the electrode incubation chamber. This force is predominantly associated with the centrifugal force applied to the system through the spin-frequency (Hz). This initial spin frequency, if too high, might cause cell lysis. Not only this, but for a fully automated device, multiple steps are actuated through an increasing spin frequency, therefore the reagents effect on the bacteria must also be understood. For this study, the known Gram-negative (GN) type sample (D017.10) was acquired from the microbiology department in St. James' Hospital, will be henceforth referred to as sample 10. Various spin-profiles were examined for both the sample and wash step, where confocal images were obtained to characterise the rotation speed effects on the pathogens.

Table 3-15 refers to the various spin – parameters subjected by each sample type. The blood culture sample was diluted 1:3 with DI H₂O before testing. Six separate samples were prepared for use with two platforms. Electrodes were removed from the eLoadS post samples, were confocal images were acquired to justify the spin-rate parameters applied to the system for automation. Image J analysis on the images was then used to determine the cell and particle numbers on the individual images (n=3) of the electrodes.

Examining the 7Hz profile for samples 10 A, B and C a high cell count exists on the GN electrode surface but there are also cells on the gram-positive (GP) and Fungal antibody

functionalised electrode which would lead to a false positive result. Sample 10 A had a flow rate of 7Hz and an incubation time of 4 minutes where the DI H₂O wash step was manually injected in and allowed to interact with the electrode surfaces for 5 minutes to determine if lysis would occur. The number of captured cells of the GN electrode was good, however debris and cells also existed on the GP electrode which may result in a false positive reading with the EIS measurements. 10 B confocal images show that the capture ability of the GN was much higher than the other two electrode surfaces, where some non-specific binding occurred, however the spin-frequency to burst the DF tab for the wash step was achieved without damage to the pathogen. As the integrity of the cell membrane remained unharmed, it was concluded that the captured pathogens were able to withstand spin frequencies of 15 Hz.

10 C gave the best results, where there was very little non-specific binding on the GP and fungal electrodes, however a low spin-frequency was used to wash the DI H₂O to the waste. The final spin profile was based upon these parameters for max pathogen capture whilst maintaining the integrity of the spin profile for DF tab actuation. Comparing the electrode surfaces of 10C to A and B, the surfaces were cleaner, where no bio-films or little non-specific binding occurred.

Large amounts of debris existed on the GP electrode for sample 10D and 10E, where bacteria or cell components have been lysed. It was evident that there was a large interference for the 20Hz spin-profile confocal images on the gram-positive electrode. Samples 10 D, E and F can automatically be ruled out for optimum spin-profile.

Justifying the results from the spin-parameters, a spin-profile of 20Hz appears to damage and spread cell contents over all electrode surfaces, therefore minimum time at this spin-speed is necessary. A spin-frequency of 15Hz was vindicated through the confocal images. The spin-profile for the automation of the device allowed for a specific spin-profile to be created to determine the specific parameters needed to operate the device. As two sample types were tested, the same spin profile can be applied to the device, where the initial spin frequency required to displace the sample to the electrode incubation chamber is different to account for the change in viscosity between whole blood and blood culture/clean buffer samples.

Table 3-15. Parameters for sample preparations used for different testing sites within eLoaD to determine optimum spin-frequency of platform where ImageJ was used to count pathogens on each electrode

Sample Name	Sample Incubation time	Testing parameters	Number of cells/pathogen clusters/fragments in image		
			Gram + Electrode	Gram - Electrode	Fungal Electrode
10 A	4 minutes	Wash step injected in and allowed incubate for 5 minutes. Sample flowed into waste at 7Hz	31 ± 9	199 ± 10	19 ± 6
10 B	4 minutes	Wash step injected and flowed to waste at 7Hz with no wash incubation	2 ± 5	188 ± 47	15 ± 22
10 C	5 minutes	Wash step triggered at 15Hz and slowed to 7Hz	19 ± 12	92 ± 43	7 ± 3
10 D	Static incubation (i.e. no flow) Sample present over electrodes for 7 minutes and then removed	Sample wash didn't trigger therefore 0.8mL injected and flowed to waste at 20Hz with no wash incubation	172 ± 81	69 ± 45	26 ± 29
10 E	4 minutes 20 seconds	0.8mL injected and incubated for 5 minutes and flowed to waste at 20 Hz	85 ± 41	46 ± 12	22 ± 41
10 F	5 minutes	Sample 10F injected in with no wash step at 20Hz	47 ± 34	70 ± 31	19 ± 26

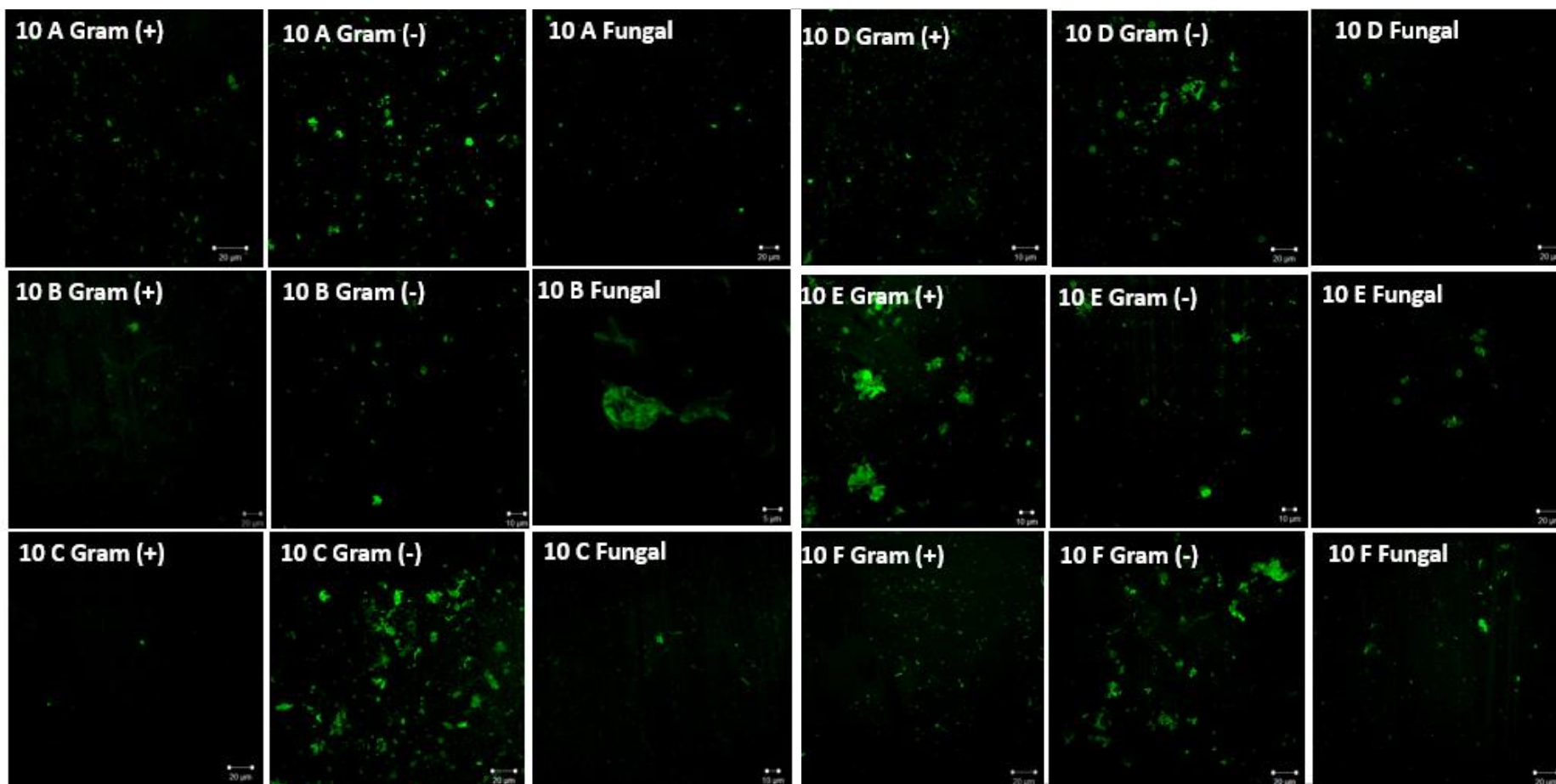


Figure 3.20. Confocal images acquired from all three working electrodes per testing site to determine optimum spin-frequency parameters to maximise pathogen capture on the antibody modified surface. 6 testing sites in total were used in conjunction with a Gram-Negative patient sample obtained from St. James' Hospital, Dublin. All images were adjusted to Brightness +20%, Contrast -20% to distinguish which testing site most efficient for pathogen capture. All confocal images acquired by Dr. Kellie Adamson

For whole blood samples, the spin frequency is higher (10Hz) as whole blood tends to aggregate under centrifuging conditions, becoming more viscous. The addition of tween20 in channels allows for the uniform distribution of the sample at 10Hz, whereas clean buffer/blood culture samples only required a spin frequency of 7Hz to flow into the electrode incubation chamber. Phase **A** of the spin profile was the initial acceleration of 10ms^{-2} followed by the displacement and incubation phase **B**. This constant spin-frequency allowed the sample to flow into the electrode incubation chamber, where it would remain until the liquid head pressure overcame the waste channel pressure which usually occurs once all the electrodes were covered. During this time, the sample also displaced into the waste chamber. Although the incubation of the sample may only last for 3-5 minutes, remnants of the sample can remain at the base of the chamber. The majority is allowed to displace under spin conditions however the actuation of the wash step DF valve at 8 minutes due to an increase in the platform frequency in phase **C** washes this additional fluid to the waste chamber.

This step was set to 15Hz to ensure all wash DF tabs trigger. After 12 minutes total run time, the spin-frequency was increased again to 20Hz to actuate the DPBS electrolyte step, considered as phase **D**. The spin-frequency was reduced down post DF tab actuation in an effort to preserve pathogen integrity on the biosensor. The 1mM DPBS would then enter the chamber and the spin-frequency of the disc is slowly reduced to 0Hz, which would be considered the final stage **E** of the test. **Phase B would be the step to alter between samples types i.e. whole blood, blood culture or clean buffer samples.**

3.10 Materials Characterisation

The fabrication of the device and its sensors required a variety of types of materials to be used, where the surface wettability was examined. As the hydrophobicity of the PDMS repels aqueous solutions, this may be problematic for antibody adsorption. Hydrophobic surfaces may not bind efficiently and therefore techniques such as plasma treatment of substrates may be necessary. Various techniques can be implemented to alter the surface energy of the substrates in order to change their wettability [26]. PDMS is used for the antibody functionalisation of the electrodes, where antibody solution is drop cast on the

patterned surface in order to carry out μ -contact printing on the gold electrodes. As the solution requires antibody adsorption to take place, the surface needs to be slightly hydrophilic for full surface interaction between the antibody solution and the surface. O_2 plasma treatment is notably effective at cleaning material surfaces, removing contaminants which can increase surface energy [27]. By removing these impurities, the surface becomes super-hydrophilic. For UV photolithographic silicon wafers, the Si surface is hydrophilic. For ease of removal of PDMS from the Si mould, the surface can be made hydrophobic through the use of Octadecyl trichlorosilane (OTS). This SAM causes a change in the surface chemistry, therefore a contact angle greater than 90° was recorded [28]. The PMMA used for the alternating layers of the device was also examined. A contact angle of approximately 74° was recorded which allows the correct lamination between the PMMA and PSA layers.

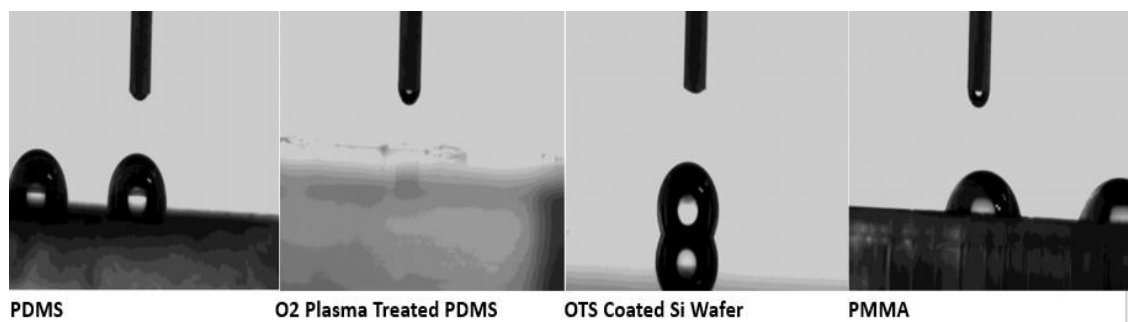


Figure 3.21. The surface wettability of four separate substrates where the water contact angle was measured with ImageJ.

The images of the surface water droplets allow for the contact angles to be measured where all results are displayed in Table 3-16

Table 3-16. The contact angle measurements recorded for four separate substrates used for the device fabrication included the platform and biosensor surface.

Substrate	PDMS	O_2 Plasma Treated PDMS	OTS Coated Si	PMMA
Contact Angle ($^\circ$)	86.84 ± 3.61	7.67 ± 1.62	120.5 ± 3.94	73.94 ± 1.32
Wettability	Slightly hydrophilic	Super hydrophilic	Hydrophobic	Hydrophilic

All angle measurements were acquired with ImageJ software (ImageJ, USA). The construction of devices and their functionality is highly dependable on the choice of materials. The use of biological substances required hydrophilic and hydrophobic interactions, therefore it was necessary for characterisation of the various materials used.

3.11 Second Generation Device

For the purpose of this project, a second-generation device was designed and tested fluidically. To reduce the layers of the device and to allow the device to be mass-manufacturable, 3D printing fabrication techniques were adopted. Initially, the device was optimised using the rapid prototyping methods. The DF tabs were removed to simplify the internal architecture.

The sample chamber, microchannel, electrode incubation chamber and waste channel were not altered, as to have replicable results compared with the original device optimised within this Chapter. This secondary device was fabricated as a proof of concept device. In an effort to reduce the cost per test, printed circuit boards (PCBs) were acquired to replace the physically inserted electrodes. The shape of the PCB electrodes was an exact replica of the electrode configuration of the first generation device. The feature comparison details the main changes between both devices, where an increased volume of both the wash and PBS step allows for better washing of the electrodes and a greater electrode to electrolyte ratio for detection purposes as detailed in *Table 3-17*.

Table 3-17. *A direct comparison between the rapid-prototyped device developed and optimised through-out this chapter versus the 2nd generation device which is 3D printed to reduce fabrication times.*

Device Feature	eLoaD device	2 nd Generation Device
Number of layers	9	2
Method of production	Rapid-Prototyping	3D Printing
Electrode type	Au plated Si 30mm x 5mm slides	Printed circuit board

Volume of sample	1.7mls	1.7mls
Volume of electrode incubation chamber	1.75mls	1.75mls
Volume of DI H₂O	0.85mls	1.6mls
Volume of DPBS	0.85mls	1.7mls
Diameter of device	130mm	130mm
Diameter of base	144mm	130mm
Triggering system	DF Tab system	Pneumatic vacuum release

The DF tabs, implemented to the eLoaD device, allowed for the automation of the device, however they require multiple layers to create pneumatic chambers on different layers. These tabs contain a variety of design factors required to be triggered at a specific spin frequency. To simplify the second-generation device, the DF valving system was removed. Instead, the DIH₂O and DPBS were pre-loaded and the vent inlets were sealed using clear tape. This created a vacuum within the chamber and does not allow the liquid to flow under spinning conditions. Once the sample was fully displaced to the waste chamber, the device would be stopped, where one vent was pierced to release the vacuum pressure. A spin-frequency was then applied to the device and the liquid is free to move between chambers.

Once all optimising was complete, the 3D device design was saved in an .stl format to be used in conjunction with the Stratasys Object260 Connex 1 3D printer. Essentially, layers 1-7 were conjoined to create one piece to be printed. This was then fused to the PCB layer (Designed by Taufeeq Elahi Diju and acquired from PCBway.com (China)) using chloroform and pressure. Figure 3.24 portrays the 2 layer 2nd generation device, where the device is printed from the vents to the channel's layers, in an inverted manner. The top view, perspective view and the final device demonstrates the design to prototype stages of the device.

The reduction of the initial device from 9 layers to 2 layers proves that the device itself may be mass-produced for large scale production. As the device itself has been proven to

be manufactured using 3D printing techniques, this design can be used in conjunction with injection moulding techniques for rapid platform production.

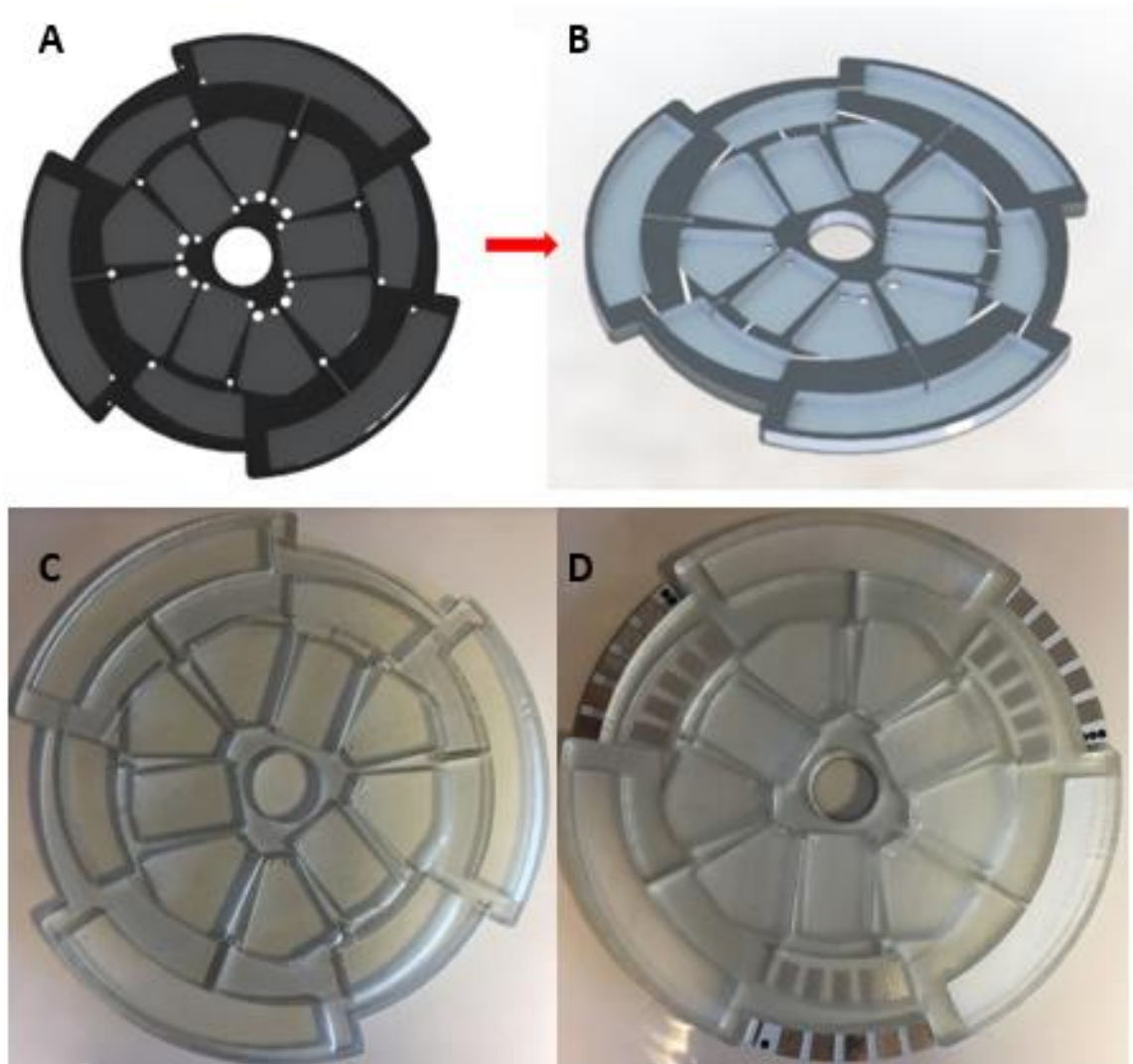


Figure 3.22. Stepwise development of the 2nd generation device where a) and b) who the SolidWorks 3D modelling of the device where the top layer was 3D printed using the Connex printer using a clear resin shown in c) where d) is this final assembled device where the 3D top layer is adhered to a PCB base layer

3.12 Conclusion

In this chapter, an extensive device optimisation was discussed. Initially, the electrodes type was the first issue encountered, where sputtered electrodes were unstable and unpredictable on the PMMA surfaces. ITO and Au coated Si slide electrodes were considered; however, the instability of the ITO reference electrode gave rise to unstable results and a reduced shelf life expectancy of the device. The microfluidics of the device was then determined, where the device went under many iterations to perfect the assay performance. Many modifications were made in an effort to maximise volumes whilst maintaining the integrity of the DF valving system. The channels were optimised for lower viscosity samples and whole blood, where tween allows more viscous samples flow. The length and width of the channels play a huge role in the displacement of liquids between reservoir chambers. The microchannel itself cannot be too large, to limit the number of platelets entering the electrode incubation chamber, and cannot be too narrow, as blood containing samples may aggregate and block the channel. It was discovered that a channel width of 0.85mm and a length of 3.31mm was the optimum design parameters, found through testing, for the channels which were coated with 10 μ l of Tween20 for whole blood samples.

The waste channel was significantly optimised to determine the incubation time of the sample over the electrodes. It was discovered that the length created the majority of the resistance within the channel which creates a pressure blockage which was overcome with either an increase in spin frequency or a pressure build up due to the majority of the sample being present in the electrode incubation chamber. The DF tab triggering optimisation work was severely altered throughout the device development stages. The overflow triggering system was unreliable, where mis-alignment and uneven lamination of the device altered the valve actuation between testing sites. Removal of this system allowed for the DPBS and wash reservoirs to increase in volume, as the architecture of the valving system was simplified. The DF tab system relied upon pneumatic chamber size, mean radial positioning of the tab and lower channel length only, reducing the source of error for the triggering system. The final version of the device was capable of testing 1.7mls of sample in triplicate where the wash and DPBS chamber could adequately hold 0.85mls of reagents each, with a waste chamber of 2.4mls. The optimisation of the

pneumatic chamber volume over the surrounding the DF tab and the mean radial positioning of the valving system were high impact factors on the tab actuation frequency.

The addition of layer 8 for V. 2.2 was introduced as a method to stop leaking over electrodes under spin-conditions which also gave rise to a control measure for the exposed electrodes area in the 1mM electrolyte solution. The area of electrode exposure zones in the electrode cover greatly influenced the EIS detection feedback for the device, so careful consideration was taken whilst implementing this layer. A full study was undertaken to determine the effect where optimum design parameters have been discussed. The effect of spin-frequency conditions was considered for the pathogens to determine whether the pathogens could survive under higher centrifugal forces. As 7-15Hz were observed to be the most favourable spin-profiles, the device is only at 20Hz for 30 seconds to burst the electrode DF tab, where to platform is then returned to 15Hz.

Confocal images were acquired to justify this parameter, where pathogens remained intact. Sample preparation was also determined to reduce non-specific binding, where RBCs and platelets tend to aggregate on the Au surfaces. A variety of pre-treatment was observed, where the culture media BacTec, saponin, and a mixture was used. High interferences still existed for a multitude of reagents added to the sample, which in turn effected the EIS measurements. The addition of fibrinogen to the sample and electrode incubation chamber significantly reduced the platelets observed on the electrode surfaces, where RBCs were reduced by the addition of DH₂O at a ratio of 1:3 with blood culture samples. Multiple, separate optimisation steps were required as the device is required to test various complex sample types. It was proven that the ELoaD platform is robust, easy to use device for use with real-samples, where the full capability of the device is carried out in the Chapter 4.

3.13 References

- [1] D. Coen, "Operative Techniques and Recent Advances in Acute Care and Emergency Surgery," *Oper. Tech. Recent Adv. Acute Care Emerg. Surg.*, 2019.
- [2] H. Won *et al.*, "A broad range assay for rapid detection and etiologic characterization of bacterial meningitis: performance testing in samples from sub-Saharan(,)," *Diagn. Microbiol. Infect. Dis.*, vol. 74, no. 1, pp. 22–27, Sep. 2012.
- [3] C. WY, "Measuring the effectiveness of mammography," *JAMA Oncol.*, vol. 1, no. 8, pp. 1037–1038, Nov. 2015.
- [4] P. Yager, G. J. Domingo, and J. Gerdes, "Point-of-Care Diagnostics for Global Health," *Annu. Rev. Biomed. Eng.*, vol. 10, no. 1, pp. 107–144, Jul. 2008.
- [5] L. X. Kong, A. Perebikovskiy, J. Moebius, L. Kulinsky, and M. Madou, "Lab-on-a-CD: A Fully Integrated Molecular Diagnostic System," *J. Lab. Autom.*, vol. 21, no. 3, pp. 323–355, 2016.
- [6] J. Ducrée, S. Haeberle, S. Lutz, S. Pausch, F. von Stetten, and R. Zengerle, "The centrifugal microfluidic Bio-Disk platform," *J. Micromechanics Microengineering*, vol. 17, no. 7, pp. S103–S115, Jul. 2007.
- [7] H. Hwang, Y. Kim, J. Cho, J. Lee, M.-S. Choi, and Y.-K. Cho, "Lab-on-a-Disc for Simultaneous Determination of Nutrients in Water," *Anal. Chem.*, vol. 85, no. 5, pp. 2954–2960, Mar. 2013.
- [8] W. Al-Faqheri *et al.*, "Vacuum/Compression Valving (VCV) Using Paraffin-Wax on a Centrifugal Microfluidic CD Platform," *PLoS One*, vol. 8, no. 3, pp. 2–10, 2013.
- [9] G. A. M. Pop *et al.*, "The clinical significance of whole blood viscosity in (cardio)vascular medicine.," *Neth. Heart J.*, vol. 10, no. 12, pp. 512–516, 2002.
- [10] Fluxion, "Understanding effects of viscosity in the BioFlux system," *Tech. Note*, pp. 1–2, 2009.
- [11] Y. Çinar, A. M. Şenyol, and K. Duman, "Blood viscosity and blood pressure: Role of temperature and hyperglycemia," *Am. J. Hypertens.*, vol. 14, no. 5 I, pp. 433–438, 2001.
- [12] C. Y. Lee, C. L. Chang, Y. N. Wang, and L. M. Fu, "Microfluidic mixing: A review," *Int. J. Mol. Sci.*, vol. 12, no. 5, pp. 3263–3287, 2011.
- [13] D. N. T. Issue, "Sputter Coating Technical Brief," vol. 2, no. 2, pp. 1–13.
- [14] R. Van Vught, R. J. Pieters, and E. Breukink, "Site-specific functionalization of proteins and their applications to therapeutic antibodies Abstract : Protein modifications are often

required to study structure and function relationships . Instead of the random labeling of lysine residues , methods ha,” *Comput. Struct. Biotechnol. J.*, vol. 9, no. 12, p. e201402001, 2014.

- [15] M. Senthilkumar, J. Mathiyarasu, J. Joseph, K. L. N. Phani, and V. Yegnaraman, “Electrochemical instability of indium tin oxide (ITO) glass in acidic pH range during cathodic polarization,” *Mater. Chem. Phys.*, vol. 108, no. 2–3, pp. 403–407, 2008.
- [16] L D Burke and P F Nugent, “The electrochemistry of gold: I. The redox behaviour of the metal in aqueous media,” *Gold Bull.*, vol. 30, no. 2, pp. 43–53, 1997.
- [17] C. A. Rusinek *et al.*, “All-Diamond Microfiber Electrodes for Neurochemical Analysis,” *J. Electrochem. Soc.*, vol. 165, no. 12, pp. G3087–G3092, 2018.
- [18] G. R. *et al.*, “Centrifugo-pneumatic valving utilizing dissolvable films,” *Lab a Chip - Miniaturisation Chem. Biol.*, vol. 12, no. 16, pp. 2894–2902, 2012.
- [19] J. Gaughran and B. S. Hons, “Development of Novel Advanced Flow Control Systems on Centrifugal Microfluidic Platforms for Nucleic Acid Testing,” no. January, 2016.
- [20] R. Gorkin *et al.*, “Centrifugo-pneumatic valving utilizing dissolvable films,” *Lab Chip*, vol. 12, no. 16, pp. 2894–2902, 2012.
- [21] C. E. Nwankire *et al.*, “A portable centrifugal analyser for liver function screening,” *Biosens. Bioelectron.*, vol. 56, pp. 352–358, 2014.
- [22] R. Ahmed and K. Reifsnider, “Study of influence of electrode geometry on impedance spectroscopy,” *Int. J. Electrochem. Sci.*, vol. 6, no. 4, pp. 1159–1174, 2011.
- [23] D. P. Mikhailidis, M. A. Barradas, A. Maris, J. Y. Jeremy, and P. Dandona, “Fibrinogen mediated activation of platelet aggregation and thromboxane A2 release: Pathological implications in vascular disease,” *J. Clin. Pathol.*, vol. 38, no. 10, pp. 1166–1171, 1985.
- [24] K. M. Koczula *et al.*, “NIH Public Access,” *Lab Chip*, vol. 7, no. 1, pp. 1–3, Jul. 2016.
- [25] S. Chanpimol, B. Seamon, H. Hernandez, M. Harris-love, and M. R. Blackman, “HHS Public Access,” vol. 32, no. 4, pp. 823–839, 2017.
- [26] S. H. Tan, N.-T. Nguyen, Y. C. Chua, and T. G. Kang, “Oxygen plasma treatment for reducing hydrophobicity of a sealed polydimethylsiloxane microchannel,” *Biomicrofluidics*, vol. 4, no. 3, p. 32204, Sep. 2010.
- [27] Y. Jin, C. Ren, L. Yang, and J. Zhang, “Nonequilibrium atmospheric pressure Ar/O2 plasma jet: Properties and application to surface cleaning,” *Plasma Sci. Technol.*, vol. 18, no. 2, pp. 168–172, 2016.
- [28] Y. Song, R. P. Nair, M. Zou, and Y. Wang, “Superhydrophobic surfaces produced by applying

a self-assembled monolayer to silicon micro/nano-textured surfaces," *Nano Res.*, vol. 2, no. 2, pp. 143–150, 2009.

Chapter 4

*Biosensor Development and
Pathogen Detection on an
Electronic Lab-on-a-Disc using
Label-Free Electrochemical
Detection Methods*

4.1 Introduction

Reflecting on the literature studied in Chapter one, there is an enormous need for a method capable of capturing disease-causing cells with high selectivity and sensitivity (<10 CFU/mL). Current techniques are still too slow at confirming whether a pathogen is present in the blood stream within the “golden-hour”. Culturing techniques have remained unchanged for many years and can take up to several days for a result to be obtained due to certain pathogens having extreme slow growth rates, or in some cases being viable but non-culturable (VNCC) needing to be resuscitated to become active again [1], [2], [3].

Biosensors are rapidly becoming a method of choice for whole cell detection due to their quick response time. A huge range of biosensor ranges exist, however bio-affinity sensors or immunosensors are of particular interest due to the strong affinity between antibodies and their respective antigen [4]. Biosensors eradicate the need for arduous pre-treatment of samples and with new fabrication methods emerging, the biosensor is prepared as a single, ready to use device. Biosensors can easily be altered for the selective capture of various cells. By fabricating the platform with specific, highly tailored antibody or capture probes, specific cells may be captured. The antibody-antigen arrangement has been described as a “lock and key” mechanism, where the antibody attaches to the antigen through a specific target region, therefore is highly selective towards the antigen. As the capture antibody can be interchanged between platforms, making it a robust method for detection. Many detection methods can be applied to biosensors, such as optical and electrochemical [5]. The response time is one major issue. For example, in a clinical setting, slow diagnosis of sepsis causes misinformed prescription of antibiotics. A surge in antibiotic resistant strains is an ever-increasing issue due to the overuse therefore, it is apparent that a biosensor capable of determining the presence of pathogens in the bloodstream, before antibiotics were administered, is highly desirable.

In recent years, there has been a significant effort to detect the whole cell, where impedimetric methods were the most commonly used [6]. The capture for the whole cell lies on the micrometre scale, rather than typical molecular analytes such as DNA, RNA and

proteins which lie on the nanometre scale, which is important when detecting the changes caused by bound cells, such as changes in capacitance and resistance. One of the main challenges presented by cell capture is the possibility of non-specific interactions with the sensor due to the presence of a variety of surface epitopes on the pathogen wall. Polyclonal antibodies (pAbs) secreted from B cell lineages against specific bacterial strains were commonly used bioreceptors for whole bacterial cell detection, where the binding sites on the cell wall were usually unknown. Selectivity is increased as isolated surface epitopes can be utilised to produce monoclonal antibodies (mAbs) [7].

As previously discussed, the top 20 pathogens found in BSIs were divided into these three categories. Gram Positive (GP), Gram Negative (GN) and Fungal. These cells were distinguished from each other due to a difference in their cell membrane proteins and composition, displayed in *Table 4-1* below.

Table 4-1. Distinguishing characteristics between Gram-positive and Gram-negative cell wall features [8].

Cell feature	GP Bacteria	GN Bacteria	Fungal Species
Peptidoglycan layer	Multi-layered	Single layer	No. Cell wall composed of N-acetylglucosamine polymer chitin
Teichoic Acids	Present	None	None
Periplasmic space	None	Present	Present in yeast
Outer Membrane	None	Present	Present
Lipopolysaccharide (LPS)	None	High	None
Lipid and lipoprotein content	Low	High	High
Toxins produced	Exotoxins	Endotoxins	Mycotoxins
Cell wall composition	100-120 Å thick single layer. Low content of lipid in the cell wall however the Murein content is up to 80%	70-120 Å double layer with both a high lipid content and low Murein content	100 µm thick composed of mannoproteins, chitins, and α- and β- linked glucans

Mesosome	More prominent	Less prominent	None
Antibiotic resistance	Susceptible	More resistant	Susceptible
Flagella	2 rings in body	4 rings	None

Bacterial cells were characterised as GP if they maintain the crystal violet dye during the gram stain process adopted after bacterial culture. GP bacteria appear blue/violet under microscopic identification, whereas GN bacterial look red/pink. This colorimetric difference is due to the distinguishes between the cell-wall components as described [5]. Asif *et al.* described the ideal biosensors, as outlines in *Table 4-2* below. There is an apparent need for a biosensor capable of whole cell detection in a clinical setting which implements a variety of these characteristics described.

Table 4-2. Requirements for an ideal biosensor for pathogen detection [7].

Characteristic	Quantity
Sensitivity	< 10 ³ CFU/ml
Selectivity	Can distinguish between different serotypes of bacteria as well as operating in complex matrices
Speed	Up to 10 minutes per test
Size	Compact, POC device
Sample processing	Label free with little or no sample processing
Stability	A shelf life for up to six months and is stable in high temperature regions
Skill of operator	No specialist training required.

In this chapter, two separate types of biosensors were fabricated. Firstly, the traditional method of self-assembled monolayer (SAM) electrode modification with EDC/NHS coupling to allow for antibody attachment was characterised. This is to quantify the effect of each subsequent layer addition to the cyclic voltammetry (CV) and Electrochemical Impedance Spectroscopy (EIS) response. This method has been previously demonstrated to be capable of the capture and sensing of microbes on an electrodes surface which is used in conjunction with EIS techniques for rapid, label-free impedance detection [8], [9].

A highly advantageous ability of this technique is the investigation of a variety of cell properties by a simple change of the applied frequency to the circuit [10],[11].

Secondly, a single use biosensor was fabricated from diced Au coated Si rectangular segments. Micro contact patterning/printing (μ CP) of an antibody layer with blocking solutions to prevent non-specific binding was also characterised and compared with the SAM method. Finally, this single use biosensor was functionalised with three separate types of biorecognition molecules which have been developed and optimised for the capture of GP, GN and Candida microbes within the centrifugal, microfluidic device.

Full optimisation studies were carried out for the production of antibody patterned surfaces for the efficient capture of microbes in blood culture samples received from St. James' Hospital. EIS methods were employed for the efficient detection of pathogens using a dilute electrolyte solution. This approach maximises the double layer thickness and increases the impedance change upon cell capture [12]. Confocal microscopy was also carried out for image profiling of the surface, to confirm that capture of the micro-organisms and to also determine the capture efficiency of the antibody modified surface.

Chapter 3 described in detail the full optimisation of an eLoaD capable of capturing and detecting pathogens with a comprehensive breakdown of each individual components and how that contributes to the overall sepsis detecting platform. Device parameters were implemented to handle more complex matrices, such as the fibrinogen functionalisation of chambers, spin rates, tween coated channels and specific sample dilution ratios. The study carried out in conjunction with St. James' Hospital Microbiology lab was used to determine whether the quick sample to answer platform was capable of capturing pathogens whilst sub-categorising them. This real sample testing was essential to determine the true capabilities of the user friendly platform to judge the potential of this device for the future of sepsis diagnosis. Compared to other methods on the market. Currently the potential of this device is an exciting and crucial development in the POC systems for pathogen detection for near patient sample analysis. According to Oeschger *et. al.*, the quickest FDA approved device available to the market for sepsis detection is based upon blood gas analysis which may be an indication of sepsis, where this is the only true POC system which may be used for rapid diagnostics [13], [14]. Blood gas levels

however may just be an indication of other forms of illnesses and therefore may not be a true indication of a blood stream infection, as serious conditions like diabetes, kidney disorders and cardiovascular system disorders could give false positives [15]. The fastest form of pathogen ID from complex sampling can be carried out in one hour. These testing procedures were predominantly carried out using real-time PCR methods, which requires extremely costly equipment and a highly trained lab technician [16]. It is proposed that the eLoaD device is capable of pathogen detection and categorisation in just 15-minutes, a significant reduction in detection time compared to a broad-range of competitors where this centrifugal microfluidic electronic lab on a disc (eLoaD) is the first of its kind.

For the validation of the eLoaD, blood culture samples acquired from the microbiology department in St. James' Hospital, Dublin, were tested to determine the potential of the device using complex matrix samples. This negation of sample filtration and purification makes this device an attractive POC system, as this reduces the need for costly filtering equipment and the need for more specialised users for the device testing. An N=3 for each sample tested was carried out to validate the results obtained from each device, where device per sample was used.

4.2 Materials and Methods

4.2.1 Chemical and Biological Reagents Used

GTX40307 GN Endotoxin [308] Mouse Monoclonal Antibody, GTX36804 GP bacteria LTA [3801] Mouse Monoclonal Antibody and Native Candida Rugose Cholesterol Esterase Purified Protein purchased from Genetex (USA). PEG₈-thiol purchased from Quanta (USA). BSA, Glutaraldehyde, Triton, DPBS, Fluoroshield mounting media, 16-mercaptohexadecanoic acid (MHDA), Sulfo-N-hydroxy succinimide (NHS), 1-ethyl-3-[3-dimethylaminopropyl] carbodiimide hydrochloride (EDC) all purchased from Sigma Aldrich (Ireland). The Live/Dead bacteria viability kit purchased from Life Sciences. ATTO 488 dye (ATTO-Tec GmbH, Germany) Ethanol, IPA, DPBS and Tween20 were purchased from Sigma-Aldrich (Ireland). Nutrient Broth No.2 and Agar No.1 Bacteriological were purchased from Lab M Limited (Ireland).

4.2.2 Materials

The eLoaD was manufactured from layers of 2mm PMMA and PSA (ARcwere7840) from Radionics and Adhesive Research respectively. The discs were assembled using the rapid-prototyping process as outlined in Chapter 3 where version 3.4 of the device was tested. The Au coated Si wafers were purchased from Platypus, which were diced into 30mm x 5mm Au electrodes. M77 glue was acquired from Scotch (United Kingdom). Gold disc electrodes, large area coiled platinum wire counter electrode, and Ag/AgCl reference electrodes were all purchased from IJ Cambria (UK).

4.3 Results and Discussion

The results obtained for the development of the biosensor is broken into four separate sections. The traditional method of sensor development by incorporating a SAM layer for antibody adhesion of 2mm gold working electrodes. Secondly, the manufacture and characterisation of the single use electrode using μ CP of antibody patterned surfaces to compare against the traditional method. Thirdly, the incorporation of the single use biosensor into the eLoaD developed in Chapter 3 and finally, the testing of blood culture samples in the LoaD for the device validation.

4.3.1 Fabrication of label-free electrochemical biosensor for use with a three electrode electrochemical cell

Initially, to create a novel biosensor platform, the traditional method of biosensor development for use with label-free impedimetric detection methods was fabricated to study the development of each stage of the fabrication process. Figure 4.1 portrays the typical setup for a three electrode electrochemical cell which contains a Counter electrode (CE), Reference electrode (RE) and Working electrode (WE) where the desired experimental response is carried out on the working electrode. A silver/silver chloride (Ag/AgCl) RE and a large area coiled platinum wire CE was used in conjunction with a gold WE, where all three electrodes were immersed in the electrolyte solution.

As sample to answer time is one of the main desirable attributes of an impedimetric biosensor, the label free method was selected. When an analyte interreacts with a selectively functionalised surface, the change in the electrical properties (resistance, dielectric constant, capacitance) are associated with the presence of the target biomolecule, therefore no label is required. Labelling can enhance sensitivity and increase selectivity through methods such as the sandwich assay approach, where a secondary probe is used, however this requires additional assay time, expense and sample handling

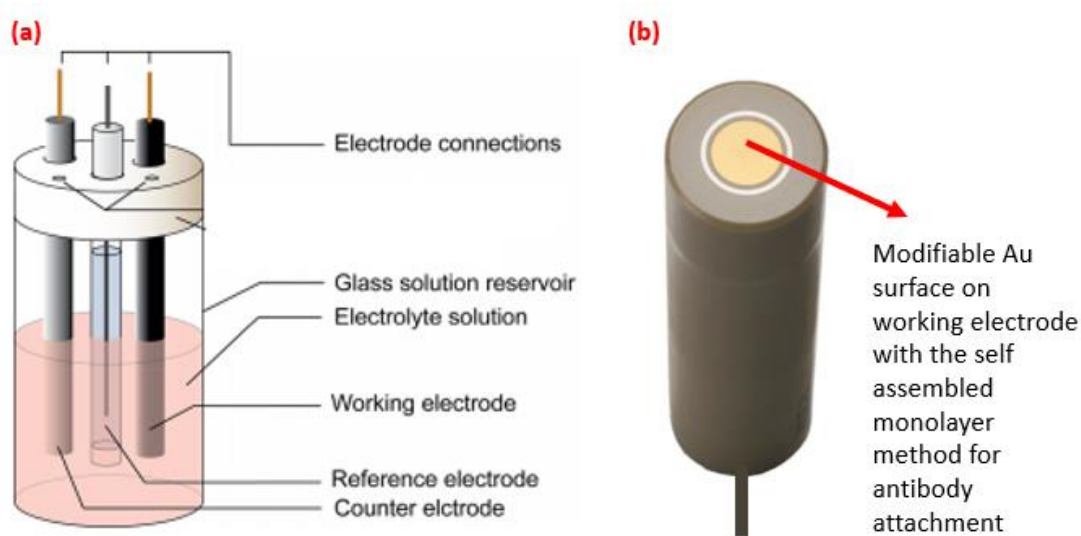


Figure 4.1. Typical 3-electrode cell configuration with a counter, reference and working electrode where (b) portrays the working electrode where the Au modifiable surface is shown.

[17].

Figure 4.2 portrays the stepwise processes in which to create a biosensor through the well-known method of SAM linked to an antibody layer. Initially, the electrode is cleaned then immersed into the SAM solution overnight. The 16-MHDA (1mM in EtOH) solution was the first modification step to promote antibody adsorption by producing a functional group in which the covalent bonding can occur [18]. This SAM is formed from active functional headgroups at both ends of the 16 carbon chain where the anchoring thiol headgroup has affinity for the gold surface, whilst the outer facing end of the molecule contains the functional group for biomolecule attachment [19].

EDC/Sulfo-NHS coupling is used to convert the carboxy group of the 16-MHDA to an active ester group to which the biomolecule covalently attaches. Carboxyl and amino groups are

omnipresent throughout the antibody structure and reside on the outside due to their charge. Amino acids and the carboxyl side chains were targeted for covalent attachment. The coupling between the amine and carboxyl groups is one of the most commonly used methods for antibody and protein attachment to a substrate [20].

Once the EDC/NHS coupling, described in Section 2.4.2 is carried out, 100 μl of the biorecognition molecule was incubated with the surface at 37°C for one hour and rinsed with DI water. With the introduction of whole pathogenic cells, the antibodies bind to the surface of the pathogens. How well they bind is dictated by the specificity and selectivity of the antibody binding layer and acts as a “lock and key” binding mechanism [21]. Finally, the sensor can be used in conjunction with CV and EIS methods to determine the change in impedance and surface coverage, if any, caused by the whole cell bound to the surface. The magnitude of the change often corresponds to the CFU/ml incubated with the surface or else the ions secreted by the pathogens once captured.

Initially, the Au WE surface was cleaned using 0.3 μm (if surface is very contaminated) and 0.05 μm alumina slurry for 10 minutes using a figure eight motion to ensure an even polish of the surface. The electrode was then rinsed with EtOH and then sonicated in DI water for 5 minutes. A CV of the working electrode was obtained in 0.1 M H_2SO_4 between -0.3 V and 1.5V at a scan rate of 0.1 V/s as described in Section 2.4.1. The characteristic sharp gold oxide reduction peak is typically found at 0.8V and overlapping oxidation peaks between 1.1 - 1.4 V versus Ag/AgCl, where a target roughness value of 1.6 is desired.

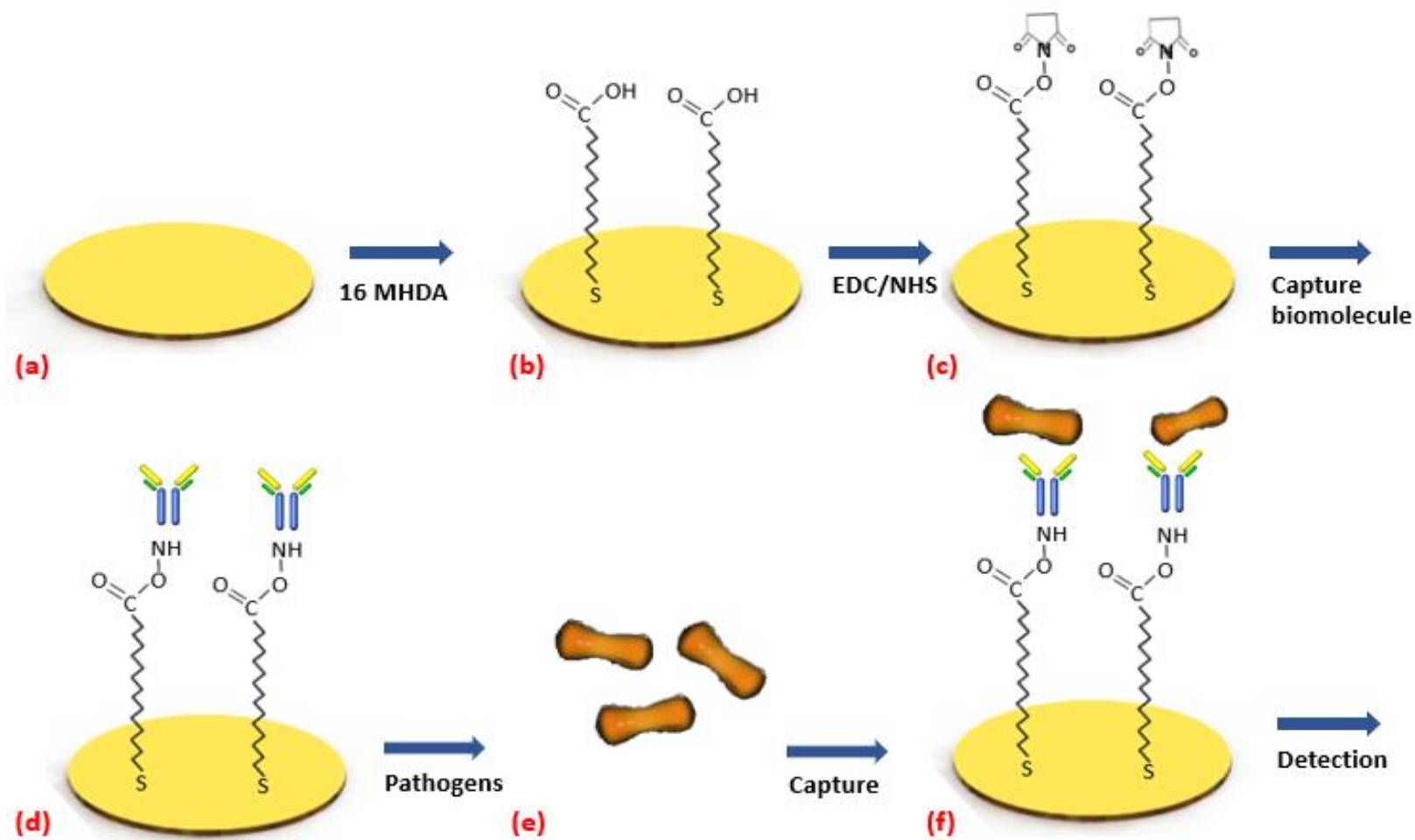


Figure 4.2. Stepwise process in which a planar gold surface is modified to be an antibody capture surface where (a) shows the planar surface only which is cleaned using alumina sludge, rinsed with EtOH and sonicated in dH₂O to create the cleanest surface possible (b) The beginning of the modification process where the surface is incubated overnight with 16-MHDA (c) The SAM is activated for EDC/NHS coupling through the carboxy group of the 16-MHDA surface (d) Incubation of the biomolecule to the SAM & incubation of the pathogens with the capture surface where (f) finally a method of detection is applied to determine if a pathogen has been captured.

Once the target surface roughness is achieved, CV and EIS measurements were performed for each fabrication step. Initially for the biosensor development, the measurements were obtained for the planar gold surface in a dilute electrolyte (1mM DPBS) as this was the desired supporting solution for the non-faradaic system response. Non-faradaic processes relate to the double layer formation and adsorption of ions present in the bulk solution which carry a positive or negative charge which interact with the charged WE surface. Due to the formation of the Double Layer Capacitance (C_{dl}) on the electrode surface, the solution-electrode interface portrays pseudocapacitive behaviour [22].

Once results were obtained, the procedure detailed in Section 2.4.2 was carried out create a SAM of 16 carbon chain length MHDA. SAMs of alkanethiols such as 16-MHDA have been demonstrated to strongly block electrochemical oxidation of gold surfaces which helps maximise the EIS response as the change in signal is associated with bound cell. The oxidation of gold surfaces may mask the response due to bound cells and therefore by blocking this process the measured response is attributed to the captured analyte [23]. These SAM layers have also been attributed to their ability to limit the access of solution phase molecules such as electrolyte ions, redox molecules and water to the electrode surface, therefore act as an insulating, blocking layer [24].

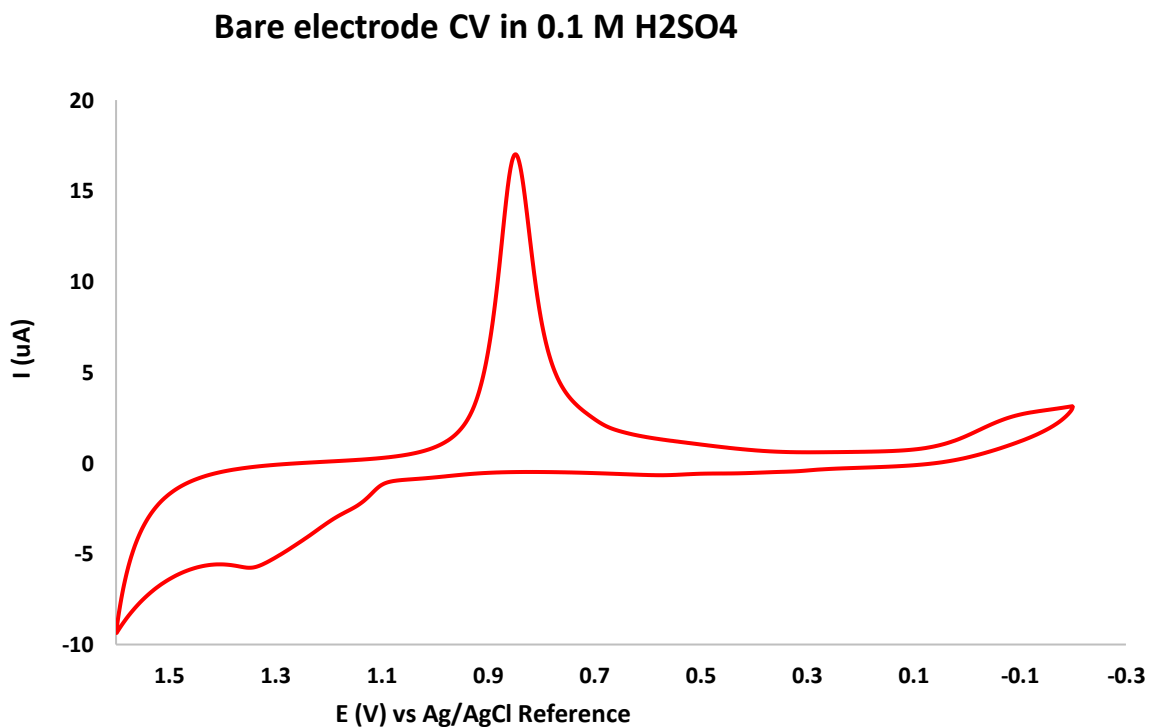


Figure 4.3. CV of planar gold surface of a typical working electrode in 0.1 M sulphuric acid showing both the reduction and oxidation peaks which has a surface roughness of 1.45. The sixth scan is presented.

The sixth cycle is portrayed for each of the CVs presented. This SAM layer results in a decrease in the capacitive current response of the surface demonstrating the formation of a low dielectric layer at this interface. For a non-faradaic sensor, a tightly packed SAM is required, in complete contrast to faradaic biosensors where the electrode surface is required to be available for the redox probe but not the adsorption of the target molecules [25]. The 16 carbon chain MHDA was chosen as SAMs with longer C-chains form more densely packed layers due to the lyophobic interactions of the chains. It's proposed in literature that C₁₁ and higher provide more packed films on the surface [26].

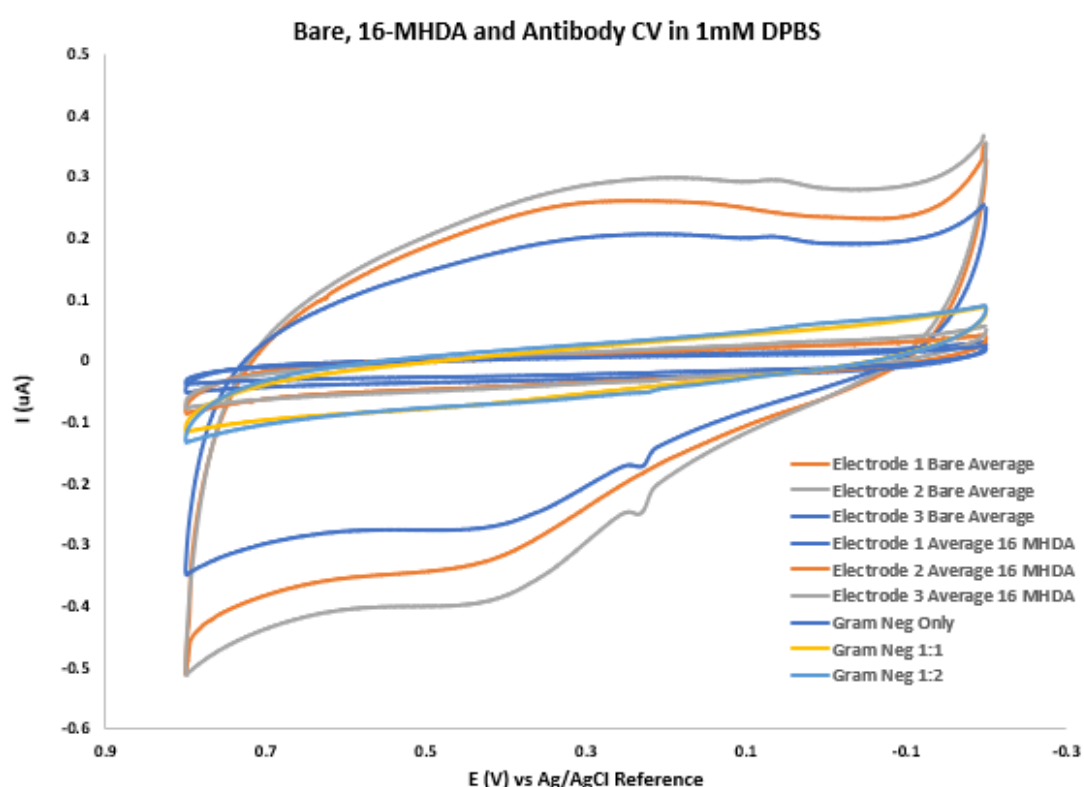


Figure 4.4. Cyclic voltammograms of the three separate stages of biosensor fabrication using a gram-negative endotoxin IgG antibody where each step was carried out using 1mM DPBS as the supporting electrolyte solution.

The modification of the SAM surface through the activation of the active ester using the EDC/NHS coupling solution before incubating with the GN endotoxin antibody. This antibody layer causes slight changes depending on the concentration of the antibody solution, as a loosely packed biomolecular recognition film is formed and therefore only minute changes in the interfacial capacitance occur [27]. Figure 4.4 portrays the comparative CVs monitoring the stepwise fabrication of the biosensor and illustrates the

responses for the unmodified gold electrode after the addition of both the SAM 16-MHDA and the immobilised GN antibody capture layer. The significant decrease in the current signifies the blocking of the WE by the formation of the SAM where further blocking occurs with the addition of the antibody layer. The voltammograms therefore prove the deposition of the biorecognition layer. The EIS response which is measured despite the blocking of the electrode is due to the changing capacitance value. The SAM R_{leak} may change the equivalent circuit modelling (ECM) of the system where the capacitance and resistance may be in parallel rather than in series.

EIS techniques were also adopted to monitor the fabrication of the biosensor to determine how the addition of the 16-MHDA and GN antibody immobilisation effects each of the responses. The Bode, Nyquist and Phase plots were all examined and explained to further understand the system. The equivalent circuit models were often used to best describe the system response is EIS. The solution resistance denoted by R_{sol} is derived from the limited conductance of the ions available in the bulk solution and therefore is typically not affected by binding of antigens to the modified surface. The capacitance between the Au WE and the ions in solution consists of the C_{dl} and the capacitance caused by surface modification can be collectively termed C_m . For an insulating probe layer on the electrode surface which will form a capacitance, the C_{dl} will appear in series with it with capacitance of the double layer [28].

SAMs act as a blocking mechanism for the prevention of ion adsorption and provide a unique method of controlling the interfacial properties at the solid/liquid interface [29], [30]. The 16-carbon chain was chosen as the linker chain alkanethiols have lower permeability due to the increased chain-chain interactions. These attractive lateral interactions as reported to increase with chain length and were ascribed to the Van der Waals interactions [31]. According to Agonafer *et. al* the capacitance of the bare gold subtract is approximately 55 times greater than the capacitance for SAMs grown from 15h-120h [24]. Small peaks were observed at ~ 0.23 V which are the results of ion adsorption on the surface.

With EIS, the Nyquist plot consists of an imaginary (Z'') vs real (Z') impedance, which may be fitted to decouple the changes in the solution phase resistance alongside the

capacitance and resistance associated with the antibody layer or the captured whole cells. The impedance response of the circuit was measured using a 1mM DPBS electrolyte solution at the open circuit potential (OCP) with the AC amplitude set at 25mV with the frequency range set from 0.01Hz to 100kHz. This electrolyte concentration was chosen as the total amount of ions in solution will determine the double layer thickness. According to Venkatanarayanan *et. al* the capture of cells typically causes the electrode capacitance and overall cell resistance to decrease and increase, respectively. The maximum sensitivity for the binding events occurs within the diffuse double layer and therefore changing the ionic strength of the buffer will determine where the sensor can detect the capture of cells. The 1mM DPBS has a double layer thickness of ~ 10 nm where the antibody layer was found to be ~ 3 nm and bacterial cells are $\sim 5 \mu\text{m}$, therefore the binding of the antibody-antigen occurs within this diffuse layer determined by the ionic strength of the supporting electrolyte solution [12]. The Bode plot of the electrochemical cell is also obtained, which plots the log of the absolute impedance ($|Z|$) against the log of the excitation frequency [32].

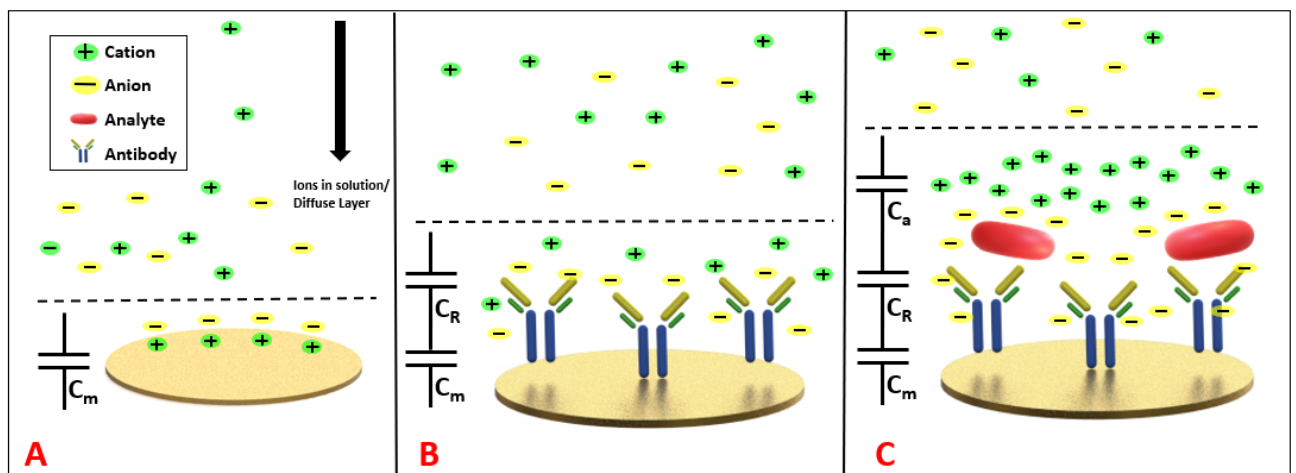


Figure 4.5 Schematic representation of the capacitance of the biosensor. The capacitive behaviour can be described by (A) The capacitance due the insulating layer denoted C_m (Double layer and SAM if present), C_R represents the capacitance of the biorecognition layer and C_a is the capacitance associated with the bound analyte.

For non-faradaic impedance the transduction occurs through changes of the surface dielectric, charge distribution or conductance of the electrode surface which are assessed through capacitance. The first capacitance arises with the electrode being immersed in the electrolyte solution where a certain potential is applied. The charged ions will be orientated at the electrode/electrolyte solution interface which in turn creates the C_{dl} as

shown in Figure 4.5 (a). This C_{dl} as previously mentioned is very sensitive to change which may be introduced by the biorecognition layer C_r (antibody or protein), and furthermore by an analyte binding to this (C_A) which further alters the capacitance of the biosensor (Figure 4.5 (b) and (c)) [33], [34]. The capacitance of the fully fabricated biosensor with the non-faradaic approach can be described as the combination of the C_M (C_{dl} and C_{SAM}), C_R and the C_A in series. The total capacitance C can be described by the equation:

Equation 4-1

$$\frac{1}{C} = \frac{1}{C_M} + \frac{1}{C_R} + \frac{1}{C_A}$$

Where the addition of each subsequent modification step will cause a decrease in the overall capacitance of the system [35]. In non-faradaic sensors, it is common to justify changes in C_R and C_A as occurring due to displacement of water and ions from the surface upon target binding. Binding should increase thickness and/or decrease ϵ (dielectric constant) of the probe layer ($\epsilon_r \approx 2 - 5$ for biomolecules, 2.7 for alkanethiols and 80 for water), both decreasing the overall capacitance [36][37].

Impedimetric responses for each fabrication step were acquired to determine the effect of the addition of each modification step. The Bode plot provides frequency information, as the logarithm of the excitation frequency is plotted against the logarithm of the impedance ($|Z|$) and the phase shift. The Nyquist plot consists of a semicircle followed by a straight line formed at an angle to the x-axis. The nyquist is composed of a real (x-axis) and imaginary (y-axis) denoted Z' and Z'' respectively. The semicircle is formed at higher frequencies, where the length of the arc as it tends towards Z''_0 correlates with the transient charge resistance, ionic resistance, or a resistive path modelled by R_{leak} . The linear aspect of the graph corresponds with the lower frequency applied to the system and portrays the diffusion process [38]. The Nyquist plots were used to study the change in both the capacitance and resistance due to the individual fabrication process which result in variances to all three EIS plots shown in Figure 4.6 [39][40]. This shows the three extracted graphs from the EIS data obtained for the three separate fabrication steps. Typically, the imaginary aspect of the Nyquist plot correlates with the capacitance, where the real component of the Nyquist plot is associated with the resistance of the recorded response. The model outlined by Equation 4-1 implied the ideal dielectric behaviour of the insulating biomolecule capture layer which could results in a straight line in the

Nyquist plot to the imaginary impedance axis. This situation however is not commonplace for real-sensors. Defects in the SAM or insulating layers, called pin-roles, would be a major factor for the non-ideal dielectric attributes. This resistance R_{leak} would act as a parallel elements to each corresponding capacitor which represent the resistance of the individual layer to the ionic species moving through the collapse sites and pin-holes within the structures [41].

The isoelectric point (pI) is the pH of a solution at which the net charge of a protein becomes zero. At solution pH that is above the pI, the surface of the protein is predominantly negatively charged. For the monoclonal antibodies used for pathogen capture, the pI of mAbs was between 6.1 and 6.5, where the buffer used has a pH of 7.4, being slightly higher to that of the antibody isoelectric point making the antibody surface slightly negatively charged [42]. The addition of more negative charge on the biosensor surface will attract more cations towards the electrode surface and therefore alter the EIS response of the system.

4.3.1.1 Nyquist Plots for Gold Disc Electrode

Figure 4.6 (a) portrays the Nyquist plot for the bare, SAM and antibody modified layer. It is noted that the magnitude of the semi-circle decreases with the addition of each modification. As the capacitance is directly correlated with the Z'' axis, a decrease in the height of the semi-circle with each additional modification step to the electrode corresponds to the model of the decreasing capacitance of the total system as each capacitor is added in series. Noting the point in which the semi-circle crosses the x-axis, a decrease in the Z' value is observed for the additional layers on the electrode also. As it is not possible to deconvolute the semicircle into its individual processes that gives rise to the overall Nyquist plot it cannot be determined with absolute certainty whether the capacitance, transient resistance or both were the cause for reducing the magnitude of the semicircle for each fabrication step. As the SAM layer has an overall negative charge due to the carboxy terminal group, and the resistance over the system appears to be reduced.

Table 4-3. Gold disc electrode Nyquist plot results for bare, SAM and antibody steps.

	Bare (1)	SAM (2)	Antibody (3)
Z'' (Ohms)	7,766 ± 1,011	5,125 ± 5,88	2,876.5 ± 396
ΔZ'' (Ohms)	NA	2,641	2,249
Z' (Ohms)	15,200 ± 1,005	11,920 ± 950	7,480 ± 880
ΔZ' (Ohms)	NA	3,280	4,400

Table 4-3 displays the data extracted from the Nyquist plots shown in Figure 4.6. Firstly, the Z'' values were considered, where the data extracted was the Z'' max values. With the initial bare electrode Z'' value obtained, the addition of the SAM layer reduced the height of the semi-circle from 7766 ohms to 5125 ohms, a difference of 2641 Ohms in total. With the antibody modified surface, the Z'' value decreases by a further 2,249 Ohms. With the imaginary graphical representation reducing by over half the initial response it would be suggested that the addition of each layer is adding a capacitance in series as the C_{total} of all modification steps significantly reduces. In a similar pattern, the Z' values which are predominately ruled by the resistive characteristics of the biosensors also reduces for each fabrication step, however as the Nyquist adopts a semi-circle shapes and with the Z'' magnitude decreasing with the modification steps, the Z' value would decrease as it is directly related to the Z'' value. It must be noted that there would be changes in the R_{leak} of the sensor, the changes appear to be dominated by the changes in the capacitance of the modified layers.

4.3.1.2 Bode Plots of Gold Disc Electrodes

Observing the Bode plots shown in Figure 4.6 the lower frequency range of 10⁰ – 10² corresponds as the bare gold has a slightly lower Log Z where both the SAM and antibody immobilised layer have very similar values in the lower range. According to Daniels *et al* the lower frequency range of a bode plot for a non-faradaic biosensor corresponds to the R_{leak} of the sensing surface [43]. As the bare gold was modified with the SAM layer, the Δ Log Z (Ohms) would suggest that the layer was formed, where the change in R_{leak} was controlled by the modification of the SAM layer. The most significant difference in the Bode plots is considered at the 10 kHz range, where the change in the Log Z (Ohms) is detailed in Table 4-4 where the most significant change was observed at the Δ Log Z (Ohms) between the SAM and antibody layer, where a difference of 0.2 Ohms was

recorded. Examining the correlated excel data, the region between Z'' max and Z' min was located between Log 4.75 – 3.75 Hz which is dominated by the C_m or C_A .

Table 4-4. Bode plot values for gold disc electrodes for bare, SAM and antibody modified steps obtained at 10 kHz.

Value at 10 kHz	Bare (1)	SAM (2)	Antibody (3)
Log Z (Ohms)	4.155 ± 0.09	4.077 ± 0.11	3.877 ± 0.01
Δ Log Z (Ohms)	NA	0.078	0.2

A clear separation was noted between the SAM and antibody Bode plots at 10,000 Hz where the change in impedance for the antibody layer was the lowest for all three plots,

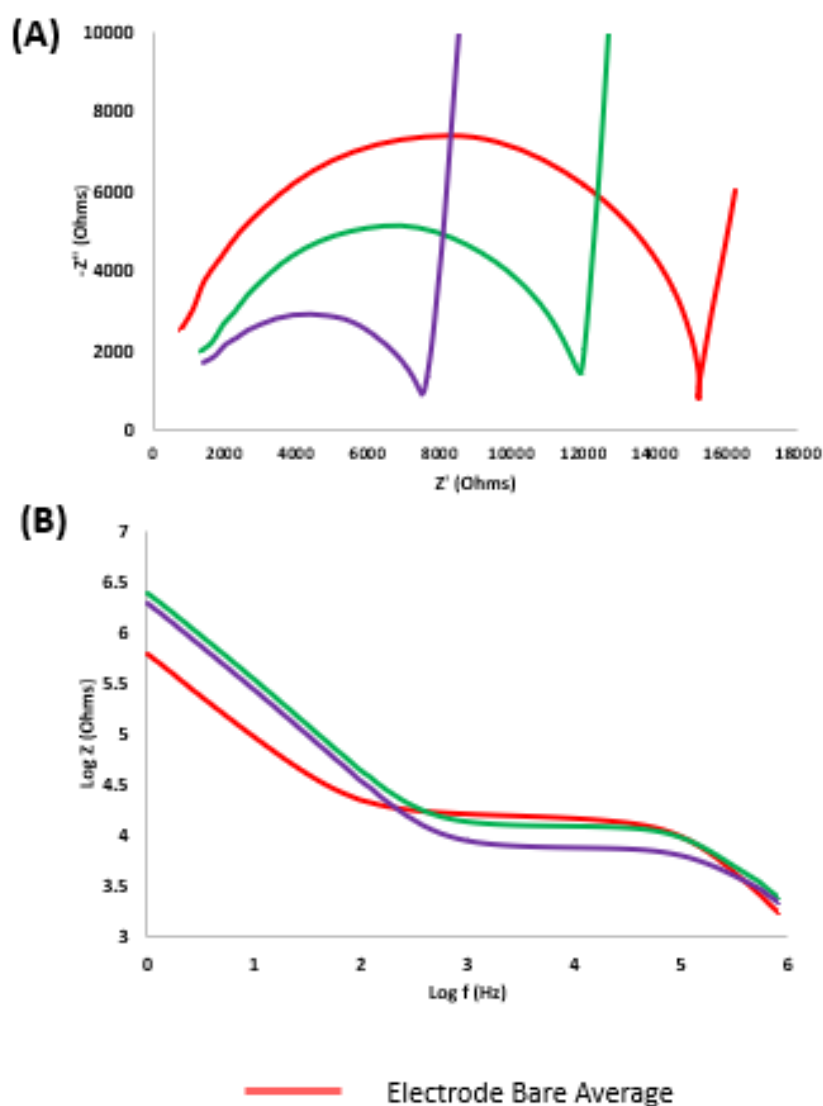


Figure 4.6 EIS plots for the Au WE electrode immersed in 1mM DPBS solution run at OCP from 0.1 - 100,000Hz against an Ag/AgCl RE where (a) portrays the zoomed Nyquist plot, where the magnitude of each semi-circle decreasing with the addition of the consecutive layers. (b) The Bode plot shows a difference between each modification step.

this corresponds to the Nyquist plot where the antibody crosses the X-axis (Z') at the lowest value of all three processes [43][44].

Figure 4.7 portrays both the Nyquist and Bode plot for seven separate antibody immobilised gold disc electrodes in 1mM DPBS. As these were brand new electrodes it is expected that the values shouldn't have much of a variance between antibody EIS results, however with an average impedance value of 8484.5 ± 1788.3 ohms for the Nyquist and 3.905 ± 0.07782 ohms at 10,000Hz for the Bode plot. No significant difference is noted amongst the data set for the Bode plots, however there is a large discrepancy obtained for the Nyquist plot. Damaging of the gold disc electrodes may therefore affect the fabrication of the biosensor for future reference as this may alter the way in which SAM and antibody layers form on the electrode surface.

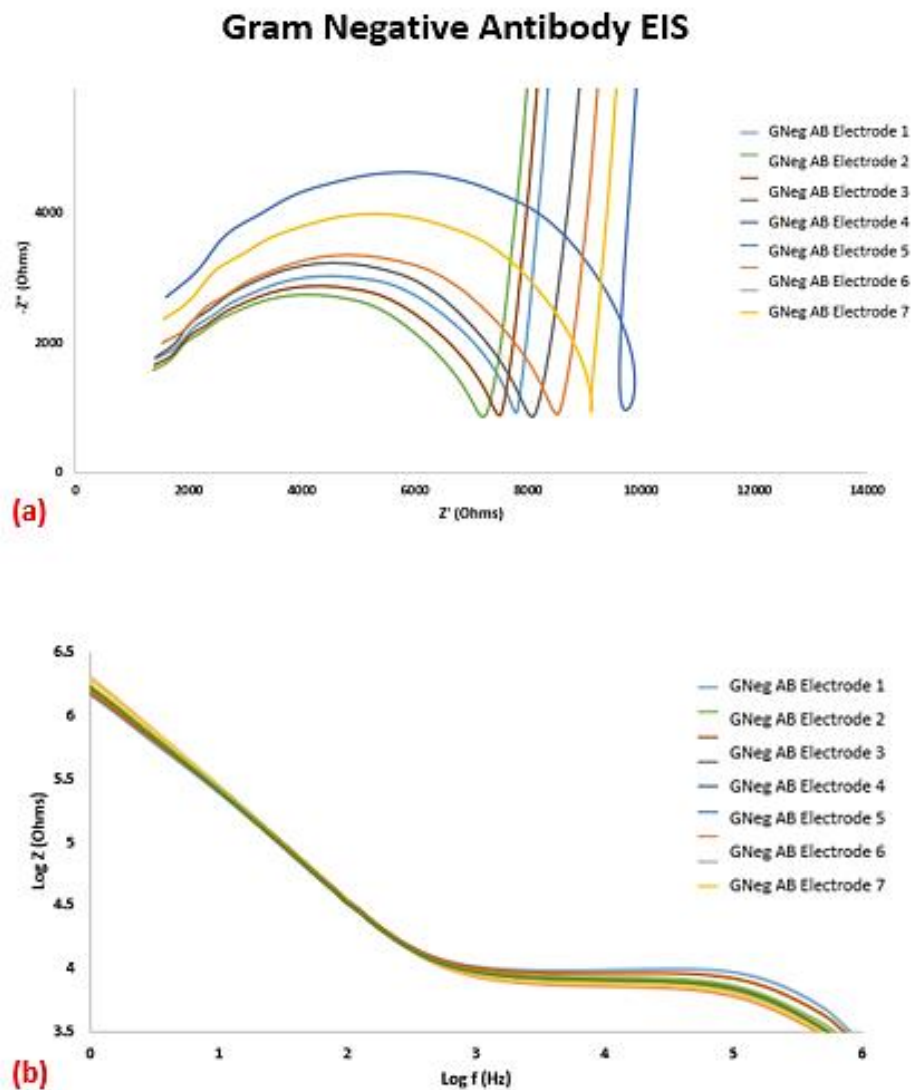


Figure 4.7. (a) Nyquist plot of gram-negative immobilised antibody for 7 separate electrodes where (b) portrays the Bode plot for the same electrode immobilised surface.

As the SAM was incubated for a 24 hour period, little defects or pinholes should exist on the surface, however the antibody solution which is coupled to this SAM layer needs to diffuse through the solution and adsorb onto the surface. Typical diffusion coefficients for small molecules in aqueous solution were in the range of 10^{-6} cm²/s where the diffusion coefficients for IgG molecules or mAbs were within the range of 10^{-7} cm²/s [45]–[47]. The diffusion coefficient can vary to the temperature and viscosity of the solution however taken as a general approximation, the diffusion rate of a monoclonal antibody with a diffusion coefficient of 10^{-7} cm²/s and a distance of 2mm (liquid height of the antibody solution) the diffusion time is calculated to be 5.55 hours for the gold disc electrodes. However, with the incubation taking place at 37°C, this diffusion time is expected to be reduced, as with an increase in temperature, the viscosity of the supporting solution decreases. According to the Einstein-stokes equation, the diffusion coefficient is directly proportional to temperature under the condition that the antibodies obey Stokes' law for drag [48]. With such a long time for the surface modification steps to successfully bind to the electrode surface. The rate in which this occurs may also affect the successful fabrication of the sensor surface and therefore may lead to additional discrepancies.

The antibody solution is only incubated for 1 hour therefore the packing of the antibody functionalised surface may be inconsistent and therefore would explain the variance in the impedance values obtained for all antibody layers for the electrode set. With time, the surface roughness changes with numerous polishes and surface scratches and therefore loses its quality and the sensor becomes extremely difficult to characterise, therefore it becomes feasible to create a single use biosensor where the antibody coverage becomes quantifiable and changes in the surface response will be solely determined by the capture of a whole cell and not discrepancies of the surface preparation.

The total time for the sensor development amounts to three days, including polishing, SAM immobilisation, coupling and antibody adhesion. This method was successfully carried out through CV and EIS characterisation however a new method was adopted to replace the gold disc electrodes to create a single-use electrode which can be implemented into the eLoad. In addition to this requirement, the reproducibility of the

gold disc electrodes is quite limited as the CV and EIS responses were initially based on the bare gold reading.

4.3.2 Justification of μ CP for the single-use biosensor

Initially, micro contact patterning (μ CP) was adopted for the new method of biosensor development to replace the SAM method. This method has been widely used for antibody patterning on a multitude of surfaces, where soft lithography methods were implemented to essentially create any desired pattern in the silicon polymer master in which PDMS is cast and divided into individual stamps with the μ -pillars which will transfer the antibody onto the electrode surface with the same pattern to that of the PDMS stamp surface. The μ CP aids in the control of antibody adhesion to the desired surface [49], [50]. Figure 4.8 portrays the photomask used with a $20\ \mu\text{m} \times 20\ \mu\text{m}$ square pattern with a $10\ \mu\text{m}$ pitch. The PDMS stamps were incubated with $100\ \mu\text{l}$ of the labelled antibody solution (ATTO 488 dye) for 15 minutes and adhered to the glass substrate for 15 minutes. Images were acquired using the Zeiss Confocal microscope using a 488nm laser line. The labelled antibody surface was clearly visible proving the efficiency of the μ CP method, where each

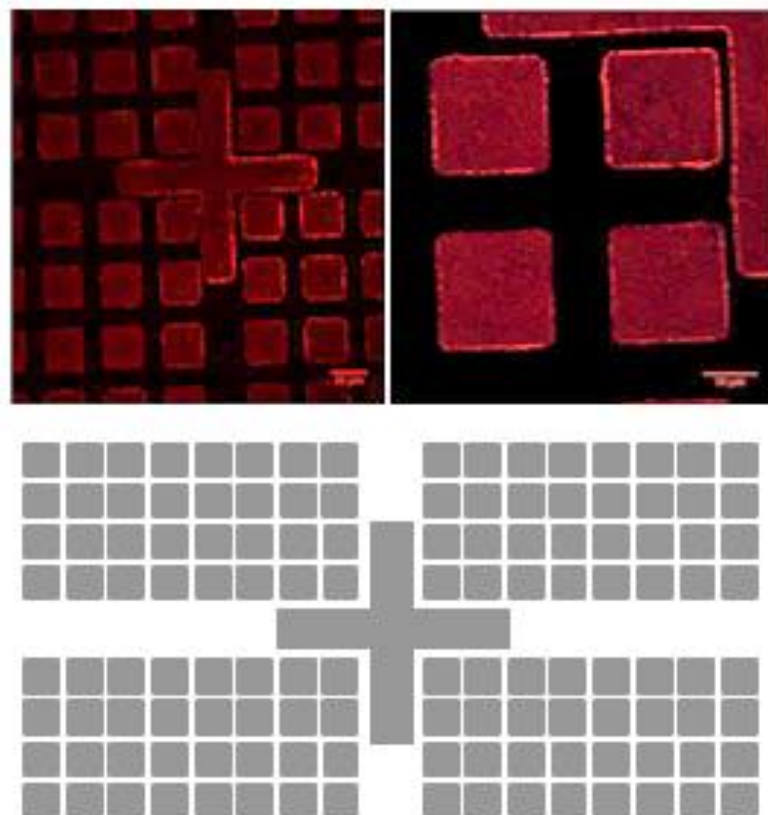


Figure 4.8. Image of initial photolithographic mask used to create an array of square structures in which a labelled antibody is printed onto glass to portray the effectiveness of the PDMS antibody stamping method. The image shown is adjusted to +40% brightness and +20% contrast. Image acquired by Dr. Kellie Adamson.

of the red visible square structures was evidence of the antibody transferred to the glass substrate surface.

While this size was achievable using soft lithography methods, the pillar structures between the $5\ \mu\text{m}^2$ cavity array which was highly selective for *E. coli* (as demonstrated in Figure 4.10) may easily collapse in the photomask after very few uses. The $10\ \mu\text{m}^2$ antibody square design was selected as a compromise between the maintenance of the silicon master integrity and the highly selective size of the cavities where the height of each pillar was $25\ \mu\text{m}$. In addition to this, the sections between each antibody square allows for blocking sections on the electrode whilst maintaining the probe density on the surface, as too much capture probe on a surface can inhibit target binding due to steric hinderance [51], [52] therefore the separation of the antibody functionalised section should reduce this effect. As the silicon wafer produced is fabricated from cross-linked photoresist, the silicon master can be re-used many times. The PDMS stamps were created using a 10:1 of elastomer to curing agent.

The new development of the single use electrode was examined. Section 2.4.3 – 2.4.7 describes the initial fabrication steps to produce the electrode. The 4" gold plated silicon wafers were diced into individual electrodes of 30mm x 5mm dimensions. After the electrodes were made hydrophilic through piranha etch and UV Ozone cleaning, the thin layer of Au is electrochemically deposited to increase surface area and roughness for antibody adsorption. The second stage of the preparation included the fabrication of the PDMS stamps. As GP antibody and *Candida Albicans* capture protein were naturally hydrophobic in nature, the correlating PDMS stamp was O_2 plasma treated for surface oxidation and hydroxylation (-OH) as outlined in Section 2.4.7 to promote antibody adsorption to the PDMS stamp surface and to maximise the solution spreading on the stamp. The GN endotoxin antibody is hydrophilic, therefore this step was excluded for the corresponding GN stamps [53]. Each PDMS stamp was cut into 50mm x 50mm squares to correspond with the width of the electrode (50mm) to increase the antibody functionalised surface.

Antibodies were prepared using 1:1 ratio of antibody/*Candida albicans* protein stock in DPBS. 100 μl of the antibody solution was incubated on the relevant PDMS stamp for 15 minutes. The solution was removed, and each stamp was dried with a N_2 stream. The

stamps were placed on the top of each Au electrodes and placed into contact with the surface for 15 minutes to allow the antibodies to adsorb onto the Au surface. This is sufficient time to transfer the antibody layer from the stamp to the Au electrode [50].

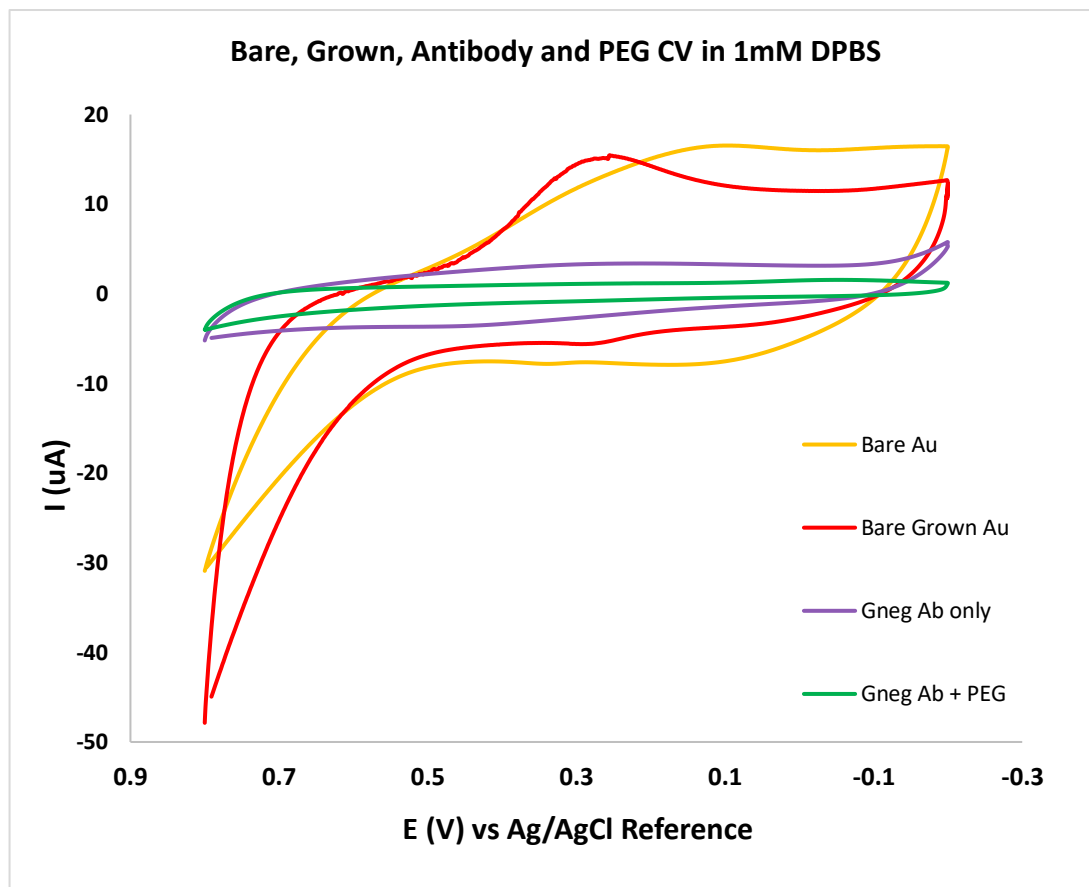


Figure 4.9. Average cyclic voltammograms of the disposable gold electrodes where the separate stages of biosensor fabrication were recorded using 1mM DPBS as the supporting electrolyte solution. The bare grown gold, antibody and PEG thiol stages were all recorded.

Electrodes were placed, overnight, in 1% PEG₈- acid to block the sections of the electrode which were not patterned with the antibody stamp. PEG is used frequently to suppress nonspecific adsorption [54]. The electrodes were then rinsed with dH₂O and incubated with a 3% BSA solution for 3 hours to further block any exposed section on the sensor surface to act as a doubled blocking system, where the BSA protein and PEG thiol block act in tandem to suppress non-specific adsorption of unwanted blood components on the surface. The electrodes were rinsed again with dH₂O and dried using a N₂ stream and placed under vacuum until use.

The effectiveness of the μ CP PDMS stamp was examined using confocal microscopy. This method of antibody functionalised electrodes reduces the fabrication time from the SAM method from 3 days to 1 day. The electrode preparation for fluorescent imaging utilised the procedure discussed in section 2.9.1. displays the effectiveness of the antibody patterned surface, as a control experiment was carried out using Cy3 labelled BSA solution was incubated on a PDMS stamp and was placed into contact with a glass slide for 15 minutes, mimicking the same procedure as the antibody solution stamping method. This was to determine how well the stamp itself interacts with the surface and how the labelled protein adsorbs onto the electrode surface. This BSA pattern is a future representation of the antibody pattern, where the Cy3 dye is excited with the 543nm laser line of the confocal. The secondary image within Figure 4.10 portrays the GN antibody stamped sections on the single use gold electrode, where the electrode itself was fabricated using the PEG and BSA blocking steps. The electrode was then incubated with 100 μ l of 10^3 CFU/ml of E. coli. This image portrays, not only the ability of the capture antibody of the antibody squares deposited by the PDMS stamp, but the blocking solution that exists between each antibody square patch as no E. coli cells have adhered on the non-antibody sections of the surface. The 10 μ m x 10 μ m stamping sections exist for a 5mm x 5mm section at the top of the electrode which is then inserted into the eLoAD detection chamber.

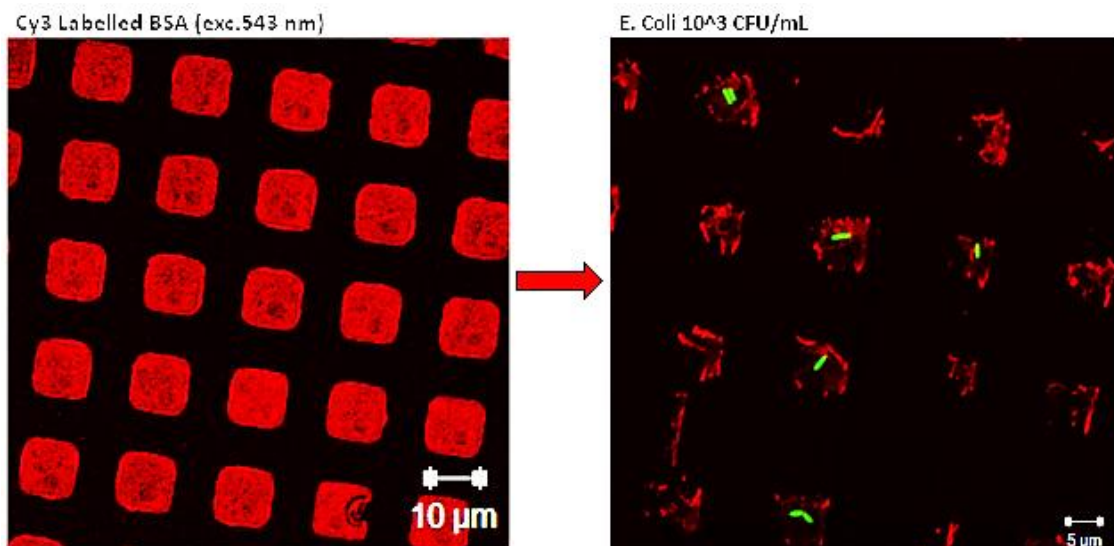


Figure 4.9. BSA patterned surface portraying the PDMS μ -contact print stamp pattern and b) the high affinity of the pathogen towards the antibody 10 μ m square sections where no E. coli attached to the blocked intermittent sections between the antibody areas. The image has been adjusted +40% brightness and +20% Contrast. Images acquired by Dr. Kellie Adamson

For the confocal image (a) shown in Figure 4.10, the calculated surface coverage using ImageJ analysis of the Cy3 labelled BSA with the μ CP pattern amounts to 39.4% of the total stamp area (i.e. 5mm x 5mm). Comparing this with the ATTO labelled antibody in image (b), the antibody surface is 11.5%. Knowing that the μ CP stamp was sufficient in transferring the BSA to the glass substrate, it must be acknowledged that gold tends to have a higher surface energy and therefore tightly packed antibody surfaces are very difficult to achieve. With a relatively high concentration of *E. coli* on the surface, the observed occupation of the individual antibody squares was no more than 3 cells per square for the static incubation. Again, CV and EIS methods were used to show the individual fabrication steps. All experiments were carried out in the dilute 1mM DPBS using the same electrochemical cell setup used in Section 4.3.1. Figure 4.9 portrays the overlapping CVs obtained for the fabrication process of the single use biosensor. With the antibody and PEG step being shown, the blocking of the electrode is evident due to the depletion of the CV current response blocking the gold oxide reduction peak that was found at 0.34 V for the grown gold electrode and 1.9 V for the bare gold electrode. This is indicative of the addition of the biomolecule layer and then further blocking of the electrode from the PEG solution where the entire biorecognition segment of the biosensor has adsorbed and blocked the gold surface where no oxide reduction peaks were evident for the PEG and antibody CV responses. These gold oxide reduction peaks

may be the results of the ionic species present in the electrolyte solution, where 1 X DPBS contains 8 g NaCl, 0.2 g KH_2PO_4 , 1.15 g Na_2PO_4 and 0.2 g KCl.

4.3.2.1 Nyquist Plot for μCP single use electrode

Figure 4.11 shows the EIS response in the 10ml electrochemical cell in 1mM DPBS. This replicated the conditions used for Section 4.3.1.1 however the electrode in this instance has a larger working area and the new method of antibody adsorption on the surface. Table 4-5 shows the extracted data for the individual Nyquist plots for the fabrication steps of the biosensor where the imaginary axis Z'' is dominated by capacitive factors and the real axis denoted resistance changes. EIS response 1 refers to the initial Z'' and Z' of the bare grown gold electrode. Interestingly for the single use electrode, the addition of the stamped antibody pattern on the surface increases both the Z'' and Z' values, causing the semi-circle to increase in magnitude. This would suggest that the antibody on the surface appears in parallel to the gold electrode for the equivalent circuit model, however

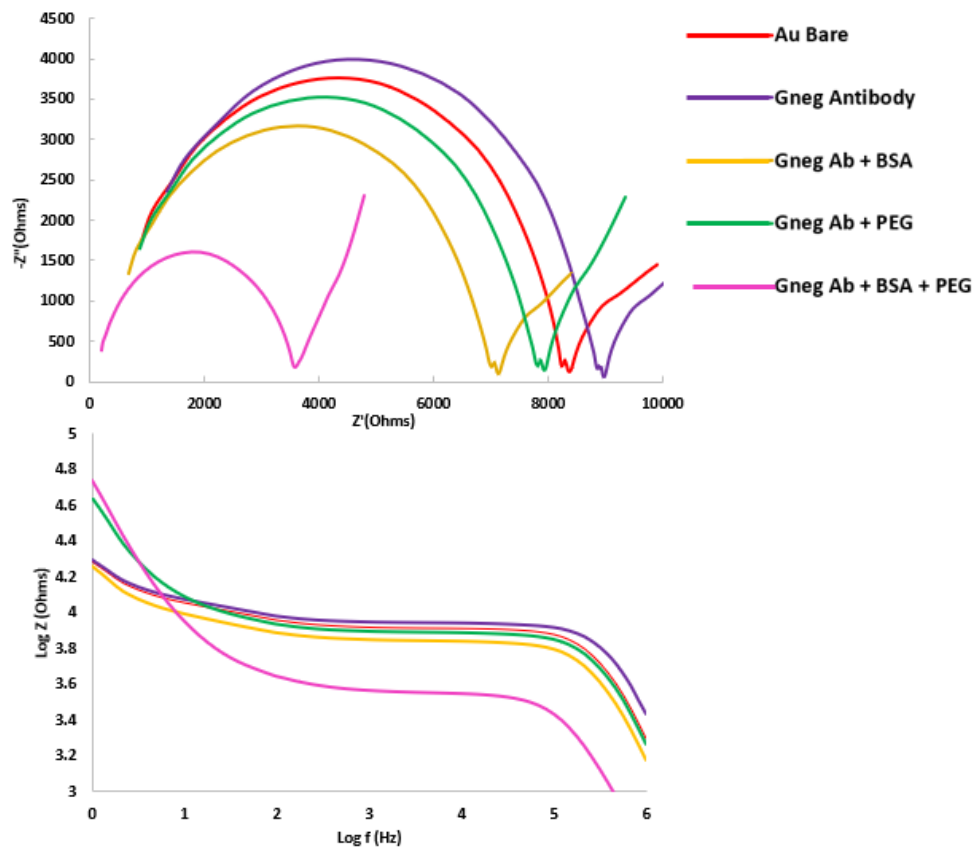


Figure 4.10. EIS plots for the disposable electrode immersed in 1mM DPBS solution run at OCP from 0.1 - 100,000Hz against an Ag/AgCl RE where (a) portrays the zoomed Nyquist plot and (b) The Bode plot between all fabrication steps of the sensor

the shift only amounts to a 5.5% increase for the Z'' value and 6.9% for the Z' . This was due to only a limited amount of the electrode being modified with the antibody μ CP. With the addition of either the PEG or BSA solution to the surface, the magnitude of the semi-circle decreases again for both cases, where the biggest change in the Z'' and Z' was observed for the BSA. As BSA is a large protein, this 3% solution that was used specifically to block the intermittent sections between the antibody modified squares. Finally, the use of the antibody, PEG and BSA solution significantly reduces the overall impedance where the Z'' reduces by 2150 ohms and 4800 ohms for the Z' compared to the bare electrode values. With the BSA and PEG solution required to considerably reduce the impedance response to be comparable to the Nyquist plot for the gold disc electrode discussed in Section 3.4.1.1, they must be used in conjunction to possibly ensure that the electrode is blocked with the bio-recognition layer.

Table 4-5 Nyquist Plot values for the single use biosensor fabrication steps for both the imaginary and real values.

	Bare (1)	Antibody (2)	Ab + PEG (3)	Ab + BSA (4)	Ab + PEG + BSA (5)
Z'' max (Ohms)	3760 ± 545	3970 ± 387	3520 ± 110	3160 ± 312	1610 ± 104
$\Delta Z''$ (Ohms)	NA	- 210	240	600	2150
Z' min (Ohms)	8390 ± 1405	8970 ± 649	7940 ± 904	7140 ± 743	3590 ± 154
$\Delta Z'$ (Ohms)	NA	-580	450	1250	4800

4.3.2.2 Bode Plot for μ CP single use electrode

The Bode plot was again observed at 10 kHz for the single use sensor as the capacitance changes appear to have the greatest effect at this frequency. Table 4-6 displays the results for the Bode plot for the modification steps. Again, this Bode plots mirror the results obtained for the Nyquist plot in Section 4.3.2.1, where there is a slight increase in the magnitude with the addition of the antibody, however the impedance reduces with the BSA and PEG layers. The biggest changes in the Bode plot is observed with the antibody,

PEG and BSA where a $\Delta \text{Log Z}$ of 0.374 from the bare electrode was observed. Its assumed that the three modifications act in series and therefore reduce the overall impedance of the system.

Table 4-6. Bode plot values for single use biosensor fabrication steps obtained at 10 kHz

Value at 10 kHz	Bare (1)	Antibody (2)	Ab + PEG (3)	Ab + BSA (4)	Ab + PEG + BSA (5)
Log Z (Ohms)	3.914 ± 0.11	3.95 ± 0.11	3.88 ± 0.07	3.84 0.07	3.54 0.05
$\Delta \text{Log Z}$ (Ohms)	NA	-0.036	0.034	0.074	0.374

4.3.3 Implementation of single use biosensor into eLoaD platform

The effectiveness of the μCP PDMS stamp was examined using confocal microscopy. This method of antibody functionalised electrodes reduces the fabrication time from the SAM method from 3 days to 1 day. The electrode preparation for fluorescent imaging utilised the procedure discussed in section 2.9.1. Figure 4.10 displays the effectiveness of the antibody patterned surface, as a control experiment was carried out using Cy3 labelled BSA solution was incubated on a PDMS stamp and was placed into contact with the Au electrode for 15 minutes, mimicking the same procedure as the antibody solution stamping method. This BSA pattern is a future representation of the antibody pattern, where the Cy3 dye is excited with the 543nm laser line of the confocal.

The secondary image within Figure 4.10 portrays the GN antibody stamped sections on the electrode, where the electrode itself was fabricated using the PEG and BSA blocking steps. The electrode was then incubated with 1000 CFU/ml of E. coli. This image portrays, not only the ability of the capture efficiency of the antibody squares deposited by the PDMS stamp, but the blocking solution that exists between each antibody square patch as no E. coli cells. Once the electrodes were modified, they were placed into a pre-made milled 2mm base disc. Here, the M77 glue was placed into a container and left under vacuum for 10 minutes to remove any air in the glue mixture. Approximately 100 μl of the glue was placed into each individual electrode slots. The electrodes were placed into the

base slots carefully to avoid glue from contaminating the antibody modified sections of the electrode. These bases were left overnight in a sterile fume hood to ensure complete drying. Excess glue removed to ensure a uniform, flat surface before the fibrinogen functionalised electrode cover (layer 8) was carefully placed over the electrodes, where the antibody functionalised sections were exposed within the PSA layer. The top section of the disc (Layer 1-7) was then laminated to the electrode cover/base section at a pressure of 80 PSI. A small amount of super glue was then pipetted to the top of the electrodes, under layer 7 of the device to ensure no leaking over the electrode once a centrifugal force is applied to the system. The device was again, left to dry in the sterile fume hood until ready to be vacuum packed and left at room temperature.

As described in Chapter 3, each device contains three separate, identical testing sites. Each detection chamber contains three antibody immobilised surfaces (GP, GN and Fungal) the reference and counter electrodes. EIS measurements of the three WEs were obtained in 1mM DPBS electrolyte solution. Compared to the electrodes fabricated in sections 4.3.1 and 4.3.2, the EIS obtained for the electrodes within the eLoaD were run in 1.7 mls rather than 10mls. Also, the electrode cover (layer 8 of the device) exposes different area sizes for each individual WE. This gives a unique range in which the initial antibody impedance value will give for the initial run in the dilute electrolyte as outlined in Section 3.8.

With the addition of the electrodes in the eLoaD, the antibody impedance value shown by the Nyquist plot became more reproducible. All EIS responses were obtained in 1mM DPBS to determine the impedance response of the antibody surfaces of the electrodes within the LoaD. The Nyquist for the GP electrode shows some variance where the impedance value of 1556.6 ± 167.42 ohms was calculated for the average runs for all three GP immobilised biosensors within the platform, where all experiments were run in triplicate. The reproducibility increased for the GN sensors as the average Nyquist obtained was 1413.33 ± 41.35 ohms. The fungal biosensors in this case provided the most stable results of 1290 ± 5 ohms for the impedance values. The Bode plots follow the same trend where the GP has the biggest difference between log Z of 3.17 ± 0.12 Ohms. The GN and Fungal Bode plots have values of Log 3.20 ± 0.04 and 3.1 ± 0.02 Ohms respectively as shown in Figure 4.12.

This reproducibility is important as it proves the effectiveness of the μ CP method for antibody adsorption onto the Au coated Si electrodes, where an average of 10% of the electrode surface was modified with the capture probes. It also proves that the integrity of the sensor remained intact after the electrodes were incorporated into the device that involves PSA layer and two types of glue were placed over the electrode. This proves that the biosensor was completely capable of being integrated into a device, allowing a microfluidic centrifugal device to be capable of electrochemical sensing. With very few eLoDs being reported in literature, this device will be one of the first of its kind to integrate an electrochemical sensor capable of detecting disease causing cells in blood culture samples [55].

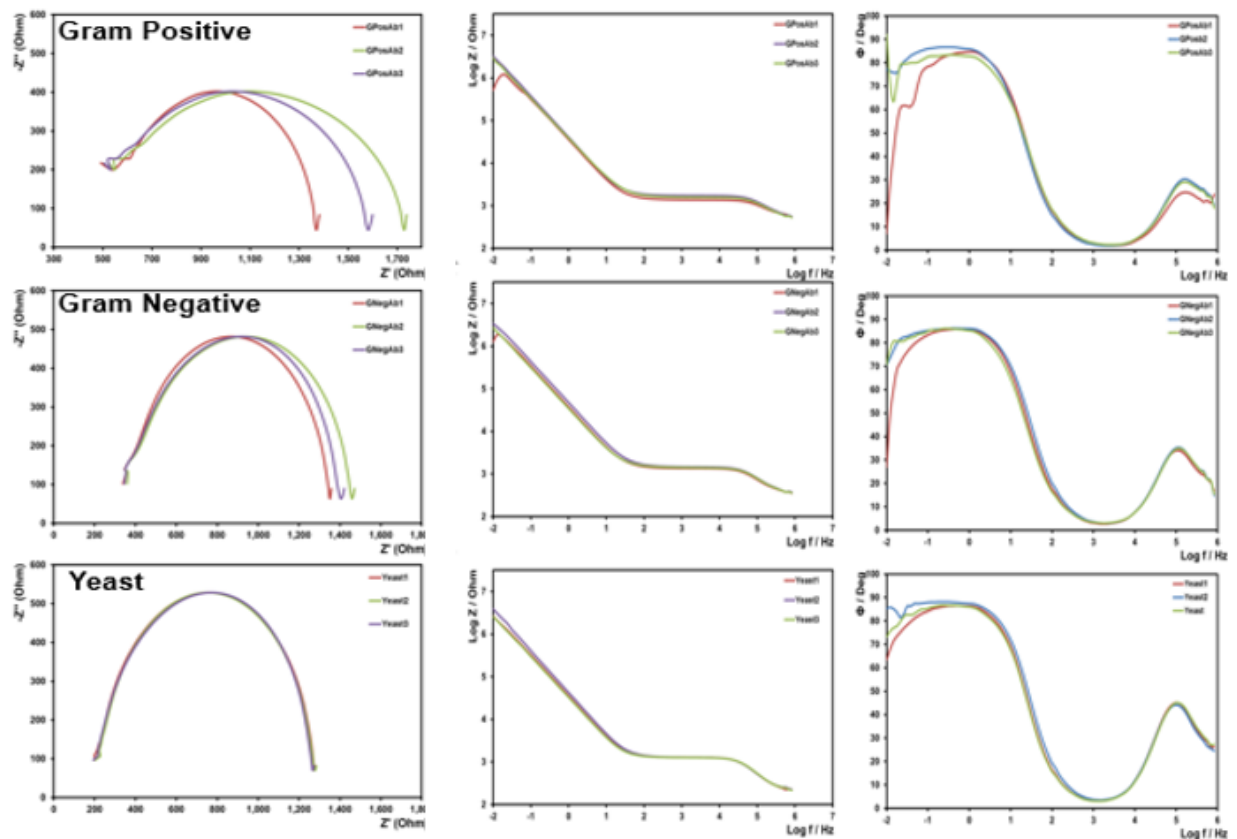


Figure 4.11. EIS response for the three separate functionalised electrodes where the Nyquist, Bode and Phase plots are shown. Image shows the reproducibility of the sensors within the device.

4.3.4 Real Sample Detection for Device Validation

The testing study of the device using real samples was carried out using blood culture samples received from the microbiology lab in St. James' hospital. These samples have been previously tested using the hospital's gold standard of pathogen testing in patient blood samples. The blood samples which were cultured within BacT bottles, which were gram-stained if returned as positive. For the purpose of this work, the samples were blind tested and later confirmed whether a pathogen is present/absent. Furthermore, the category of the pathogen; GP, GN, Fungal or a combination was provided after LoD testing to determine the discriminating capabilities of the device. Both the sensitivity and the specificity will be determined for the prospective retrospective study. The sensitivity measures the proportion of positives that were correctly identified as having the condition, also known as the true positive rate. The specificity on the other hand measures the proportion of negative samples that were correctly identified for not having the condition. This is also known as the true negative rate.

As the samples obtained are blood injected BacT blood culture bottles, the effect of this media on the EIS response was first determined. Common culture media is composed of sugars, salts, complex carbohydrates, amino acids and nitrogen (from yeast extract, beef etc) and a nutrient media such as nutrient agar [56], [57]. Figure 4.13 portrays the difference of the EIS of the antibody and the BacT media solution. The BacT media was tested at a spin rate of 7Hz where a water wash step and 1mM DPBS solution was sequentially triggered. The huge changes in impedance are shown in *Table 4-7* where the shift for both plots indicates a significant interference from the BacT media. This reduction in impedance would be considered a positive result for pathogen capture on all surfaces, however as the sample used was only the culture media this would be considered a false positive result. Therefore, this was the first issue addressed for the assay optimisation of the device with real blood culture samples.

Table 4-7. Nyquist and Bode response of BacT sample for GP, GN and Fungal capture probe surfaces.

Capture Probe	G (+)	G (-)	Fungal
---------------	-------	-------	--------

Capture probe Z' (Ohms)	1410 ± 101	1407 ± 128	1230 ± 88
BacT Z' (Ohms)	657 ± 94	554 ± 116	443 ± 54
Δ Z'	753	853	787
Capture Z Log Z (Ohms)	3.14 ± 0.04	3.14 ± 0.05	3.07 ± 0.03
BacT Log Z (Ohms)	2.82 ± 0.05	2.74 ± 0.03	2.64 ± 0.07
Δ Log Z (Ohms)	0.32	0.40	0.43

Nyquist and Bode plots of BacT media EIS in eLoad

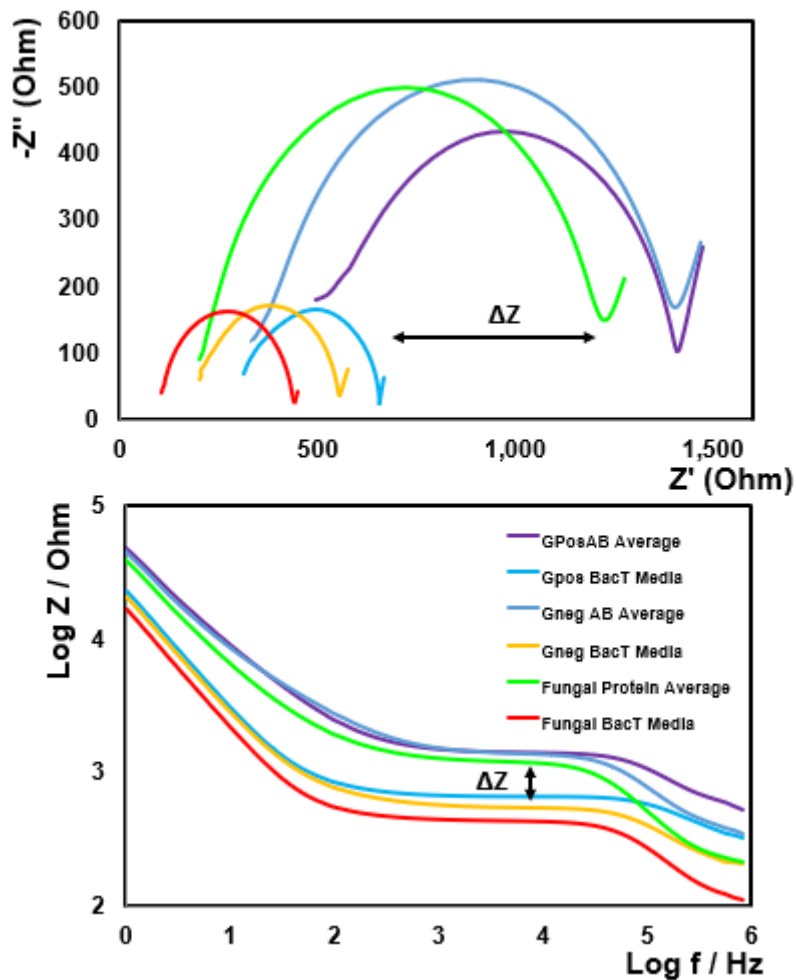


Figure 4.12. Nyquist and Bode plots of the eLoad response of the difference between the GP, GN and Fungal antibody/fungal protein capture surfaces with and without BacT media was tested on the platform.

For the duration of this experimental section, all samples were diluted at a ratio of 3:1 DH₂O to sample, to reduce the viscosity of the sample to allow for proper flow of the fluid through-out the device and to reduce the overall interference from the media components. This dilution is performed within a sterile fume hood outside of the device. The sample was left within the sample chamber for 5 minutes to allow the sample to incubate with the fibrinogen coated chamber. This helps reduce the platelet interference on the electrodes which may provide a false positive result due to non-specific binding. With the initial EIS measurements of the three-individual antibody modified working electrodes within each system on the platform obtained, the disc was pre-loaded with the DH₂O and 1mM DPBS electrolyte reagents. Applying a spin-frequency of 7Hz to the system, the sample enters the electrode chamber in a downwards, transitional flow from the microchannel into a much larger chamber. The sample enters the much larger electrode chamber where it fills up under a constant spin frequency. This allows the samples to mix within the chamber, allowing suspended pathogens to come into contact with the functionalised electrodes. The exit, waste channel also lies on the same level as the electrodes, which promotes the sample to flow in a downwards flow through the z-axis of the device in order to pass to the waste channel. This downward flow maximises the sample to electrode contact, increasing the chance of pathogen capture.

Table 4-8 tabulates all the EIS data for all 26 patient samples received and tested from St. James' hospital. All EIS values have corresponding confocal images (Appendix A). The EIS data shows the Nyquist and Bode plot data for the individual patient samples where the response for the Nyquist and Bode plot was tabulated. The Δ (Ohms) for Nyquist and Bode is the difference between the antibody value and sample value. The also indicated the species of pathogens as confirmed by the microbiology department and whether they were correctly identified by the eLoad.

As previously indicated, each sample was tested on one device, therefore three separate EIS results were obtained as the device is capable of testing N=3. Any sample with * is indicative of a contamination from the hospital sample obtaining stages, where skin flora bacteria such as *Staphylococcus epidermis* may be cultured and cause a false positive in the culturing process in the microbiology departments. This is further described by Figure. 4.17.

Table 4-8. Results of tested patient samples received from St. James' hospital indicating the Δ Ohms for the Nyquist and Bode plot. A total of 26 patient samples were used in the study for the eLoaD prospective retrospective validation for 26 samples contained in BacT blood culture bottles.

Sample Number	eLoaD Result	Gram (+) Nyquist Z'' Δ Z	Gram (+) Bode Δ (Ohms)	Gram (-) Nyquist Z'' Δ Z	Gram (-) Bode Δ (Ohms)	Fungal Nyquist Z'' Δ Z	Fungal Bode Δ (Ohms)	St. James' species results	Correctly identified	Aerobic/Anaerobic BacT bottle
422217.1	GN	151 \pm 25	0.05 \pm 0.01	327 \pm 68	0.1 \pm 0.02	221 \pm 56	0.09 \pm 0.02	Capnocytophaga gingivalis	✓	Aerobic
422462.2	GP	513 \pm 56	0.19 \pm 0.02	208 \pm 74	0.07 \pm 0.04	314 \pm 40	0.11 \pm 0.03	Staphylococcus epidermis	✓	Anaerobic
422460.3	Mixture GP/GN	346 \pm 89	0.11 \pm 0.03	331 \pm 66	0.14 \pm 0.04	7 \pm 38	0.01 \pm 0.01	E.coli, Staphylococcus hominis & Streptococcus mitis oralis	✓	
422421.4	GP	321 \pm 11	0.16 \pm 0.01	221 \pm 15	0.09 \pm 0.01	313 \pm 83	0.11 \pm 0.02	Enterococcus faecium	X	
422517.5	GN	207 \pm 49	0.08 \pm 0.02	484 \pm 18	0.21 \pm 0.1	246 \pm 62	0.16 \pm 0.03	E.coli	✓	
422517.6	GN	182 \pm 57	0.08 \pm 0.05	281 \pm 86	0.19 \pm 0.02	318 \pm 102	0.11 \pm 0.01	E.coli	✓	
422175.7	GP	523 \pm 17	0.18 \pm 0.01	167 \pm 108	0.07 \pm 0.03	351 \pm 153	0.07 \pm 0.04	Clostridia	✓	

422008.8	GP	835 ± 110	0.19 ± 0.02	179 ± 81	0.08 ± 0.06	194 ± 79	0.11 ± 0.1	No Growth	✓*	
422564.9	Mixture GP/GN	508 ± 24	0.11 ± 0.01	530 ± 277	0.11 ± 0.05	326 ± 95	0.07 ± 0.01	Staphylococcus & streptococcus	✓	
422605.10	GN	260 ± 9	0.06 ± 0.005	830 ± 127	0.16 ± 0.01	138 ± 56	0.03 ± 0.01	GN with Enterococcus faecalis	✓	
422673.11	GP	539 ± 37	0.14 ± 0.03	376 ± 172	0.06 ± 0.01	346 ± 117	0.07 ± 0.03	Paenibacillus pabuli	✓	
424439.12	GP	343 ± 50	0.2 ± 0.07	10 ± 45	0.01 ± 0.04	68 ± 19	0.04 ± 0.06	Staphylococcus	✓	
424414.13	GN	75 ± 32	0.04 ± 0.02	288 ± 88	0.21 ± 0.04	84 ± 74	0.05 ± 0.04	GN bacilli	✓	
424840.14	Negative sample	126 ± 43	0.03 ± 0.04	128 ± 91	0.03 ± 0.005	113 ± 6	0.03 ± 0.005	Negative sample	✓	
425090.15	GN	291 ± 65	0.1 ± 0.03	342 ± 119	0.20 ± 0.04	335 ± 244	0.02 ± 0.08	GN	✓	
425040.16	GN	261 ± 51	0.16 ± 0.02	424 ± 101	0.15 ± 0.01	126 ± 153	0.04 ± 0.06	GN	✓	
426215.17	GP	710 ± 196	0.23 ± 0.12	183 ± 102	0.05 ± 0.04	163 ± 122	0.06 ± 0.03	GP Cocci	✓	

426115.18	Mixture Fungal/ GP	898 ± 409	0.52 ± 0.25	237 ± 102	0.13 ± 0.05	204 ± 255	0.24 ± 0.02	Yeast	✓*	
400639.19	GP	1069 ± 204	0.21 ± 0.09	594 ± 178	0.21 ± 0.19	522 ± 109	0.2 ± 0.07	GP Bacilli	✓	
426180.20	Mixture GP/GN	535 ± 124	0.11 ± 0.08	469 ± 107	0.10 ± 0.5	58 ± 81	0.01 ± 0.03	GN Bacilli	✓*	
426105.21	GP	817 ± 129	0.26 ± 0.05	280 ± 60	0.09 ± 0.03	94 ± 173	0.04 ± 0.10	GP Cocci	✓	
426393.22	Mixture GP/GN	296 ± 71	0.14 ± 0.06	386 ± 81	0.13 ± 0.04	193 ± 83	0.05 ± 0.03	Staphylococcus	✓	
426500.23	GP	337 ± 135	0.10 ± 0.07	290 ± 49	0.06 ± 0.02	325 ± 65	0.07 ± 0.04	GN	X	
426548.24	GN	228 ± 108	0.06 ± 0.04	398 ± 49	0.12 ± 0.06	176 ± 22	0.05 ± 0.005	GN	✓	
426589.25	GN	184 ± 195	0.1 ± 0.05	628 ± 140	0.26 ± 0.13	616 ± 341	0.19 ± 0.03	Streptococci	✓*	
426591.26	GP	368 ± 128	0.11 ± 0.04	151 ± 43	0.03 ± 0.02	141 ± 91	0.08 ± 0.04	Staph	✓	

Once the EIS measurements were obtained, the results were further compared with confocal imaging for post-analysis. To determine the threshold, it was necessary to match Nyquist plot data against confocal imaging, determining whether the shift in impedance is caused by pathogen capture or non-specific binding of platelets or red blood cells to the surface where initial data showed that >300 Ohms for the Nyquist was sufficient. These contaminants do cause a shift in impedance; however, this is less than the threshold just discussed. The dilution factor introduced into the sample also reduces these contaminants which can cause these interferences.

After EIS analysis the electrodes were later removed and prepared for confocal imaging for further confirmation of results, following the procedure discussed in section 2.10. Figure 4.14 portrays an example of a non-positive sample (424840.14). All three Nyquist and Bode plots for GP, GN and the Fungal from the EIS measurements were shown.

The overlay of the semi-circles shows the slight shift between the ($R_{\text{Antibody}} - R_{\text{Antibody} + \text{bacteria}}$). As this shift is below the threshold for the Nyquist plot (>300 ohms) it is determined that the sample is negative for pathogens. The Bode plots were also below the threshold of 0.15 Ohms, where in this case the change in the Bode plot for all three electrodes is 0.03. These results were later confirmed using confocal imaging, where all surfaces were free of pathogens. The slight change between the $R_{\text{Antibody}} - R_{\text{Antibody} + \text{bacteria}}$ is a common response of the biosensor for EIS obtained in clean buffer or a negative blood culture sample. The ions in solution from the 1mM electrolyte solution may adsorb onto the clean/or relatively clean electrode surface, create a slight change in the resistance and capacitance value, therefore the exact same value will never be obtained for two runs of the antibody surface in an electrolyte solution.

This result compared to that displayed for the undiluted BacT media portrays in Figure 4.13 proves the need for the sample dilution to significantly reduce background interferences from the media solution.

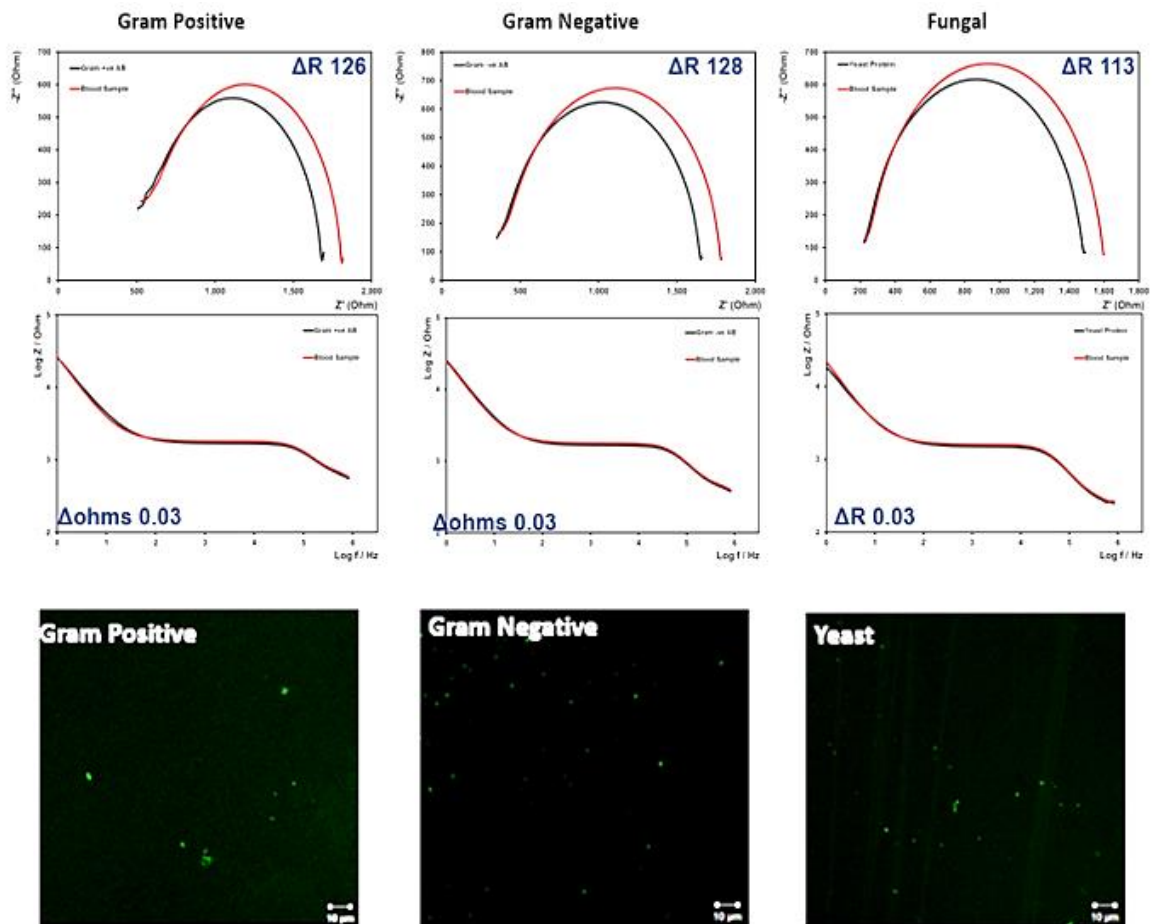


Figure 4.13. Nyquist and Bode plots for all three working electrodes associated with a negative blood culture sample with supporting confocal images.

Table 4-9. Tabulated results for the EIS measurements obtained for the non-sepsis patient, portraying an insignificant change between the impedance of the antibody and antibody + sample measurement for all three working electrodes.

Capture Antibody/Protein	GP Electrode	GN Electrode	Fungal Electrode
Nyquist Plot Z'' ΔR	126 ± 41	128 ± 9	113 ± 33
Bode Plot ΔZ (Ohms)	0.03 ± 0.01	0.03 ± 0.004	0.03 ± 0.012

Considering that the negative patient sample is a mixture of the culture media and whole blood, this dilution along with the incubation with the fibrinogen functionalised chambers was highly successful in reducing the ΔZ . The change in the impedance as shown in Table 4-9 was under the threshold and therefore the sample was determined to be negative for pathogens. This result was indicative of three factors;

1. **Non-specific binding of blood components was hugely reduced by both the sample dilution and use of fibrinogen on the surrounding chamber structure.**
2. **Threshold of negative samples was reliable, where confocal imaging was used as a secondary confirmation source.**

4.3.4.1 Gram-Positive pathogen detection on eLoaD

Figure 4.15 is an example of a patient sample (426105.21) positive for a GP type bacteria. A huge shift of 817 ± 129 ohms was evident for the GP Nyquist plot which greatly exceeds the limit of $\Delta R \geq 300$ ohms. The Bode plot confirms the captured bacteria as a change of 0.26 ohms was also detected and also qualifies the sample as positive for the secondary confirmation source. All corresponding data is shown in Table 4-10. The GN impedance value was just below the threshold for the Nyquist plot change, however by examining the Bode plot, the shift is below the threshold of 0.1 ohms and therefore was determined to be negative for GN pathogens. As the changes for the fungal pathogens were inconsequential, the sample was also determined to be negative for fungal pathogens. The electrodes were removed from the device and prepared for confocal imaging which confirmed the presence of GP pathogens and confirms the validity of the EIS results. Although the sensitivity and selectivity are based on the EIS results alone, the supporting confocal images were extremely useful to determine and correlate the signal change to the surface coverage and also monitor whether platelets or RBCs are attaching to the electrode surfaces.

By combining both EIS methods to determine the effective capture of pathogens, it reduces the chances of false positives/false negatives. The threshold was determined but is not a LOD, as the initial concentration of the sample was unknown. The time the initial sample spent incubating within the culture system varies, with the routine checks carried out every 4 hours by the monitoring system within the microbiology lab. Also, specific pathogens' growth times can greatly vary from hours to days [58].

Table 4-10. Results showing the difference between the Nyquist and Bode plot, resulting in positive results for Gram-Positive pathogens in patient sample 426105.21.

Pathogen	Antibody/Protein	Gram (+)	Gram (-)	Fungal
Gram (+)	Nyquist Plot Z'' ΔR	817 ± 216	280 ± 109	94 ± 71
Cocci	Bode Plot Δ (Ohms)	0.26 ± 0.11	0.09 ± 0.04	0.04 ± 0.01

For GP type bacteria, the negative charge resides on the cell wall of the pathogen. Figure 4.16 is a graphical representation of all the positive GP samples tested where the change in the impedance from the antibody to the sample, denoted by ΔZ , is plotted against the surface coverage of the pathogens and debris on the electrode surface.

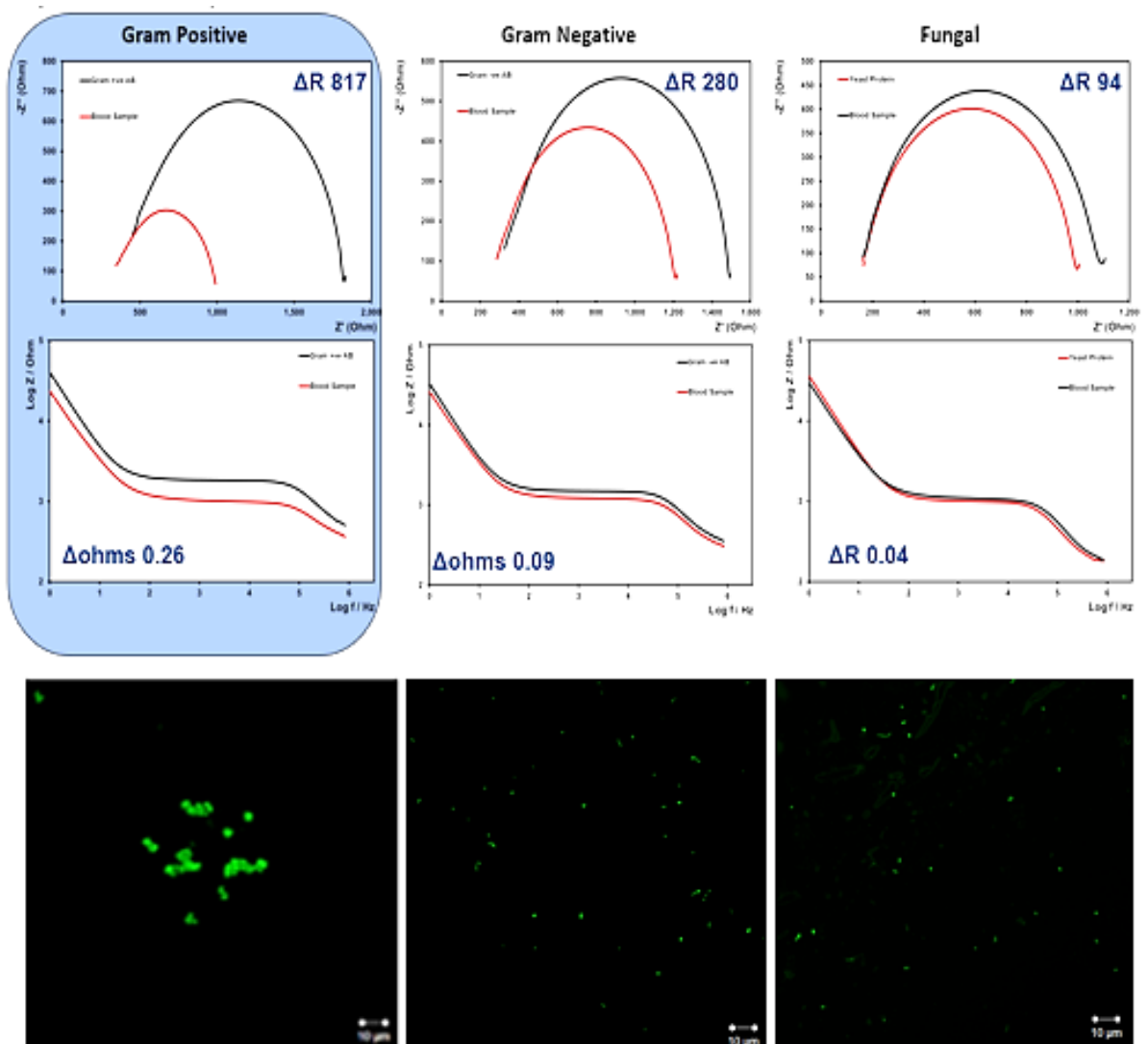


Figure 4.14. EIS results obtained for a gram-positive sepsis confirmed patient sample tested using the eLoAD device displaying the corresponding Nyquist, Bode and Confocal images.

After testing, all electrodes were imaged using confocal microscopy. Using ImageJ, the percentage of the electrode that was covered with biological structures was determined where all data was obtained in triplicate for the change in EIS versus surface coverage values. As blood culture samples were used, it was extremely difficult to differentiate between the captured pathogen and other blood components on the surface on the electrode and therefore a total % coverage was calculated using the image analysis software. The confocal images associated with the GP samples from the sample set were examined are shown in Figure 4.16.

The threshold was adjusted to reduce the background fluorescence however as the attached cell components would have an effect on the ΔZ , this was also considered when determining the % of the electrode which had captured cells. Referring to the graph, a linear relationship exists between the percentage of the electrode which captured bacteria against the increasing impedance value. GP bacteria has an overall negative charge on the cell membrane. This is due to the teichoic acids linked to the large peptidoglycan layer found in the cell membrane. For the GP samples, there appears to be a directly proportional relationship between the % of the covered electrode against the change in impedance.

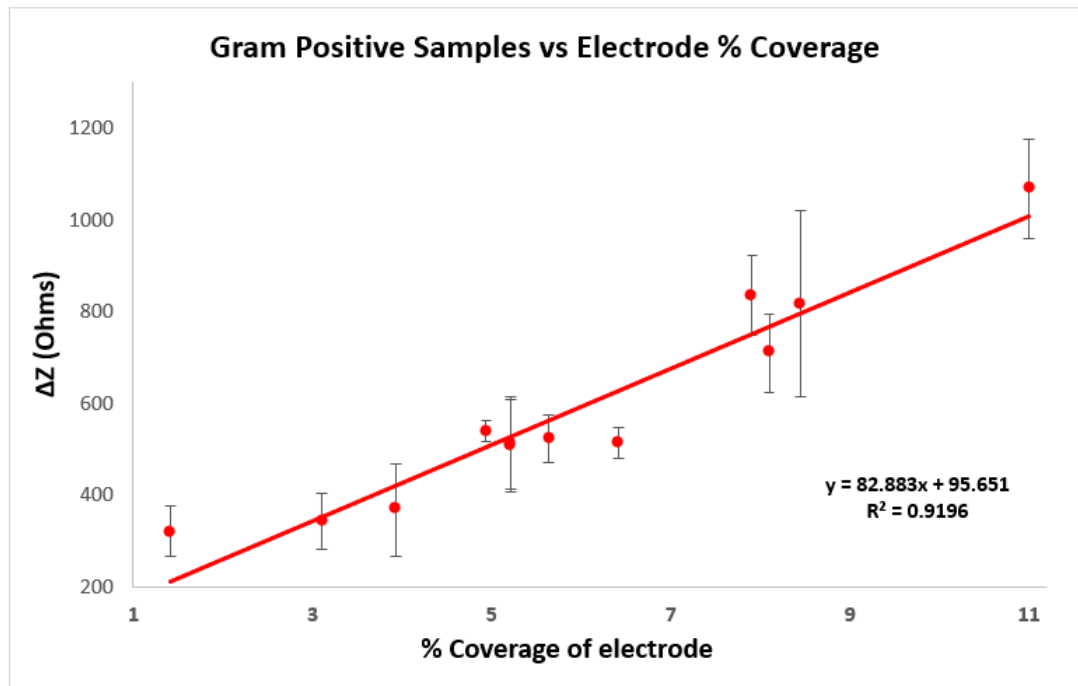


Figure 4.16. Graphical representation of all positive GP samples where the change in the Nyquist impedance value was plotted against the % surface coverage on electrodes.

These teichoic acids are negatively charged due to the phosphates in their structure [59]. With an increasing negative charge existing on the biosensor surface which correlates to the percentage of the electrode coverage, the overall impedance decreases and therefore the larger the change the more GP pathogen cells have been captured. A good linear fit of 0.9196 was determined which determines that the fit of the data determined a good correlation between the data sets and therefore the EIS and captured pathogens are directly proportional.

4.3.4.2 Gram-Negative pathogen detection on eLoad

Figure 4.17 portrays the EIS and confocal results for a positive GN patient sample (422605.10). Similar to the results obtained in 4.3.4.1, the GN EIS response greatly exceeds the threshold of >300 Ohms for the Nyquist and also exceeds the second threshold of > 0.15 ohms for the Bode plot. *Table 4-11* shows the EIS data which again shows the difference between the antibody and sample EIS values where only the delta values are shown. With both sets of results positive for the GN modified electrode, the

GN morphology is confirmed using confocal microscopy that shows to capture of the pathogens on the corresponding electrodes. Neither EIS plots show a significant change in the response for the GP and Fungal electrodes and therefore are determined to be negative for both GP and Fungal pathogens. The sample was confirmed to be GN *Enterococcus faecalis* by the St. James' Hospital microbiology lab.

Table 4-11. Results showing the difference between the Nyquist and Bode plot, resulting in positive results for Gram-Negative pathogens in patient sample 422605.10.

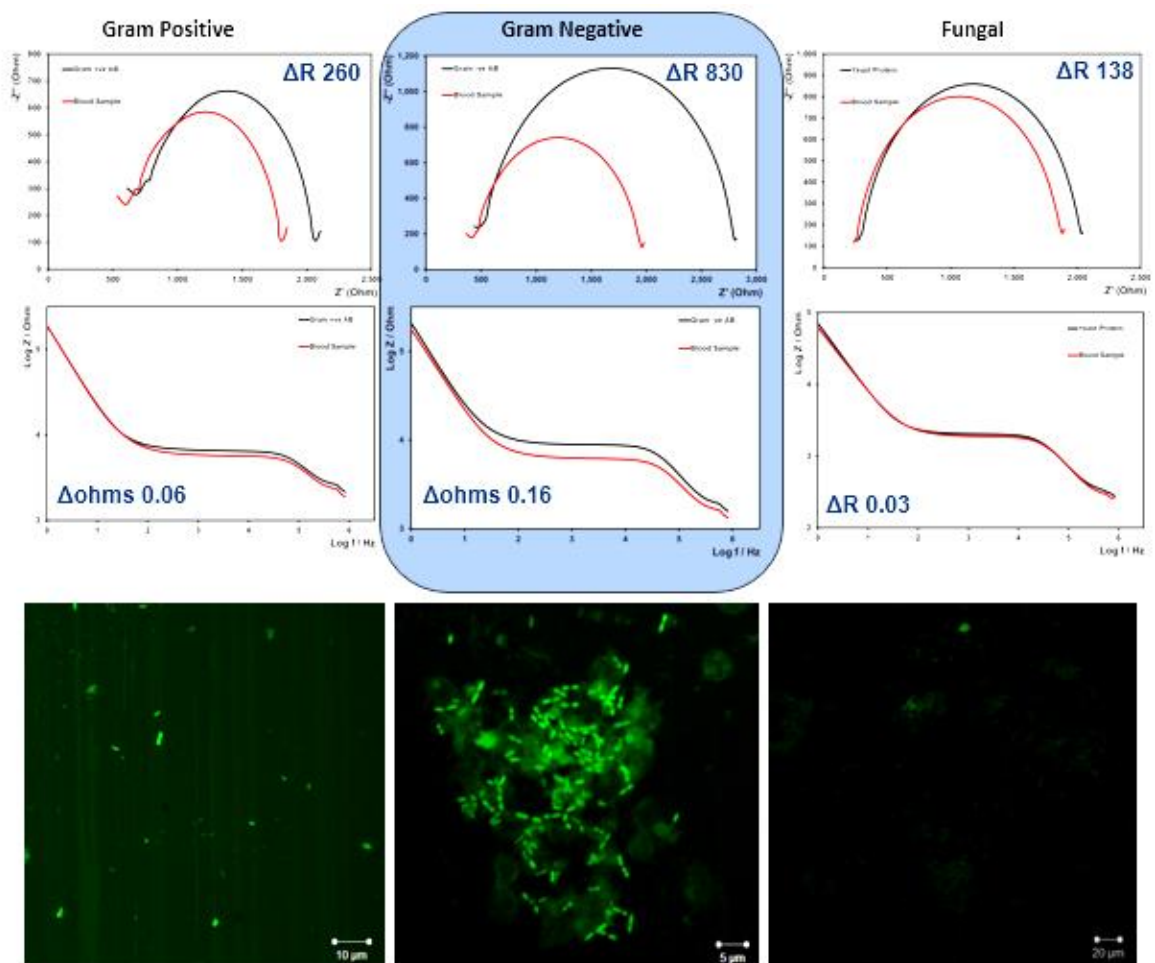


Figure 4.15. EIS results obtained for a gram-negative sepsis confirmed patient sample tested using the eLoaD device displaying the corresponding Nyquist, Bode and Confocal images.

These results still greatly indicated that it is a GN sample and would suggest the GN endotoxin antibody was highly selective for this type of pathogen. Figure 4.18 portrays the linear relationship between the % of the surface coverage of the pathogens/debris and the ΔZ of all positive GN blood culture samples. With an increasing number of captured pathogens on the GN electrode, the change in impedance also increases. This is

due to the negative charge that exists on the GN cell membrane, similarly to that of the GP type pathogen. The cell wall is also composed of a peptidoglycan layer which is negatively charged due to the phosphates present. The addition of a more negatively charged biomolecule on the surface of the electrode increasing the change of the EIS response. The ImageJ analysis was carried out in triplicate to ensure a broad scope of the electrode topography where a good fit of 0.9227 was obtained for the positive GN samples [60], [61]. As this determined the linear relationship of the capture surface ability to the increasing EIS response, it also proves that the GN biosensor has a high affinity towards GN type pathogens.

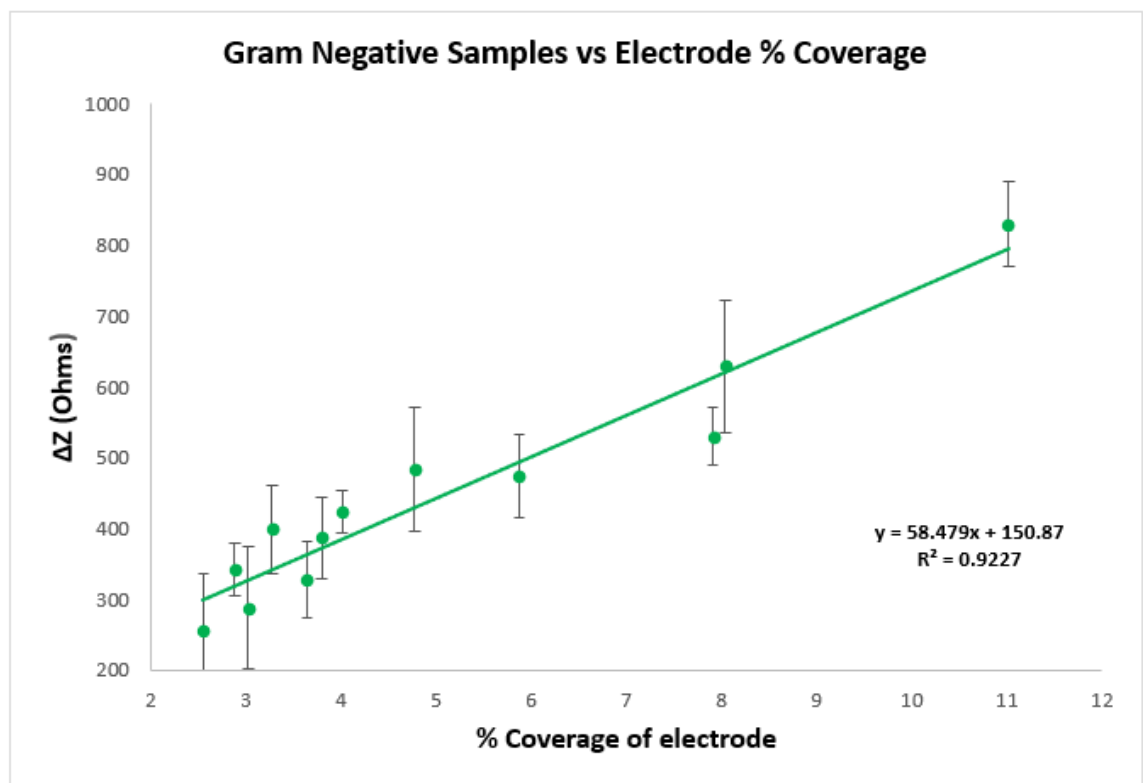


Figure 4.18. Graphical representation of all positive GN samples where the change in the Nyquist impedance value was plotted against the % surface coverage on electrodes.

4.3.4.3 Mixed pathogen detection on eLoaD

Figure 4.19 shows the EIS and confocal data for a positive GP and GN mixed patient sample (426180.20) where the quantified data is shown in Table 4-12. As it is possible for patients to have mixed pathogens present in the bloodstream it is highly desirable to be able to not only prove the presence of pathogens but to identify that there is more than one type

of pathogen present. Again, both the ΔR for the GP and GN exceeded the threshold for the Nyquist. In this case, the Bode plots for both pathogen readouts were below 0.15 ohms. However, with such a large shift in the semi-circle profiles, the samples were identified as positive for sepsis causing pathogens. The fungal showed very little change for both types of plots and was immediately determined to be negative.

The morphology of GP and GN pathogens was investigated using confocal microscopy where spherical whole cells were captured on the GP electrode, which is a characteristic for most GP bacteria, and rod shaped for the GN pathogens which is also representative of the common morphology of GN pathogens. The fungal electrode was relatively clean, with very few indistinguishable cell components visible. This however did not provide a false positive which was a hugely successful result considering the huge pathogen counts found on the other two Wes located in the same chamber.

This proves that the antibody and protein functionalised surfaces were highly selective and suggested that the frequency of 7Hz allowed the sample to come into contact with the electrode surfaces while not forcing non-specific adsorption of cell-components and pathogens onto the electrodes. The sample was confirmed to be GP Streptococcus and GN Staphylococcus by the St. James' Hospital microbiology lab.

Table 4-12. Results showing the difference between the Nyquist and Bode plot, resulting in positive results for Gram-Negative pathogens in patient sample 426180.20.

Pathogen	Antibody/Protein	Gram (+)	Gram (-)	Fungal
Gram (+) & (-) Streptococcus and GN Staphylococcus	Nyquist Plot $Z'' \Delta R$	535 ± 9	469 ± 127	58 ± 56
	Bode Plot Δ (Ohms)	0.11 ± 0.005	0.1 ± 0.01	0.01 ± 0.01

All results portrayed were carried out in triplicate (n=3). The Nyquist plots were examined to determine if pathogens were present. The change in impedance for the Z' ($R_{\text{Antibody}} - R_{\text{Antibody + pathogen}}$) was examined for each working electrode. It has been determined that $\Delta R \geq 300$ Ohms provided a positive answer for that system. Bode plots which were greater than 0.15 Ohms would also suggest a positive answer. Initially the Nyquist plots were

examined for a simple, quick read-out answer however, if there is a noticeable change across all electrodes, the Bode plots were also examined for a more in-depth analysis. A noticeable shift in the Nyquist plot across all three electrodes is the result of debris or biofilm formed on the surface on the sensors.

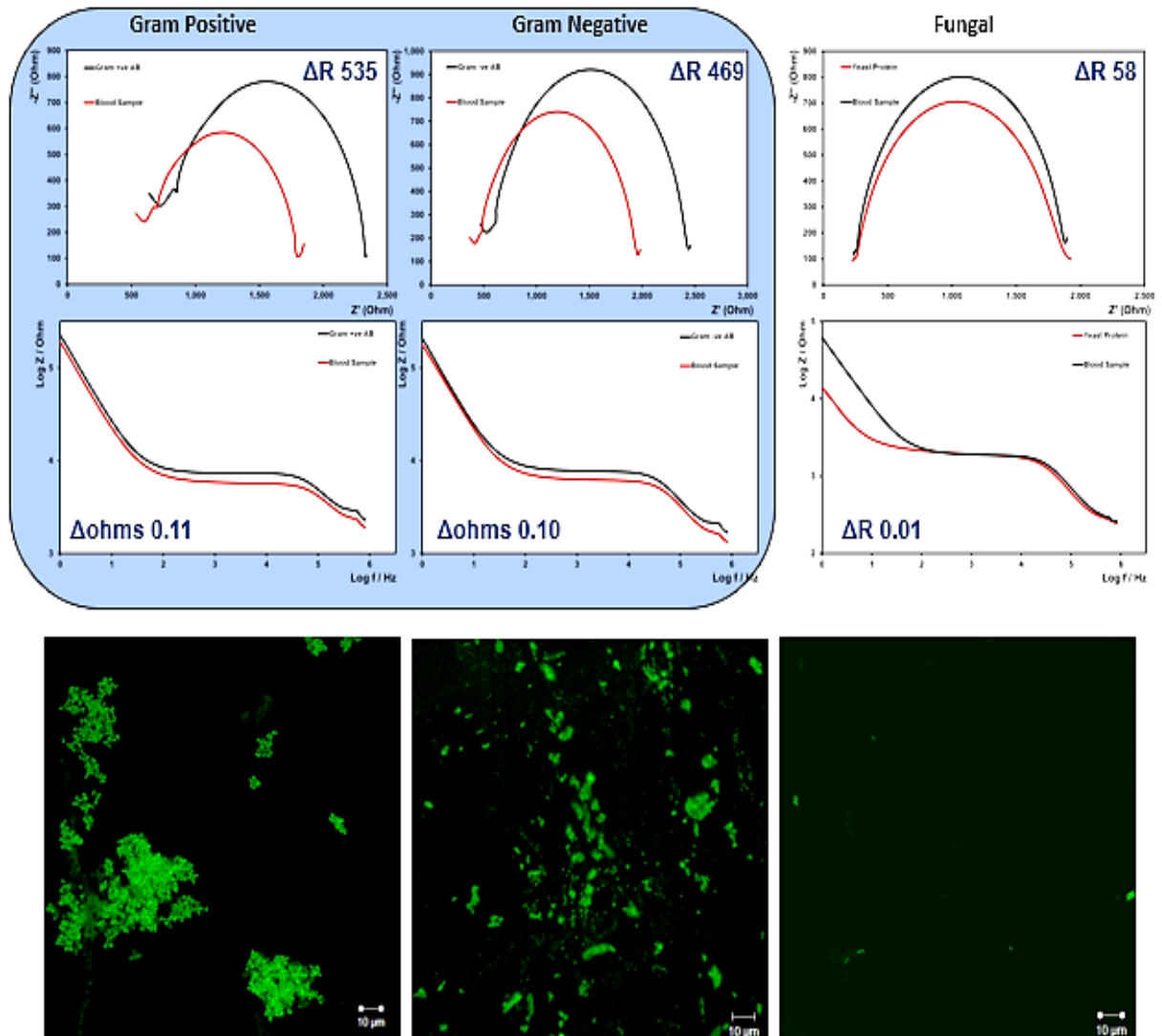


Figure 4.16. EIS results obtained for a GP and GN s confirmed patient sample tested using the eLoaD device displaying the corresponding Nyquist, Bode and Confocal images.

A number of factors can cause this, but it is usually due to the viscosity of the individual sample which is unique to the patient due to haematocrit and other blood components. There were a huge range of factors that differ between male, female and infant samples; such as higher platelet counts for males, which can aggregate due to illness. These can contribute to a high shift in the Nyquist plot for the GP, GN and Fungal electrodes. By

looking at both the Nyquist and Bode plots in these cases, the “false positives” can be ruled out by subtracting the background, which consists of the lowest Nyquist shift, from all three electrodes’ Nyquist plots. The Bode plot were also examined in the same way. From here it can be determined if the sample is positive for pathogens and what category they were in.

By applying the normal threshold previously indicated, there are 23/26 certain positive samples which were confirmed by the change in ΔR therefore 88.5% of the samples tested are positive for the indicated eLoaD result (marked green).

For this sample set it must also be considered that the BacT blood culture bottles used by the hospital staff contains a certain amount of yeast media to promote microbial growth. This may have an effect on the fungal EIS for this particular study as yeast present in the sample should have a high affinity towards the fungal capture surface on the third WE. An interesting trend was observed when studying the EIS measurements obtained. It appeared that the fungal electrode for samples tested that were originally cultured in aerobic bottles exceeded the threshold of >300 ohms for the Nyquist plot. When factoring in that the sample was obtained in an aerobic container, the Bode plot must be examined and become the overall determining factor, else, increase the threshold to >350 ohms for the fungal EIS for aerobic samples. This significantly reduces any false positives for fungal pathogens. This is a similar parameter implementation if the EIS testing system was automated, where sample source type would be an input parameter where the threshold would alter to suit the tested sample.

Contaminants such as skin flora microbes represent 15-30% of the isolated organisms in some hospitals. Overall, the success of recovering pathogens and eliminating contaminants is directly related to the techniques used to collect and process blood cultures, and the patient population being evaluated. Aseptic techniques are employed during blood drawing however the point of access for a blood sample can cause different contaminations due the changing skin flora and where these bacteria tend to reside on the body. 70% EtOH rubbing alcohol is used in conjunction with other preparation solutions and when two or 3 collections are required, changing needles between each is required to further reduce the chance of contamination [55]. Referring to the results

obtained, it was discovered that the EIS and confocal results for four samples (422008.8, 426115.18, 426180.20, 426589.25) detected pathogens which were believed by St. James' to be a contamination from the time of sample collection which was cultured as normal in the lab culture system. This contamination however was detected by the eLoaD whilst the causative class of organism for the sepsis response was also detected. These contaminated samples amount to 15% of the tested samples and directly correlates to the contaminations figures of blood culture samples reported in literature [58].

One sample required further explanation to why the EIS response was indicative of what functionalised electrode provided the positive result (marked orange) in *Table 4-8*. Patient sample number 426115.18 was one of the false positive results detected by the eLoaD. The sepsis inducing microbe for the patient's illness was a response to a fungal blood stream infection. However, the sample was contaminated with a GP organism which caused a huge EIS shift of 898 ± 409 ohms for the Nyquist detected by the n=3 sampling. This was likely an *S. aureus* contamination as this is the most common bacteria of the skin flora [62]. Confocal imaging confirmed the presence of a GP type pathogen as shown in *Figure 4.20*. When comparing (b) and (c) of the figure, the morphology of the microbes is identical. Both have a spherical shape and are clustered together, where (b) is the pathogen detected by the GP electrode and (c) is an image of cultured gram-stained *S. aureus* pathogens [63]. In conjunction with this, a significant change in the Bode plot was also noted and therefore the sample was also marked as positive for fungal microbes.

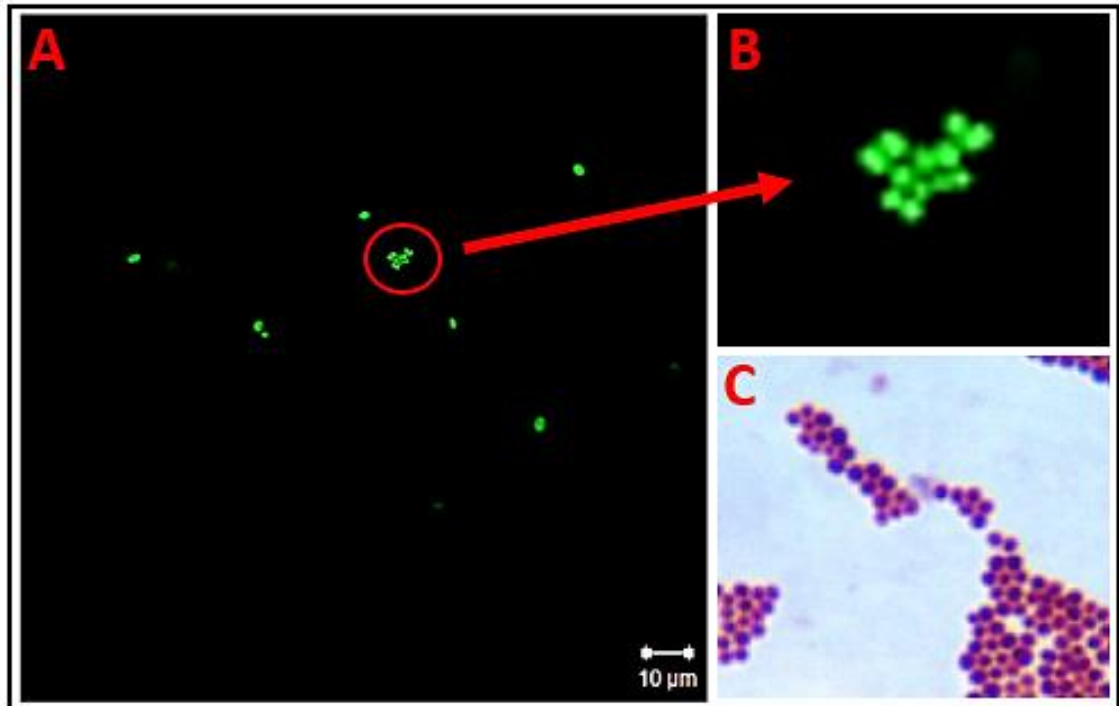


Figure 4.17. Image of GP electrode for patient sample 426115.18 to prove that the positive result obtained for the GP electrode was valid where the initial sample contamination was induced at sample collection where (a) is the confocal image acquired confirming the presence of pathogens, (b) the zoomed in image showing the spherical morphology when compared with (c) confirms that the cell shape directly corresponds to the morphology of a typical *S. aureus* microbe [18].

Finally, two false negative were also determined when the EIS results were cross-referenced with the clinical data. The EIS response of samples, 422421.4 and 426500.23, suggested both samples were GP as the change in the ΔR was significant. Examining the supporting confocal images, sample 422421.4 displayed very little evidence of pathogens captured on the surface. Remnants of cells were detected on both the GP and GN electrodes. Sample 426500.23 provided similar results, where the EIS would indicate a positive GP however the sample contained GN as confirmed by the hospital clinician and also by confocal imaging. With the confocal images clearly indicating a high cell count on the GN electrode only, it may have been the case where the RE or CE in the detection chamber may have been contaminated with a biofilm or the pathogen itself, hindering the detection ability of the electrochemical cell. As the confocal imaging is only used as a tool to correlate the EIS results with the electrode surface, the confocal images obtained cannot be an influencing factor in the determination of the causative pathogen. All supporting confocal imagery is found in Appendix A (acquired in conjunction with Dr. Kellie Adamson and David Boyle), where only one image per functionalised electrode is shown as a quick reference guide.

Consulting *Table 4-8*, 24 out of 26 patient samples tested on the eLoaD were correctly identified.

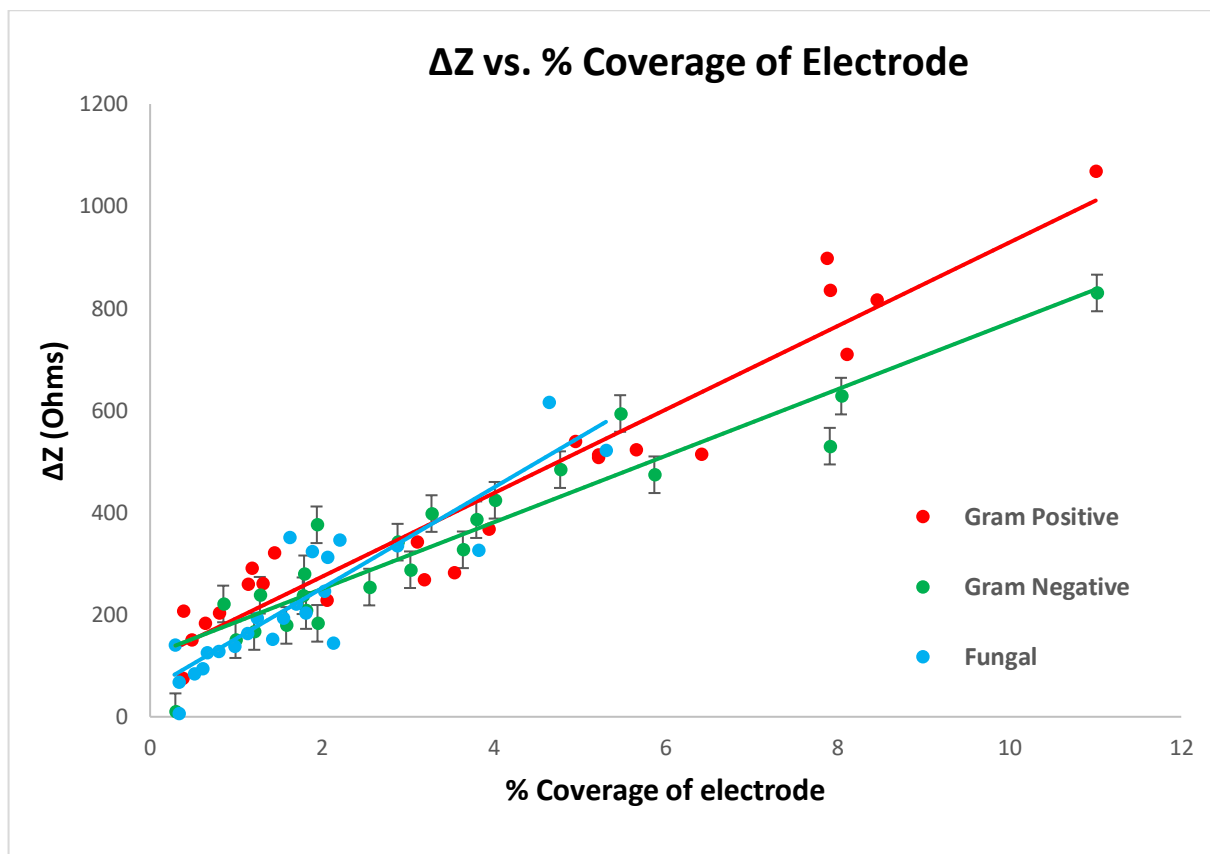


Figure 4.21. Graphical representation of all samples used in the St. James' Hospital validation study, where the change in the Nyquist impedance value was plotted against the % surface coverage of pathogens and debris on the surface. All image analysis was carried out using ImageJ where the average of three images per electrode was used.

Figure 4.21 represents all the data from the clinical samples in relation to the surface coverage percentage. 23 samples are shown where the negative sample and two false positives are excluded. For each electrode that was tested and imaged, the surface coverage of three separate sections of the electrode was determined and plotted against the ΔZ . The GP, GN and Fungal modified electrodes portrayed a linear relationship against the ΔZ , where the more capture cells and components on the surface increasing the change of impedance. In each case, the value of the real impedance on the Nyquist plot is reduced and therefore the change in impedance lowers the response value. By reducing the overall impedance value of the surface due to an increase in the negative charge on the surface due to the negatively charged captured biomolecules, the change in impedance

is directly related to the number of cells captured. GP cells contain more negative charges than that of the GN cell wall. This is due to thicker peptidoglycan layer which contains the teichoic acids. For GP pathogens this layer ranges from 20-100nm where-as the GN layer is only a few nanometres thick [59]. This variance in the charge density of the cell wall will have an overall effect on the change in impedance, which is shown by the slopes of the GN and GP graphs.

The results of this study are tremendously encouraging as the potential of the eLoaD is only being realised. The use of macro sampling being processed through microchannels allows for the detection of whole cells. The use of label-free, EIS methods of detection were validated as a reliable tool for pathogen detection. In 15 minutes, the sample was incubated with the fibrinogen solution to activate and coagulate the platelets within the device sample chamber to prevent these blood components from causing interferences on the electrodes themselves. With the optimised spin frequency of 7 Hz applied to the system forcing the sample down over the functionalised electrode surfaces, maximising sample-to-surface contact time, the integrity of the pathogen cells was preserved, where the dilution of the blood culture samples reduced interferences from the culture media. With the complexity of the sample being considered with such a short testing time, the overall result of the eLoaD provided to be a significant development in the rapid detection of sepsis causing pathogens in real-samples.

4.4 Conclusion

The fabrication of a traditional SAM functionalised electrode was shown, where individual steps of the sensor production was investigated via CV and EIS methods. The CV was used as a common characterisation tool where the blocking of the surface was demonstrated through the decreasing recorded as the modification steps proceeded. With the biosensor being successfully fabricated and characterised, it was shown that the traditional method of self-assembling monolayers activated through EDC coupling for the antibody layer can vary highly where the Nyquist and Bode ohmic values had a high discrepancy between each electrodes. Although the fabrication was a simple technique to adopt, the time for sensor completion was three days to allow for the proper formation of the monolayer and biorecognition layer.

The single-use biosensor was developed to be implemented into the centrifugal, microfluidic device designed and optimised in Chapter 3. As the aim of the platform was to handle biohazardous fluids, the biosensor had to be disposed of after one use, therefore the commercial gold discs were no longer a feasible option. The dicing of the Au coated Si wafers into rectangular shapes allowed for the device to become single-use for use with biohazardous samples was reported. μ CP methods produced very reproducible EIS results for all three working electrodes and the fabrication time was reduced to one day. The method using a PEG and BSA blocking layers to impede non-specific adsorption in the intermittent sections between the capture antibody/protein functionalised squares was used and characterised using EIS and CVs. Voltammograms were again used to determine the layer formation of each fabrication step of the sensor. An electrodeposited grown gold layer was used to increase the surface roughness the area of the overall area of the CV increases. The EIS response for the biosensor recorded under the same conditions of the rotating gold disc electrode shows similar results, where the Nyquist ΔR from the bare gold to the final antibody functionalised surface is significantly reduced. The overall reduction between the bare electrode and the antibody surface for both the Bode and Nyquist plots is a possibly due to a reduction in the capacitance on the surface due to the negatively charged amino groups on both the antibody and BSA structures as both isoelectric point of both biomolecules is below the pH of the electrolyte

solution, where the capacitance of the modification layers appear in series. With the characterisation of the sensor complete, the sensor was then integrated into the centrifugal, microfluidic device.

The reproducibility of the single use electrodes significantly increased when inserted into eLoaD. The eLoaD reduced the discrepancy between the impedance on each antibody surface (GP, GN and fungal) possibility helped by the electrode cover (layer 8) as the fixed exposed area of the electrodes remains constant. The distance between electrodes is also fixed due to their position on layer 9 of the device. When using a 10ml electrochemical cell it was extremely difficult to keep the electrode positions constant between batches. With the eLoaD, this problem was solved and has had a positive impact on the reproducibility of the system.

The performance of the platform using real, blood culture samples received from St. James' Hospital microbiology department. The study determined that the platform was highly selective between pathogens and blood cell components. With only two false positives being reported, the sensor is capable of differentiating between the target analyte and the other unwanted cells in the sample. This is due to the high affinity of the antibody and protein recognition layers. The blocking, coupled with the fibrinogen functionalised chambers, greatly reduced non-specific binding of cell components to the electrode surfaces, as revealed by the confocal images. This allowed for complex sample handling on the device whilst able to correctly identify the pathogen category. The dilution of the sample was also a necessary step to reduce interferences and the possibility of false positive results. The dilution not only appeared to lyse RBCs but also significantly reduced the binding of pathogens to the other electrodes, increasing the specificity.

The eLoaD was very effective for its dual functionality, where;

The samples were determined to be either positive or negative for sepsis causing microbes.

Which subclass of pathogens they belong to: GP, GN, Fungal or a mixture.

The optimised test confirmed in 15 minutes the presence of these pathogens and therefore has the potential to become a rapid diagnostic tool can pave the way for simple POC testing for suspected sepsis sufferers. Supporting confocal images confirmed the relationship that existed for the surface coverage against the overall change in the Nyquist Z' value (ohms). The percentage of the electrodes covered for the GP positive samples had a seemingly directly proportional relationship against the ΔZ (Ohms) where the GN electrode coverage against the corresponding ΔZ (Ohms) also showed a high correlation. With the epidemic of antibiotic resistance strains of pathogens emerging, the need for rapid sepsis detection is at an all-time high. By confirming in a short space of time whether a patient is in need of an antibiotic due to the presence of pathogens in the blood streams, the overuse of drugs through “blind prescription” will be eradicated. The time for producing rapid, accurate results is a significantly lower time-frame to that of the turn-around time for results obtained in our own hospitals.

4.5 References

- [1] J. A. Pienaar, A. Singh, and T. G. Barnard, "The viable but non-culturable state in pathogenic *Escherichia coli*: A general review," *Afr. J. Lab. Med.*, vol. 5, no. 1, p. 368, May 2016.
- [2] J. Straub *et al.*, "Diagnostic accuracy of the ROCHE Septifast PCR system for the rapid detection of blood pathogens in neonatal sepsis—A prospective clinical trial," *PLoS One*, vol. 12, no. 11, p. e0187688, Nov. 2017.
- [3] B. Piknova and A. N. Schechter, "Measurement of nitrite in blood samples using the ferricyanide-based hemoglobin oxidation assay," *Methods Mol. Biol.*, vol. 704, pp. 39–56, 2011.
- [4] P. Mehrotra, "Biosensors and their applications – A review," *J. Oral Biol. Craniofacial Res.*, vol. 6, no. 2, pp. 153–159, Jan. 2016.
- [5] M. E. E. Alahi and S. C. Mukhopadhyay, "Detection methodologies for pathogen and toxins: A review," *Sensors (Switzerland)*, vol. 17, no. 8, pp. 1–20, 2017.
- [6] M. Barreiros dos Santos, J. P. Aguil, B. Prieto-Simón, C. Sporer, V. Teixeira, and J. Samitier, "Highly sensitive detection of pathogen *Escherichia coli* O157:H7 by electrochemical impedance spectroscopy," *Biosens. Bioelectron.*, vol. 45, pp. 174–180, Jul. 2013.
- [7] F. Ricci, G. Volpe, L. Micheli, and G. Palleschi, "A review on novel developments and applications of immunosensors in food analysis," *Anal. Chim. Acta*, vol. 605, no. 2, pp. 111–129, Dec. 2007.
- [8] Y. Jun, X. Y. Zhu, and J. W. P. Hsu, "Formation of alkanethiol and alkanedithiol monolayers on GaAs(001)," *Langmuir*, vol. 22, no. 8, pp. 3627–3632, 2006.
- [9] A. Hasan and L. M. Pandey, *Self-assembled monolayers in biomaterials*, no. December. Elsevier Ltd., 2017.
- [10] K. F. Lei, "Review on impedance detection of cellular responses in micro/nano environment," *Micromachines*, vol. 5, no. 1, pp. 1–12, 2014.
- [11] M. J. Mitchell and M. R. King, "NIH Public Access," vol. 132, no. 1, pp. 1–23, 2014.
- [12] A. Venkatanarayanan, T. E. Keyes, and R. J. Forster, "Label-free impedance detection of cancer cells," *Anal. Chem.*, vol. 85, no. 4, pp. 2216–2222, 2013.

- [13] B. A. Stotler and A. Kratz, "Analytical and Clinical Performance of the epoc Blood Analysis System," *Am. J. Clin. Pathol.*, vol. 140, no. 5, pp. 715–720, 2013.
- [14] T. Oeschger, D. McCloskey, V. Koppaarth, A. Singh, and D. Erickson, "Point of care technologies for sepsis diagnosis and treatment," *Lab Chip*, vol. 19, no. 5, pp. 728–737, 2019.
- [15] V. Singh, S. Khatana, and P. Gupta, "Blood gas analysis for bedside diagnosis," *Natl. J. Maxillofac. Surg.*, vol. 4, no. 2, pp. 136–141, 2013.
- [16] H. Salimnia *et al.*, "Evaluation of the FilmArray Blood Culture Identification Panel: Results of a Multicenter Controlled Trial," *J. Clin. Microbiol.*, vol. 54, no. 3, p. 687 LP-698, Mar. 2016.
- [17] R. Halai, D. E. Croker, J. Y. Suen, D. P. Fairlie, and M. A. Cooper, "A Comparative Study of Impedance versus Optical Label-Free Systems Relative to Labelled Assays in a Predominantly Gi Coupled GPCR (C5aR) Signalling," *Biosensors*, vol. 2, no. 3, pp. 273–290, Jul. 2012.
- [18] J. L. Acero Sánchez, A. Fragoso, H. Joda, G. Suárez, C. J. McNeil, and C. K. O'Sullivan, "Site-directed introduction of disulfide groups on antibodies for highly sensitive immunosensors," *Anal. Bioanal. Chem.*, vol. 408, no. 19, pp. 5337–5346, 2016.
- [19] J. E. Butler *et al.*, "The immunochemistry of sandwich elisas—VI. Greater than 90% of monoclonal and 75% of polyclonal anti-fluorescyl capture antibodies (CAbs) are denatured by passive adsorption," *Mol. Immunol.*, vol. 30, no. 13, pp. 1165–1175, 1993.
- [20] H. Sharma and R. Mutharasan, "Half antibody fragments improve biosensor sensitivity without loss of selectivity," *Anal. Chem.*, vol. 85, no. 4, pp. 2472–2477, 2013.
- [21] D. N. Forthal, "Functions of Antibodies," *Microbiol. Spectr.*, vol. 2, no. 4, pp. 1–17, Aug. 2014.
- [22] H. D. Abbruña, Y. Kiya, and J. C. Henderson, "Batteries and Electrochemical Capacitors," *Phys. Today*, no. December, pp. 43–47, 2008.
- [23] E. P. Randviir, J. P. Metters, J. Stainton, and C. E. Banks, "Electrochemical impedance spectroscopy versus cyclic voltammetry for the electroanalytical sensing of capsaicin utilising screen printed carbon nanotube electrodes," *Analyst*, vol. 138, no. 10, pp. 2970–2981, 2013.

- [24] D. D. Agonafer, E. Chainani, M. E. Oruc, K. S. Lee, and M. A. Shannon, "Study of Insulating Properties of Alkanethiol Self-Assembled Monolayers Formed Under Prolonged Incubation Using Electrochemical Impedance Spectroscopy," *J. Nanotechnol. Eng. Med.*, vol. 3, no. 3, p. 31006, 2013.
- [25] F. Ricci *et al.*, "Surface chemistry effects on the performance of an electrochemical DNA sensor," *Bioelectrochemistry*, vol. 76, no. 1–2, pp. 208–213, Sep. 2009.
- [26] W. Wang, H. Piao, D. Choi, and Y. Son, "Nanodielectric properties of 16-MHDA self-assembled monolayers," *RSC Adv.*, vol. 4, no. 82, pp. 43387–43391, 2014.
- [27] E. Katz and I. Willner, "Probing Biomolecular Interactions at Conductive and Semiconductive Surfaces by Impedance Spectroscopy: Routes to Impedimetric Immunosensors, DNA-Sensors, and Enzyme Biosensors," *Electroanalysis*, pp. 913–947, 2003.
- [28] L. Bard, Allen J.: Faulkner, *Electrochemical methods, fundamentals and applications*. New York, 2001.
- [29] B. Thi, T. Nguyen, and C. S. Toh, *Development of an electrode-membrane-electrode system for selective Faradaic response towards charged redox species*, vol. 54. 2009.
- [30] C. Gupta, M. A. Shannon, and P. J. A. Kenis, *Mechanisms of Charge Transport through Monolayer-Modified Polycrystalline Gold Electrodes in the Absence of Redox-Active Moieties*, vol. 113. 2009.
- [31] F. Schreiber, *Structure and Growth of Self-Assembling Monolayers*, vol. 65. 2000.
- [32] Y. Wang, Z. Ye, and Y. Ying, "New trends in impedimetric biosensors for the detection of foodborne pathogenic bacteria," *Sensors*, vol. 12, no. 3, pp. 3449–3471, 2012.
- [33] A. Santos, "Fundamentals and Applications of Impedimetric and Redox Capacitive Biosensors," *J. Anal. Bioanal. Tech.*, vol. S7, no. 12, 2014.
- [34] B. Mattiasson and M. Hedström, "Capacitive biosensors for ultra-sensitive assays," *TrAC - Trends Anal. Chem.*, vol. 79, pp. 233–238, 2016.
- [35] K. C. Lin, V. Kunduru, M. Bothara, K. Rege, S. Prasad, and B. L. Ramakrishna, "Biogenic nanoporous silica-based sensor for enhanced electrochemical detection of cardiovascular biomarkers proteins," *Biosens. Bioelectron.*, vol. 25, no. 10, pp.

2336–2342, 2010.

- [36] Y. Sun, Y. Zhang, and E. Pickwell-Macpherson, “Investigating antibody interactions with a polar liquid using terahertz pulsed spectroscopy,” *Biophys. J.*, vol. 100, no. 1, pp. 225–231, Jan. 2011.
- [37] M. A. Rampi, O. J. A. Schueller, and G. M. Whitesides, “Alkanethiol self-assembled monolayers as the dielectric of capacitors with nanoscale thickness,” *Appl. Phys. Lett.*, vol. 72, no. 14, pp. 1781–1783, 1998.
- [38] M. Zhang *et al.*, “Ultrasensitive electrochemiluminescence immunoassay for tumor marker detection using functionalized Ru-silica@nanoporous gold composite as labels,” *Analyst*, vol. 137, no. 3, pp. 680–685, 2012.
- [39] C. H. Chu *et al.*, “Beyond the Debye length in high ionic strength solution: Direct protein detection with field-effect transistors (FETs) in human serum,” *Sci. Rep.*, vol. 7, no. 1, pp. 1–15, 2017.
- [40] E. Spain *et al.*, “Detection of prostate specific antigen based on electrocatalytic platinum nanoparticles conjugated to a recombinant scFv antibody,” *Biosens. Bioelectron.*, vol. 77, pp. 759–766, Mar. 2016.
- [41] F. Malvano *et al.*, “Fabrication of SrTiO₃ layer on Pt Electrode for label-free capacitive biosensors,” *Biosensors*, vol. 8, no. 1, pp. 1–11, 2018.
- [42] P. Novák and V. Havlíček, “4 - Protein Extraction and Precipitation,” P. Ciborowski and J. B. T.-P. P. and A. C. (Second E. Silberring, Eds. Boston: Elsevier, 2016, pp. 51–62.
- [43] N. Daniels, J.S., Pourmand, “Label-free impedance Biosensors:,” *Retrieved Sept.*, vol. 19, no. 12, pp. 1239–1257, 2007.
- [44] C. Fernández-Sánchez, C. J. McNeil, and K. Rawson, “Electrochemical impedance spectroscopy studies of polymer degradation: Application to biosensor development,” *TrAC - Trends Anal. Chem.*, vol. 24, no. 1, pp. 37–48, 2005.
- [45] K. Smith *et al.*, “Rapid generation of fully human monoclonal antibodies specific to a vaccinating antigen,” *Nat. Protoc.*, vol. 4, no. 3, pp. 372–384, 2009.
- [46] B. Pokrić and Z. Pučar, “The two-cross immunodiffusion technique: Diffusion coefficients and precipitating titers of IgG in human serum and rabbit serum antibodies,” *Anal. Biochem.*, vol. 93, pp. 103–114, 1979.

- [47] J. Vajda, W. Conze, and E. Müller, "Kinetic plots in aqueous size exclusion chromatography of monoclonal antibodies and virus particles," *J. Chromatogr. A*, vol. 1426, pp. 118–125, 2015.
- [48] Y. Cu and W. M. Saltzman, "Mathematical modeling of molecular diffusion through mucus," *Adv. Drug Deliv. Rev.*, vol. 61, no. 2, pp. 101–114, Feb. 2009.
- [49] J. Foncy *et al.*, "Dynamic inking of large-scale stamps for multiplexed microcontact printing and fabrication of cell microarrays," *PLoS One*, vol. 13, no. 8, p. e0202531, Aug. 2018.
- [50] J. A. Wiggenius, S. Fransson, F. von Post, and O. Inganäs, "Protein biochips patterned by microcontact printing or by adsorption-soft lithography in two modes," *Biointerphases*, vol. 3, no. 3, pp. 75–82, 2009.
- [51] A. W. Peterson, R. J. Heaton, and R. M. Georgiadis, "The effect of surface probe density on DNA hybridization," *Nucleic Acids Res.*, vol. 29, no. 24, pp. 5163–5168, Dec. 2001.
- [52] A. Vainrub and B. M. Pettitt, "Coulomb blockage of hybridization in two-dimensional DNA arrays," *Phys. Rev. E*, vol. 66, no. 4, p. 41905, Oct. 2002.
- [53] O. Haji-Ghassemi *et al.*, "Structural Basis for Antibody Recognition of Lipid A," *J. Biol. Chem.*, vol. 290, no. 32, pp. 19629–19640, 2015.
- [54] H. Sunayama, Y. Kitayama, and T. Takeuchi, "Regulation of protein-binding activities of molecularly imprinted polymers via post-imprinting modifications to exchange functional groups within the imprinted cavity," *J. Mol. Recognit.*, vol. 31, no. 3, pp. 1–6, 2018.
- [55] J. Gilmore, M. Islam, and R. Martinez-Duarte, "Challenges in the use of compact disc-based centrifugal microfluidics for healthcare diagnostics at the extreme point of care," *Micromachines*, vol. 7, no. 4, 2016.
- [56] K. Waseem *et al.*, "Effect of different growing media on the growth and flowering of stock (*Matthiola incana*) under the agro-climatic condition of dera Ismail Khan," *Pakistan J. Agric. Sci.*, vol. 50, no. 3, pp. 523–527, 2013.
- [57] I. Use, E. Of, T. H. E. Procedure, S. Life, and U. Q. Control, "BD BHI Media Compositions," pp. 24–26, 2013.
- [58] P. R. Murray and H. Masur, "Current approaches to the diagnosis of bacterial and

fungal bloodstream infections in the intensive care unit,” *Crit. Care Med.*, vol. 40, no. 12, pp. 3277–3282, Dec. 2012.

- [59] T. J. Silhavy, D. Kahne, and S. Walker, “The Bacterial Cell Envelope” T. J. Silhavy, D. Kahne and S. Walker, .,” pp. 1–16, 2010.
- [60] N. Malanovic and K. Lohner, “Gram-positive bacterial cell envelopes: The impact on the activity of antimicrobial peptides,” *Biochim. Biophys. Acta - Biomembr.*, vol. 1858, no. 5, pp. 936–946, 2016.
- [61] K. C. Huang, R. Mukhopadhyay, B. Wen, Z. Gitai, and N. S. Wingreen, “Cell shape and cell-wall organization in Gram-negative bacteria,” *Proc. Natl. Acad. Sci.*, vol. 105, no. 49, pp. 19282–19287, 2008.
- [62] F. Tamer, M. E. Yuksel, E. Sarifakioglu, and Y. Karabag, “Staphylococcus aureus is the most common bacterial agent of the skin flora of patients with seborrheic dermatitis,” *Dermatol. Pract. Concept.*, vol. 8, no. 2, pp. 80–84, Apr. 2018.
- [63] A. M. Soliman, M.K. , Ellakany, H.F., Gaafar, A.Y., Elbially, A.K, Zaki, M.S. and Younes, “Epidemiology and antimicrobial activity of methicillin-resistant Staphylococcus aureus (MRSA) isolated from Nile tilapia (*Oreochromis niloticus*) during an outbreak in Egypt.,” no. June 2016, 2014.

Chapter 5

E. coli Capture and Detection using ELONA, Apta-PCR and Apta-RPA Assays

5.1 Introduction

Aptamers are single stranded DNA (ssDNA) or ribonucleic acid (RNA) oligonucleotides which bind to their target through DNA base pair sequencing with high affinity and specificity [1]. RNA and ssDNA aptamers can be differentiated from each other due to their folding patterns although they can bind to the same target. Aptamers are being increasingly used as replacements for expensive antibody systems and assays as they are synthetically produced, with lower cost whilst maintaining a high affinity towards the analyte [2]. They have the capacity to associate with small molecules, proteins, cells or viruses. Aptamers can range in length from 25 to 90 bases [3]. Antibodies and proteins are easily denatured at high temperatures due to loss of their tertiary structure. As aptamers are able to recover their natural formation and have the ability to bind to targets after re-annealing they can be used in regions of severe temperatures [4].

The development of antibodies requires the use of live-animals and increase the need for mammalian cell culture. Aptamers eradicate the use of a live host and therefore are consistent across batch production, unlike antibodies. As aptamers are synthesised, they are easily modified to contain moieties such as targets, nanoparticles or fluorophores. Aptamers can also be chemically stabilised to further increase thermal and pH stability [5]. Furthermore, aptamers show a high affinity and specificity for some ligands that are not captured or recognized by antibodies, such as small molecules or antigens, indicating that the use of these highly specific oligonucleotides as recognition components are broadening their applications [6]. In 2012 Nadal *et. al* produced a highly specific and high affinity DNA aptamer for the β -conglutin food allergen using *in-vitro* selection. ssDNA was produced from a randomised pool using the T7 Gene 6 exonuclease and incubated against magnetic beads where the captured ssDNA was eluted and amplified before another round of the Systematic Evolution of Ligands by Exponential Enrichment (SELEX) process [7]. This procedure used a large population of randomised sequences in a produced library of synthetic nucleic acids used to select specific aptamers by repeating rounds of binding, competition, selection, amplification, and enrichment of the final selected aptamer. This SELEX process, through competitive binding to the analyte, produced the aptamer with a high affinity [8].

Aptamers have increasingly been used for enzyme linked oligonucleotide assays (ELONAs) due to their specificity and stability [9]. A sandwich aptamer assay consists of an aptamer-target-aptamer configuration where two different types of aptamers attach to separate binding sites of the target molecule for capture and detection purposes. As aptamers are easily labelled it's simpler to design the reporter probe to contain moiety, such as biotin, which can bind to biotin binding protein conjugated with signal changing polymers for colorimetric detection [10]. A secondary approach for analyte detection may use amplifying techniques such Polymerase chain reaction (PCR) and recombinase polymerase amplification (RPA). For the aptamer-target-aptamer assay, the reporter probe may be eluted and amplified when signal changes may be low. PCR requires cycling temperature to amplify DNA where-as RPA is an isothermal technique utilising enzymes to carry out the denaturation and annealing of the target to amplify the products [11]. RPA is a highly sensitive and selective technique which has been reported to amplify as little as 1-10 DNA and RNA copies in less than ten minutes [12].

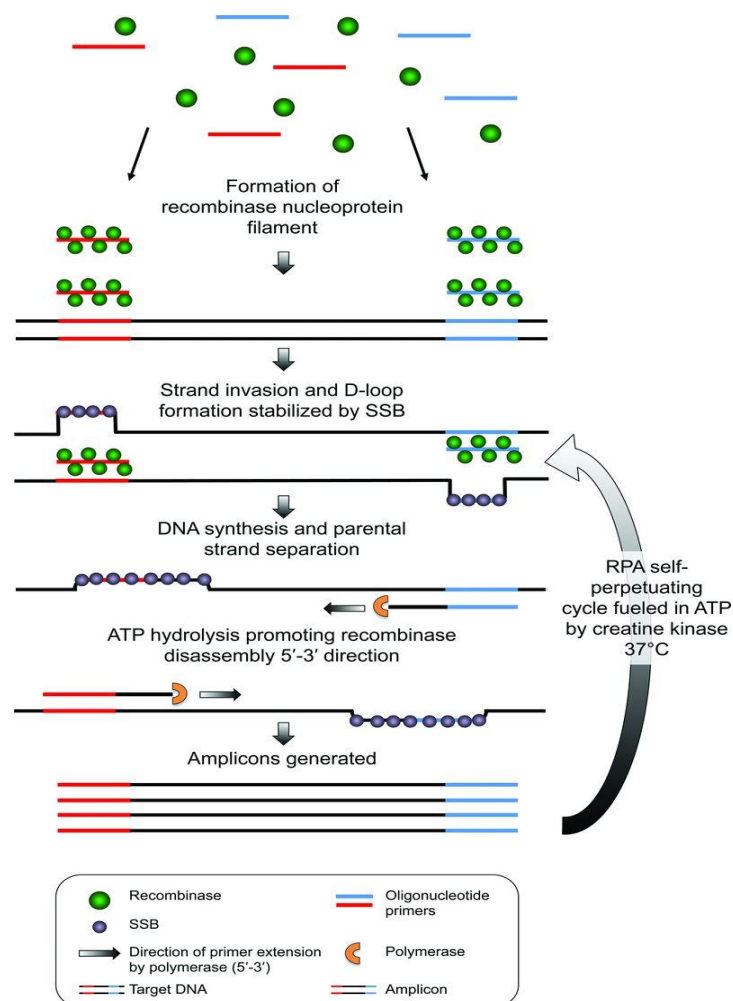


Figure 5.1 Recombinase polymerase amplification stepwise process.

RPA disregards the use of thermocycling used in PCR, as three core proteins are used which operate at 37 °C. This means that RPA can be used in a conventional oven, rather than requiring a thermocycler, ideal for labs that may not have access to such specific equipment.

Figure 5.1 portrays the RPA process where the first protein used in RPA is a recombinase. This binds to the primers which forms filaments which then recombine with the DNA, forcing the displacement of the non-complimentary strand. The second protein present is a ssDNA binding protein which adheres to the strand of DNA which has been displaced by the primer. This prevents the dissociation of the primer strand and hybridisation of the duplex target. The final protein displaces the polymerase that copies the DNA whilst adding bases to the 3' end of the primer which consequently forces the double helix to open and it progresses. While opposing primers are used, the amplification rate is exponential [13][14], [15]. The RPA method is altered from the original process, instead to use tailed primers which creates an amplicon with duplex with two ssDNA tails, which create an overhang on each end of the ssDNA. This tailed DNA amplicon aids in detection through hybridisation to the immobilised capture probe.

In 2015, Bruno *et al* introduced aptamers capable of capturing and detection pathogenic *E. coli* cells (O157:H7) on a lateral flow system using both AuNPs and Quantum Nanodots [16]. These aptamers were created using the SELEX process, in which the analyte is hybridised with a library containing up to 10^{15} DNA or RNA sequences, where the bound sequences are extracted and amplified [17]. 44 aptamers were identified through this process, where ECO3R had the highest affinity towards a multitude of *E. coli* strains with the aptamers attaching to the outer membrane proteins (OMPs). Surface Plasmon Resonance (SPR) studies using a Biacore X-100 confirmed that the ECO3R and the ECO4F showed the highest affinity towards the bacteria, where both pathogenic and non-pathogenic species were studied [18]. The SPR data also suggested that the aptamers had a low or negative response to high concentrations of both *Salmonella enterica* and *Campylobacter jejuni* (2.5×10^6 CFU/ ml), where both pathogens are gram-negative rod shaped species which have very similar attributes to that of *E. coli* cells as they are associated with food poisoning outbreaks [19].

These aptamers first used by Bruno *et. al.* were used to capture and detect a dynamic range of DH5 α E. coli cells using ELONA, PCR and RPA methods for a fully robust detection system for bacterial cells. Initially, the ECO4F – 5' amine was termed the capture aptamer as it is a thiolated molecule which initially binds to the maleimide coated microwells. The ECO3R – 3' digoxigenin aptamer was the secondary aptamer and used as the reporter probe, which cleaves to streptavidin (SA) poly horseradish peroxidase (HRP) which reacts with TMB to produce a signal, quantified by a plate reader for ELONA analysis. All assay conditions were optimised for whole cell capture and detection was used for quantification. Spectrophotometric analysis allowed for quantification of the colorimetric response of the assay. Once optimised, the same assay was employed as a capture platform for the cells. Eluted samples were acquired for both PCR and RPA assays were carried out. A limit of detection for each experimental platform was determined in clean buffer samples using GraphPad Prism software.

5.2 Chemical and Biological reagents used

Reagents were sourced as follows:

Phosphate-buffered saline, bovine serum albumin and skimmed milk powder (Sigma, Ireland and Spain), PBS-Tween (10mM phosphate, 138mM NaCl, 2,7mM KCl, 0,05% v/v Tween 20, pH 7.4), maleimide coated plates (Fischer Scientific, Spain), horseradish peroxide-linked streptavidin (SA-HRP), 3,3', 5, 5' – tetramethylbenzidine (TMB), sulphuric acid (Sigma, Spain), DH5 α E. coli (Sigma, Ireland), Twist amp basic kit (TwistDX, UK) DNA polymerase, loading buffer and 10bp DNA ladder (life sciences, Ireland) (Sigma, Ireland). All solutions were prepared in in high purity water obtained from Milli-Q (18M Ω cm⁻¹) RG systems. All DNA sequences were purchased from Biomers (Ulm, Germany) which are detailed in *Table 5-1*

Table 5-1. Composition of aptamers used for e. coli capture and detection with an initial concentration of 1000 μ M.

Forward Primer	5'-GTTTTCCCAGTCACGAC-C3-AGCTCCAGAAGATAAATTACAGG-3'
-----------------------	--

Reverse Primer	5'-TGTA AACGACGGCCAGT-C3-GGGGTCATAGTATCCTAGTTG-3
ECO4F - Thiol Capture	Thiol-5'-TTTTTTTT... ATACGGGAGCCAACACCATAATATGCCGTAAGGAGAGGCCTGTTGGGAGCG CCGTAGAGCAGGTGTGACGGAT-3'
ECO3R - Biotin Reporter	Biotin-5'-TTTTTTTT... CACACCTGCTCTGTCTGCGAGCGGGGCGCGGGCCCCGGCGGGGGATGCGTG GTGTTGGCTC- 3'
ECO3R - Unmodified	5'-TTTTTTTT... CACACCTGCTCTGTCTGCGAGCGGGGCGCGGGCCCCGGCGGGGGATGCGTG GTGTTGGCTC- 3'
ECO3R Thiol - Capture	Thiol-5'-TTTTTTTT... CACACCTGCTCTGTCTGCGAGCGGGGCGCGGGCCCCGGCGGGGGATGCGTG GTGTTGGCTC- 3'
ECO4F Biotin - Reporter	Biotin-5'-TTTTTTTT... ATACGGGAGCCAACACCATAATATGCCGTAAGGAGAGGCCTGTTGGGAGCG CCGTAGAGCAGGTGTGACGGAT-3'

5.3 Experimentation

Three separate assays were optimised for the capture and detection of *E. coli* cells. Firstly, an ELONA assay was carried out and would be used for the entirety of the experiments as a cell capture platform. PCR and RPA methods were carried out in parallel to determine if one method was more robust for the aptamer amplification.

5.3.1 Enzyme linked oligonucleotide assay (ELONA)

The thiolated ECO4F capture aptamer has a high affinity to the Thermo Scientific Pierce Maleimide Activated plate through Sulfhydryl-binding. The affinity of streptavidin (SA) for biotin is the strongest noncovalent biological interaction known, with a dissociation constant (K_d) in the femtomolar range [20]. Each SA monomer can bind one biotin molecule, allowing a SA protein to maximally bind four biotins (shown in Figure 5.2), which is synthetically attached to the ECO3R reporter probe, for detection through SA Poly HRP – TMB colorimetric detection.

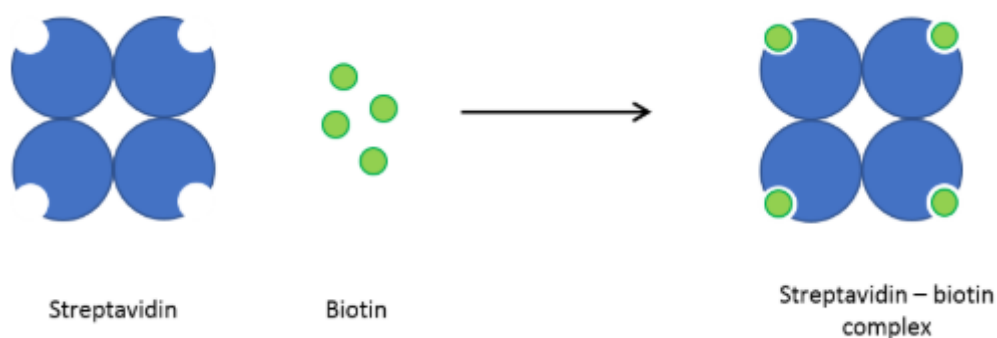


Figure 5.2. Binding ability of streptavidin and biotin creating a SA-biotin complex, required for detection of analytes in ELONAs

Figure 5.3 represents the ELONA assay carried out for the capture and detection of *E. coli* cells. The maleimide coated wells were initially washed twice with 200 μl PBST (0.05%). 100 μl of 125nM capture aptamer (ECO4F) was incubated in each well overnight at 4°. The wells underwent three wash steps before being blocked with 200 μl of skimmed milk blocking solution (5%) in PBST for 1 hour under rocking conditions to prevent/reduce non-specific adsorption of *E. coli* cells to the wells. The plate was again washed three times before incubating 50 μl of *E. coli* containing buffer for one hour. The bacteria were previously grown and plated for cell counting as previously described in section 2.7. The concentration(s) of the ECO3R reporter probe were prepared where 50 μl of this solution was placed in each well and incubated for 30 minutes at room temperature under rocking conditions. The wells underwent a further three washes and incubated with 50 μl of SA Poly HRP solution (1:20,000 in PBS) for 30 minutes under rocking conditions. The wells were washed 5 times with PBST to ensure all unbound SA Poly HRP was removed. 50 μl of TMB (used as received) was incubated with each well for 5 minutes whilst covered with foil. Here, a noticeable blue colour forms in the liquid and is dependent on the amount of SA poly HRP that has bound to the reporter aptamer which in turn is dependent on the concentration of captured cells. Finally, 50 μl of H_2SO_4 (1M) was used to stop the reaction

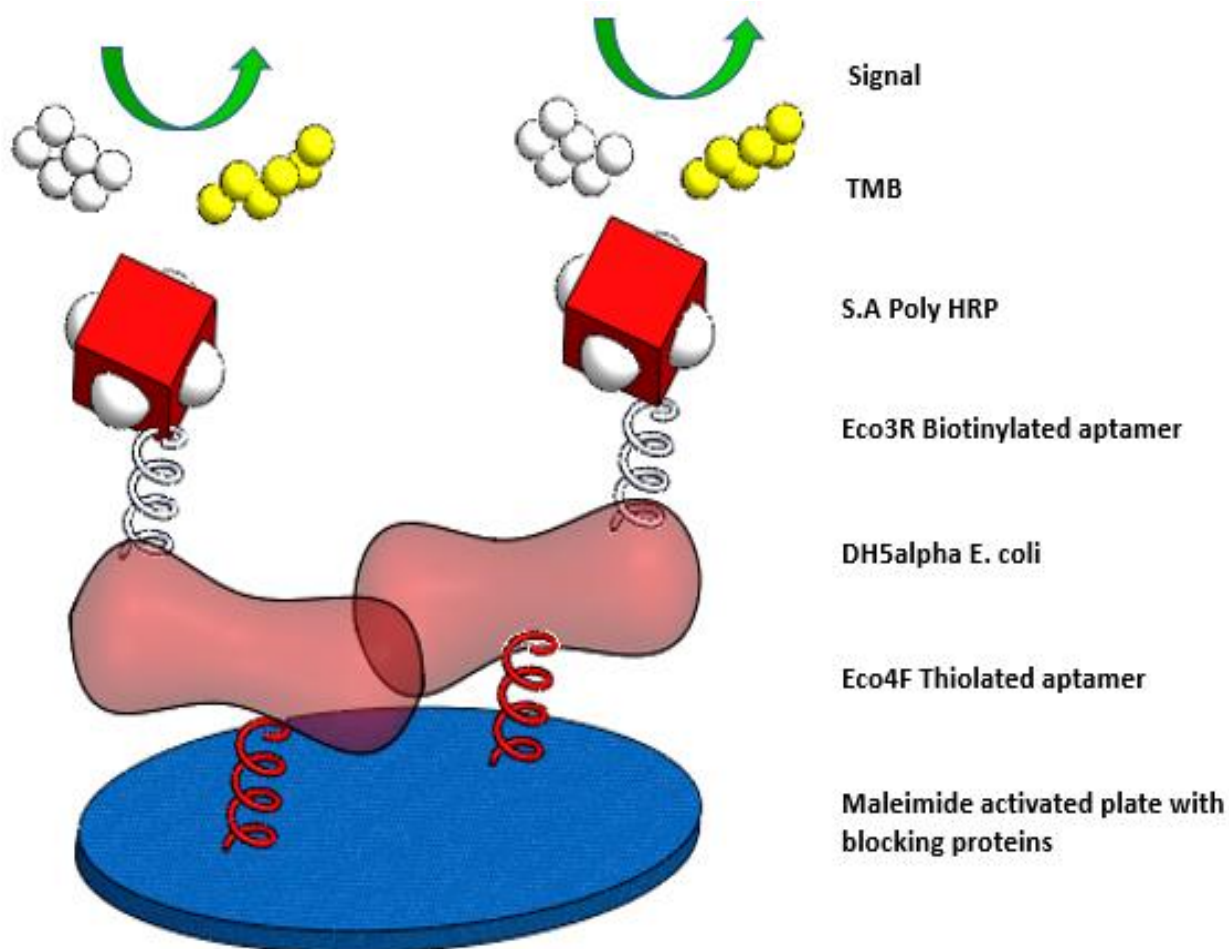


Figure 5.3. Components of the ELONA test carried out for the detection of *E. coli* cells where TMB is used to determine the presence, and concentration, of the analyte present.

All readings were obtained using the Spectramax 340 PC (bioNova, Scientifica Spain) spectrophotometer. All results obtained are based upon the Beer Lambert law where the concentration of compound has a linear correlation to its absorbance at a defined wavelength at a constant pathlength.

An initial checkerboard assay was carried out to determine the optimum concentration of capture and reporter aptamer probes be used to detect a dynamic range of DH5 α *E. coli* cells. Eight different concentrations of the capture probe were incubated in a maleimide plate overnight as previously described. Five separate reporter probes concentrations were used in conjunction with the *E. coli* cells (0nM – 1000nM) as shown in Figure 5.4.

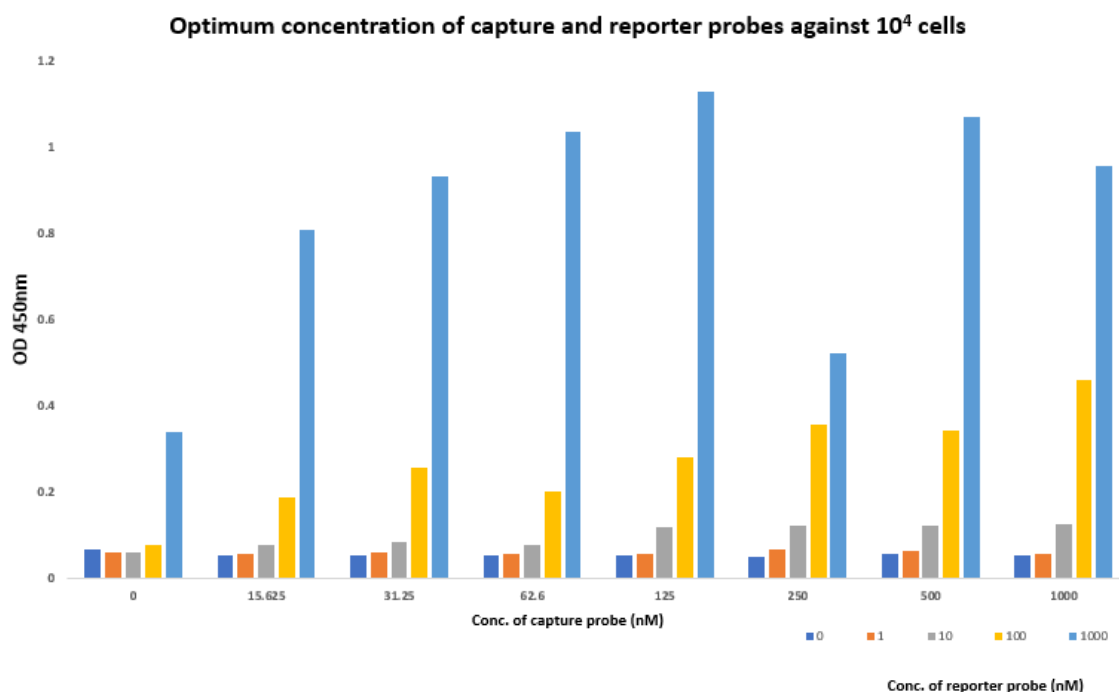


Figure 5.4. Bar chart indicating the optimum capture aptamer concentration based on the optical density of the ELONA assay against 10⁴ E. coli cells.

Consulting the bar chart results, the optical density (OD) for the 0nM capture probe incubated with 10⁴ E. coli cells shows very low signal against the 0, 1, 10 and 100 nM reporter probes. As no E. coli should be present for this control, as no capture probe was present, the background was found to be 0.0665 ± 0.01 OD. Based on the background signal it was determined that a capture probe of 125nM and two concentrations of the reporter probe (100nM and 1000nM) provided sufficient signal to be used for the remaining assays to determine a limit of detection (LOD). The maximum OD of 1.1264 was recorded and associated with the 125 nM capture probe and the 1000nM reporter. As this was the highest noted OD, this would provide the highest signal change for the ELONA assay. A secondary reporter probe concentration of 100nM used in conjunction with the 125nM capture probe was also considered for the ELONA assay, as the reporter probe still provided a good OD signal of 0.2791 even with a ten-fold dilution from the maximum signal provided by the 1000nM probe. The capture probe of 125nM was a fixed concentration of the aptamer applied to all further experiments. A distinguishable signal was also proven for 100nM and 1000nM, where they were both used for the detection 10⁴ E. coli cells (per 50 µl) for the initial experiment. Once the optimum capture probe concentration was determined, the ELONA plate optimisation parameters were regulated to find the LOD of the captured cells. To carry out an ELONA assay using the two reporter

aptamers (100nM, 1000nM ECO3R) used for detection of *E. coli* against a range of concentration of cultured *E. coli* cells. A 1:10 dilution of the cultured cells was prepared in PBS for use with a pre-functionalised plate.

5.3.1.1 Optimisation of ELONA

The initial experiment carried out to determine the LOD of the assay followed the ELONA protocol outlines in Section 5.3.1. The increase of OD with an increasing *E. coli* concentration against both reporter aptamers provided sufficient evidence that the assay was capable of detecting *E. coli* cells using spectrophotometric detection as shown in Figure 5.5, where the colorimetric intensity reduced with the reducing concentration of the bacteria in the wells, where a 1:100 dilution was incubated in the subsequent wells. The colour change from TMB (blue) to the stopped enzymatic reaction (yellow) from the 1M H₂SO₄ where the OD of the stopped reaction samples were recorded. The concentration of incubated cells from top to bottom corresponds to the decreasing cell amounts and therefore correlates to the decreasing OD obtained. With a visible colour change detected for the last wells for all reporter probes, the background was found to be too high and would become the first issue addressed for the optimisation of the ELONA. All OD values were inputted and plotted using GraphPad Prism 6 software where a sigmoidal curve was returned, where a saturation point was found for very high concentrations of bacteria (~10⁷ cells). A lower plateau on the graph was also found for the very low counts of bacteria (0-1000 cells) where the OD was very low and showed little discrimination between each value. The Prism software used automatically fit the data, where each experiment was carried out in duplicate. The R² and LOD were determined and shown in *Table 5-2*. The LOD was calculated by the formula bottom value + 3x standard deviation of the bottom value provided by the analysis parameters.

Table 5-2. R² and LOD for 1000nM and 100nM against a dynamic range of *E. coli* cells (10⁸ – 10⁰) CFU/50 µl.

	1000nM	100nM
R ²	0.7009	0.8237
LOD per ml	198787.9	5469.345
LOD per 50uL	9939.395	273.467

A high background existed for this assay, where the lowest OD for the 100nM reporter was 0.601 ± 0.076 where-as the 1000nM had a much higher background of 0.9012 ± 0.1102 . The point in which the lowest OD of the sigmoidal curve intercepts the y axis should be close to zero as it contains no pathogens, therefore a clear need to increase the washing steps was evident.

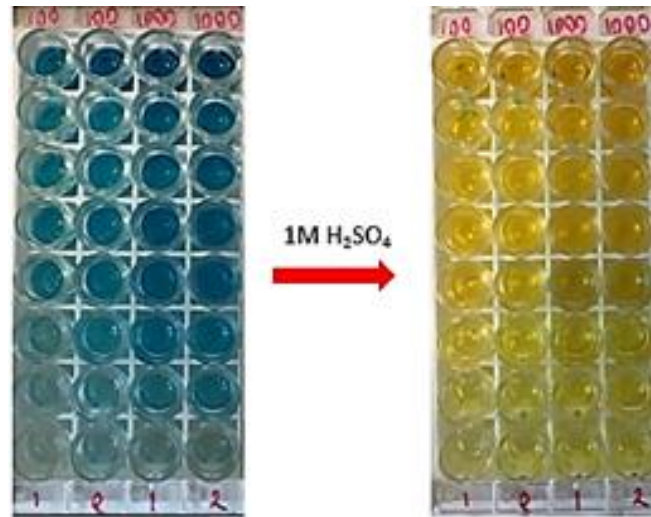


Figure 5.4. Displays the decreasing optical density (OD) vs. Log of *E. coli* where the OD of each well was then obtained using a plate reader set to 450nm wavelength.

A number of factors which may be responsible for the high background signal were examined by implemented a variety of changes to future ELONA assays, such as less incubation time with TMB solution, more washing steps between incubations and combined incubation steps between cells and aptamers. Implementation of heat during incubations steps to increase binding efficiency of *E. coli* and reporter aptamer. Incubating cells at 37°C to increase binding aptamer to cell binding efficiency and using PBS at room temperature rather than PBS stored at 4°C . Contaminated or inactive blocking buffer may lead to non-specific binding of the analyte. High concentrations of the SA Poly HRP or TMB may also have an effect on the background signal [21].

The initial attempt to reduce the background signal of the ELONA assay was to combine the *E. coli* and the two concentrations of the reporter probes to reduce the need of washing steps between incubations, where all remaining wash steps were increased to 4 between incubations. Both reporter probes concentrations were incubated with $50 \mu\text{l}$ of *E. coli* cells at a range of concentration (1:100 dilution) to give a total volume of $100 \mu\text{l}$ for

1 hour within well at constant temperature of $20 \pm 2^\circ\text{C}$ under rocking conditions. *Table 5-3* shows the extracted data from both the 1000nM and 100nM sigmoidal curves, where a significant decrease in the LOD for both probes was determined. The background was reduced to 0.69 ± 0.053 for the 1000nM and slightly reduced to 0.51 ± 0.005 for the 100nM.

Table 5-3. *Prism results for extrapolated data from response curves for 1000nM and 100nM reporter probes for E. coli and probe mixed incubation.*

	1000nM	100nM
R ²	0.7315	0.7341
LOD/ml	4124.56	669.934
LOD/50 µl	206.23	33.5

The reporter probes and E. coli appear to bind within same incubation step, reducing one washing and incubation step, which would contribute to a lower background signal than the previous experiment and reduce the assay time. The sigmoidal shape of the response curves was maintained where the same colorimetric change was observed for reducing E. coli concentrations.

The R² values for 1000nM and 100nM reporter probes combined with e. coli for a one step 1-hour incubation was relatively low, where further optimisation was required to increase the R² value and reduce background signal of the assays. To try increase this value, more values at lower range of concentration to try get a better fit on the curve. By comparing the data from *Table 5-3* the background interference was very similar for the 100nM probe, however both LOD values decreased for the 1-step E. coli and reporter probe incubation step [22]. By combining the e. coli and reporter aptamer incubation steps, the LOD decreased by 97.9% for the 1000nM and 87.75% for the 100nM. This provides promising for results for the assay, however a different strategic approach to reduce the background and increase the LOD was still required. A variety of assays were tested where the assay alteration, R² and LOD was shown for each.

Table 5-4 refers to four separate tests carried out with different variants to determine the best approach to improve the assay, where each LOD was clearly defined. Optimisation assay 1 refers to the same assay procedure as previously described, however a 1:20 E. coli

dilution approach was considered to increase data range tending toward 0 CFU/ml. The LOD of 135 CFU/ 50 μ l for the 1000nM reporter and 13 CFU /50 μ l for the 100nM where the altering the dilution factor significantly reduced the LOD from the previous assays carried out. Placing the plate under rocking conditions to promote analyte, capture and reporter probe contact. Optimisation assay 2 was carried out at 37°C to determine the effect of temperature on the assay for a 1:10 dilution of sample, following the same procedure as the assay results shown in *Table 5-3*. The LOD decreased for 1000nM reporter concentration to that previously reported for the same assay carried out at room temperature, however increased the LOD for the 100nM. The background signal was notably high for the 100nM probe, where an OD of 0.524 ± 0.11 was recorded. With such a high background signal, the results may have been the true value of the assay, as the background for the 1000nM probe was logged at 0.317 ± 0.087 . The LOD for the 1000nM probe was calculated to be 167.5 50 μ l which was still considered high however the results were promising as the 1:10 dilution only allowed for a condensed concentration range. Another approach adopted for optimisation assay 3 was to incubate the SA poly HRP complex under rocking conditions at 37°C for 30 minutes. Both LOD for the reporter probes were significantly higher, where values of 7,227 and 15,308 were calculated for the 1000nM and 100nM respectively. The background signal for both concentrations of reporter probe was significantly higher than the other assays. ODs of 0.542 ± 0.245 and 0.981 ± 0.487 were far too high for realistic results to be obtained and therefore this modification would be excluded for the ELONA. It would appear that elevating the temperature for the SA poly HRP increased the binding of the polymer to the well plates as well as the analyte probe complex. With 6 wash steps to remove unbound SA poly HRP, the huge background signal would imply the increase of temperature for the incubation of the polymer to increase non-specific adsorption to the wells themselves. Finally, optimisation assay 4 provides the LOD for a 1:100 dilution of *E. coli* samples where a thiolated ECO3R was used for a capture and the biotinylated ECO4F was utilised as a

Table 5-4. Four separate ELONA optimisation assay alterations to determine the effect of incubation and heating parameters on the LOD and R^2 values of the results

Method	Measurement	1000nM	100nM
1. 1:20 dilution of E. coli and reporter in a 1-step incubation at $20 \pm 2^\circ\text{C}$	R^2 Value	0.9908	0.9843
	LOD per mL	2716.45	258.226
	LOD per 50 μl	135.8225	12.9113
2. 1:10 dilution of E. Coli and Reporter in a 1-step incubation at 37°C	R^2 Value	0.9704	0.9815
	LOD per mL	3349.6544	15381.5464
	LOD per 50 μl	167.4825	769.05
3. SA Poly HRP incubation at 37°C with reporter and e. coli incubation	R^2 Value	0.9538	0.9471
	LOD per mL	144543.9771	306196.3434
	LOD per 50 μl	7227.15	15,308.45
4. 1:100 dilution of E. coli using inverted aptamers at $20 \pm 2^\circ\text{C}$	R^2 Value	N/A	0.9861
	LOD per mL	N/A	783
	LOD per 50 μl	N/A	39.15

reporter i.e. the aptamers were inverted to determine the binding ability of the oligonucleotides. This assay was only carried out for 100nM concentration however the LOD provided an interested result of 39.15 CFU /50 µl proving the robust nature of the assay. Considering the results, the best results were retrieved from optimisation assay 1 and 2, where assay 2 required a larger concentration range to determine.

Applying the findings from the optimisation assays, a 1:100 dilution of the E. coli samples was carried out where the bacteria and reporter were mixed together in a 1-step 1 hour incubation of the E. coli and reporter aptamer concentration at 37 °C under rocking conditions. By extending out the concentration range and incubating at a higher temperature the LOD for both reporter concentrations were significantly reduced. Figure 5.6 shows the overlay of the graphs for both reporter probe concentrations. The background signal of both assays was reduced to 0.181 ± 0.02 and 0.19 ± 0.023 for the 1000nM and 100nM respectively.

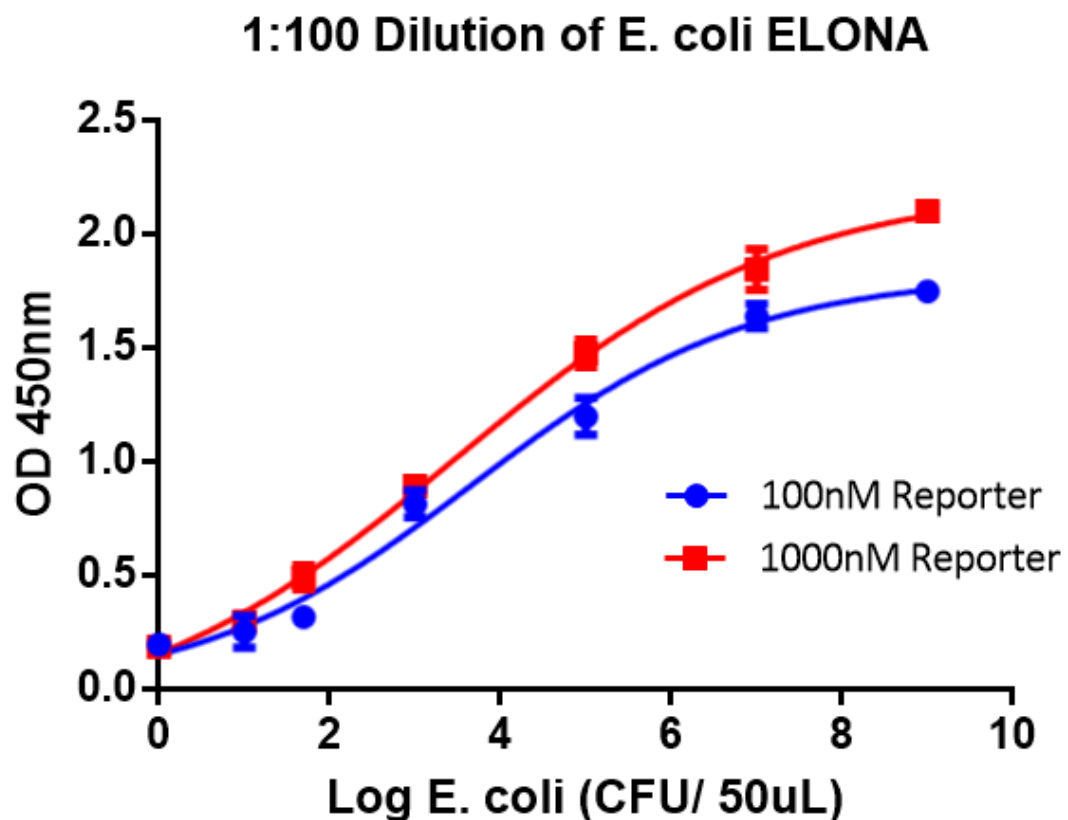


Figure 5.5. Graphical representation for the 1:100 dilution of e. coli incubated with 1000nM and 100nM reporter aptamer.

Table 5-5. Data associated with the 1:100 dilution of *E. coli* for 1000nM and 100nM reporter probes

	1000nM	100nM
R²	0.9964	0.9866
LOD/ml	41.81	23.065
LOD/50 µl	2.44	1.15

The calculated LODs of 42 CFU/ ml and 2.44 cell(s) per 50 µl for the 1000nM reporter probe which was a sizable reduction in the detection limit for the assay compared with previous efforts. The 100nM probe allowed for more sensitive detection, where 23 CFU/ml and 1.15 cell(s) per 50 µl was calculated. As 1 cell was the absolute minimum that could have been detected with the sample volume, the 100nM reporter probe with the optimised assay conditions proved to be the optimised probe concentration. Reflecting on both concentrations for the optimisation studies, the 100nM reporter probe had a lower LOD for the majority of the studies. The 1000nM may have had an increase of competitive binding to the analyte and therefore the 100nM probe was the superior concentration [21].

By increasing the washing steps between each incubation steps, the background was greatly reducing, as shown by the Y-intercept of the graphs previously described. The closer the value to zero, the less background noise of the assay. It has also reduced the probability that the colorimetric response of the ELONA plates is due to unbound SA Poly HRP molecules. The optimisation of the assay has proven that the ELONA analyte incubation carried out 37°C. The LODs of 1 and 2 cell(s) per 50 µl was demonstrated for both reporter aptamer concentrations. In conclusion, a range of concentration of *E. coli* cells can be captured and detected using a standard ELONA assay, thus proving that these aptamers are capable of binding to these cells at specific membrane regions. Preliminary tests also provided promising results that an inversion of the aptamers was still capable of binding to and detecting *E. coli* in the same ELONA assay. With the plates pre-functionalised with the capture aptamer, a sample to answer can be achieved in approximately 160 minutes.

5.3.2 Polymerase Chain Reaction Assays

PCR is a molecular biology technique for amplifying segments of DNA, by generating multiple copies using DNA polymerase enzymes under controlled conditions. As little as a single copy of a DNA segment can be amplified into millions of copies, allowing detection using dyes visible under UV light. The PCR procedure is as follows:

- Initialization: The initial step is necessary only for DNA polymerases that require hot-start PCR. The reaction is heated to 96 °C and held for 1-9 minutes.
- Denaturation: The reaction is heated to 94-98 °C for 20-30 seconds. The DNA template's hydrogen bonds are disrupted, and ssDNA molecules are created.
- Annealing: The reaction temperature is lower to between 50 and 65 °C and held for 20-40 seconds. The primers anneal to one end of the ssDNA template. The temperature is extremely important during this step. If it's too hot, the primer may not bind; and too cold, the primer might bind imperfectly. A good bond is formed when the primer sequence closely matches the template sequence.
- Extension/Elongation: The temperature during this step varies depending upon the type of polymerase. The DNA polymerase synthesizes a completely new DNA strand.
- Final elongation: This step is performed at 70-74 °C for 5-15 minutes after the final PCR cycle.
- Final hold: This step is optional. The temperature is kept at 4-15 °C and stops the enzymatic reaction [23].

Each step of the PCR is critical for the correct amplification of the eluted target probes, where cycle lengths and temperatures were optimised [24]. To initially determine whether the unmodified reporter aptamer was being successfully eluted, two maleimide strips were prepared with a 125nM capture aptamer and incubated overnight. The ELONA plate was prepared as previously described in Section 5.3.1, where all wells were incubated with 10^4 E. coli cells and a reducing concentration of the unmodified reporter aptamer (1000nM – 1fM) for 1 hour at 37°C. MilliQ H₂O was heated to 95°C were 20 µl was placed into each well for 3 minutes where it was aspirated and removed. Each sample was stored in individual eppendorf tubes and was stored at -20°C. The agarose gels were prepared by mixing 1.3g of agarose in 50mls of 1x TBE buffer and heated within a

microwave for 2 minutes, with regular stirring to ensure all agarose has been dissolved. 3 μ l of GelRed was mixed into the agarose solution where it was poured to set with the relevant comb size to create the loading pores. Gels can be stored in 1x TBE buffer at 4°C for 1 week. This assay type was termed Apta-PCR where the ELONA and PCR methods were combined for the whole cell capture and elution for amplification.

Table 5-6. Volumes of each component of PCR master mix required to carry out each amplification of the aptamers eluted from ELONA plates

PCR Master Mix	Volume Required for 100 μ l
10x Buffer	10 μ l
dNTPS	10 μ l
Fw. primer (10uM)	2 μ l
Rev. primer (10uM)	2 μ l
Sterile Milli Q	74 μ l
BSA (50mg/ml stock)	1 μ l
Dream Taq Polymerase (5U/ μ l)	1 μ l

Table 5-7. PCR program for thermocycler indicating temperature and times for each cycle

PCR program	
1 x 95 °C for 2 mins	
95 °C for 30 seconds	Optimised cycle number
60 °C for 30 seconds	
72 °C for 30 seconds	
1 x 72 °C for 5 mins	

1 μ L of eluted sample with 9 μ L of PCR master mix (Table 5-6) = total sample to be amplified. 10 μ l of total sample was placed into a PCR thermocycler where the PCR protocol (Table 5-7) was initiated. Once complete, the sample tubes were removed and were run using gel electrophoresis to determine the concentration of the amplicons. 5 μ l of total sample mixed with 4 μ l of loading buffer = total sample loaded into each well in gel. 5 μ l of stock DNA (0.5 μ g/ μ l) is added to 355 μ l ladder buffer (295 μ l Milli Q + 60 μ l loading buffer) to make stock solution. 3.5 μ l of stock solution is loaded into the well for the DNA ladder which contains 0.02 μ g (20ng) of DNA for analysis purposes.

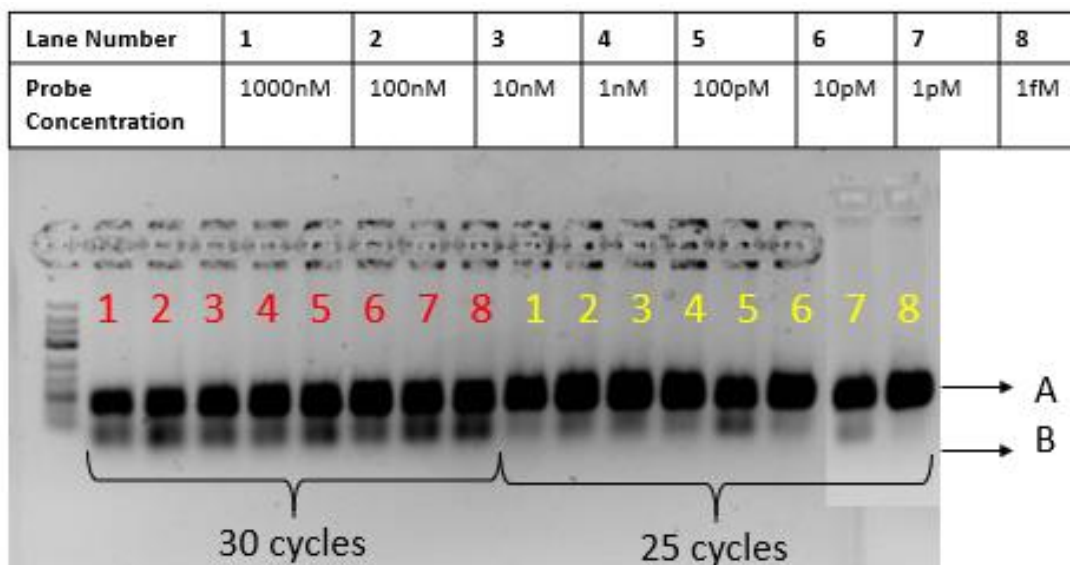


Figure 5.6. PCR of eluted reporter probe for a reducing reporter aptamer concentration incubated against 10^4 cells for 30(red) and 25(yellow) cycles. The upper band (A) represents the over-amplified eluted aptamer (~80bp) where the lower band is an indication of the primers (B).

The initial PCR that was run for the eluted reporter aptamer (unmodified ECO3R) from a concentration of 1000nM to 100fM incubated with 10^4 e. coli cells in 50 μ l PBS. Figure 5.7 portrays the PCR amplicons which were run for 15 minutes in a 2.6% agarose gel. The lanes numbered from 1-8 represent the eluted aptamer concentration where the lanes labelled red represent the elution samples which underwent 30 cycles of PCR compared to the yellow lanes which went through 25 cycles. The thick black bands (denoted by A) between each lane are indistinguishable, as with a reducing reporter aptamer concentration, a decrease in band intensity should be observed. From this, it can be deduced that the reporter aptamer was successfully eluted as the overamplified bands are present just below the 100bp ladder indicator. The second band produced below are the primers used for the PCR process which are present in the master mix (denoted by B). For a successful PCR assay, both probe and primers should be visible in the gel image. A pilot PCR was carried out to determine the optimum cycle number. The reducing aptamer concentration against 10^4 E. coli cells were run for 5, 10, 15 and 20 cycles to determine to optimum cycle conditions for amplicon production. Each gel was run with a positive and negative control, where the positive control contained of 1 μ l of the ECO3R (1 μ M) unmodified probe with 9 μ l of Mastermix. The negative control contained 1 μ l Milli Q water and 9 μ l of master mix.

Figure 5.8 displays the difference between the amplicons produced between the four separate cycle conditions.

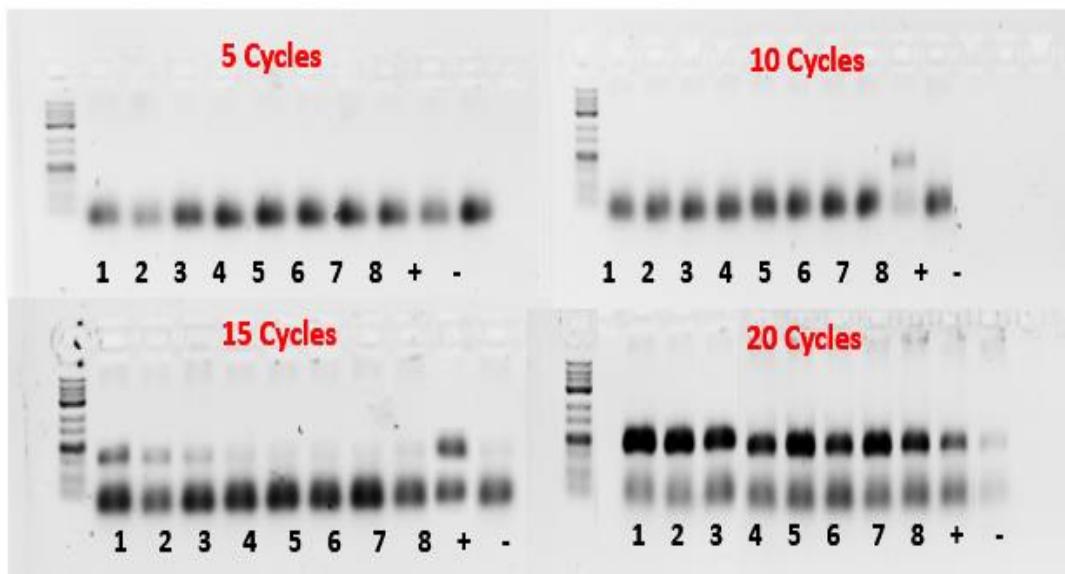


Figure 5.7. PCR pilot study to determine optimum cycle conditions for eluted reporter aptamer for 5, 10, 15 and 20 cycles.

The first image displays the products of 5 cycles, where there are no amplicons were produced or visible at the 80bp ladder indicator. Only primers are present at the 20bp line of the DNA ladder. The second image which displays the 10 cycles gel has the same results as 5 cycles, however the positive control is present. The third image provides more promising results as the reducing band intensity is present at the 80bp mark on the DNA ladder with a strong positive control line.

Despite the amplicons being present, the products are slightly under amplified as only a distinction can be made between lanes 1, 2 and 3. The most prominent amplification occurred for 20 cycles where the products are over amplified as it's very difficult to differentiate between the band intensity, however there is a slightly reducing intensity between each lane as the height of the bands appear to diminish slightly with a reducing probe concentration. At this cycle number, there is also some contamination observed for the negative control being amplified. The pilot PCR proved essential in the initial optimisation of the PCR process, where successful amplification is observed. The PCR master mix and PCR cycle program were adequate for DNA amplification. However, the

specific cycle number must be determined before specific reporter aptamer concentrations are used against a reducing range of *E. coli* cells. Both 15 and 20 cycles of PCR produce bands of reducing intensity with a decreased concentration of the reporter aptamer. 15 cycles portray a clear decrease in band intensity against the decrease in reporter aptamer where-as 20 cycles produces over-amplified products as no differentiation is present between amplicon bands. 17 cycles were applied to the same system of reducing eluted aptamer concentrations. Figure 5.9 displays the gel image acquired from the UV transilluminator where the ladder provides an insight into the amount of DNA produced by the amplification at 17 cycles.

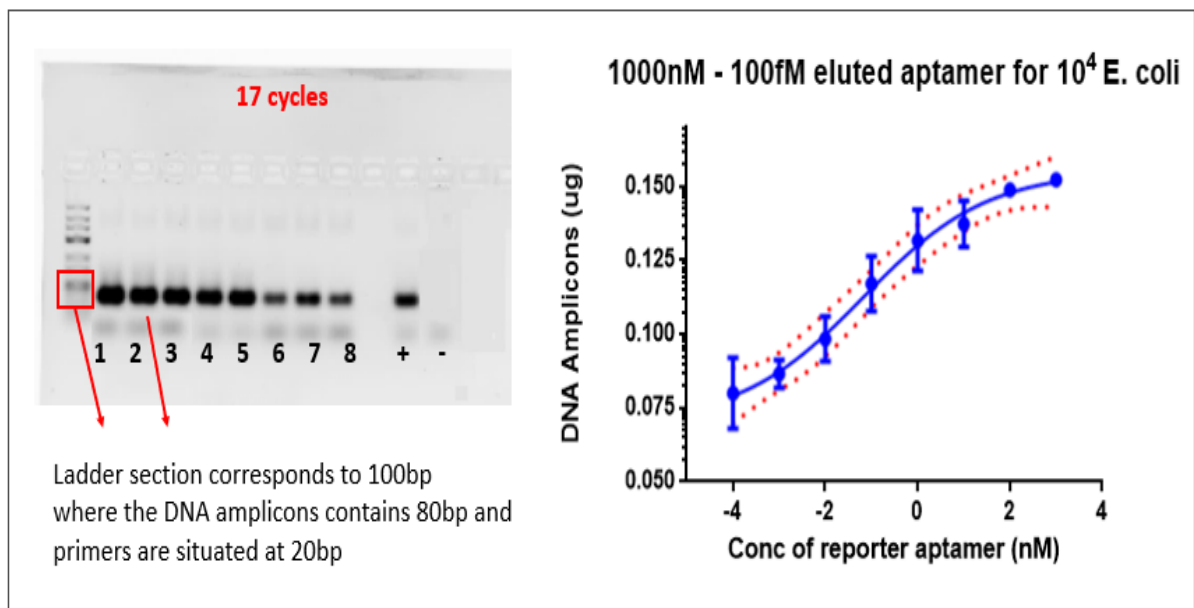


Figure 5.8. Gel image represents the amplicons and primers produced from 17 PCR cycles where there is a clear reduction in band intensity from lane 1 to 8. A graphical representation portrays the sigmoidal curve of the amount of DNA amplified from the concentration of the initial reporter aptamer incubated with the 10^4 *e. coli* per well.

The ladder contains $0.02\mu\text{g}$ of DNA which is used to determine the DNA produced through the PCR method. ImageJ analysis was used to determine the pixel density of each band, which is correlated to the pixel density of the $0.02\mu\text{g}$ ladder. This data was analysed using GraphPad Prism 6, where the DNA amplicons are plotted vs the concentration of the eluted reporter aptamer. In this case, lane 1 represents the highest concentration of 1000nM where each lane contains a 1:10 dilution from the previous lane.

Once the cycle number and master mix solution were optimised, the PCR assay for the detection of *E. coli* cells suspended in 1x DPBS buffer was carried out using a fixed concentration of unmodified reporter concentration. A reducing concentration of 10^8 - 1

cells per 50 μ l was prepared. Observing the results obtained in Figure 5.9 there is a difference in the band intensity between the eluted probes in lane 4 (1nM), 5 (100pM) and 6 (10pM). Initially, the 1nM reporter aptamer was observed for 15 and 17 cycles.

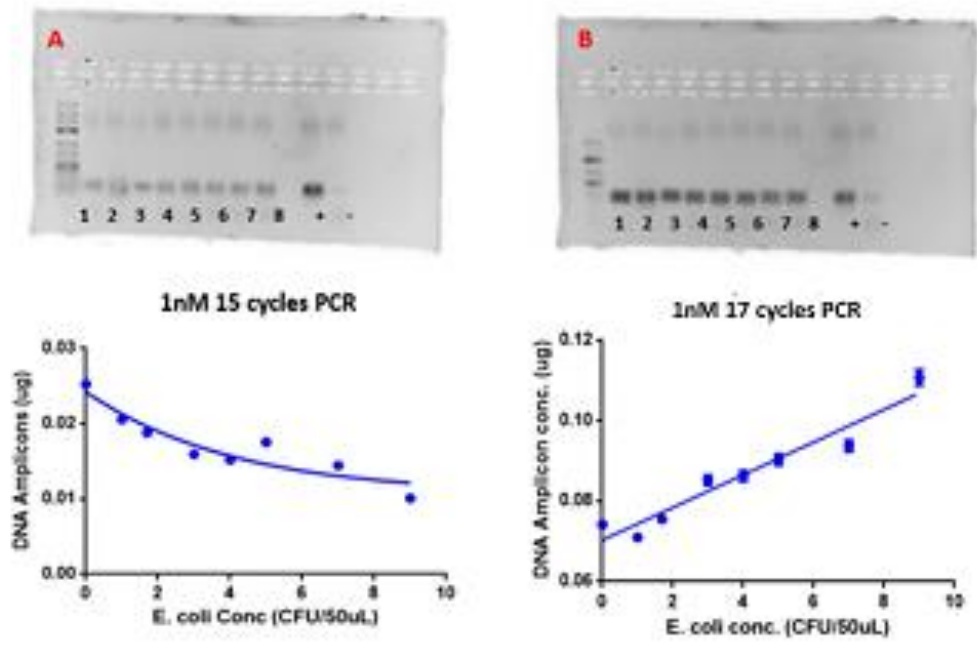


Figure 5.9. Difference in amplification for ECO3R unmodified reporter (1nM) for 15 cycles (A) and 17 cycles (B) where 15 cycles has under-amplified products

Figure 5.10 (A) portrays the difference in band intensity produced between 15 and 17 cycles for the same reporter aptamer concentration. The DNA amplicons for the 1nM eluted probe amplified for 15 cycles under amplified the eluted aptamer un-evenly without an observational decrease in band intensity for the decreasing concentration of e. coli cells and was immediately discredited from the optimisation. The graphical representation of the DNA concentration proves the unreliability of 15 cycles to determine and detect a difference in cell concentration. As a sigmoidal response was expected, as previously observed by the ELONA response in Section 5.3.1.1, the cycle number was too low to analyse for the DNA amplicons. Figure 5.10 (B) displays the gel image acquired for 17 cycles of the eluted aptamer for the same reducing concentration. The decrease in band pixel density corresponds to the decrease in cell concentration, however a more linear response is observed rather than a sigmoidal graph. A lower saturated lower range plateau allows for a more accurate representation of the amplified

eluted probes, where lanes 7 and 8 were incubated against very low cell counts (10 and 1 respectively) and therefore were expected to have similar amplicon quantities. The LOD extrapolated from the graphical data is 7 CFU/ml. A strong band intensity for 1nM allows the possibility of reducing the concentration of the reporter aptamer whilst maintaining the integrity of the LOD for the PCR assay. All data obtained was carried out in triplicate to ensure the reproducibility of the obtained results. To ensure the correct transfer of the elution solution, all pipette tips were autoclaved, and O₂ plasma treated for 5 mins at 10sccm to improve the repeatability of the assay. As the cycle number was optimised, further studies were carried out in an effort to reduce the LOD of the assay for lower probe concentrations.

A range of initial reporter aptamer concentrations were incubated against a dynamic range of *E. coli* cells, as previously described. A 1:10 dilution of reporter aptamer was individually incubated against the cells for one hour at 37°C under rocking conditions. 100pM – 10fM of the reporter probe concentrations were eluted and amplified for 17 cycles. All amplicons were run on a 2.6% agarose gel containing 3 µl of 10,000x GelRed (Biotium, UK). All gels were run for 20 minutes at 120V in 1x TBE buffer and examined on the Syngene G:Box UV transilluminator (Cambridge, UK). All images were examined using ImageJ to determine the pixel density of the individual amplicon bands, which was analysed against the DNA ladder to determine the amplicon DNA concentration.

Figure 5.11 portrays the five separate concentrations of the reporter aptamer incubated against the dynamic range of *E. coli* cells, where the corresponding DNA amplicons vs. cell concentration was plotted to form a dose response (variable model) sigmoidal curve which is the most typical method for data analysis for PCR-ELONA type assays. The graphical representation of the results shows the decreasing concentration of DNA amplicons as the initial reporter probe concentration was reduced. 10fM is the minimum concentration of reporter aptamer that can be used as the LOD significantly increases for lower concentrations of the reporter probe as band intensity diminishes to a point where it's difficult to distinguish between the amplicon bands observed with UV imaging. As 10fM is a low concentration of reporter aptamer, any concentration lower than this would be difficult to elute for maximum retrieval of the ssDNA.

The tabulated results indicate that the use of 100pM as the reporter aptamer for use with the PCR assay was the optimum concentration to be eluted and amplified for 17 cycles. A good R^2 value of 0.9934 validates the fitting of the data, whilst an LOD of 5 CFU/ml was obtained. Again, the LOD was determined using the formula of the bottom value + 3x standard deviation of the bottom value provided by the analysis parameters from the Prism software. From the associated gel images for the 100pM aptamer, a very distinctive decrease in band intensity exists, where little to no contamination for the negative control was visible. The 10pM aptamer concentration experiments and PCR provided the highest LOD from the overall tabulated data. With an LOD of 46 CFU/ ml and an R^2 value of 0.9756 The 10pM eluted aptamer provided alternating band intensities for the higher E. coli concentration, where large error bars were observed. The 1pM aptamer proved the best fit values with an R^2 value of 0.9923 with a calculated LOD of 37 CFU/ml.

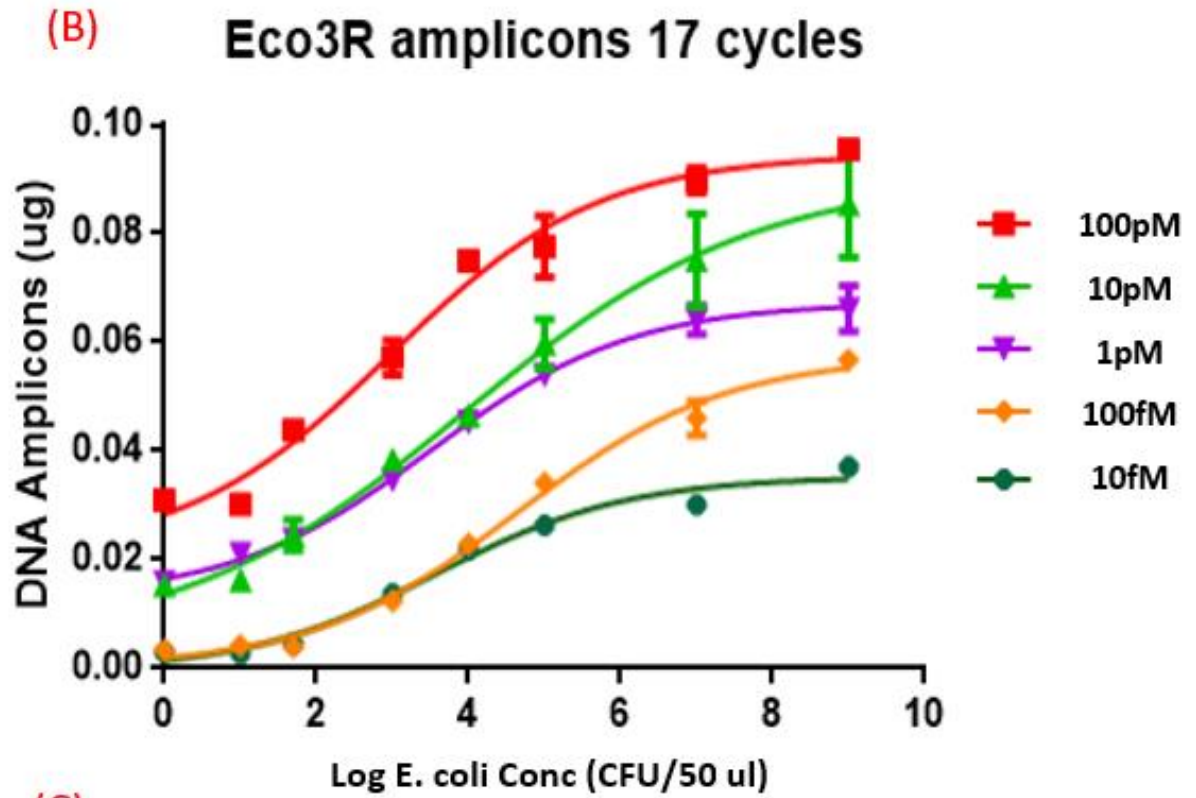
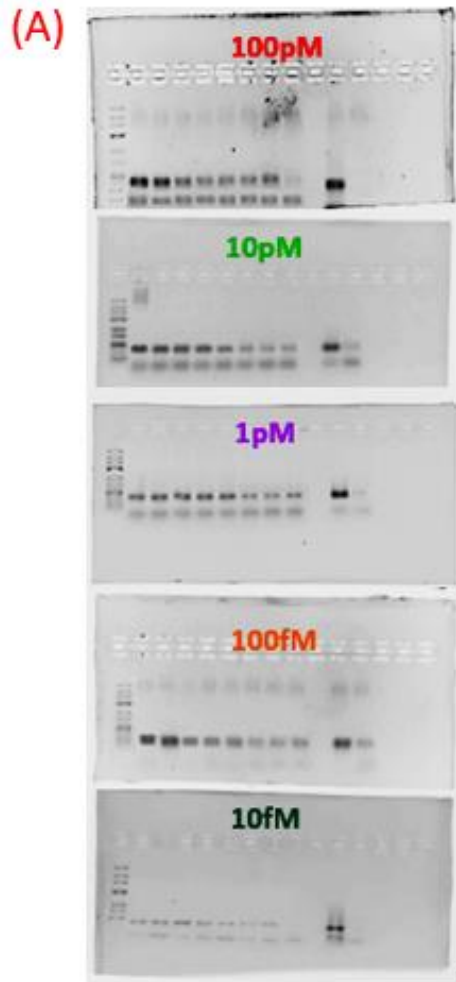
Reducing the concentration of the aptamer by a tenfold dilution again, the 100fM aptamer also provided a good R^2 and LOD value of 0.9884 and 6 CFU/ ml. With this low LOD it must also be noted that some contamination was observed for the negative control. This may be from contaminated MilliQ water or a contamination of the master mix during preparation. As the band intensity of the negative control was subtracted from the band intensity of the amplicon concentration, the true values of the amplicons are plotted. Observing the graphs plotted in Figure 5.11 the linear range of the sigmoidal graph has a high slope, where by removing the background from the negative control significantly reduced the number of observed amplicons for the lower E. coli range.

Finally, the 10fM eluted aptamer provided good results, where the R^2 and LOD were 0.9833 and 25 CFU/ ml respectively. Observing the gel image however it is very difficult to distinguish by observation between the presence of the high and low E. coli concentration. Using the ImageJ to determine the pixel density and utilising excel and Prism software to determine the absolute value of these bands It would be difficult to gauge whether the detected E. coli concentration is high or low. Comparing the band intensity of the 10fM to 100pM, is it simple to qualitatively determine if the E. coli is abundant or not compared to that of the 10fM gel image. For the higher range of the E. coli cells, the sigmoidal graph saturates. Again, the lower plateau of the graph shows little amplification of the reporter probes for the very low concentrations of the E. coli cells.

The linear range of the sigmoidal graph shows the most interested data, where the DNA amplicons correlates to the E. coli cell concentration. The sensitivity of the assay depends of the optimum probe concentration, as too much may lead to non-specific binding of the probe to the plate well walls and too little may be too difficult to elute and amplify.

Observing the gel images, the band intensity of the negative control increases as the reporter aptamer concentration decreases which is possibly due to the intensity of the amplicons present. For large amounts of DNA amplified for the 100pM probe, the amplicon bands may be intense enough that the UV transilluminator automatically adjusts the camera focus and saturation, and therefore if a band is present for the negative control, the software cannot detect it and the band isn't amplified as much as the other amplicons present. This contamination could be introduced at any stage of the sample preparation or even from the elution of the reporter aptamer, where sometimes the capture aptamer could be eluted and become amplified during the PCR process. Comparing the 100pM to the 10fM gel images, the pixel density obtained from ImageJ analysis for both aptamer concentration increased more than ten-fold, therefore the risk of contamination and false results increases as the reporter concentration is reduced.

The PCR assay provides good results regarding a low limit of detection for all aptamer concentrations, Taking the negative control into consideration, the 100pM reporter aptamer provided the best results regarding E. coli detection in clean buffer. With a very low LOD of 5 CFU/ ml and a good R^2 value it was found that the optimum conditions for the PCR-ELONA assay employed for the calibration curves were 100pM reporter aptamer eluted using O_2 plasma treated pipettes, one hour total incubation time of the E. coli and reporter tamer at 37°C under rocking conditions, 17 PCR cycles using the parameters outlined and a total gel run time of 20 minutes at 120V with the total assay duration of 195 minutes.



(C)

	100pM	10pM	1pM	100fM	10fM
R ² value	0.9934	0.9756	0.9923	0.9884	0.9833
CFU per ml	5.121	45.993	36.755	5.93	25.43

Figure 5.10. (A) Five PCR gel electrophoresis images for each concentration of reporter probes incubated against a dynamic range of *E. coli* cells (10^8 – 1 CFU/ 50 μ l). (B) portrays the overlaid sigmoidal curves obtained for all 5 images where the amount of DNA amplicons is plotted against the concentration of bacteria where (C) shows the tabulated data from the 5 gels presented.

5.3.3 Recombinase Polymerase Amplification

Recombinase Polymerase Amplification (RPA) was studied in an effort to reduce assay time and to increase the simplicity and feasibility of the E. coli detection procedure. The isothermal amplification method avoids the need for thermo-cycling as a standard optimised temperature is obtained and applied for a specific length of time to allow the three core proteins to amplify the ssDNA rather than using heat to denature and amplify the target as previously carried out using PCR methods. Initially, the RPA time is optimised, to avoid both under and over amplification of the amplicons. Five separate RPA reactions were carried out for a reducing concentration of the ECO3R unmodified reporter (1000nM – 1fM) against a fixed concentration of 10^4 E. coli cells using the same elution conditions as used in Section 5.3.2.

1 μ l of eluted sample was added to 9 μ l of RPA master mix (*Table 5-8*) which determines the total sample to be amplified. The Master-Mix must be prepared fresh before each test to avoid contamination and damaging the proteins. This solution must be prepared on ice to avoid the activation of the core proteins until added to the sample and amplified under heating conditions. Using a TwistAmp basic kit, the desired volume of the master mix was prepared and added to the sample before the application of heat to the PCR tubes.

Table 5-8. *Required volumes of each component of RPA master mix required to carry out each amplification of the aptamers eluted from ELONA plates.*

RPA Master Mix	Volume Required for 100 μ l
Twist DX Buffer	50 μ l
Fw. primer (10uM)	4.8 μ l
Rev. primer (10uM)	4.8 μ l
Sterile Milli Q	26.4 μ l
MgOAc (280mM)	5 μ l
Reaction Pellets (From kit)	2

The RPA reaction is carried out for 5, 10, 15, 20 and 30 minutes for a reducing concentration of the reporter aptamer to determine to optimum amplification times for the process and what concentration of aptamer to use for the future RPA assays.

9 μ l of sample was individually loaded into each well of the gel (5 μ l RPA product and 4 μ l loading buffer). 3.5 μ l of the DNA ladder was also added to the first well and where the gel was run for 15 minutes at 120V.

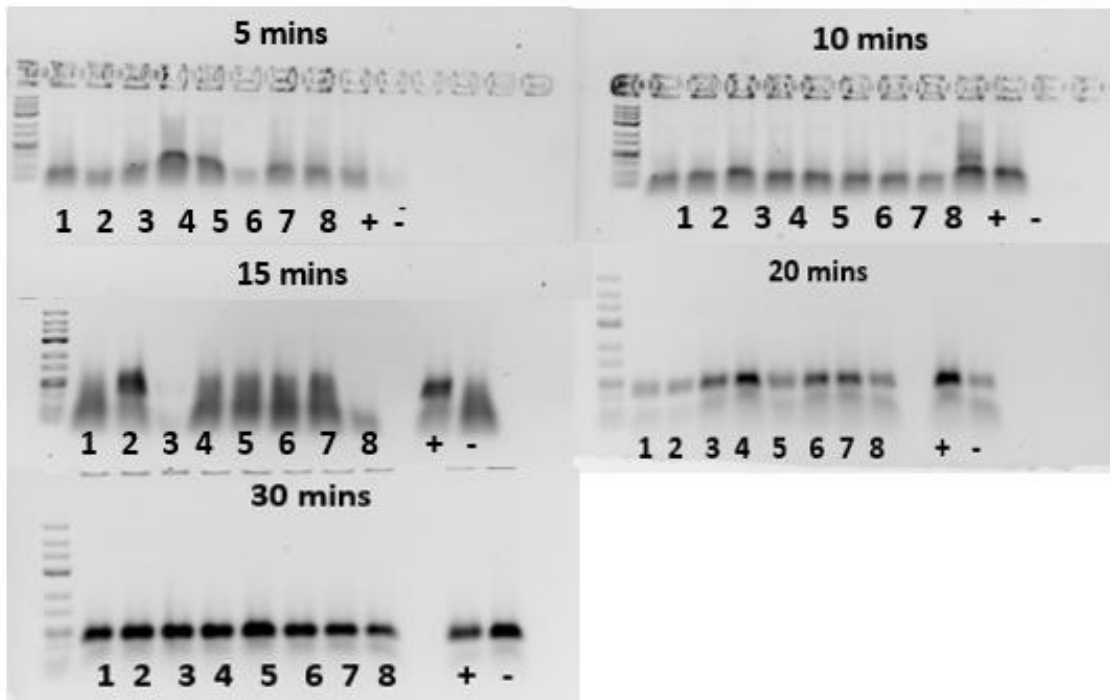


Figure 5.11. *Effect of incubation times for the amplification of RPA amplicons, where under-amplification is observed for 10 minutes and less and over-amplified for 30 minutes for a reducing concentration of eluted aptamers incubated against 10^4 E. coli.*

Figure 5.12 portrays five separate gels to determine whether the RPA was successful at a given time and which concentration of aptamers to incubate against the reducing concentration of E. coli cells. As the amplicons can be under or over amplified, a specific incubation time must be determined for optimum amplification time. Double bands are observed for 15 and 20 minutes for the reducing concentration of the ECO3R reporter probe. Smearing was observed for the RPA gels as the DNA amplicons migrated through the agarose gel. There are a multitude of reasons which may affect the band sharpness of the amplicons. The voltage applied to the system for band separation plays a pivotal role in reducing the amplicons smearing for UV imaging [25]. When the voltage is too low the mobility of small DNA fragments (< 1kb), such as the aptamers tested, is reduced which results in band broadening due to diffusion and dispersion. Too high a voltage can cause thermal diffusion and asymmetric heating to occur. The pore size of the agarose also has an effect in the DNA migration. However, a 2.6% gel allows for good band separation which is evident as both RPA products and primers are visible [26]. As it was proved that

RPA was a suitable process for the amplification of the eluted aptamers and the mastermix was adequate for this amplification, the effect of time on the assay was observed. Three concentrations of the reporter probes (10nM, 1nM and 100pM) were chosen based on the amplification of the products shown in Figure 5.12. Effect of incubation times for the amplification of RPA amplicons, where under-amplification is observed for 10 minutes and less and over-amplified for 30 minutes for a reducing concentration of eluted aptamers incubated against 10^4 E. coli. as there is some differentiation between bands 3, 4 and 5 for the 20 minutes incubation. Despite the amplicons smearing and unequal amplification of products, the RPA assay still amplified and therefore proves the hypothesis that the ssDNA can be amplified under isothermal conditions. The voltage was decreased to 100V for 25 minutes to reduce the effect of band broadening. The same RPA procedure is followed for sample preparation, where the RPA time of 10, 15 and 20 minutes were examined for a difference in band intensity corresponding to the bacterial concentrations

RPA optimisation reactions were carried out for the three eluted reporter probes (10nM, 1nM and 100pM) against a range of concentrations of E. coli (10^8 -1 CFU/ 50 μ l) using 20 μ l of Milli Q water heated to 95°C. The heated water was pipetted into each well and aspirated on removal after 10 minutes. The lower voltage reduced the band broadening and the effect of time for the isothermal amplification is shown to overamplify the higher concentration of reporter aptamers at 20 minutes and under amplify all products at 10 minutes. It was determined that the optimal time for amplification was 18 minutes which was applied to all further RPA assays. Five separate concentrations of the reporter aptamer were used (10nM – 1pM) and incubated against the reducing concentration of E. coli cells, where the same analysis was carried out as previously described in Section 5.3.2 for the PCR assays.

Figure 5.13 portrays all five RPA assays with corresponding gel images. The highest concentration of 10nM gave the highest LOD from all the assays. With the calculated LOD of 140 CFU/ ml, the 10nM probe was disregarded. results

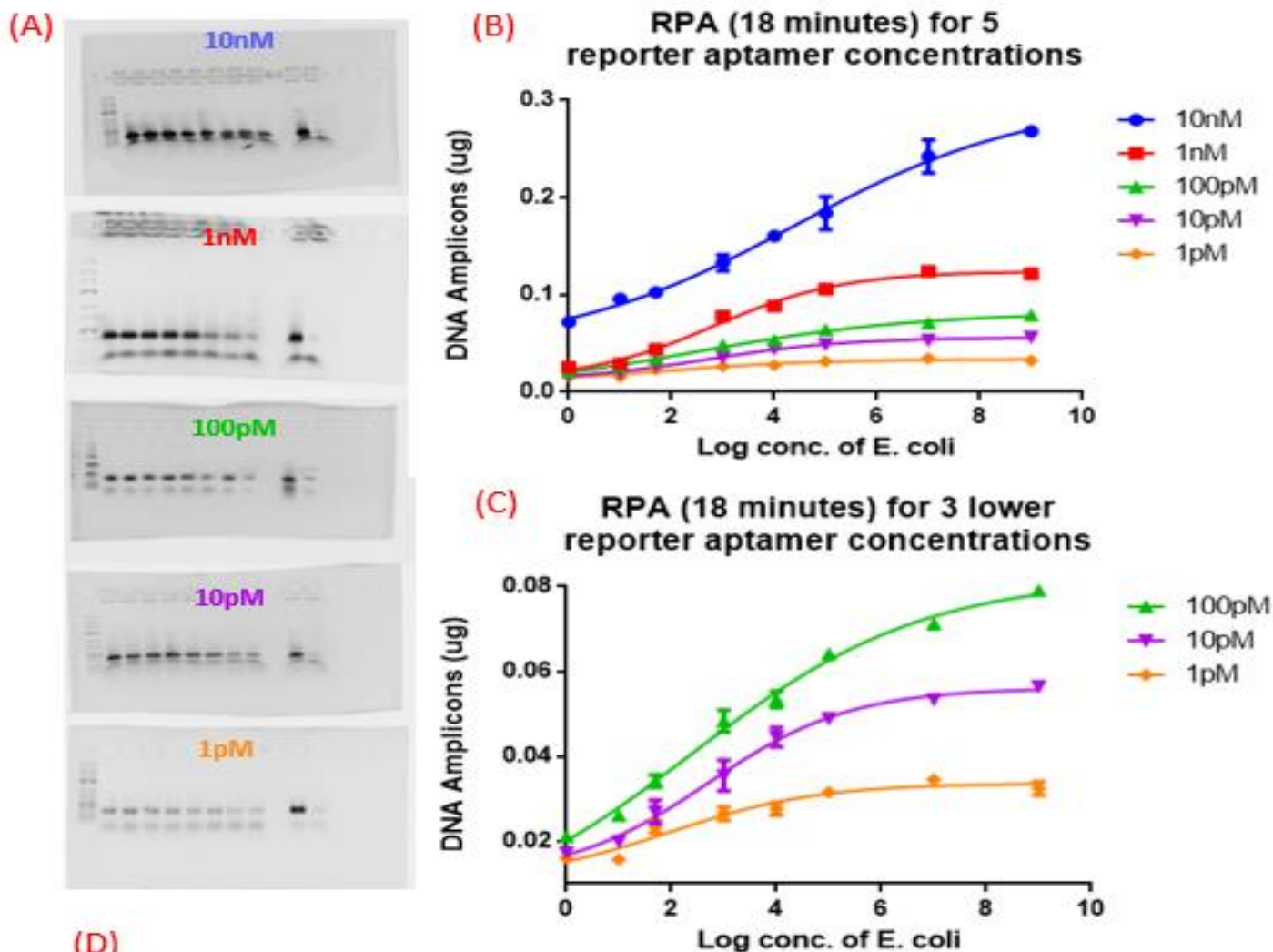


Figure 5.12. (A) Five RPA gel electrophoresis images for each concentration of reporter probes incubated against a dynamic range of *E. coli* cells ($10^8 - 1$ CFU/ 50 μ l) with an amplification time of 18 minutes (B) portrays the overlaid sigmoidal curves obtained for all 5 images where the amount of DNA amplicons is plotted against the concentration of bacteria where (C) shows the three lower concentration of the probes and (D) the tabulated data for all 5 gels.

With the concentration of the reporter aptamer being so high in comparison to the reporter aptamer used for the PCR assay, this concentration of aptamer would not be a good basis for further experiments due to the discrepancy between the n=3 assays. The fitting of the sigmoidal curve improves for all additional RPA assays. The 1nM assay provided good results where an LOD of 9 CFU/ml was obtained. Comparing the LOD obtained for the 100pM and 10pM the obtained were quite similar where an LOD of 32 CFU/ml and 37 CFU/ml was recorded. Finally, an LOD of 10 CFU/ml for the 1pM aptamer was recorded for the final RPA assay. It is safe to assume that the LOD obtained for both the PCR and RPA are quite similar, proving the robust nature of the RPA technique. Reflecting on the results, the 1nM reporter probe provided the lowest LOD of 9 CFU/ml, where the corresponding gel image does show a decrease in the band intensity. The amplification time of 18 minutes was sufficient enough to amplify to products and allow discrimination between the amplicons produced against the reducing E. coli range. With a total assay run time of 103 minutes, there is a difference of 92 minutes between the PCR and RPA methods. This proves promising results that the RPA method of DNA amplification can be used as an alternative method of amplicon production if assay duration was a concern.

Another optimisation process which may be examined is the type of elution solution to be used for the removal of the reporter probes. Salt solutions have been proven to remove the ssDNA from cells without disturbing the cells themselves [27]. Two salt solutions are examined; 2M NaCl and 100nM NaOH. These salt solutions are left for 10 minutes within each ELONA well, aspirated and removed to be amplified using RPA. The samples were left for 20 minutes under previously described RPA conditions. A gel run-time of 20 minutes was applied to the gels at 100V. 100nM NaOH looks promisingly as a preliminary result as the negative control is very low despite the DNA being over-amplified in all cases. Again, optimisation conditions need to be further explored in order to achieve a gel with decreasing band intensity corresponding to the E. coli dilutions. As cells tend to burst at high temperature, which may release a plasmid which may interfere with the PCR and RPA amplification, it is interesting to note that salt solutions may be used as easy to prepare elution solutions where other, more delicate whole cells, may be incubated with aptamers which may need to be eluted. Despite the negative control being contaminated in both cases, evidence of a double band exists in both gel images, therefore providing

enough evidence to show that the eluted and amplified aptamer is that of the reporter ECO3R-unmodified ssDNA.

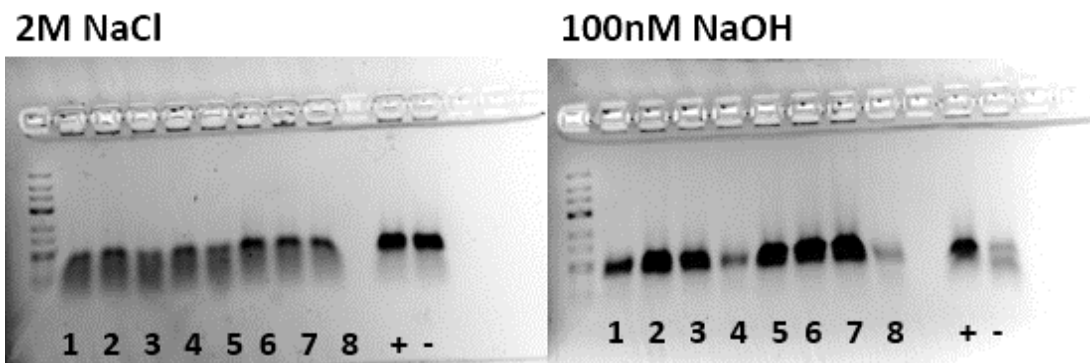


Figure 5.13. Two gel images where two separate salt solutions were used to elute the reporter probe from a reducing concentration of *E. coli* cells.

Comparing both sets of PCR and RPA assays, both assays provided good results for the low CFU count for *E. coli*. For the PCR assay, an LOD range of 5-46 CFU/ ml was obtained, compared to 9-140 CFU/ ml for the RPA assay. With low counts of CFU being detected, the aptamers proved to be a reliable capture and detection source, where the use of antibodies was completely disregarded. In comparison the Apta-PCR, the Apta RPA assay was more rapid, as the amplification process was complete within 18 minutes whilst also achieving an LOD of 9 CFU/ ml. This is evidence to support that RPA assays are potentially suitable for low resource settings [28].

Comparing all three methodologies, the best LOD for two concentrations of reporter aptamers were compared to determine the best approach for *E. coli* detection using the assays as shown in **Table 5-9**. The ELONA assay was a simple procedure which used the highest concentration of the reporter aptamers and gave the highest LOD values for both concentrations. The PCR assay offered the lowest LOD for two extremely low concentrations of the ECO3R-unmodified aptamer. Due to the nature of the assay, low concentrations amplified during the cyclic process gave an adequate band intensity to detect *E. coli* within the range of 5-6 CFU/ml for the 100pM and 100fM reporter respectively. The assay time however was the longest of all three studied, with the PCR process taking 55 minutes and the gel run time of 20 minutes, including the initial ELONA plate preparation for the while cell capture. This is the biggest drawback of the assay as

the lengthy thermocycling process depends on the required amount of cycles and their individual time constraints. In an effort to reduce assay time and the complexity of the Apta-PCR process, the Apta RPA assay was studied. This process was notably faster, where the amplification being accomplished in just 18 minutes at 37°C.

Table 5-9. Comparison of three assay types and their correlated LOD.

Method	Optimum Reporter Aptamer Conc.	LOD (CFU/ ml)	Assay Time (min)
ELONA	1000nM	42	160
	100nM	23	
Apta-PCR	100pM	5	195
	100fM	6	
Apta-RPA	1nM	9	103
	1pM	10	

With all LOD existing within the range of $10^0 - 10^2$ CFU/ml, the aptamers have been established as a sensitive capture and detection complex which is highly robust for use with a variety of biological assays.

5.4 Conclusion

The use of aptamers instead of antibodies have proven to work very effectively when combined with ELONA, Apta-PCR and Apta-RPA assays for whole cell detection. The use of these synthetically produced ssDNA as a capture and detection tool is an exciting alternative to eradicate the use of animal produced antibodies for bio-assay development. These high affinity oligonucleotides are sensitive as they only bind to complimentary sites on the analyte, reducing the chance of non-specific binding by other biomolecules. As they are synthetically produced, they are also highly reproducible, unlike antibodies which can widely vary between batches [29].

The use of aptamers in the ELONA delivered an LOD of 23 and 42 CFU/ml for the 100nM and 1000nM aptamer concentration respectively with a total assay duration of 160 minutes. The optimised assay comprised of a 1-step incubation between analyte and the secondary aptamer at 37 °C which provided the best results regarding the lowest achievable LOD. The robust assay allowed for low CFU detection of whole cells in PBS buffer proving the ability of the aptamers to recognise and bind specifically to the target analyte for a dynamic range of *E. coli* (10^8 – 1 CFU/ml). Carrying out the *E. coli* and aptamer incubation step under shaking conditions helped replicate the initial conditions in which the *E. coli* was grown, where the shaking of the plate helps introduce and circulate oxygen into the plate, essentially creating an ideal environment for the *E. coli*. Heating the environment to 37°C also replicated model conditions in which *E. coli* tends to thrive [30].

In addition to this, the shaking of the plate increased the probability of aptamer and whole cell contact in which the bio-recognition site the ECO4F aptamer would adhere to. By implementing these specific conditions, the LOD of the assay was reduced to 42 and 23 CFU/ ml for the 1000nM and 100nM probes. As previously described, both ECO3R and ECO4F aptamers have a high affinity towards to OMPs of the *E. coli* species and therefore a preliminary test to ensure the integrity of the assay was carried out where the capture and detection aptamers were inverted. An LOD of 7.83×10^2 CFU/ ml for the 100nM was obtained, however with the optimised ELONA assay conditions it is highly suspected that this LOD would be significantly reduced.

The Apta-PCR assay was optimised to detect the same dynamic range of *E. coli* to detect lower counts of CFUs. Utilising the initial steps of the ELONA, the PCR and RPA elution samples were obtained however much lower concentrations of the secondary aptamer were required, as the amplification aspect of the assays required a much lower concentration. The Apta-PCR was optimised for 17 cycles were the optimum concentrations of the reporter aptamer was deemed to be 100pM and 100fM giving a LOD of 5 and 6 CFU /ml. The minimum concentration of aptamer required for the PCR assay was 10fM, where the negative control showed signs of contamination from that point onwards. Similarly, the Apta-RPA had two optimum concentrations of reporter aptamer, where 1nM and 1pM gave LOD values of 9 and 10 CFU/ml. Considering the LOD and assay times, RPA appeared to be superior in that the LOD values of the RPA and PCR are within the same range of 1-10 CFU/ml. Results were obtainable in nearly half the time required for the PCR assay.

With amplification being carried out in just 18 minutes, the RPA method was a rapid source of exponential increase of ssDNA strands with the use of a forward and reverse primer set. As RPA is one of the newest isothermal amplification methods, its application and use in research is likely to develop due to its numerous advantages which include portability, simplicity, sensitivity, rapid sample to answer time and ability to be used in low-resource settings.

5.5 References

- [1] K. M. Song, S. Lee, and C. Ban, "Aptamers and their biological applications," *Sensors*, vol. 12, no. 1, pp. 612–631, 2012.
- [2] N. Alizadeh, M. Y. Memar, S. R. Moaddab, and H. S. Kafil, "Aptamer-assisted novel technologies for detecting bacterial pathogens," *Biomed. Pharmacother.*, vol. 93, pp. 737–745, 2017.
- [3] J. H. Lee, M. V Yigit, D. Mazumdar, and Y. Lu, "Molecular diagnostic and drug delivery agents based on aptamer-nanomaterial conjugates," *Adv. Drug Deliv. Rev.*, vol. 62, no. 6, pp. 592–605, Apr. 2010.
- [4] K. Han, Z. Liang, and N. Zhou, "Design strategies for aptamer-based biosensors," *Sensors*, vol. 10, no. 5, pp. 4541–4557, 2010.
- [5] J. J. Trausch, M. Shank-Retzlaff, and T. Verch, "Replacing antibodies with modified DNA aptamers in vaccine potency assays," *Vaccine*, vol. 35, no. 41, pp. 5495–5502, 2017.
- [6] S. C. B. Gopinath and P. K. R. Kumar, "Aptamers that bind to the hemagglutinin of the recent pandemic influenza virus H1N1 and efficiently inhibit agglutination," *Acta Biomater.*, vol. 9, no. 11, pp. 8932–8941, 2013.
- [7] P. Nadal, A. Pinto, M. Svobodova, N. Canela, and C. K. O'Sullivan, "DNA aptamers against the lup an 1 food allergen," *PLoS One*, vol. 7, no. 4, pp. 17–19, 2012.
- [8] A. D. Keefe, S. Pai, and A. Ellington, "Aptamers as therapeutics," *Nat. Rev. Drug Discov.*, vol. 9, no. 7, pp. 537–550, 2010.
- [9] K.-A. Frith *et al.*, "Towards development of aptamers that specifically bind to lactate dehydrogenase of Plasmodium falciparum through epitopic targeting," *Malar. J.*, vol. 17, no. 1, p. 191, May 2018.
- [10] S. Y. Toh, M. Citartan, S. C. B. Gopinath, and T. H. Tang, "Aptamers as a replacement for antibodies in enzyme-linked immunosorbent assay," *Biosens. Bioelectron.*, vol. 64, pp. 392–403, 2014.
- [11] S. M. Mirmajlessi, M. Destefanis, R. A. Gottsberger, M. Mänd, and E. Loit, "PCR-based specific techniques used for detecting the most important pathogens on

strawberry: a systematic review,” *Syst. Rev.*, vol. 4, no. 1, p. 9, Jan. 2015.

- [12] I. M. Lobato and C. K. O’Sullivan, “Recombinase polymerase amplification: Basics, applications and recent advances,” *TrAC - Trends Anal. Chem.*, vol. 98, pp. 19–35, 2018.
- [13] M. Jauset-rubio *et al.*, “Ultrasensitive , rapid and inexpensive detection of DNA using paper based lateral flow assay,” *Nat. Publ. Gr.*, no. October, pp. 1–10, 2016.
- [14] M. Euler *et al.*, “Recombinase Polymerase Amplification Assay for Rapid Detection of *Francisella tularensis*,” vol. 50, no. 7, pp. 2234–2238, 2012.
- [15] M. Euler *et al.*, “Development of a Panel of Recombinase Polymerase Amplification Assays for Detection of Biothreat Agents,” *J. Clin. Microbiol.*, vol. 51, no. 4, p. 1110 LP-1117, Apr. 2013.
- [16] J. Bruno, “Application of DNA Aptamers and Quantum Dots to Lateral Flow Test Strips for Detection of Foodborne Pathogens with Improved Sensitivity versus Colloidal Gold,” *Pathogens*, vol. 3, no. 2, pp. 341–355, 2014.
- [17] Z. Zhuo *et al.*, “Recent Advances in SELEX Technology and Aptamer Applications in Biomedicine,” *Int. J. Mol. Sci.*, vol. 18, no. 10, p. 2142, Oct. 2017.
- [18] J. G. Bruno, M. P. Carrillo, T. Phillips, and C. J. Andrews, “A novel screening method for competitive FRET-aptamers applied to *E. coli* assay development,” *J. Fluoresc.*, vol. 20, no. 6, pp. 1211–1223, 2010.
- [19] J. G. Bruno, T. Phillips, M. P. Carrillo, and R. Crowell, “Plastic-adherent DNA aptamer-magnetic bead and quantum dot sandwich assay for *Campylobacter* detection,” *J. Fluoresc.*, vol. 19, no. 3, pp. 427–435, 2009.
- [20] C. M. Dundas, D. Demonte, and S. Park, “Streptavidin–biotin technology: improvements and innovations in chemical and biological applications,” *Appl. Microbiol. Biotechnol.*, vol. 97, no. 21, pp. 9343–9353, 2013.
- [21] C. K. Dixit, S. K. Vashist, B. D. MacCraith, and R. O’Kennedy, “Multisubstrate-compatible ELISA procedures for rapid and high-sensitivity immunoassays,” *Nat. Protoc.*, vol. 6, p. 439, Mar. 2011.
- [22] M. Sypabekova, A. Bekmurzayeva, R. Wang, Y. Li, C. Noguez, and D. Kanayeva, “Selection, characterization, and application of DNA aptamers for detection of *Mycobacterium tuberculosis* secreted protein MPT64,” *Tuberculosis*, vol. 104, pp.

70–78, 2017.

- [23] S. L. Jun and K. P. McNatty, "Aptamer-based regionally protected PCR for protein detection," *Clin. Chem.*, vol. 55, no. 9, pp. 1686–1693, 2009.
- [24] T. C. Lorenz, "Polymerase Chain Reaction: Basic Protocol Plus Troubleshooting and Optimization Strategies," *J. Vis. Exp.*, no. 63, p. 3998, May 2012.
- [25] R. Kuhn, J. Böllmann, K. Krahl, I. M. Bryant, and M. Martienssen, "Data on DNA gel sample load, gel electrophoresis, PCR and cost analysis," *Data Br.*, vol. 16, pp. 732–751, Dec. 2017.
- [26] B. A. Sanderson, N. Araki, J. L. Lilley, G. Guerrero, and L. K. Lewis, "Modification of gel architecture and TBE/TAE buffer composition to minimize heating during agarose gel electrophoresis," *Anal. Biochem.*, pp. 44–52, 2015.
- [27] S. C. Tan and B. C. Yiap, "DNA, RNA, and Protein Extraction: The Past and The Present," *J. Biomed. Biotechnol.*, vol. 2009, pp. 1–10, 2009.
- [28] V. Skouridou *et al.*, "Duplex PCR-ELONA for the detection of pork adulteration in meat products," *Food Chem.*, vol. 287, no. November 2018, pp. 354–362, 2019.
- [29] J. Hidding, "A therapeutic battle: Antibodies vs. Aptamers," *Nanosci. master Progr.*, pp. 1–20, 2017.
- [30] J. D. van Elsas, A. V Semenov, R. Costa, and J. T. Trevors, "Survival of *Escherichia coli* in the environment: fundamental and public health aspects," *ISME J.*, vol. 5, no. 2, pp. 173–183, Feb. 2011.

Chapter 6

Future Outlook and Final Conclusions

6.1 Future Outlook

Building on this work, there are a multitude of directions the research may be taken to future develop the device portrayed in Chapters 3 and 4 and furthermore, explore further possibility of the aptamer research in Chapter 5.

6.1.1 Prospective study for eLoaD for use with real samples

For commercialisation prospects, alternative samples must be tested on the platform used in Chapter 4. As blood culture samples were used for the retrospective study, whole blood samples must be tested as part of a validation process to determine whether the platform is capable of detecting low CFU counts (<10 CFU/ml). As no pre-treatment is desirable for a POC or near patient device where time is critical, this enrichment process must be eradicated. Whole blood was previously tested in the device to determine how the fluid behaves within microchannels and how the viscous matrix responds under centrifugal conditions. Taking that research one step further would be to determine how whole, untreated blood interacts with the sensor and whether the sensor is capable of detecting low pathogen counts in the complex matrix. An interesting study would consist of determining the sensitivity of the device using a sample set of sepsis-suspect whole blood patient samples. The patients would have the signs of sepsis; however, statistics have shown that people displaying the symptoms suspected of being associated with sepsis that 90% was caused by inflammation only, where no pathogen was detected [1]. When an individual is sick, platelets and WBC count in the blood rise, which increases the amount of possible interferences with the biosensor.

The future work for this device will be to determine the LOD of the device using real-blood samples acquired from sick patients who are sepsis free. As illnesses cause the components in the blood to act abnormally. Spiking these samples with a dynamic concentration range of pathogens would allow the true capability of the device to be determined in a hospital setting. This secondary validation process will be highly beneficial and allow the project to progress from a validated proof of principle to a validated device. A secondary proposal is to develop a second generation device where instead of having a

generic gram-positive, gram-negative and fungal device; each working electrode will be functionalised with a species specific capture antibody. This will allow for specific ID of the captured pathogen if present and will allow for the precise treatment of the microbial infection.

6.1.2 Integrated System for eLoaD Testing

With a potential scope for commercialisation of the eLoaD, a fully integrated testing system would be an ideal POC instrument which could be located near the patient for rapid sepsis detection. Considering that Samsung have already brought to market a fully automated centrifugal, POC system for biomarker detection, the technology already exists for testing of the LoaD devices. Rather than using OD detection, the novel eLoaD presented in this work would require a built in potentiostat to carry out the EIS measurements. PalmSens offers compact electrochemical interfaces which may be incorporated with programmable centrifuge. The interface could control the spin parameters of the device, where upon completion of the spin profile, probes connected to the built-in potentiostat can be lowered to make contact with the protruding electrodes from the eLoaD for an EIS response acquisition. As the threshold of >300 Ohms is the required change in impedance required for a sepsis positive result, the interface may be designed with a simple algorithm where <300 Ohms will state a “negative” response and >300 ohms “positive” for GP, GN and/or Fungal.

6.1.3 Alternative Electrode Fabrication for eLoaD Device

Reflecting on the literature regarding a POC device, the cost per test is a key component to the overall desirability of the platform. As the eLoaD was prepared using diced gold coated Si wafer slides, the cost per disc was extremely expensive (~€80) where each device contained 15 electrodes, 9 of which were functionalised with antibody, thiol and BSA blocking solutions. In an effort to reduce the cost of the device, alternative approaches of sensor fabrication were explored. Carbon paste cost €150 per pot and could produce between 40-50 bases costing approximately €3.50 per base included PMMA and PSA costs. This is a significant difference compared to the extremely costly, single use eLoaD and therefore these alternative approaches to electrode fabrication

must be explored. The PCBs also used for research purposes cost €10 per base for the eLoaD, including all fabrication and functionalisation costs, however with large bulk order this cost also significantly reduces. The effort in researching potential alternatives to the gold electrodes is paramount for the future prototypes of the eLoaD to allow to device to be low-cost and for ease of manufacturability.

6.1.3.1 Carbon Screen Printed Electrodes

The method of screen printing was investigated where carbon sensor ink (acquired from Gwent (UK)) ink was specifically designed to be used for working electrodes tested with EIS methods for bio-sensing assays. The same microfluidic platform tested in Chapter 4 was used to determine the EIS and CV spectra of the carbon electrodes. As per the previous design, 5 milled wells were required for each testing chamber. This requirement was no longer needed as the screen-printed carbon paste was directly placed onto the device base. Carbon ink was studied as a replacement to the gold electrodes in an effort to reduce the cost per device

The base disc of 144mm diameter was used to maintain the weight of LoaD, as this would affect the force exerted on the platform under spinning conditions as the centrifugal force is related to the mass of the platform. This was also used to maintain all aspects of the design to determine the response of the electrodes to directly correlate the EIS measurements of the screen printed electrode (SPE) to the original Au coated Si biosensor used in Chapter 4. The base was reverse engineered to house the SPEs, where there was no longer a requirement to mill the electrode slots. The first design of the SPE base used a plain PMMA disc with an attached PSA layer that contained the electrode slots attached as shown in Figure 6.1 (a). The PMMA disc was heated to 70°C for 10 minutes to allow for expansion and shrinking for later curing stages, as PMMA is known to expand with an increasing temperature. A spatula tip of the carbon paste was placed at the top of the five electrode slots, where a heavy steel block was used to slowly displace the ink into the electrode slots cut into the PSA layer on the heated PMMA. Using the PSA as the scaffold of the ink, the SPEs had a known height of 86µm. To allow the ink to cure, the base was placed into a convection oven for a further 10-15 minutes, or until the ink was dry on the top surface. The disc was then left at room temperature to allow to cool.

Regardless of all pre-heating steps, the SPEs cracked severely when placed onto the PMMA base as shown in Figure 6.1 (c). To rectify this, a secondary method was used where only the electrode shapes were cut into the protective layer of the PSA layer, rather than entirely through it to reveal the PMMA underneath. With the electrode shapes only cut into the top layer of the PSA, white spirits were used to remove the PSA glue to leave a smooth acrylic, flexible layer underneath on which the carbon ink was placed. This allowed the SPEs to remain a uniform shapes whilst the ink was now sitting on top of the PSA layer which doesn't allow cracks to form [2].

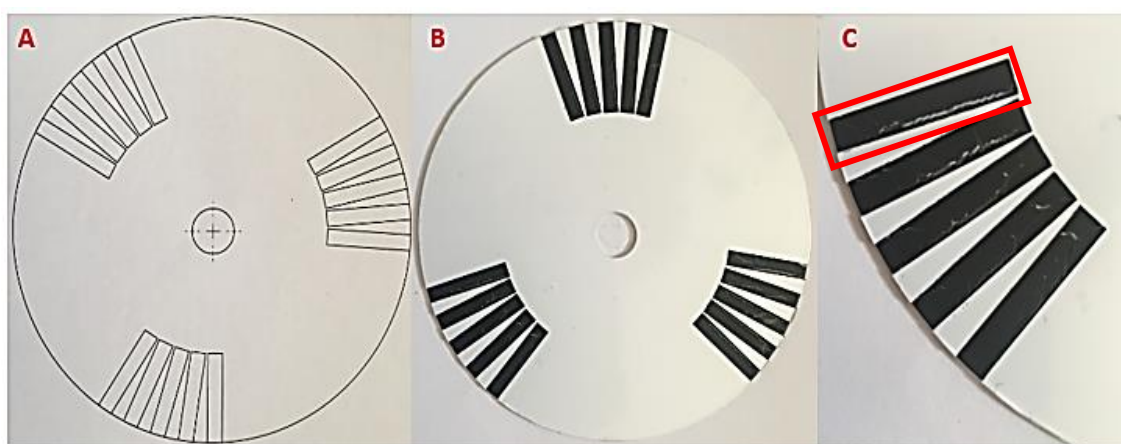


Figure 6.1. (a) CAD drawing of base for the SPEs where the design is cut into a PSA layer where each rectangular shape represents each of the electrodes. (b) portrays the SPE base to be used in conjunction with layers 1-7 of the eLoaD discussed in chapter 4 and (c) shows the crack formations of the SPE on the PMMA base.

With the issue of the cracked electrodes resolved by printing directly onto the PSA, the sensors themselves were functionalised using the previous μ CP of antibody solution on the electrodes as described in Chapter 4. For the carbon electrodes, the PEG thiol solution incubation was omitted as the alkanethiol has a high affinity towards gold and therefore no longer required for the SPEs. The EIS of the bare, antibody, and antibody BSA stages were obtained using the standard 1mM DPBS solution, where the results obtained are shown in Figure 6.2 All EIS were run in triplicate, where the average of each run was plotted and displayed. The GP, GN and Fungal capture layers were characterised based upon the Nyquist and Bode plots, as previously described. With the EIS of the three capture surfaces acquired, the capacitance and/or resistance of the surface increases with the addition of the capture bio-molecule. The 3% BSA blocking solution was used on the surface to block between the antibody patterning. With the carbon electrodes being quite

hydrophobic, the EIS results do portray a change on the surface due to the addition of the antibody and BSA solutions to the surface. All three electrodes follow the same pattern for both the Nyquist and Bode, where the overall impedance increases for the antibody adsorption step and then decreases with the addition of the BSA. The equivalent circuit model (ECM) of the system or else the overall negative charge of the BSA protein layer reduces the impedance by acting in series with the antibody modified layer [3].

It would be assumed that the addition of the capture biomolecule layer increases the capacitance and resistivity of the system as these components possibly lie in parallel for the antibody layer for this increase to occur. By placing the BSA solution on the surface, the overall impedance of the surface slightly decreases, allowing the assumption that the BSA layer acts in series to the antibody layer in the circuit. The almost circular shape of the Nyquist plot is due to a change in the ECM, where the shape is possibly due to a “low frequency hook” or an “inductive loop” which would only have an effect at high frequencies if connected in series. The inductive loop refers to a section in the complex plane of the Nyquist, where the positive half imaginary plane (inductor) and the negative half imaginary plane (capacitance). According to Klotz the formation of the imperfect semicircle Nyquist may be one of two possible ECMs either containing a circuit phase elements in series or inductor elements in parallel. It would be estimated that with the increasing overall shape of the Nyquist plots with the addition of the antibody layer, the circuit phase elements were added in parallel containing an inductor element causing the change in shape to the previously studied Nyquist plots in Chapter 4 [13].

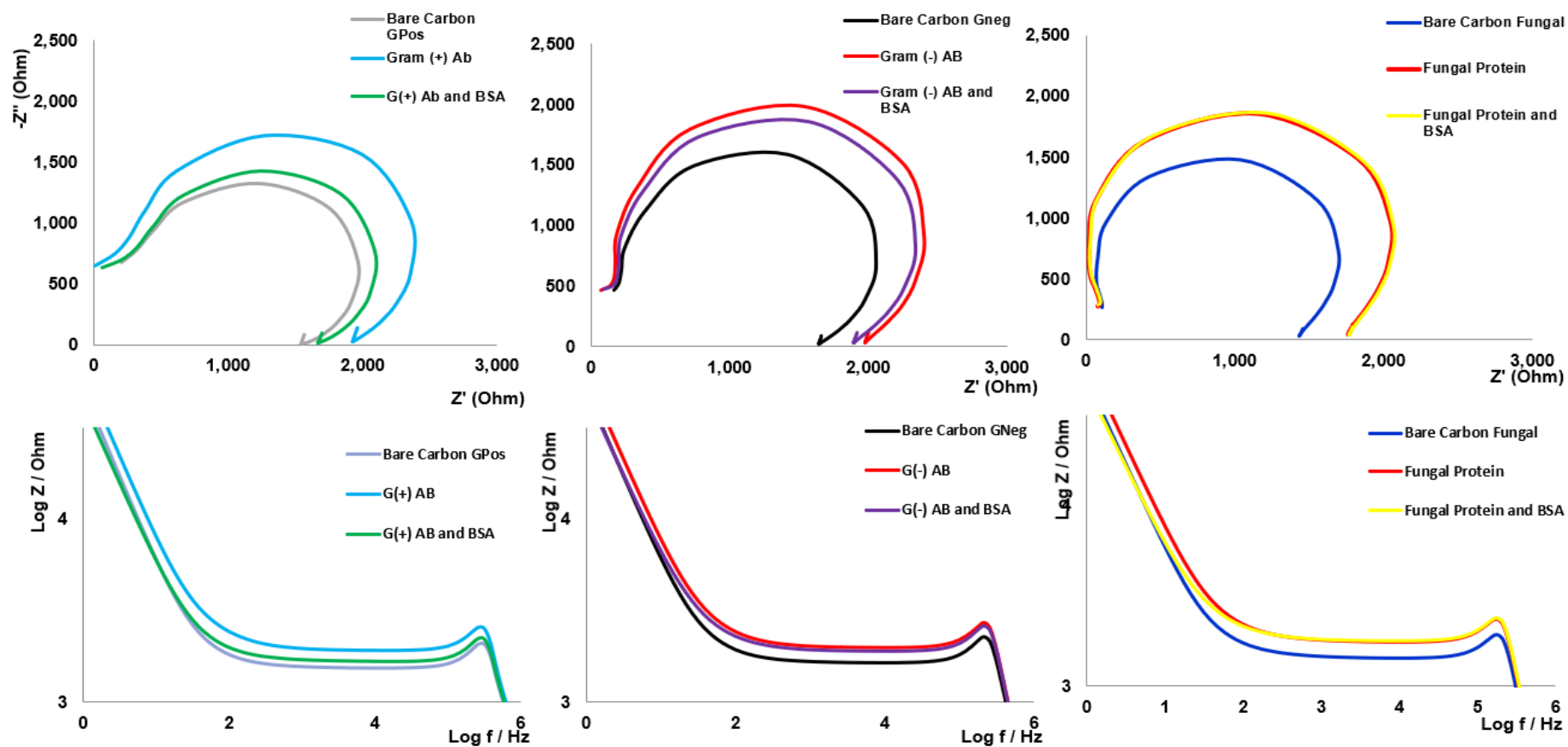


Figure 6.2. EIS nyquist and bode plots of the functionalised screen-printed carbon electrodes for GP, GN and Fungal surface tested with the V3.4 of the centrifugal device fabricated in chapter 3.

To determine the capabilities of the carbon SPEs, the eLoaD discussed in Chapters 3 and 4 was fabricated with the carbon electrode base replacing the Au coated Si wafer electrodes. This SPE LoaD was tested with the samples acquired from St. James' Hospital for a direct comparison between the gold electrodes and the carbon electrodes. Two blood culture samples were tested in conjunction with the SPE LoaD, where samples 14 and 15 were a negative and gram-negative samples respectively as previously determined with the eLoaD in Chapter 4. It was noted the SPEs themselves were hydrophobic and repelled the stamps and therefore an additional fabrication step was examined to determine the effect of plasma treating the electrode surface in an attempt to create a more hydrophilic surface to promote the stamp adhesion to the surface to allow the adsorption of the antibody solution from stamp to electrode.

The Oxford Plasma lab 100 system was used to plasma etch the surface to modify the surface chemistry of the electrodes. A mixture of argon and oxygen plasma deposition was used at different rates, where the Ar gas was used to create defects in the surface in which the oxygen gas penetrates to oxidise the surface making it hydrophilic by creating oxygen surface functional groups. The parameters for the plasma surface etch of the carbon electrodes consisted of 10 sccm of argon (volumetric flow rate or standard cubic centimetres per minute) and 40 sccm of oxygen for 5 minutes at 100mT power.

Contact angle measurements (CAM) of the carbon SPEs before and after Ar and O₂ treatment. A CAM of $88.98 \pm 6.54^\circ$ for the untreated carbon, the ink is considered slightly hydrophilic according to literature, however an angle obtained over 90° is considered hydrophobic. In this case as the angle obtained was on that threshold, it would be considered hydrophobic due to the PDMS stamps not adhering to the surface. Carrying out the Ar O₂ plasma etch on the surface of the SPE carbon base, the CAM was reduced to $45.93 \pm 3.45^\circ$ which was considerably lower than the previous measurement. This pre-treatment of the surface was necessary to create a more hydrophilic surface; however, it was noted that the PDMS stamps were detaching from the surface after a few minutes. To promote the antibody adsorption from the stamp to the carbon electrode, all antibody adsorbed stamps were weighted down onto the surface. Table 6-1 portrays the table of results obtained for samples 14 (424840.14 -negative blood culture sample) and 15 (425909.15 gram-negative clinical sample) for the carbon SPEs, treated and untreated,

where all samples are diluted 3:1 with DH₂O. Considering that the Δ Ohms should be observed for sample 15 for the GN capture surface, the best result obtained was for the O₂ and argon plasma etched surface with the BSA blocking protein. It is noted that the EIS measurements note the difference from the $R_{\text{Antibody}} - R_{\text{Antibody} + \text{bacteria}}$, the minus sign in front of certain results indicated that the impedance value has increased, compared to the results obtained in Chapter 4 where capture bacteria reduces the overall impedance of the system.

Table 6-1. EIS results obtained for carbon SPEs used in conjunction with the optimised microfluidic Load to determine the effect of electrode treatment on the capture of pathogens.

Sample Type	G (+) AB Nyquist (Ohms)	G (+) AB Bode (Ohms)	G (-) AB Nyquist (Ohms)	G (-) AB Bode (Ohms)	Fungal AB Nyquist (Ohms)	Fungal AB Bode (Ohms)
Sample 14	-28 ± 15	-0.01 ± 0.01	-60 ± -10	-0.02 ± 0.0	22 ± 48	0.02 ± 0.01
Sample 15	-21 ± 97	-0.01 ± 0.03	-8 ± 111	0 ± 0.04	10 ± 64	-0.01 ± 0.05
Sample 15 No BSA	-91 ± 54	0.03 ± 0.02	-111 ± 84	-0.04 ± 0.02	-82 ± 76	-0.04 ± 0.02
Sample 15 O ₂ Argon treated SPE	24 ± 233	0.03 ± 0.12	183 ± 77	0.09 ± 0.05	96 ± 57	0.05 ± 0
Sample 15 O ₂ Argon treated SPE no BSA	90 ± 45	0.02 ± 0.01	130 ± 67	0.05 ± 0.03	80 ± 95	0.04 ± 0.01

Both O₂ and Argon plasma treatment of the SPEs were carried out to make the surface more hydrophilic to reduce the repulsion of the antibody surface. However, the attempts were unsuccessful as the carbon SPEs were unable to detect the GN pathogens present in sample 4265909.15 as no significant change in impedance was noted. This is possibly due to little or no antibody coverage present on the SPEs due to their hydrophobic nature. The

carbon inks would need to incorporate a component which allows to ink formulation itself to become hydrophilic or contain molecules or a functional group which may be modified to allow for antibody or protein attachment rather than changing the surface energy of the electrodes.

6.1.3.3 Printed Circuit Board Electrodes

Printed circuit boards (PCBs) were also explored as a secondary attempt at creating a cheap alternative to the Au coated Si electrodes to reduce the cost of the eLoaD. The PCBs were designed using CAD software and converted to Gerber files, where the electrodes were manufactured by Beta Electronics LTD (Ireland). Initially, the second generation of the eLoaD was used to determine whether the PCB electrodes were suitable for pathogen capture and detection. The base was a two tiered electrode configuration. The connection points for the potentiostat were connected to the 5 electrode configuration where the size of the electrodes mimicked that of the electrode cover electrode areas. These screen printed gold electrodes were connected via copper wiring to create the electrical connection between both the contact point and the functionalised electrode area. Copper tracking is located underneath the base which connect the electrodes and the contact point for the potentiostat crocodile connections. This copper tracking was used to reduce the amount of gold needed for the electrodes to further reduce cost of the platform. Figure 6.3 portrays the PCB base where (b) shows one of three electrode sites on the acrylic platform. The associated legend highlights the four main features of each sites, where an alignment hole is located to the left of each electrode configuration. This is to allow for a more accurate placement of the top section of the centrifugal platform on the base during assembly. The gold SPEs of the PCB was designed as an exact replica of the electrode exposed areas in the eLoaD characterised in Chapters 3 and 4.

Only the GN electrode was functionalised as previously described in Chapter 4, followed by an overnight incubation in 1% PEG solution and a 2 hour incubation in 3% BSA. This functionalised PCB base was covered with the fibrinogen modified electrode cover PSA layer. This base and electrode cover section was then pressure rolled to the second generation 5-layer device at 80 PSI. 1.7mls of 10^7 CFU/ml *Klebsiella Pneumoniae* GN type bacteria was injected into the sample chamber which was spun at 7Hz where a sample

incubation time of 3 minutes was recorded. The DH₂O wash step was manually triggered where the wash step was displaced to the electrode detection chamber at 10Hz. The 1mM DPBS electrolyte solution was also triggered under the same conditions to mimic that of the optimised eLoaD assay. The base was removed where the GN electrodes were fixed and stained for confocal imaging, as shown in Figure 6.3 (C). The images shown were a clear indication that the pathogens on the surfaces burst, where the spreading of the cell membrane and its contents in a downward fashion is visible which corresponds to the downwards flow of the samples over the electrodes.

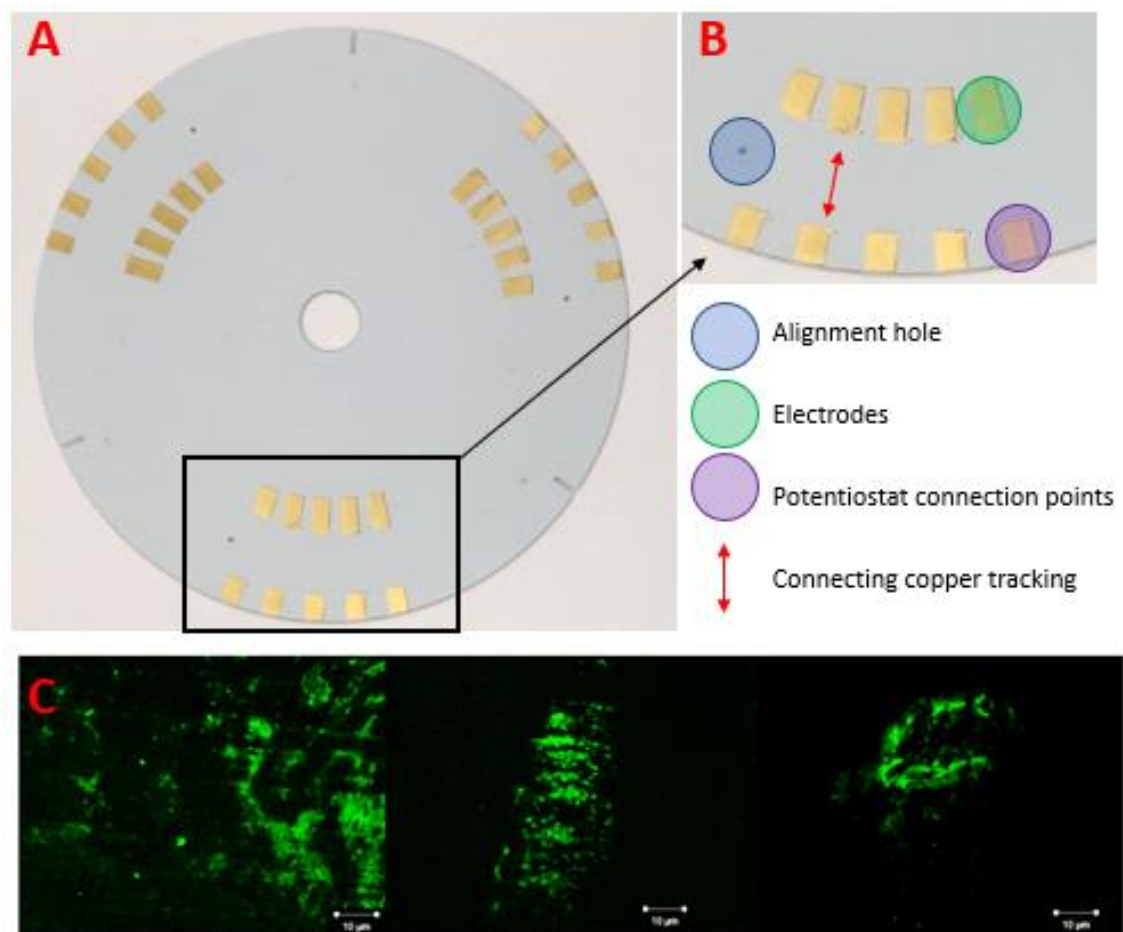


Figure 6.3. (a) Portrays the PCB electrode base acquired from PCBway (Designed by Taufeeq Elahi Diju). (b) Shows one of three separate electrode sites on the base with a corresponding legend (c) Portrays the PCB of the GN functionalised PCB electrode tested against 1.7mls of 10^7 CFU/ml GN type bacteria, *Klebsiella Pneumoniae* where evidence of cell lysis and cell membrane debris are evident using confocal microscopy imaging.

With some evidence of rod shaped cells on the surface, it was apparent the pathogens were captured by the biorecognition layer; however, surface roughness and the spin frequency of the device caused the majority of the cells to burst. Other sources of PCB

electrodes were tested to determine the optimum source to create the mass manufacturable base.

An array of sample PCB screen printed gold was acquired from Mint Tek (Ireland) where preliminary tests were carried out to determine how bacteria behaves on these gold surfaces, which was imaged using confocal microscopy. Four separate types of PCB gold samples were received and prepared by sonicating in EtOH for 2 minutes and rinsed with DH₂O. All electrodes were functionalised with the GN endotoxin antibody solution via μ CP as previously described. Blocking solutions were not used for these experiments as this was to determine whether the gold was suitable for the antibody to adsorb to and also smooth enough to not damage the pathogens on the surface. Figure 6.4 displays the four separate samples of PCB gold which were incubated with a high concentration (10^7 CFU/ml) of GN type bacteria, Klebsiella Pneumoniae which were cultured overnight in LB broth and counted using the traditional cell counting on agar plates. 100 μ l of the pathogen solution in DPBS was incubated on the surface on the gold for 1 hour to allow sufficient time to bind to the capture antibody. All gold surfaces were washed 3 times with DPBS with to remove unbound whole cells.

PCB00007 displays three separate images of the same gold type where it is evident that the stained, fixed pathogens on the surface are bursting, where the cytoplasm surrounds the cell membrane which is fixed to the surface. The halo ring surrounding the whole cell on the surface is evidence of the pathogen lysis due to the surface roughness of the electrode. Very few pathogens were also captured on the surface which also suggests that the antibody didn't adsorb to the surface either due to the surface energy of the gold SPE being too high and therefore too hydrophobic to allow the attachment of the antibody.

PCB00007 (b) portrays another set of PCB gold surfaces which show no evidence of pathogen capture. It was noted the PDMS stamp would not adhere to the surface and therefore was forced to remain in contact in hopes that hydrophobic interactions between the gold surface and antibody solution would allow the biomolecules to adsorb onto the surface. With only one cell visible on the entire surface, this PCB was considered highly unsuitable for the working electrodes, however as non-specific adsorption of blood components was an issue in Chapter 4, it could be possible to use this type of gold PCB

for the counter and reference electrodes to avoid these electrodes becoming contaminated when testing more complex samples.

The third gold PCB proved the most successful, where this electrode type had a high surface capture of the desired pathogens. There was no evidence of cell lysis as portrayed with PCB00007 and therefore this electrode was successful at adsorbing the antibody solution for the pathogen capture possibly due to a smooth gold surface.

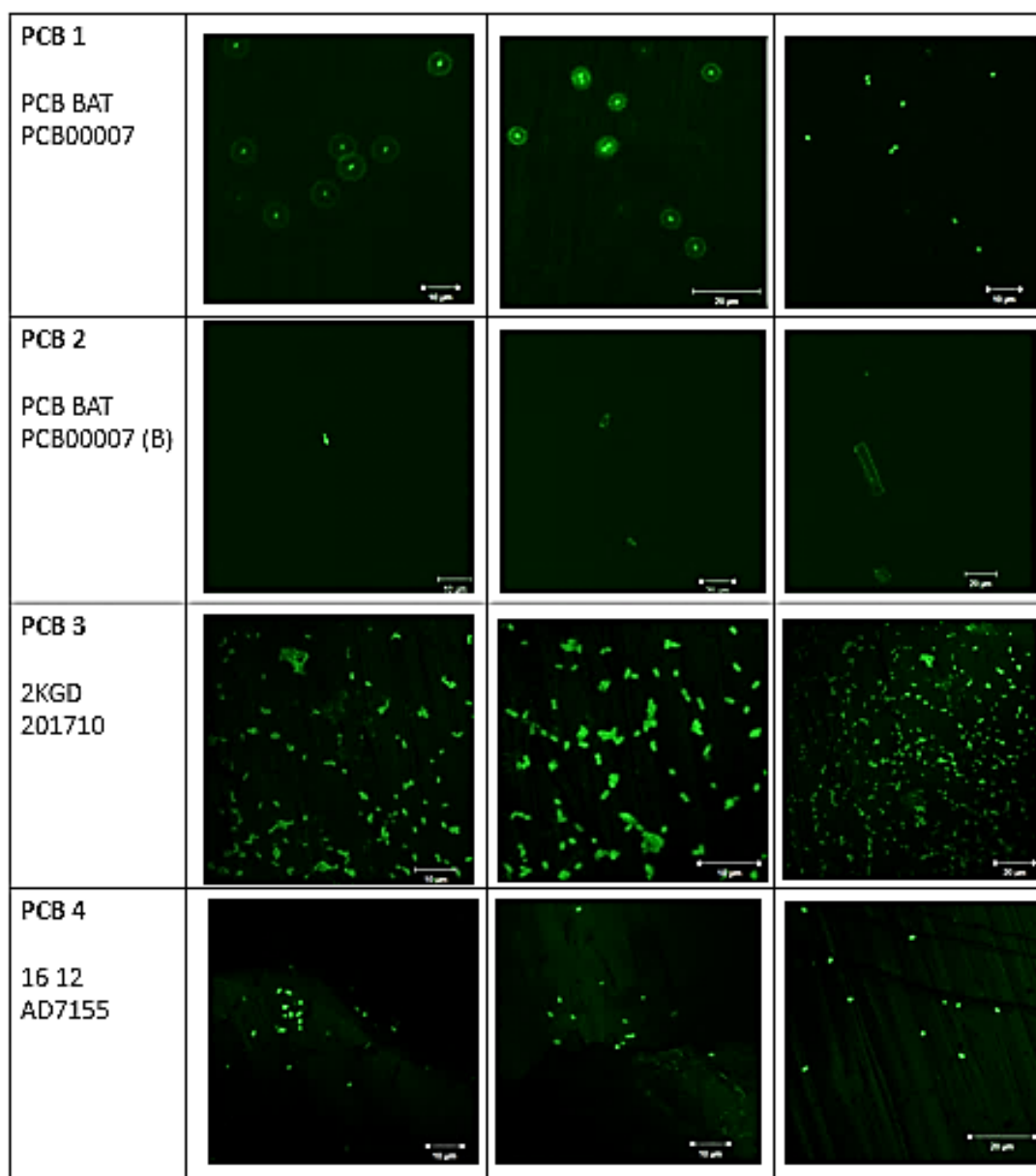


Figure 6.4. Comparison of four separate PCB electrodes manufactured by Mint Tek (Ireland) stamped with GP antibody solution and incubated with *Klebsiella Pneumoniae* (GN type bacteria) to determine best electrode type.

PCB 4 shows some evidence of whole cell capture however compared to PCB3, this electrode type was also disregarded. The cell coverage was far too low compared to the initial CFU/ml incubated on the surface and therefore it was also assumed that the antibody solution adsorption was minimal on the surface. As the initial steps taken to investigate the gold PCB electrodes were successful, it would be suggested that the gold surface for PCB3 (displayed in Figure 6.4) would be used for the working electrodes where PCB2 could be a possible type of gold surface used as the counter and reference electrode.

PBC3 proved to be the most successful for the pathogen capture, where the surface energy was low enough to allow the PDMS antibody stamping where no evidence of cell lysis was found. The clean gold surfaces for PCB2 would be ideal for the counter and reference electrodes as non-specific adsorption of cells on these electrodes hinder the detection ability of the sensor platform. Another suggestion could be to have a dual-ink sensor, where the working electrodes would remain the same however a carbon ink could be substituted for the counter and reference electrodes which may reduce the cost per base even further.

It has been shown that the manufacturable PCB base is possible to produce and therefore further exploitation of this is required to optimise the second generation device.

6.1.4 Lateral Flow Assays (LFAs) detection with aptamer conjugated AuNPs

Lateral flow assays (LFAs) have been previously used to detect biomarkers however their use in capturing and detecting whole cells has rarely achieved low LODs. The capture and detection aptamer probes studied in Chapter 5 had the ability to adapt with three separate bio-assays for the detection of *E. coli* cells. Realising the potential of the oligonucleotides for cell capture, further applications could be explored. Aptamers have previously been used to replace antibodies in lateral flow assays (LFAs) [4], [5]. LFAs are immunochromatographic strip tests that utilise capillary action of a membrane to drive a sample over a test and control line to determine the presence and concentration of an analyte. LFAs are popular immunoassays due to its rapid and sensitive nature. They are a highly desirable test due to their portability, stability, cost and ability to detect a wide range of analytes [6]. Gold nanoparticles (AuNPs) cause the colorimetric change which originates from the aggregation of the particles. The binding affinity of the functionalised AuNPs to the capture-immobilisation sites line on the LFA determines the sensitivity of the assay. This colour change allows the user to qualitatively determine without the use of equipment, making it a highly desirable platform as a POC device [7] [8].

Two types of LFAs were fabricated for the detection of *E. coli* cells and *E. coli* RPA tailed amplicons. The standard sandwich LFA consisted of a capture and reporter probe which surround the analyte, where the reporter aptamer was pre-functionalised with AuNPs for detection. The secondary LFA was designed to capture the RPA product which was the

amplified eluted product which was previously detected through UV imaging in Chapter 5. The biotinylated capture probe was immobilised on a streptavidin (SA) test line where the analyte binds. The immobilised test line, the analyte and the reporter probe functionalised AuNPs bond to create a visible line to determine a positive sample. The control line was composed of a SA, biotinylated DNA probe complementary to the AuNP aptamer [9]. The same case applied for the secondary LFA, where the tailed RPA product replaces the *E. coli* whole cell as the analyte. In both cases where the AuNPs bind to the immobilised capture probes to create a red line visible to the naked eye, as shown in Figure 6.5. It has been reported that detecting DNA products rather than whole cells reduces the LOD, and therefore both LFAs were examined in tandem [10].

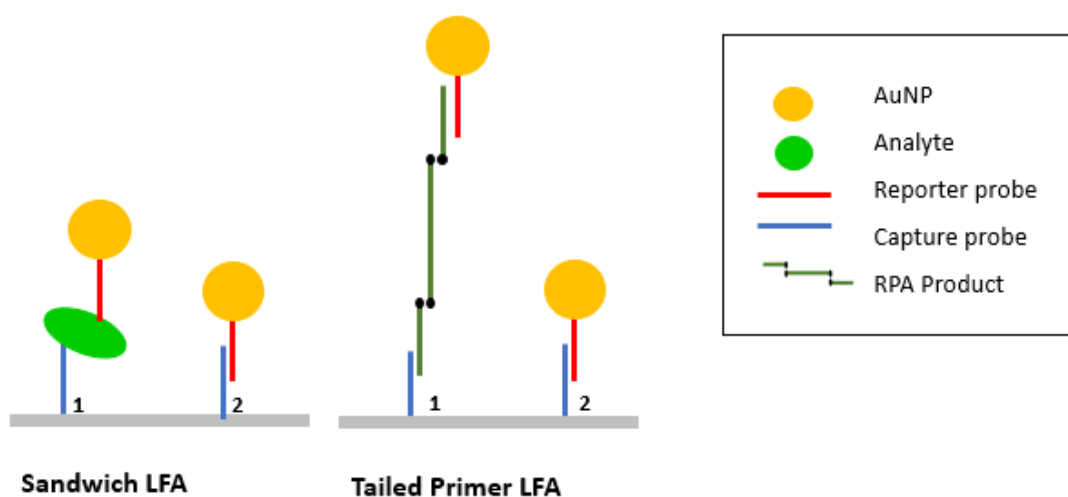


Figure 6.5. Two LFAs utilised for the capture and detection of *E. coli* cells/*E. coli* RPA products where 1. portrays the test line and 2. denotes the control line.

For the sandwich LFA the analyte being detected was the *E. coli* cells which are cultured and suspended in DPBS. The second analyte was the RPA product which was the amplified eluted reporter probe incubated against the reducing *E. coli* cells from the ELONA plates. Both methods were identical, however the AuNPs are prepared with different reporter aptamers and the immobilised test and control lines are different aptamers. Gold nanoparticles (AuNPs) with an approximate average diameter of 13nm were prepared by citrate reduction of HAuCl₄ where 2mL of 1% sodium citrate was added to boiling HAuCl₄

solution (1 μl in 50 ml MilliQ water) under vigorous stirring. A solution of 30 μl of the desired reporter aptamer in 100 μl of MilliQ water, 1ml 10mM TCEP and 2 μl 500mM acetate buffer (pH 5.2) was added to the thermomixer for 1 hour at RT at 850 RPM. 1mL of AuNPs was added to the solution and left in the thermomixer under the same conditions. 10 μl of 500mM Tris acetate buffer (pH 8.2) and 100 μl 1M NaCl was prepared, where 10 μl of this solution was added to the AuNPs every 20 minutes and finally left overnight under thermomixing conditions. The AuNPs were finally centrifuged at 15,000 RPM for 25 minutes and washed x3 500 μl MilliQ and resuspended in 30 μl MilliQ.

6.3.2.2 AuNP Characterisation

The Aptamer-AuNPs conjugates were evaluated using UV-visible spectroscopy, where data was collected by scanning the wavelength from 800nm to 200nm.

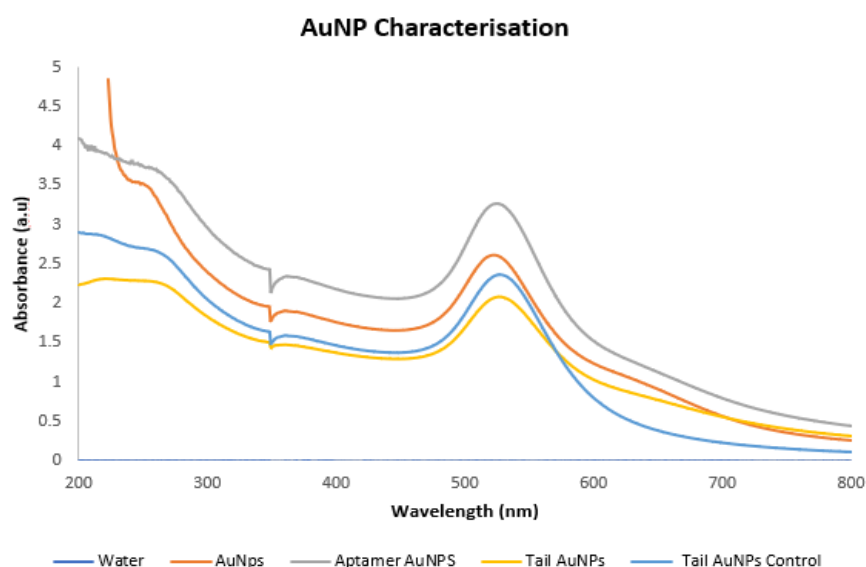


Figure 6.6. UV spectra of the functionalised AuNPs compared against naked AuNPs where MilliQ water was used as a control base line.

The peak observed at 520nm is typical for the AuNPs where the DNA peak was observed at 260nm, where the absorbance was dampened between 260nm – 200nm. Four separate AuNPs were characterised, where the sandwich LFA AuNPs, tailed AuNPs, control tail AuNPs all displays the same characteristics of the sampled absorbance peak between 200nm and 260nm where the naked AuNPs absorbance increases directly between this range as shown in Figure 6.6. A secondary method which determined whether DNA had bound was to run the AuNPs in an agarose gel [11]. As DNA travels downwards in parallel

with the DNA ladder, any DNA conjugated to the AuNPs will force the ssDNA-AuNPs to travel in a downwards direction also. The tabulated data displays each sample loaded into each well. A 1.3% agarose gel was prepared, allowing the nanoparticles to pass through the gel.

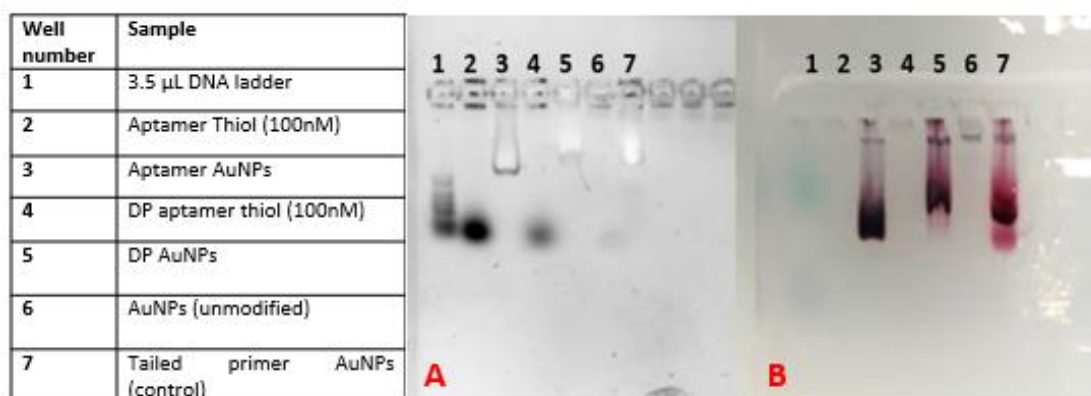


Figure 6.7. Functionalised AuNPs run in agarose gel to determine bound DNA where (a) portrays the UV transilluminator image and (b) running of functionalised AuNP under non-UV imaging conditions

A voltage of 100mV was applied for 25 minutes where the all DNA and DNA-AuNPs shown either on the transilluminator or to the naked eye. No movement is reported for the AuNPs only. 4 μ L of loading buffer was added to 5 μ L each sample. Each sample loaded into each well was detailed in Figure 6.7 where image (a) displays the UV image of the gel which was required to observed the DNA ladder and the probes (well 1, 2 and 4) and (b) where the AuNPs functionalised with the DNA from well 2 and 4 are observed in wells 3, 5 and 7. The unmodified AuNPs which were loaded into well 6 did not run as no charged DNA was presence to displace the unmodified NPs through the gel.

Two lateral flow assay membranes were prepared; sandwich assay LFA and the tailed primer detection LFA. For initial optimisation, four types of nitrocellulose membranes were prepared to determine the optimum flow conditions and pore size for cell flow. Millipore (Sigma) Hi-Flow™ Plus (HF080, HF120, HF170 and HF180) nitrocellulose membranes were pre-functionalised with both the test and control lines aptamers and solution as detailed in Table 6-2.

Table 6-2. Test and control line immobilisation solution.

LFA Type	Sandwich	Tailed Primer
----------	----------	---------------

Test line	Eco 4F Biotin 100uM (9 µL)	S.A Poly + IP Test (9 µL)
Control line	S.A Poly Biotin (5 µL)	S.A Poly + IP Control (9 µL)

The tailed primer aptamers were prepared by adding 9 µL (100 µM Immobilisation probe) with 4.5 µL SA (5mg/ml) giving a total concentration of 0.66 µM. This is prepared for both the IP test and control. The stated volume of liquid was pipetted in a straight line across a 4cm wide membrane in a horizontal direction, where the test was the first line the sample will come into contact with and the control was placed in the second position. This placement was critical to ensure that the control line must be visible to verify that sample has crossed both the test and control line. All prepared membranes were blocked with 2% skimmed milk solution w/ 0.1% tween for 15 minutes under rocking conditions and left to dry for 2 hours.

To determine the optimum membrane, 20 µl of the control sample (2µl of AuNPs and 18µl 0.05% PBST) were added to each type of membrane and observed after 10 minutes of development. If background interference from the AuNPs was high, 50 µl PBS was used to wash the membrane. As no control line was detected for the HF080 and HF120 membranes, no further tests were carried out with these membranes as the samples travels too fast through the membranes, allowing little time for AuNPs to bind to the control lines. Both the HF170 and HF180 nitrocellulose membranes showed equal control line intensity however only the HF170 was used for the LFA optimisation as it was easier to functionalise. These membranes have a much slower flow rate and therefore are ideal for assay requiring high sensitivity [12]. Only AuNPs and PBS solution were used as initial samples in order to determine the optimum AuNP concentration to be used with real-samples. *Table 6-3* portrays each of the sample compositions pipetted onto the individual LFAs where assays 1-2 was carried out on the sandwich assay where 3-7 contained the tail primer control line. Samples 8-10, 14 contains E. coli cells to determine the effect on the control and test line where all remaining samples were an attempt to find the optimal AuNP concentration.

Table 6-3. 20 µl sample pipetted into each LFA where each samples type is detailed to shown optimum AuNP concentration for assay on the HF170 functionalised membranes.

1	5 µl AuNPs + 15 µl PBST (Sandwich)
----------	------------------------------------

2	8 µl AuNPs + 12 µl PBS Tween (Sandwich)
3	8 µl AuNPs + 12 µl PBS Tween (Tailed Primers)
4	8 µl AuNPs + 12 µl PBS Tween (Tailed Primer Control)
5	5 µl AuNPs + 15 µl PBS Tween (Tailed Primers)
6	5 µl AuNPs + 15 µl PBS Tween (Tailed Primers Control)
7	8 µl AuNPs + 12 µl PBS Tween (Tailed Primer Solution from stock)
8	2 µl sample (From 10 ⁸ E. coli stock) + 5 µl AuNPs + 13 µl PBS Tween. 3 min incubation in eppendorph tube.
9	10 µl e. coli sample + 5 µl AuNPs 5uL PBS Tween. 3-minute development time
10	10 µl e. coli sample + 10 µl PBS Tween. 30-minute development time
11	1 µl AuNPs+ 19 µl MilliQ
12	3 µl AuNPs + 17 µl MilliQ
13	13 µl MilliQ + 5 µl salmon sperm +3 µl AuNPs (No pre-incubation)
14	8 µl MilliQ + 4 µl E. coli +5 µl salmon sperm + 2 µl AuNPs (No pre-incubation)
15	18 µl salmon sperm DNA + 2 µl AuNPs. 3-minute incubation in eppendorph tube

As no analyte were being tested for samples 1-7, only the control line should be visible. It was evident that for the sandwich LFAs (LFA 1-2) there was interaction between the AuNPs and the test line and no control line appeared for the tailed primer AuNPs as shown in Figure 6.8. A test line is apparent for LFA 7; however, this was a high concentration from the stock to determine if the control line was correctly immobilised in the production process. Reviewing the AuNP UV spectra for the tailed primer AuNPs, the absorbance was significantly lower for these AuNPs compared to the sandwich AuNPs. The bound DNA may be insufficient to create a visible line, therefore new AuNPs for the tailed primers should be prepared again with a higher concentration of DNA.

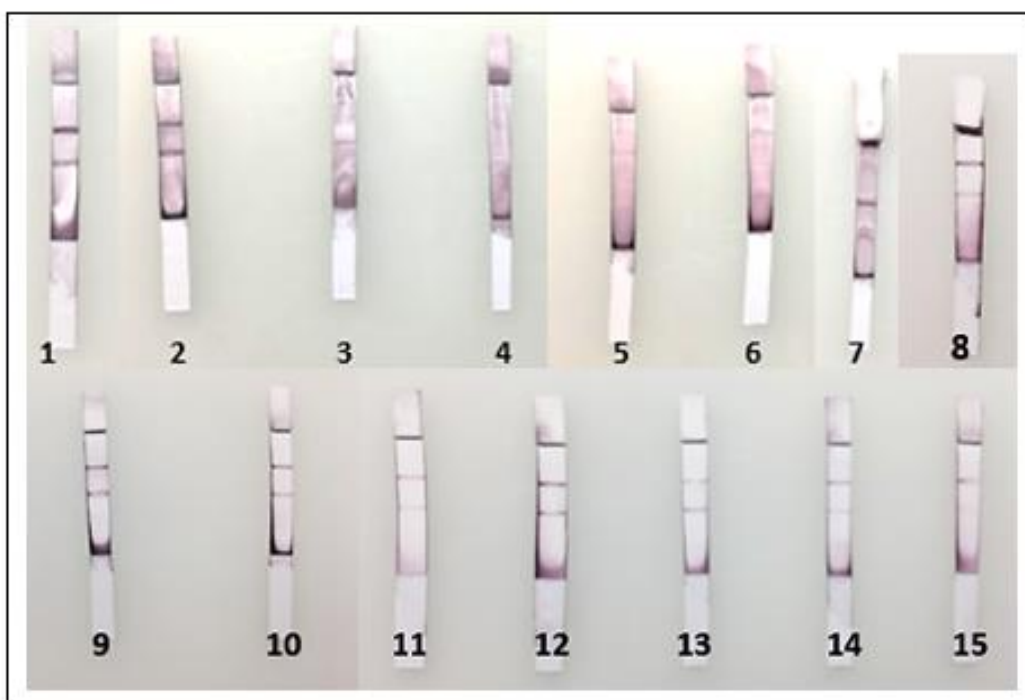


Figure 6.8. LFA where each test strip number corresponds to the sample described in Table 6.3.

To further investigate the sandwich LFA strips a variety of AuNP mixtures were investigated to determine optimum conditions in which the control line only appears in the case no analyte present in the sample. The introduction of salmon sperm DNA to the 20 μ l sample appeared to displace the test line AuNP whilst still conjugating with the control line. In order to reduce the amount of salmon sperm DNA to be used, other blocking agents were tested. The new membrane blocking agent was composed of 400 μ l of 10nM Carbonate Bicarbonate buffer, 0.2g skimmed milk and 10 μ l of empigen (Sigma) in 10ml MilliQ water. The HF170 membranes were prepared with the sandwich LFA control and test immobilised aptamers followed by 15 minutes in blocking solution and allowed to dry overnight however reflecting on the LFA displayed in Figure 6.8 non-specific binding of the AuNPs was clearly evident. Much more optimisation work would be required to fully develop the LFAs for both sandwich and tailed primer assays. Membrane preparation and blocking was needed to assist the movement of cells and AuNPs whilst reducing non-specific binding of analytes to the membrane pores. The flow rate is a major factor in the development of the visible control line with the AuNPs.

The lateral flow assays require optimisation for both sample and membrane preparation. As sandwich and RPA tailed primers were considered, both require optimisation. However, as RPA used DNA-AuNP conjugates, the blocking shouldn't require as much optimisation to that of the whole cell detection. Reviewing the data in the AuNP UV spectra, the tailed primer AuNPs were not coated in sufficient DNA, therefore they would need to be conjugated with a higher amount of initial DNA to increase the coverage.

A second observation was also made between the reporter aptamers and both the test line aptamers where base matching was observed between the aptamer sequencing. Up to 10 bases matched between the sandwich assay AuNP conjugated probe and the test line probe and 8 matching bases for the tailed LF assay. Better design of the aptamers would highly increase the specificity of the assay and avoid false positive results of the modified AuNPs binding to both the test and control line.

6.2 Final Conclusions

With a huge necessity for innovative, rapid sepsis detection technologies, the traditional methods of blood culture and sample pre-treatments must be re-evaluated in an effort to address this serious condition. Although blood culture techniques have been considered the gold standard of pathogen detection with clinical microbiology departments globally, the time of detection relies on the growth of the pathogens to a high CFU count to be capable of detecting CO₂ levels within the culture media. With the conditions being initially caused by bacteria, fungi and viruses the focus was placed upon the whole cell pathogens. Blood culture can take several days before being reported as negative and therefore a pre-screening device would be highly advantageous to rapidly diagnose the patient where in the case of a positive blood sample, other, more complex methods of susceptibility testing can be carried out. A revised system must be imposed to reduce to the time to diagnosis to decrease the huge mortality rates caused by this traditional, laborious methodology which in effect, increases antibiotics administrations and therefore increases antibiotic resistant strains of pathogens in clinical settings. This domino effect can be stopped with initial detection of the low CFU count of pathogens in blood samples where lengthy blood culture processes are eradicated.

This thesis has explored alternative methods of the capture and detection of pathogenic whole cells by integrating a biosensor into a novel centrifugal, microfluidic platform capable of label-free electrochemical impedance spectroscopy detection of the bound cells. With a near-patient device or bio-assays accompanied with a short sample-to-answer process, the diagnosis time will be reduced and therefore improve the patient outcomes.

Chapter one reviewed the common and state-of-the-art methods of pathogen detection. Electrochemical methods were then explored where finally, the theory and practical uses of centrifugal microfluidics and other bio-assay used for the detection of harmful microbes was explored with the intention to exploit this knowledge to develop new assays to reduce sampling times.

Chapter two reviewed all methods and materials used throughout this body of work. As a variety of protocols were implemented for each of the results chapters, this section explored the individual instruments used and their rationale. The materials type and production process for the centrifugal platforms was clearly justified, where the protocol for each develop stage was presented in a clear, concise manner for future references for other potential users. As the body of work discussed an array of interdisciplinary projects, the protocols for each manufacturing process, assay development, testing and post-analysis were discussed in detail.

Chapter three presented the research that was primarily involved with the fabrication and development of a novel centrifugal microfluidic platform capable of handling and processing complex matrices. Initially, a centrifugal platform was chosen as the intended end sample would be a bio-hazardous substance and therefore the device would have to be disposable. In an effort to create a platform that would be easily tested, the LoAD was determined to be the best option. A full optimisation study was carried out, where each feature was scrutinised to determine the optimum parameters for testing pathogen containing samples. The platform itself went under many iterations to perfect the flow of the sample, triggering frequencies of the assay reagents, incubation times of the sample

over the sample and electrode cover optimisation to increase sensor sensitivity. To eradicate the need for pre-sample treatment, the device sample chamber was pre-functionalised with fibrinogen which causes platelet aggregation, reducing the overall contamination of the electrode surfaces to increase the sensitivity of the sensor cell. A spin-rate study was also used to determine the prime frequency in which the sample is forced over the sensors to maximise sample to sensor surface time whilst maintaining the integrity of the pathogen cell without forcing non-specific binding of unwanted blood components on the surface. The device was manufactured in a way that the design could be used in conjunction with other manufacturing processes, such as 3D printing.

Chapter four reported two separate methods of biosensor development. The traditional SAM modified antibody surface was characterised to determine the effect of each fabrication step on the gold working electrode and how this would influence the EIS and CV responses of the electrochemical cell in a dilute electrolyte solution. With the addition of each sequential modifying solution, the overall impedance of the cell reduced. This was caused by an amalgamation of the thickness of the modified layers forming that contains negative charges due to the isoelectric point of the amino acid structures of the antibody being lower than the pH of the supporting electrolyte solution. With the addition of the biosensor fabrication steps, the capacitors acting in series reduces the overall capacitive response of the system. The capacitance of the layers also alters the response which was previously shown by the Nyquist semi-circle plots. For a single use sensor to be fabricated, the method of μ CP was explored as an alternative approach to create a bio-recognition layer of the gold sensor surface. With the electrodes being tested outside and inside the device, the sensor was proved to be highly reproducible where the sensor preparation time was reduced from 3 days to 1. A full validation of the new eLoaD was carried out with a total of 26 blood culture samples received from St. James' Hospital.

Chapter 5 reported alternative approaches to whole cell detection which excluded the use of expensive antibodies. Aptamers are robust oligonucleotides which are easily modifiable with a variety of moieties and therefore were selected as an alternative capture and detection probe for E. coli cells. Three separate assays were optimised where ELONA, PCR and RPA techniques were used to detect a dynamic range of the whole cell in clean buffer. Initially, the ELONA assay was optimised. The intensity of the colorimetric

change of the assay was in indication of the concentration of the E. coli cell present in the assay. An LOD of 23 and 42 CFU/ml for the 100nM and 1000nM reporter probes was detected. This low detection limit confirmed the use of aptamers instead of antibodies for this type of bio-assay, proving the negation of the complex biomolecule. The synthetically produced aptamers proved to be successful probes for the capture and detection of cells. Apta-PCR and Apta-RPA methods were also used to detect low CFU counts of the whole cell. Initially, the ELONA assay was performed where the reporter probe was eluted and amplified and detected using gel-electrophoresis and UV-transilluminator imaging to determine the concentration of the amplified DNA. The robust PCR technique proved most successful with an LOD of 5 CFU/ml for the 100pM reporter probe concentration. The isothermal RPA method was also very similar with its lowest LOD being 9 CFU/ml with the 1nM reporter probe. With all three assays compared, the Apta-RPA was theoretically the best assay due to the shortest assay time with a very low LOD which only requires one temperature, and therefore one cycle, for the amplification process.

The novel eLoaD discussed in both Chapter 3 and 4 may pave the way forward for a near-patient device capable of detecting sepsis inducing whole cells within a reasonable time-frame in which clinicians may make an informed diagnosis. With the antibody based biosensor implemented into the device, the work carried out in Chapter 5 proves the use of aptamers over antibodies as a robust capture and detection methodology. The optimised bio-assays carried out for E. coli detection included well establishes techniques of ELONA and PCR. However, very little literature exists for the RPA methodology for detection purposes.

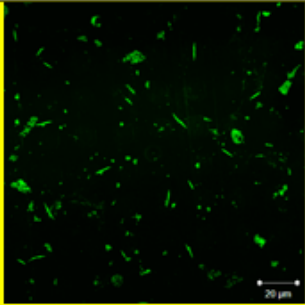
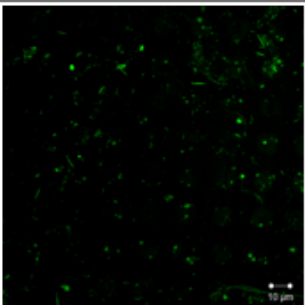
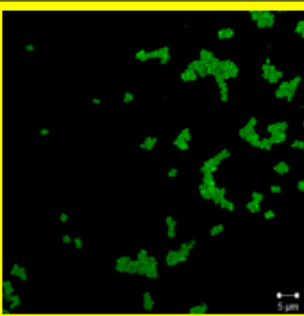
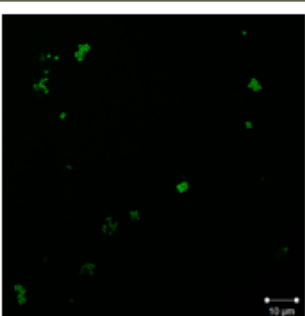
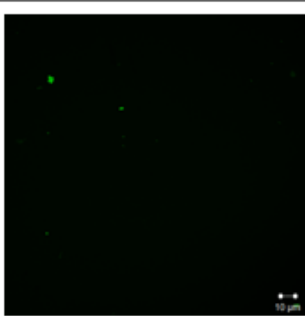
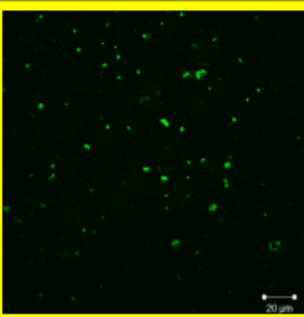
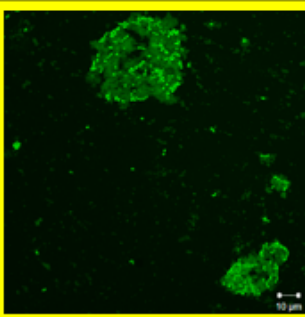
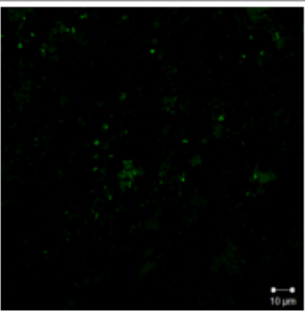
Chapter 6 showed the future work of the individual Chapters in this thesis and portrayed the potential of each project. The SPEs and LFA, if optimised, would allow for low cost sensors to be produce

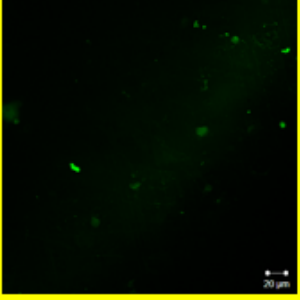
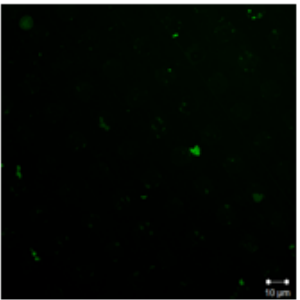
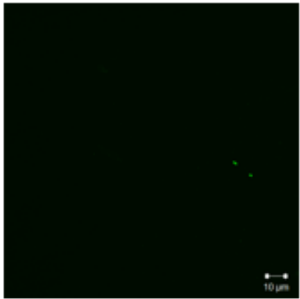
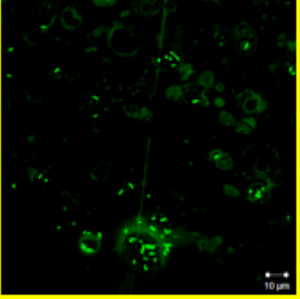
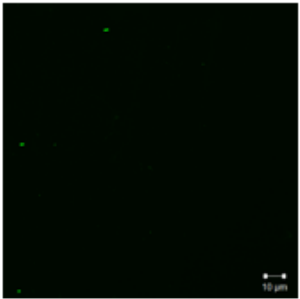
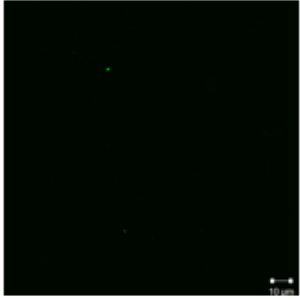
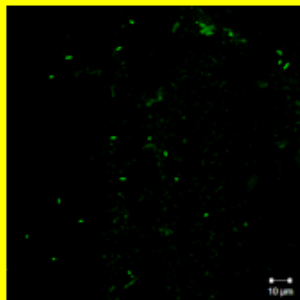
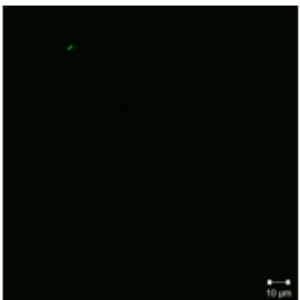
6.3 References

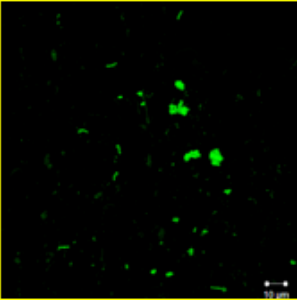
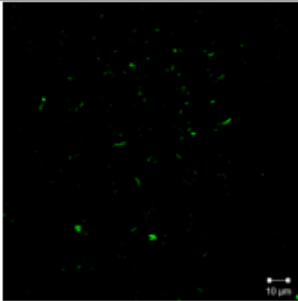
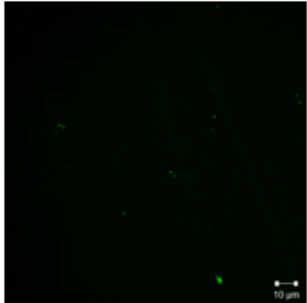
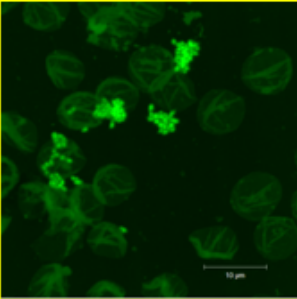
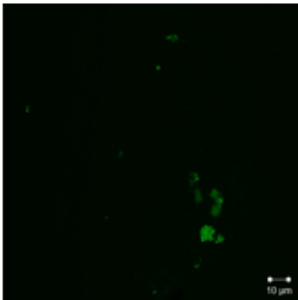
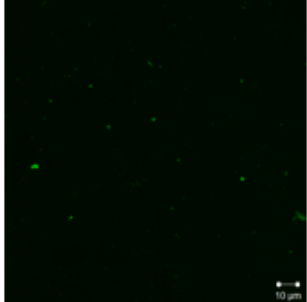
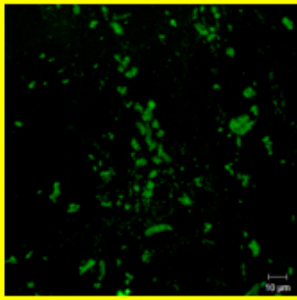
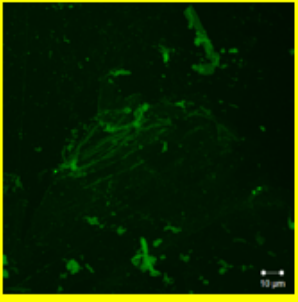
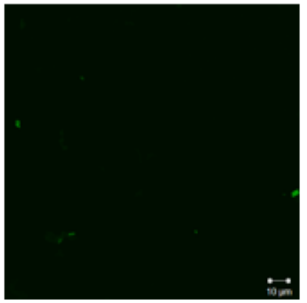
- [1] S. L. in. Chong, G. Y. K. Ong, A. Venkataraman, and Y. H. we. Chan, "The golden hours in paediatric septic shock--current updates and recommendations," *Ann. Acad. Med. Singapore*, vol. 43, no. 5, pp. 267–274, 2014.
- [2] A. Hayat and J. L. Marty, "Disposable screen printed electrochemical sensors: Tools for environmental monitoring," *Sensors (Switzerland)*, vol. 14, no. 6, pp. 10432–10453, 2014.
- [3] C. Fernández-Sánchez, C. J. McNeil, and K. Rawson, "Electrochemical impedance spectroscopy studies of polymer degradation: Application to biosensor development," *TrAC - Trends Anal. Chem.*, vol. 24, no. 1, pp. 37–48, 2005.
- [4] M. Jauset-rubio *et al.*, "Ultrasensitive , rapid and inexpensive detection of DNA using paper based lateral flow assay," *Nat. Publ. Gr.*, no. October, pp. 1–10, 2016.
- [5] M. Jauset-Rubio, M. S. El-Shahawi, A. S. Bashammakh, A. O. Alyoubi, and C. K. O'Sullivan, "Advances in aptamers-based lateral flow assays," *TrAC - Trends Anal. Chem.*, vol. 97, pp. 385–398, 2017.
- [6] K. M. Koczula and A. Gallotta, "Lateral flow assays," *Essays Biochem.*, vol. 60, no. 1, pp. 111–120, Jun. 2016.
- [7] D. S. Kim *et al.*, "Development of Lateral Flow Assay Based on Size-Controlled Gold Nanoparticles for Detection of Hepatitis B Surface Antigen," *Sensors (Basel).*, vol. 16, no. 12, p. 2154, Dec. 2016.
- [8] O. Spadiut, S. Capone, F. Krainer, A. Glieder, and C. Herwig, "Microbials for the production of monoclonal antibodies and antibody fragments," *Trends Biotechnol.*, vol. 32, no. 1, pp. 54–60, Jan. 2014.
- [9] T. Mairal, C. Mcneil, and N. Keegan, "Aptamer Lateral Flow Assays for Ultrasensitive Detection of β - Conglutin Combining Recombinase Polymerase Ampli fi cation and Tailed Primers," 2016.
- [10] M. Sajid, A. N. Kawde, and M. Daud, "Designs, formats and applications of lateral flow assay: A literature review," *J. Saudi Chem. Soc.*, vol. 19, no. 6, pp. 689–705, 2015.

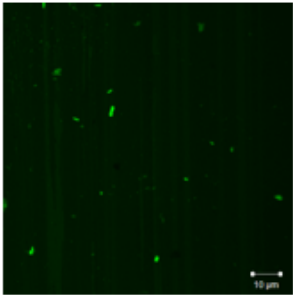
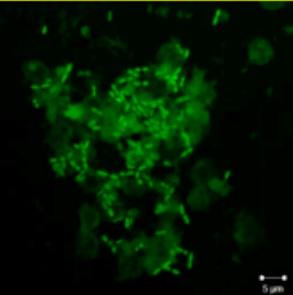
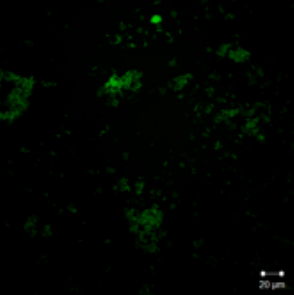
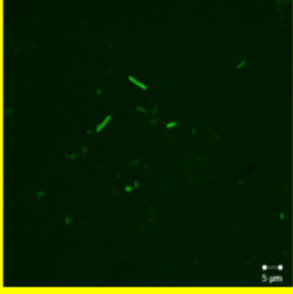
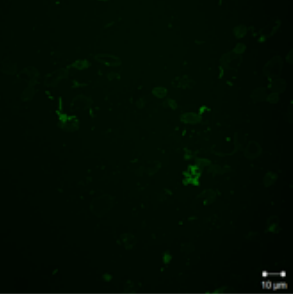
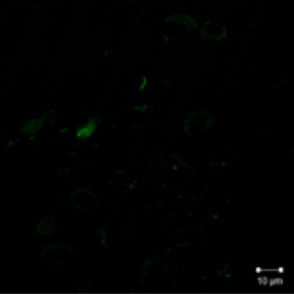
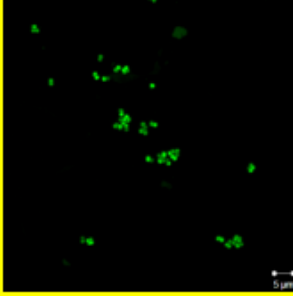
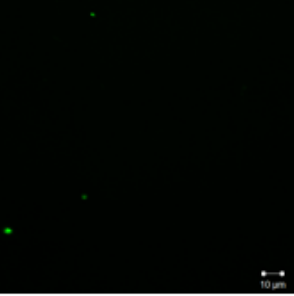
- [11] “Analytical Tools to Improve Optimization Procedures for Lateral Flow Assays,” *Diagnostics*, vol. 7, no. 2, p. 29, 2017.
- [12] Merck-Millipore, “Hi-Flow Plus Membranes and SureWick Pad Materials,” 2015.
- [13] D. Klotz, “Negative capacitance or inductive loop? – A general assessment of a common low frequency impedance feature,” *Electrochem. commun.*, vol. 98, no. November 2018, pp. 58–62, 2019.

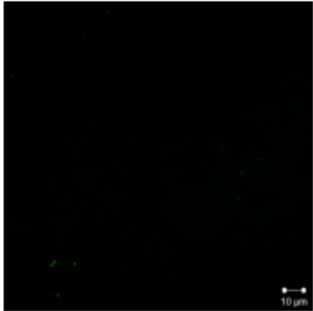
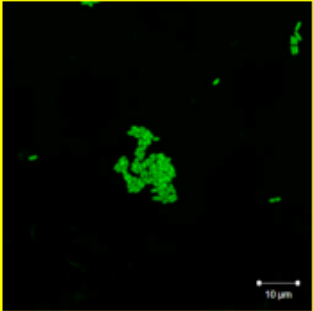
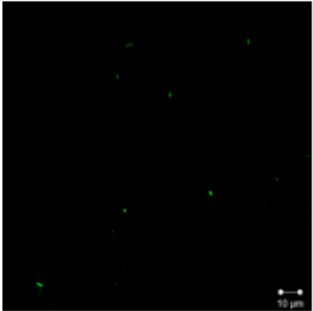
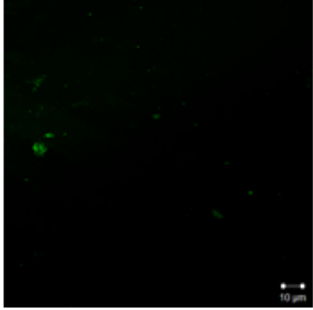
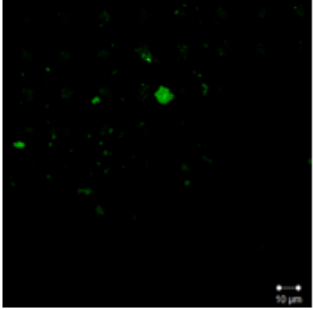
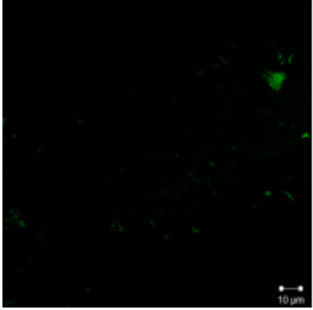
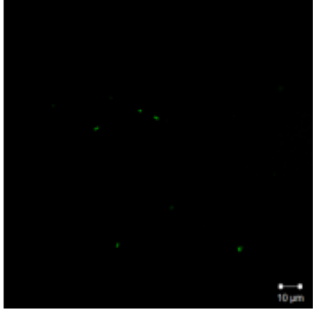
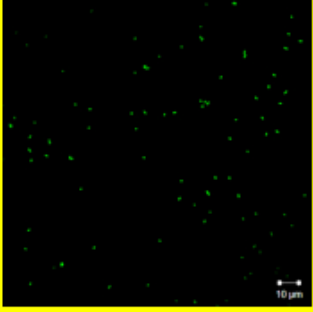
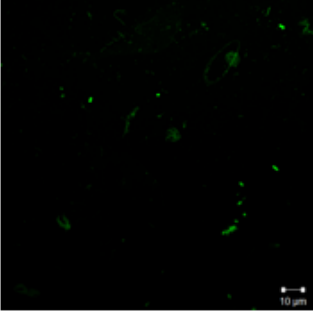
Appendix A

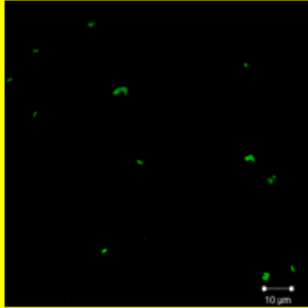
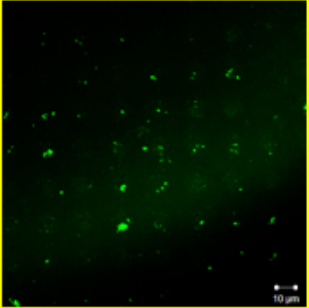
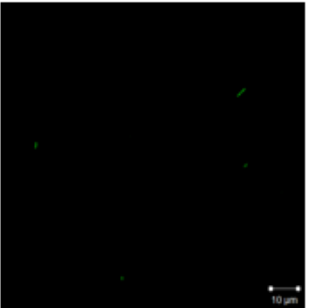
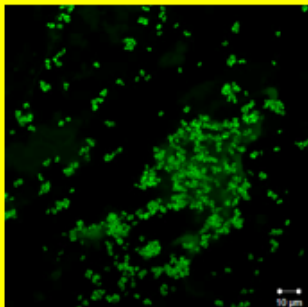
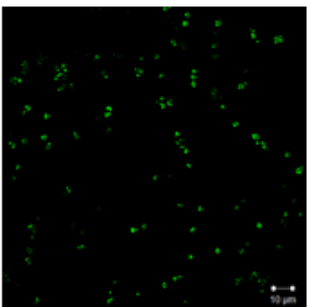
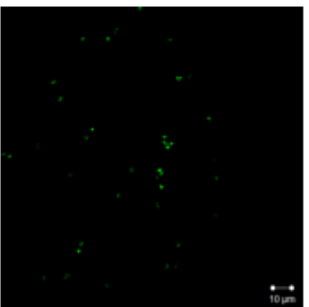
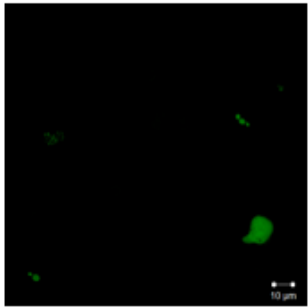
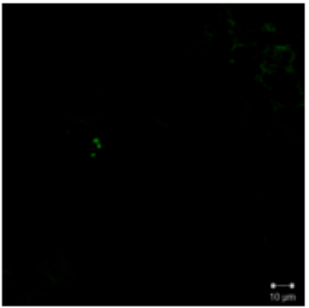
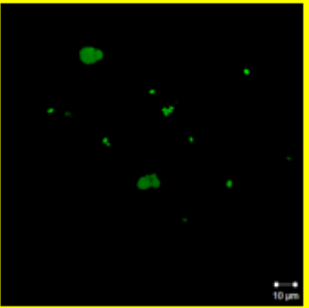
Patient Number	Gram Positive	Gram Negative	Fungal
<p><u>Patient Sample 1</u> <u>422217.1 (Anaerobic)</u></p>			
<p><u>Patient Sample 2</u> <u>422462.2 (Aerobic)</u></p>			
<p><u>Patient Sample 3</u> <u>422460.3 (Anaerobic)</u></p>			

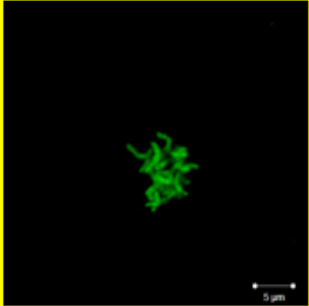
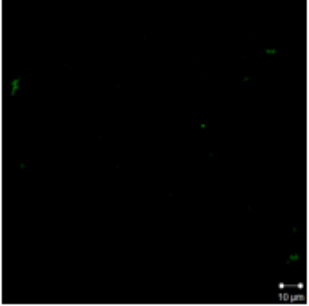
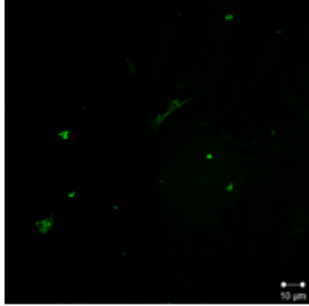
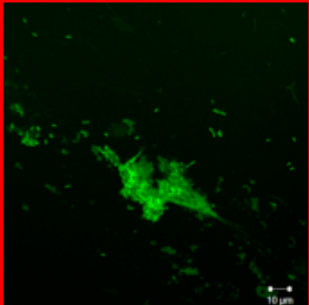
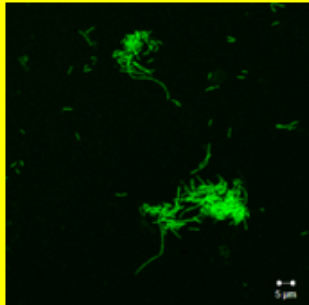
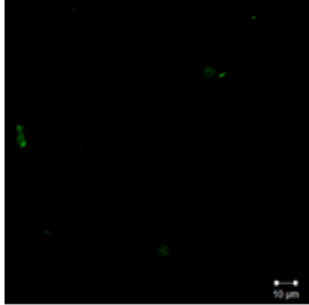
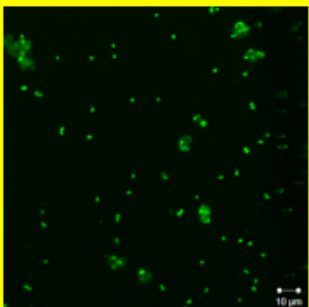
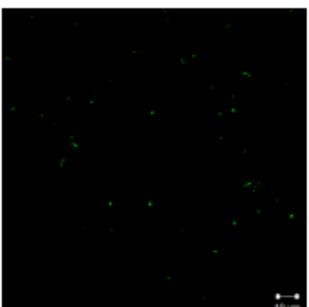
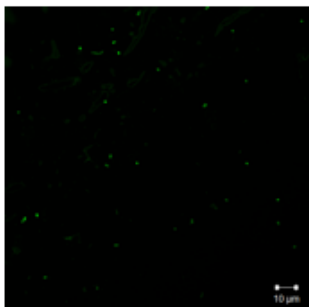
Patient Number	Gram Positive	Gram Negative	Fungal
<p><u>Patient Sample 4</u> <u>422421.4 (Aerobic)</u></p>			
<p><u>Patient Sample 5</u> <u>422517.5 (Anaerobic)</u></p>			
<p><u>Patient Sample 6</u> <u>422517.6 (Aerobic)</u></p>			

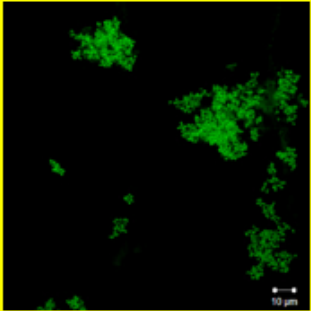
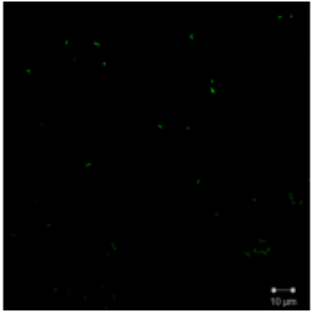
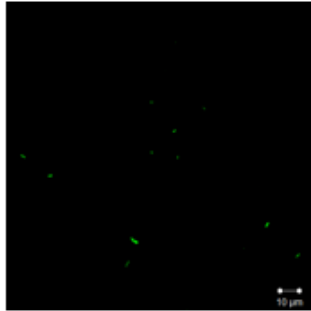
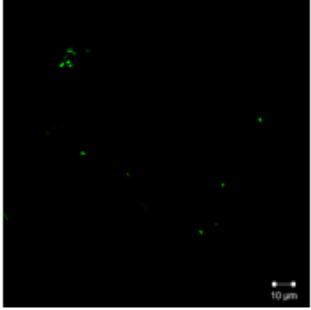
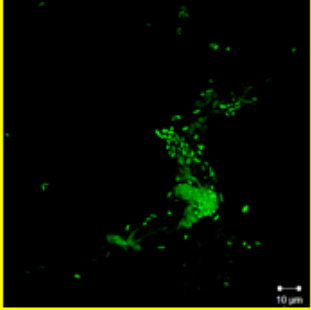
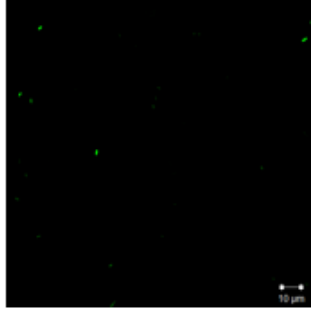
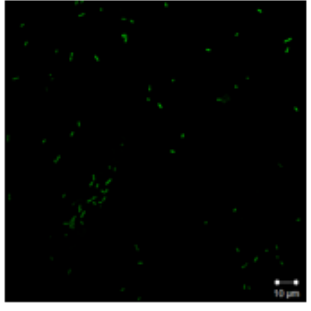
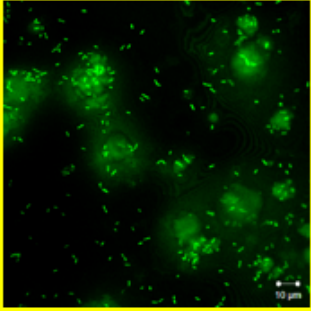
Patient Number	Gram Positive	Gram Negative	Fungal
<p><u>Patient Sample 7</u> <u>422175.7 (Anaerobic)</u></p>			
<p><u>Patient Sample 8</u> <u>422008.8 (Anaerobic)</u></p>			
<p><u>Patient Sample 9</u> <u>422564.9 (Aerobic)</u></p>			

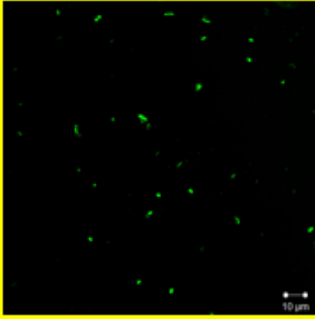
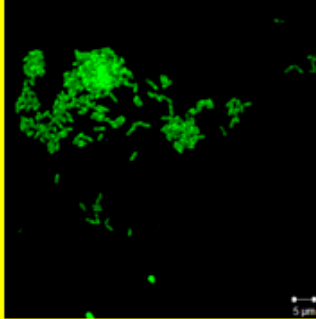
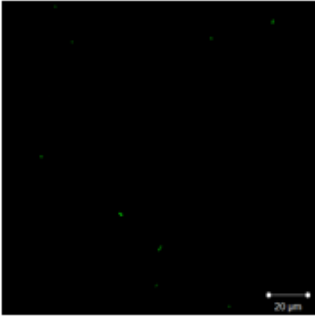
Patient Number	Gram Positive	Gram Negative	Fungal
<p><u>Patient Sample 10</u> <u>422605.10 (Anaerobic)</u></p>			
<p><u>Patient Sample 11</u> <u>422673.11 (Aerobic)</u></p>			
<p><u>Patient Sample 12</u> <u>424439.12 (Aerobic)</u></p>			

Patient Number	Gram Positive	Gram Negative	Fungal
<p><u>Patient Sample 13</u> <u>424414.13 (Anaerobic)</u></p>			
<p><u>Patient Sample 14</u> <u>424840.14 (Aerobic)</u></p>			
<p><u>Patient Sample 15</u> <u>425090. 15 (Aerobic)</u></p>			

Patient Number	Gram Positive	Gram Negative	Fungal
<p><u>Patient Sample 16</u> <u>424414.13 (Anaerobic)</u></p>			
<p><u>Patient Sample 17</u> <u>424414.13 (Aerobic)</u></p>			
<p><u>Patient Sample 18</u> <u>424414.13 (Aerobic)</u></p>			

Patient Number	Gram Positive	Gram Negative	Fungal
<p><u>Patient Sample 19</u> <u>400639.19 (Aerobic)</u></p>			
<p><u>Patient Sample 20</u> <u>426180.20 (Anaerobic)</u></p>			
<p><u>Patient Sample 21</u> <u>426105.21 (Anaerobic)</u></p>			

Patient Number	Gram Positive	Gram Negative	Fungal
<p><u>Patient Sample 22</u> <u>426393.22 (Aerobic)</u></p>			
<p><u>Patient Sample 23</u> <u>426500.23 (Aerobic)</u></p>			
<p><u>Patient Sample 24</u> <u>426548.24 (Anaerobic)</u></p>			

Patient Number	Gram Positive	Gram Negative	Fungal
<p><u>Patient Sample 25</u> <u>426589.25 (Anaerobic)</u></p>			
<p><u>Patient Sample 26</u> <u>426591.26 (Aerobic)</u></p>	